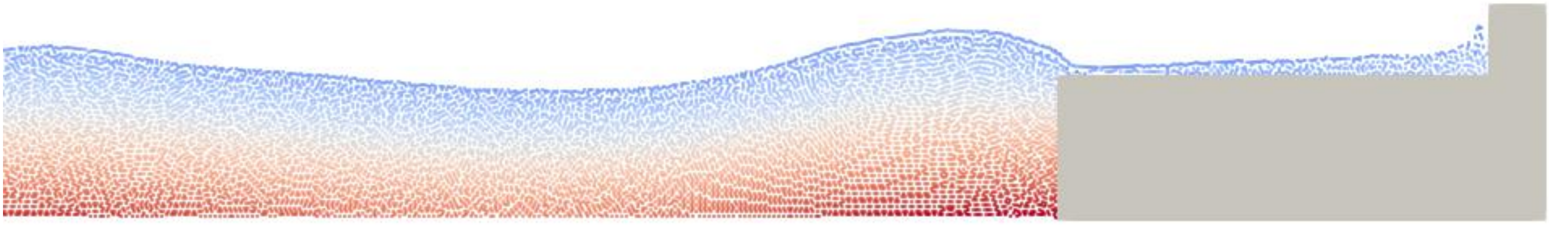

WAVE FORCING ON RETREATED STORM WALLS ON TOP OF VERTICAL QUAY WALLS

Master Thesis

TU Delft
Faculty Civil Engineering and Geosciences

Annika Schalk
5019222

Delft University of Technology

Design & Consultancy for natural and built assets

Wave forcing on retreated storm walls on top of vertical quay walls

by

A.E. Schalk

Final requirement of the degree of Master of Science in Civil Engineering at the Delft University of Technology

to be defended publicly on July 29th, 2024 at Lecture Hall G, Civil Engineering & Geosciences, TU Delft

Student number:	5019222	
Thesis committee:	Dr. ir. Bas Hofland	TU Delft
	Dr. ir. Alessandro Antonini	TU Delft
	Ir. Henry G. Tuin	Arcadis

Preface

This Master thesis is the final part of obtaining my Master's degree in Civil Engineering with the specialty Hydraulic and Offshore Structures at the Delft University of Technology. The research has been carried out at Arcadis, for which I am very grateful. I have met many people who showed a lot of enthusiasm and support during my thesis.

The results of my research would not be there without my thesis committee. To start with, I would like to thank the chair of the committee, Bas Hofland, for his feedback and guidance during the meetings. I also want to thank Alessandro Antonini for providing solutions and asking questions during the meetings to make my research more thorough. And of course a lot of gratitude to my supervisor at Arcadis, Henry Tuin, who weekly guided me through the process, answering my questions.

Besides the committee, I would also like to thank Ermano de Almeida for discussing and helping with the set-up of the laboratory experiment. I would also like to thank Job Oude Vrielink and Stefan Been for their advice on SWASH and DualSPHysics respectively.

Lastly, I would like to thank my family and friends who proofread my thesis and helped me practicing my presentation.

Wishing you an enjoyable read.

Annika Schalk
Rotterdam, July 2024

Summary

Globally the sea level is rising. One of the problems arising from a higher sea level is the increase in wave overtopping discharge at quays. With increasing overtopping discharges, the duration that a quay becomes unusable increases as well. The overtopping problem becomes even larger due to new uses for quays, which require stricter requirements on overtopping discharge due to human involvement or larger economic value, e.g. a shopping area.

To decrease wave overtopping discharge, multiple solutions are available, like placing a storm wall on top of the vertical quay. This wall should be placed at the seaside of the vertical quay wall to limit forcing and space requirements. However, due to requirements regarding e.g. landscaping, ship access or monumental status this is not always possible. Therefore, the storm wall is in some cases placed at a distance from the quay wall's edge. With such a setback wall impact wave loads can occur which cause much higher loads than with a straight vertical wall. There is however limited knowledge on the computing of these impact loads. Empirical formulas for a first estimation exist, but they do not consider the geometry of the structure (height storm wall, length quay) or are not applicable for negative freeboard, or both.

Due to this limitation, the main research question of this research is "What is the influence of the geometry of a retreated storm wall on top of a quay wall on the wave forcing exerted on the storm wall?".

The main method used for this research is numerical modelling. Several models are considered, including SWASH (Simulating Waves till SHore) and DualSPHysics, from which DualSPHysics has appeared the most suitable. DualSPHysics makes use of Smoothed Particle Hydrodynamics (SPH), which is a Lagrangian method where all matter consists of particles instead of a grid. At every time step the new properties of each particle are computed. The particles move according to these new values. The model is verified with a qualitative laboratory experiment. In this experiment it is observed which type of wave occurs (quasi-standing, slightly breaking, breaking or broken) under different circumstances (wave steepness, quay length, etc.). There is no pressure or forcing measured in this experiment. The results of the experiment are used to see if the numerical model predicts the same type of wave occurring. The forcing results from the numerical model are compared to simplified methods from literature to see which corresponds the best.

The DualSPHysics model appears well suitable to simulate different waves when comparing them with the results of the lab experiment. In the validation, using experiments from Den Heijer (1998), it appears that the model performs well in predicting the highest 1% and 10% force of an irregular wave field as well. The maximum wave force is however often overestimated by the DualSPHysics model. The poor prediction for the maximum force is likely due to the randomness of irregular waves (sampling error). In addition, the experiments used for the validation contained a relatively coarse measuring frequency which can cause the omission of high peaks in the forcing.

The DualSPHysics model is not able to simulate positive freeboard accurately, as only a few particles would reach the top of the quay and the storm wall. This low resolution results in numerical instabilities. DualSPHysics might be able to model it well with a large increase in the number of particles. For negative freeboard the resolution is limited from 5 to 10 particles in the mean depth.

According to the laboratory experiment, the quay length appears to have a large influence on the types of waves occurring and therefore also on the wave forcing, as appears in the DualSPHysics model. When the quay length is 0.15 to 0.30 times the wavelength, a significant increase in wave pressure of a factor around 5 can be expected. Making the quay longer leads to broken waves

occurring more often with only an increase in wave pressure of a factor 1.1. The exact increase also depends on the relative depth on top of the quay and the wave steepness (d_{wq} / H), as these also influence the type of waves occurring. A linear relationship between the relative quay length (L_{quay} / L) and relative water depth (d_{wq} / H) is found, creating a breaking wave range.

The formulas which come closest to the forcing found by DualSPHysics are the Cooker-Peregrine formula with added coefficients and an exponential fit. The Cooker-Peregrine formula is a field solution for an idealized wave impact which provides the pressure impulse. To this formula two coefficients are added to obtain a better fit with the DualSPHysics data. The exponential fit is not based on physics, it is just fitted to the data. Both formulas should only be used in the ranges $0.15 \leq L_{quay} / L \leq 0.30$ and $0.17 \leq d_{wq} / H \leq 0.80$ (regular waves) or $0.43 \leq d_{wq} / H_s \leq 2.0$ (irregular waves). This is the range where the highest forcing is expected caused by impact loads.

It should be taken into account that the numerical model itself contains inaccuracies and that the formulas can only be used for a rough first estimation. Use the wave height according to the standards applicable in the project's country in the formulas for an estimation of the wave force in the conceptual design. For the follow-up designs laboratory experiments or CFD models are recommended for a better force estimation.

List of symbols

Greek symbols

Symbol	Definition	Unit
β	= Angle of incidence	°
γ	= Peak enhancement factor	-
Δt	= Time step	s
Δx	= Horizontal grid size	m
Δz	= Vertical step size	m
ζ	= Free surface	m
η^*	= Elevation to which the wave pressure is exerted	m
θ	= Phase	rad
λ_n	= $(n - ½)\pi$, constant Cooker-Peregrine	-
μ	= Mean	Depends
μ^*	= Fraction of water height	-
ν	= Kinematic viscosity	m^2/s
ρ	= Density	kg/m^3
ρ_w	= Density water	kg/m^3
σ	= Standard deviation	Depends
ω	= Angular wave frequency	rad/s

Latin symbols

Symbol	Definition	Unit
a	= Wave amplitude	m
B	= Width of structure	m
B_M	= Width of berm in front of structure	m
b	= Width of fluid	m
c	= Wave celerity	m/s
C	= Scaling factor of Willmott's refined index of agreement	-
-d	= Vertical coordinate of the bottom	m
d	= Still water depth	m
dp	= Particle distance	m
d_r	= Willmott's refined index of agreement	-
d_w	= Water depth in front of the quay	m
d_{wq}	= Water depth on top of the quay	m
F	= Force	N
$F_{h,max}$	= Maximum horizontal force	N
F_{max}	= Maximum force	N
F_{peaks}	= Average force of all peaks	N
f	= Wave frequency	Hz
f_{max}	= Maximum wave frequency	Hz
f_p	= Peak wave frequency	Hz
$f_{sliding}$	= Friction coefficient	-
g	= Gravitational acceleration = 9.81	m/s^2
H	= Wave height	m
H_c	= Height of wave crest with respect to the bed	m
H_{m0}	= Estimate of significant wave height from spectral analysis	m
H_{max}	= Maximum wave height	m
H_s	= Significant wave height, average height of highest third of waves	m

h	= Water depth at a distance of 5 times H_s from the structure	m
h'	= Depth of structure under water	m
h_{sl}	= Smoothing length	
h_{sw}	= Storm wall height	m
k	= Wave number	rad/m
L	= Wavelength = $\frac{gT^2}{2\pi}\tanh\left(\frac{2\pi d_w}{L}\right)$	m
L_{op}	= Peak deep water wavelength = $\frac{gT_p^2}{2\pi}$	m
L_{quay}	= Length of the quay = distance of storm wall from the edge	m
MAD	= Mean absolute deviation	Depends
MAE	= Mean absolute error	Depends
N	= Number of samples	-
N_s	= Number of sensors	-
n	= Porosity	-
$\bar{O}$	= Mean of observed series	Depends
O_i	= Sample of observed series	Depends
P	= Momentum	Ns
P_I	= Pressure impulse	Pa·s
P_i	= Sample of predicted series	Depends
p	= Pressure	Pa
$\mathbf{q}$	= Mass flux	m^2/s
q	= Wave overtopping discharge	m^2/s
R^2	= Coefficient of determination	-
R_c	= Freeboard	m
S	= Elevation above bottom	m
$S_{var}(f)$	= Wave variance spectrum	m^2/Hz
s_{op}	= Wave steepness in deep water	-
T	= Wave period	s
T_p	= Peak wave period	s
t	= Time	s
U_0	= Velocity before impact	m/s
$\mathbf{u}$	= Depth averages flow velocity vector	m/s
u_x	= Horizontal flow velocity	m/s
$u_{x,max}$	= Maximum horizontal flow velocity	m/s
u_z	= Vertical flow velocity	m/s
x	= Horizontal coordinate	m
z	= Vertical coordinate	m

Other

Symbol	Definition	Unit
∇	= Two-dimensional gradient operator = (∂_x, ∂_y)	[-]

Contents

Chapter 1 Introduction

Globally the sea level is rising. These rising sea levels are posing new challenges to maritime infrastructure. One of the problems that arise from a higher sea level is that the wave overtopping discharge at quays and other vertical structures increases. Also, the number of waves on structures, due to the overtopping, increases. With increasing overtopping discharges, the duration that a quay becomes unusable increases as well.

On the other hand, the allowed overtopping discharge can also decrease due to the change of purpose of the quay. Examples include the placement of housing, which involves human lives, or the placement of buildings with high economic value. In this case, discharges which might have been allowable before are now no longer acceptable.

1.1 Relevance

Examples in practice

An example of the problem in practice is the sea lock at Ijmuiden. To prevent wave overtopping in the ship lock, a storm wall was applied at the lock door, shown at the right side of the road in the lower picture in Figure 1.1. The storm wall was placed towards the lock side instead of the seaside because of aesthetic sightlines. However, the placement of the storm wall on the lock side instead of the seaside led to the need for a new design method (Tuin, 2016). This is because due to the sudden decrease in water depth, breaking waves can occur. Breaking waves are preferably prevented, as they exert high forcing on structures.

Figure 1.1: Lock door Ijmuiden with retreated wall on the right (design wave enters from left to right). By H. G. Tuin, n.d.

An example of a breaking wave impact is shown in Figure 1.2. The photos show the incoming wave in the upper left picture and the moment after impact on the lower right picture. The retreated storm wall was placed on a vertical structure, indicated with a red arrow. The photos are part of a video from experiments done in the Deltaflume at Deltares (2024).

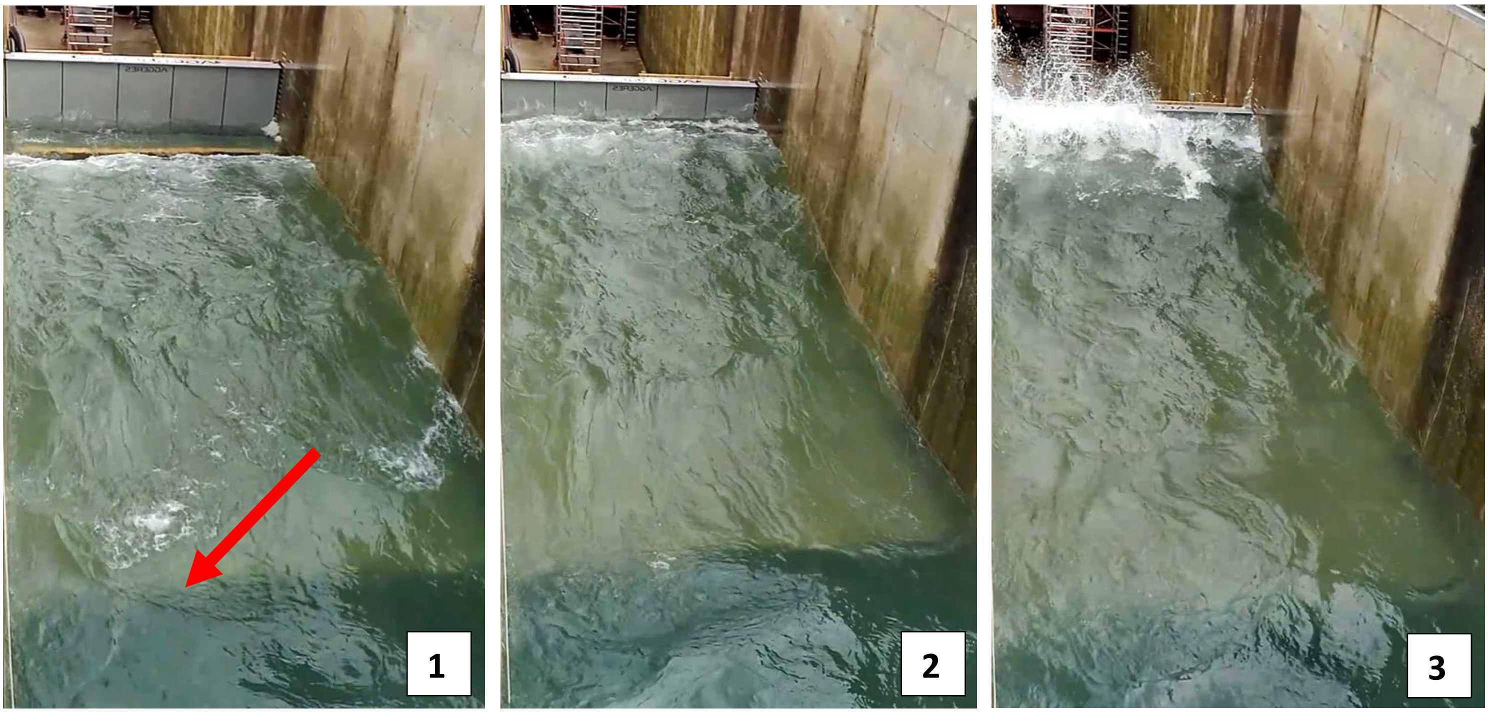

Figure 1.2: Wave impact on retreated storm wall on top of a vertical structure. By H.G. Tuin, 2024.

The tests at Deltares were performed to validate the design of an automatic storm wall which is going to be put at the quays at the Scheldt in Antwerp. The storm wall is going to be placed to protect the hinterland against flooding. An artist impression of the new situation is shown in Figure 1.3. The wall is located in the ground and will automatically rise when the water level in the Scheldt rises above a certain level. Similar to the lock door in Ijmuiden, the storm wall is set back, which introduces the potential for breaking waves to occur.

Figure 1.3: Artist impression of automated storm wall in Antwerp. By Artes, 2024.

Case study

In this thesis the wave impacts on such set back storm walls are studied. A case study is used, which will be presented here. The case study is the Kop Van Zuid neighbourhood in Rotterdam, located on the south side of the river Nieuwe Maas, shown in Figure 1.4. Due to sea level rise and a lower allowed overtopping discharge, a storm wall might need to be placed to prevent flooding of the neighbourhood. By modelling different sizes of storm walls at different distances from the edge of the quay, the effect of the geometry can be found. This allows for more precise estimation of the forcing.

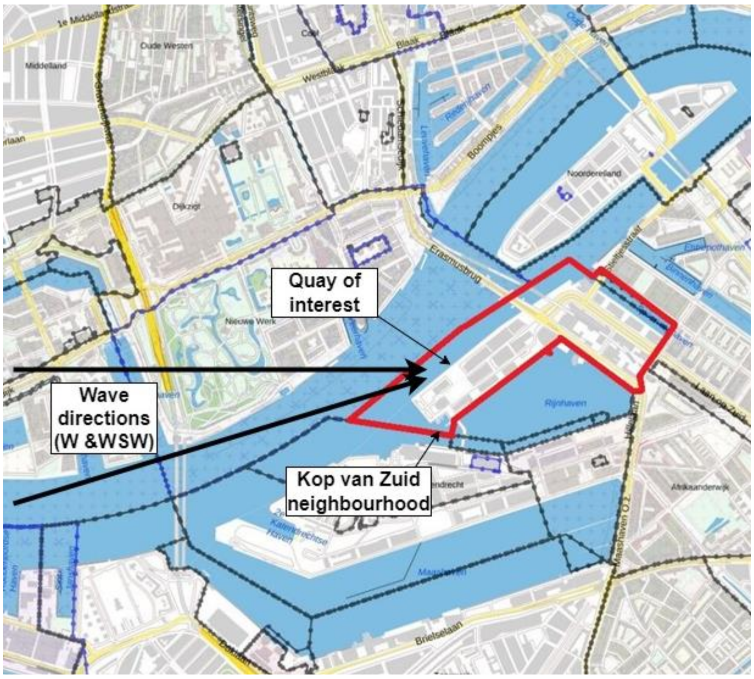

Figure 1.4: Location Kop van Zuid. From "Gemeente Rotterdam", by R. Volman, n.d.

As seen in the examples, placing a storm wall on top of the vertical structure is one way to limit wave overtopping. A general layout of such a scheme is given in Figure 1.5. The incoming wave is characterized by the incoming significant wave height H_s and the peak period T_p. The geometry of the retreated storm wall is described by the length of the quay in front L_{quay} and the height of the storm wall h_{sw}. The other parameters describe the water depth in front of the quay, d_w, and on top of the quay d_{wq}. The water depth in front of the quay can be omitted in case of deep water waves, but it is still mentioned to compare with literature which does not use deep water.

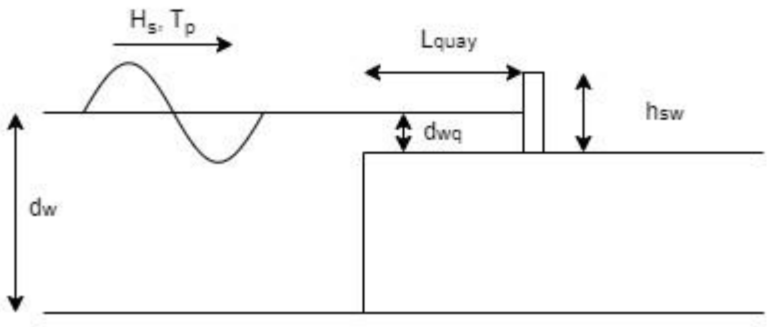

Figure 1.5: Lay-out storm wall on top of a quay wall

1.2 Prior knowledge and gaps

Knowledge about computing wave forcing on a retreated storm wall on top of a vertical quay is limited. Primary experimental research to determine the wave forcing was done by Den Heijer (1998), who performed experiments in the "Scheldegoot" of WL Delft Hydraulics (now known as Deltares). Den Heijer used irregular waves in intermediate water (d_w / L_{op} = 0.152 to 0.195) on a small scale. The experiments delivered empirical formulas for the maximum occurring wave load with negative freeboard, dependent only on the significant wave height and wave steepness. Den Heijer gives a first estimation of the possible occurring force, but the formulas are only usable in the tested ranges shown in Table 1.1. Additionally, the formulas are empirically derived instead of analytically. Parameters like the water level or the distance of the storm wall from the edge of the quay are missing.

Van Doorslaer et al. (2015) obtained formulas as well by performing tests with a 1:6 scaled model. The model consists of a retreated storm wall on a vertical quay with a layer of sand in front of the quay. Van Doorslaer used irregular non-breaking waves in intermediate water (d_w / L_{op} = 0.134 to 0.236) with zero and positive freeboard. In the formulas the freeboard is taken into consideration, but the forcing is independent of the distance from the storm wall to the edge of the quay wall. This parameter was studied by Romano and Bellotti (2023) who looked at the forcing on a crown wall on top of a vertical breakwater / caisson by doing experiments where the distance of the crown wall to the edge of the vertical breakwater varied. They used regular waves in intermediate water (d_w / L = 0.207 to 0.406) with a positive freeboard. They found that the forcing on the breakwater decreases when placing the crown wall further from the edge, but the forcing on the crown wall itself increased (up to 300% for low energy wave conditions). They suggested that the increase in forcing of the wall was caused by the occurrence of impulsive loads. They recommended follow-up research using irregular waves and CFD models. As can be noted, the studies on wave impact on a storm wall described, were conducted entirely through laboratory experiments.

Table 1.1 gives an overview of the dimensionless parameters which were tested in the references described above. Two relevant parameters were the same in all these references. First, the waves were always entering straight on the quay. Second, even though in all experiments the pressure over time was measured, the analysis was focused on the total horizontal force, not the impulse.

Table 1.1: Overview of relevant dimensionless parameter ranges for different studies on wave impact on a retreated storm wall

Irregular waves Author(s) (year)	L_{quay} / L_{op}	(h_{sw} – d_{wq}) / H_s	h_{sw} / H_s	H_s / L_{op}	kd_w	d_{wq} / H_s	Freeboard (w.r.t. quay)
Den Heijer (1998)	0.25 – 0.5	1.5 – 3.0	1.63 – 3.02	1 – 4%	0.71 – 1.79	0.5 – 2.0	Negative
Van Doorslaer et al. (2015)*	0.133; 0.065	-	0.4 – 1.54	0.5 – 4%	0.58 – 1.92	<= 0	Zero and positive
Regular waves	L_{quay} / L	-	h_{sw} / H	H / L	kd_w	d_{wq} / H	Freeboard (w.r.t. quay)
Romano & Bellotti (2023)	0 – 0.20	-	0.94 – 1.88	2.5 – 10%	1.12 – 2.52	< 0	Positive

*H_{m0} was used instead of H_s

Research up to now has been done experimentally, resulting in first insights and formulas for first estimations. The formulas derived are however still limited. None of them contain the relative quay length L_{quay} / L and they are not applicable for waves steeper than 4%. Romano and Bellotti (2023) tested for wider ranges of wave steepness and water depth, but only for positive freeboard and regular waves. They described a linear increase in forcing on the retreated wall with an increased quay length but did not provide a formula.

The applicability of computational models for the retreated storm wall on a vertical quay has not been reported yet.

1.3 Aim

This research aims to determine the influence of the geometry of a retreated storm on top of a quay wall on the wave forcing, with both positive and negative freeboard, exerted on the storm wall, and compare/explain the differences between basic physical considerations and both computational models. Here, the geometry refers to the storm wall's height and location.

In this study two types of computational models are used: non-hydrostatic wave-flow (SWASH) and Smoothed Particle Hydrodynamics (DualSPHysics).
The main research question is: "What is the influence of the geometry of a retreated storm wall on top of a quay wall on the wave forcing exerted on the storm wall?"

Sub-questions to answer the main research question are:

1. When are breaking waves on a retreated storm wall expected?
2. To what extent are SWASH and DualSPHysics suitable for modelling wave-structure interactions?
3. How does the wave force on the storm wall change with increased storm wall height / distance of the storm wall from the edge of the quay wall based on computational model predictions?
4. To what rate are the results of sub-question 1 and 3 similar with different freeboards?
5. What are the differences between the numerical model and the laboratory experiment and what are the corresponding possible explanations?
6. What are the differences between the results found and simplified methods from literature?

1.4 Approach

An overview of the thesis approach is shown in Figure 1.6. The methods are shown on the left and the desired knowledge on the right. With different line types it is indicated which method is used to get which information.

To answer the research questions, first the available literature is studied. The literature provides insight into which hydraulic situations are relevant to answer the research questions. It also helps to understand the physical processes happening in the model. Next, the two previous mentioned models are introduced. The physical model experiment is used to see which type of wave occurs when altering the relevant dimensionless parameters (relative quay length, wave steepness, etc.). The results are used as validation for the computational models.

For the numerical model, both SWASH (Simulating Waves till SHore) and DualSPHysics are used, because of limited calculation time while still providing reasonable to good results (Gruwez et al., 2020). However, SWASH appeared unsuitable for the studied type of geometry and therefore the research continued with DualSPHysics. SWASH is only used to answer sub-question 2. The primary model parameters are validated using the laboratory experiments of Den Heijer (1998). The calibrated model is additionally validated with the use of a qualitative lab experiment. To determine the order of magnitude of the variables in the model, the Kop van Zuid case study is used.

Sub-question 1 is answered using both the results from the laboratory experiments and the DualSPHysics model. Videos from the laboratory experiment are used to observe the wave types and determine the relevant dimensions using pixel sizes. For the DualSPHysics model the type of waves are observed by making animations of the simulation. To answer sub-question 2 the SWASH model is used as well. The suitability of the models can be determined using the lab experiment and expected results from the literature study. Sub-question 3 and 4 are answered using the results from the DualSPHysics model and fitting a formula. Sub-question 5 is answered by comparing the results of the laboratory experiment and the DualSPHysics model. Explanations in differences are found by looking into the model's assumptions and limitations. Sub-question 6 is answered by comparing the results of the laboratory experiment and the DualSPHysics model with the simplified methods from literature.

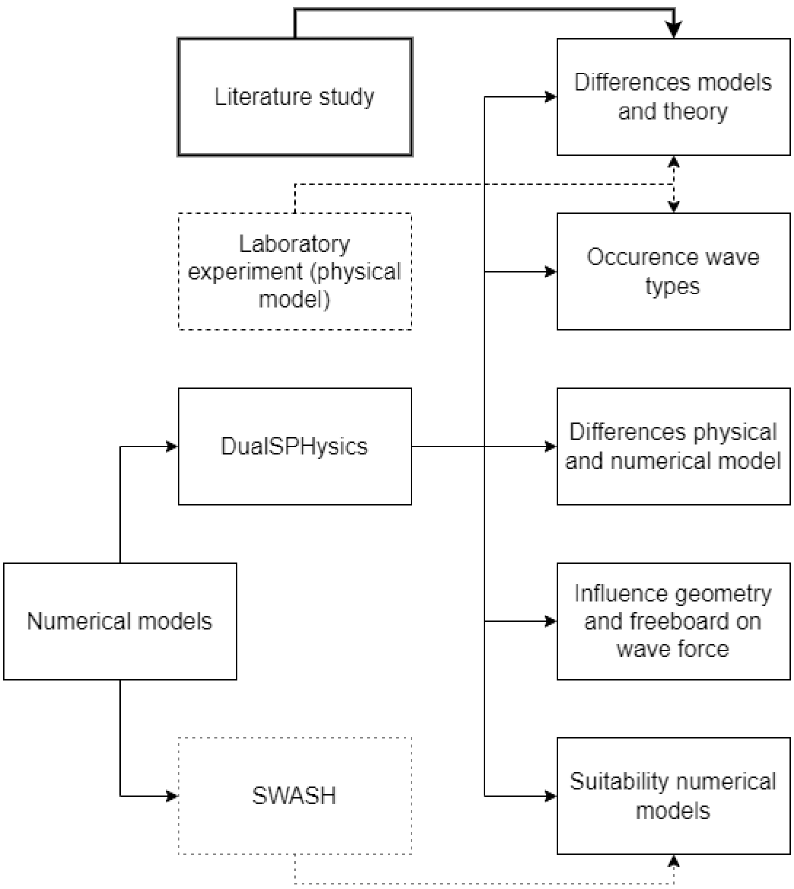

Figure 1.6: Thesis approach with methods (left) and desired knowledge (right). Different line types are used for different methods.

1.5 Scope

There are many parameters that can be investigated. In this study, the focus lies on the effect of the storm wall's geometry on the wave forcing. Therefore, certain phenomena are interesting to consider while others can be simplified as described below.

Freeboard

For the freeboard, the focus lies on the negative freeboard, as here the knowledge gap is the largest. The influence of the change from positive to negative will be investigated as well.

Geometry variations

The geometry variations will contain variations in storm wall height (h_{sw}) and the distance of the storm wall to the edge of the quay wall (L_{quay}). Also the freeboard (d_{wq} - d_w) is varied, to see if the same effects occur for different freeboards.
The slope of the quay is assumed flat.

Wave characteristics

This research uses both irregular and regular wave forcing. The model results are qualitatively validated using an experiment in the wave flume with regular waves.
The waves considered are perpendicular to the quay. The wave steepnesses considered are 2% and 5%.

Bathymetry
Since the case study deals with deep water, the bottom will likely have a minor influence on the wave behavior. Therefore, it is assumed to be flat.

Overtopping
Note that the research is focussed on the forcing and the effect of the geometry on the overtopping discharge is not part of the research. Overtopping computations are only used to determine a reasonable storm wall height.

1.6 Thesis outline

The thesis outline will, after the introduction, first contain the literature review, forming Chapter 2. This is then followed by Chapter 3 which contains the methods used. The set-ups of both the physical and numerical model are described. Next, the results of the lab tests follow in Chapter 4. In Chapter 5 the results of the DualSPHysics model are discussed. In Chapter 6 the results are compared to each other. This chapter also contains possible explanations for the differences. 0 compares the results to the theory from Chapter 2. In Chapter 8 fits are generated to predict the force based on the results and theory. Chapter 9 contains the discussion of this research. Finally, Chapter 10 contains the conclusions and recommendations, and the main research question is answered.

Chapter 2 Literature

This chapter describes the relevant literature for this study. The state-of-the-art has already been treated in Chapter 1. This chapter first focuses on different wave types and boundary conditions. Next, the already existing theories for force computation for vertical structures are described. Lastly, different types of numerical models and their applicability are discussed.

2.1 Wave types

Different types of waves can occur depending on the geometry of the structure and the hydraulic boundary conditions. One type of wave can result in higher wave forcing than another, which is why it is important to know which type of waves are expected. For a vertical breakwater, the types of waves and their occurrences are described by the extended parameter map given by Kortenhaus and Oumeraci (1998), shown in Figure 2.1. The occurrence of the wave types is determined based on laboratory tests at four different institutes and large-scale model tests in the Hannover wave flume. The parameter map helps determine which type of waves are expected to occur (quasi-standing, slightly breaking, impact or broken waves) based on the geometry of the berm, if present, and hydraulic boundary conditions. Below, the different wave types seen in Figure 2.1 are explained.

Quasi-standing wave

In a perfectly standing wave the nodes and antinodes of the wave stay at the same position. They are caused by the interfering of two waves with the same frequency moving in opposite directions, which for example occurs at a vertical wall with perfect reflection. This causes the amplitude of a standing wave to be twice as high as the amplitude of the incoming waves.
A quasi-standing wave might still have some movement of the nodes and antinodes, but its behaviour is similar to a standing wave.

Slightly breaking wave

A slightly breaking wave is a wave that is in the beginning stage of the breaking process. It has not collapsed yet, but it shows characteristics of the beginning stage, like an increased wave steepness or foam caps.

Impact / breaking wave

A breaking wave is a wave at its moment of collapsing. When this happens at a vertical wall a lot of energy is exerted on the wall. This wave force can be four times as high as the wave load from a quasi-standing wave.

Broken wave

A broken wave has fully collapsed. What remains is turbulent water movement. The maximum wave load is in magnitude comparable to a quasi-standing wave. According to the parameter map shown in Figure 2.1, broken waves instead of breaking waves are expected to occur for a berm width of at least 0.4 of the wavelength.

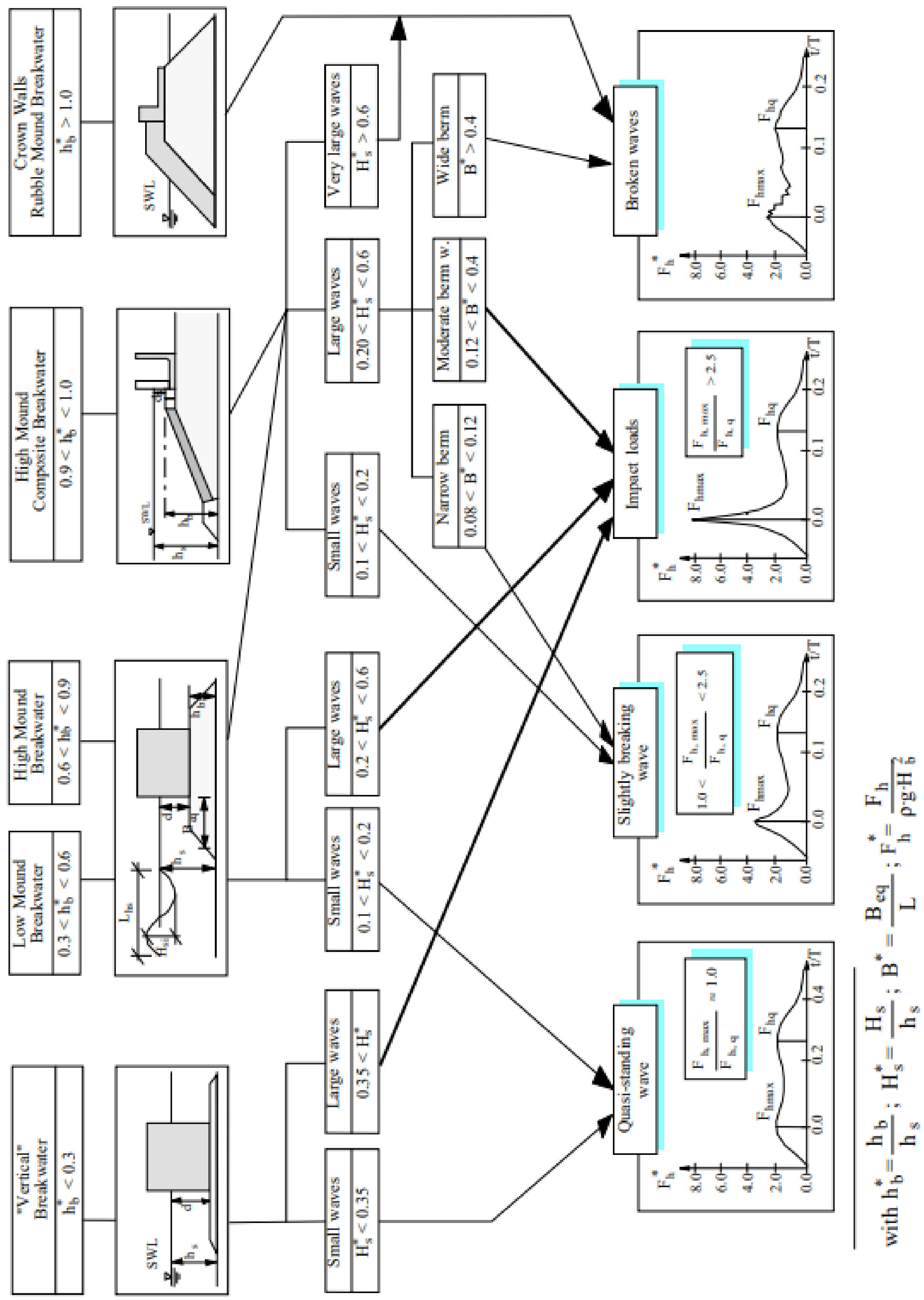

Figure 2.1: Parameter map, Kortenhaus & Oumeraci (1998)

2.2 Wave boundary conditions

This paragraph introduces the boundary conditions which are used for the waves in this research. A distinction is made between irregular and regular waves. Regular waves are waves with the same wave height and period. Irregular waves come from a distribution and their wave height and period can vary. First, the irregular waves are discussed as they are closest to the real-life situation. After the irregular waves, the translation to the regular waves is made. Lastly, the theories and their applicability to describe the incoming waves are discussed.

Irregular waves

Irregular waves come from a distribution or spectrum. An irregular wave field can consist of multiple distributions or a single one. For the irregular wave models in this research a unimodal wave spectrum is used. This means that only one group of waves is considered, but that within the group the wave heights and wave periods vary. A widely used wave spectrum for modelling is the JONSWAP (JOint North Sea WAve Project) spectrum (Hasselman et al., 1973). The shape of this spectrum is based on the Pierson and Moskowitz spectrum (Pierson and Moskowitz, 1964), but has as additional parameter, the peak enhancement factor γ. This factor can give the spectrum a sharp peak to represent a certain sea state. Examples are $\gamma = 3.3$ for a mean JONSWAP spectrum, which represents a young sea state, and $\gamma = 20$ for a very sharp JONSWAP spectrum, which represents swell. For this study a mean JONSWAP spectrum is used.

The shape of the JONSWAP spectrum is influenced by the spectral significant wave height H_{m0} and the peak wave period T_p. In this research, deep water waves are considered, which means that the significant wave height H_s and the spectral significant wave height H_{m0} are approximately the same.

Regular waves

Regular waves all have the same wave height and period. To compare irregular and regular waves, a wave from the irregular wave field has to be selected to use for the regular waves. The most interesting wave in the irregular wave field is the wave which gives the maximum wave force. Therefore, this maximum wave is used for the regular waves. With rules of thumb, the corresponding wave height and period of such a maximum wave are 2 H_s and 0.9 T_p respectively. H_s is the significant wave height and T_p is the peak period which together characterize the irregular wave field.

Wave theories

The valid ranges for wave theories for stable waves are shown in Figure 2.2. The red lines and rectangle show the region of incoming waves which is investigated in this research. The waves in front of the quay can be described by Stokes of the 2nd or 3rd order as seen in the red rectangle in Figure 2.2. For the waves on top of the quay, none of the theories are applicable, as the waves will break due to the depth induced breaking criterion.

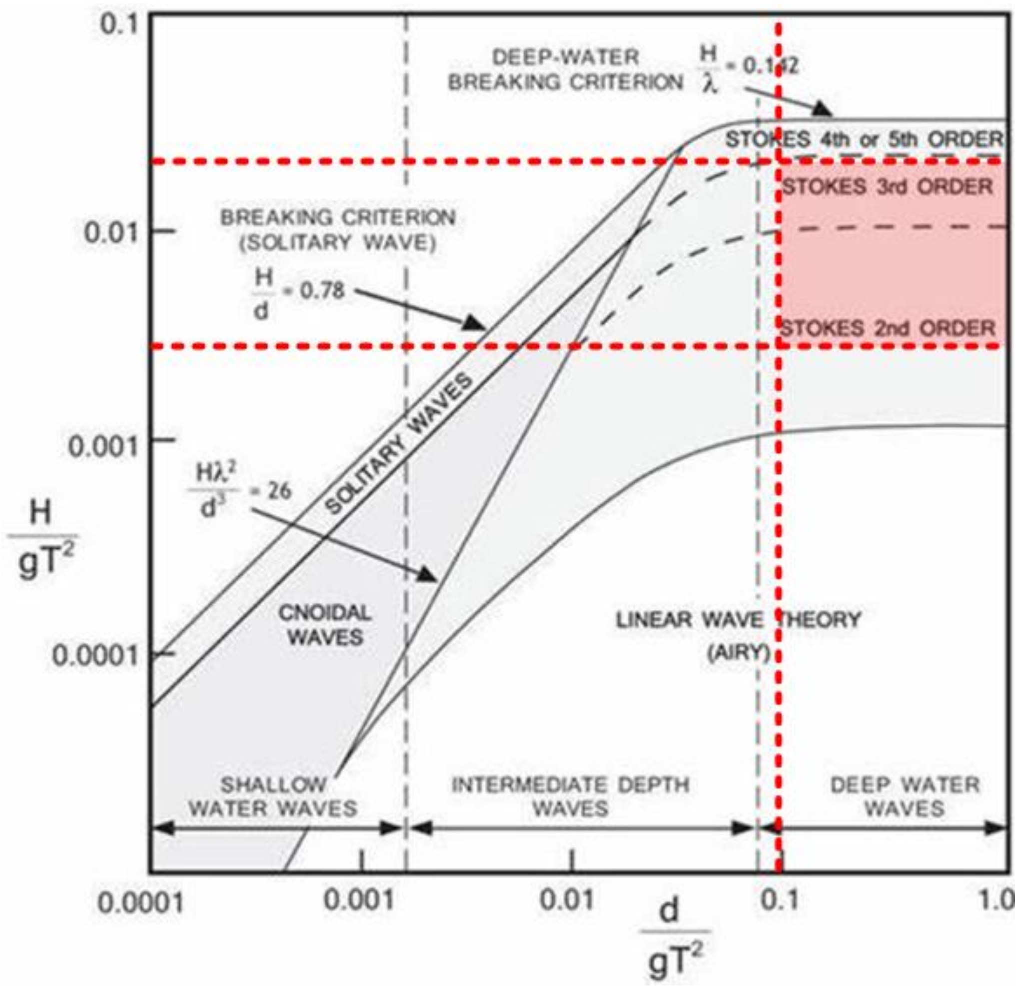

Figure 2.2: Valid ranges wave theories, red rectangle indicates ranges studied in this thesis

2.3 Wave force theories

In this paragraph, the wave force theories are discussed. Figure 2.2 showed that the approaching waves can be best described by Stokes 2nd or 3rd order. The wave force is however caused by the waves breaking on the quay which are no longer at the same depth as the approaching waves. To see which theory lies closest to this phenomenon multiple wave forcing theories are considered.

The paragraph starts with the linear wave theory. Next, the empirical wave force theories are considered. Last, the force based on the conservation of momentum is explained.

Linear wave theory

In case of a non-breaking wave, the force can be computed by integrating the pressure distribution over the storm wall height.

For a progressive wave the pressure by linear wave theory is given by Equation 2.1.

$$p_{wave} = \hat{p}_{wave} \sin(\omega t - kx) \quad \text{with} \quad \hat{p}_{wave} = \rho_w g a \frac{\cosh(k(d_w+z))}{\cosh(k(d_w))} \qquad \text{Equation 2.1}$$

With:

- p_{wave} [Pa] = Wave pressure
- $\hat{p}_{wave}$ [Pa] = Wave pressure amplitude
- ω [rad/s] = Angular wave frequency

- k [rad/m] = Wave number
- g [m/s²] = Gravitational acceleration = 9.81
- d_w [m] = Water depth (in front of quay)
- z [m] = Vertical coordinate

For a standing wave against a vertical structure, the wave height increases due to reflection. The pressure above the still water level is defined as a hydrostatic pressure, as shown in Equation 2.2. Below the still water level Equation 2.3 holds.

$$p_{wave} = (1+\chi)\rho_w g a\left(1-\frac{z}{(1+\chi)a}\right) \quad with\ z \geq SWL$$ Equation 2.2

$$p_{wave} = (1+\chi)\rho_w g a\frac{\cosh(k(d_w+z))}{\cosh(k(d_w))} \quad with\ z \leq SWL$$ Equation 2.3

With:
- χ [-] = Reflection coefficient

Applicability
The force following from the wave pressured caused by a linear wave is representative for a standing or quasi-standing wave. These types of waves are expected when the reflection coefficient is close to 1.

Goda and Takahashi
An empirical method often used is the method of Goda (1974) or Takahashi (2002). The method provides the values of the pressures as shown in Figure 2.3.

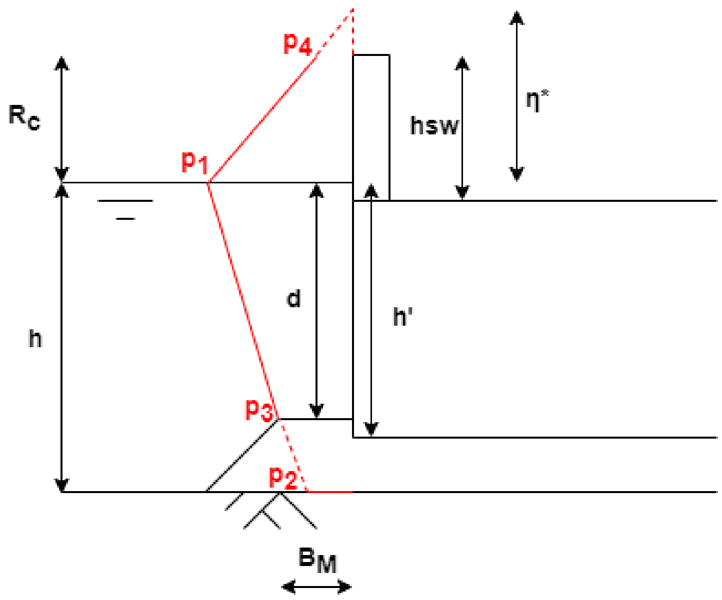

Figure 2.3: Pressures on a vertical wall according to Goda-Takahashi

The difference in the Goda and Takahashi method is the definition of the α_2 parameter. The definition using the Goda method, for non-impulsive conditions, is given by Equation 2.4. The definition using the Takahashi method, for impulsive conditions, is given by Equations 2.5 – 2.6.
Goda:

$$\alpha_2 = \min\left\{\frac{h-d}{3h}\left(\frac{H_{max}}{d}\right)^2, \frac{2d}{H_{max}}\right\}$$ in absence of a berm $\alpha_2 = 0$ Equation 2.4

Takahashi et al.:

$\alpha_2 = \max\{\alpha_{2,Goda}, \alpha_I\}$ Equation 2.5

$\alpha_I = \alpha_{IH}\alpha_{IB}$ Equation 2.6

With:

$$\alpha_{IH} = \min\{H/d, 2.0\}$$

$$\alpha_{IB} = \begin{cases} \cos\delta_2 / \cosh\delta_1 & \text{if } \delta_2 \le 0 \\ 1/(\cosh\delta_1 \cosh^{1/2}\delta_2) & \text{if } \delta_2 > 0 \end{cases}$$

$$\delta_1 = \begin{cases} 20\delta_{11} & \text{if } \delta_{11} \le 0 \\ 15\delta_{11} & \text{if } \delta_{11} > 0 \end{cases}$$

$$\delta_2 = \begin{cases} 4.9\delta_{22} & \text{if } \delta_{22} \le 0 \\ 3.0\delta_{22} & \text{if } \delta_{22} > 0 \end{cases}$$

$$\delta_{11} = 0.93\left(\frac{B_M}{L} - 0.12\right) + 0.36\left(0.4 - \frac{d}{h}\right)$$

$$\delta_{22} = -0.36\left(\frac{B_M}{L} - 0.12\right) + 0.93\left(0.4 - \frac{d}{h}\right)$$

The other formulas are given by Equations 2.7 – 2.13.

$\alpha_1 = 0.6 + \frac{1}{2}\left(\frac{2kh}{\sinh(2kh)}\right)^2$ Equation 2.7

$\alpha_3 = 1 - \frac{h'}{h}(1 - \frac{1}{\cosh(kh)})$ Equation 2.8

$p_1 = \frac{1}{2}(1 + cos\beta)(\lambda_1\alpha_1 + \lambda_2\alpha_2 cos^2\beta)\rho_w g H_{max}$ Equation 2.9

$p_2 = \frac{p_1}{\cosh(kh)}$ Equation 2.10

$p_3 = \alpha_3 p_1$ Equation 2.11

$p_4 = p_1\left(1 - \frac{R_c}{\eta^*}\right)$ Equation 2.12

$\eta^* = 0.75\lambda_1(1 + cos\beta)H_{max}$ Equation 2.13

With:

- $\beta = 15°$, but for larger values of the angle of incidence reduction can be applied.
- $\lambda_1 = \lambda_2 = 1$ for preliminary design

(Takahashi, 2002)

- h [m] = Water depth at a distance of 5 times H_s from the structure
- d [m] = Water depth in front of structure
- H_{max} [m] = Maximum wave height = 1.8 · H_s (in deep water)
- B_M [m] = Width of berm in front of structure
- L [m] = Local wavelength
- k [rad/m] = Wave number
- h' [m] = Depth of structure under water

- β [°] = Angle of incidence
- ρ_w [kg/m^3] = Density water
- g [m/s^2] = Gravitational acceleration
- R_c [m] = Freeboard
- η^* [m] = Elevation to which the wave pressure is exerted

Applicability
The Goda-Takahashi method is applicable for unimodal spectra in both deep and shallow water, but, for the latter, shoaling and breaking should be considered as well. It was found by Meinen et al. (2020) that Goda-Takahashi shows systematic over- or under estimations with breaking or impact wave loads up to 200%. Therefore, in case of a breaking wave force on a storm wall, deviations might be expected as well.

To be more specific, Goda-Takahashi is expected to perform well for $kd_w \lesssim 0.5$, to underestimate for $0.5 \lesssim kd_w \lesssim 2.5$ and to overestimate for $kd_w \gtrsim 2.5$ for the situation without berm (Tuin et al. 2022).

Empirical wave force: Den Heijer
Den Heijer (1998) preformed experiments in the "Scheldegoot" of WL Delft Hydraulics (nowadays known as Deltares). The quay was 0.66 m high, and the storm wall was located 2 m from the edge. The experiments delivered the formulas in Equations 2.14-2.16. These formulas give an estimation of the maximum force which could occur on the storm wall.

$$F_{max} = 15\rho_w g H_s^2 \quad \text{for } s_{op} < 0.0051 \qquad \text{Equation 2.14}$$

$$F_{max} = (16.5 - 294 s_{op})\rho_w g H_s^2 \quad \text{for } 0.0051 < s_{op} < 0.022 \qquad \text{Equation 2.15}$$

$$F_{max} = 10\rho_w g H_s^2 \quad \text{for } s_{op} > 0.022 \qquad \text{Equation 2.16}$$

With:

- F_{max} [N/m] = Maximum horizontal force on storm wall
- ρ_w [kg/m^3] = Density water
- g [m/s^2] = Gravitational acceleration
- H_s [m] = Significant wave height
- s_{op} [-] = Wave steepness in deep water

Applicability
Equations 2.16-2.18 are only usable in the range of $0.8 < d_{wq} / H_s < 2$, which is the range in which the experiments were performed. They only give a primary estimation as the force in these formulas is independent of several factors which should play a role like the height of the wall and the distance from the wall to the edge.

Conservation of momentum Tuin
The Tuin method gives a first rough estimation of the wave force caused by a wave breaking on the storm wall. To estimate the wave force, the water mass of the wave and its velocity are used to determine the momentum. Then using a short time step one can compute an impulsive force which impacts on the storm wall (Tuin, 2016).

The maximum horizontal velocity is determined using linear wave theory, given in Equation 2.17.

$$u_{x,max} = \omega a \frac{\cosh(k(S))}{\sinh(kd_w)} \qquad \text{Equation 2.17}$$

With:

- $u_{x,max}$ [m/s] = Maximum horizontal velocity
- ω [rad/s] = Angular frequency
- a [m] = Wave amplitude
- k [rad/m] = Wave number
- d_w [m] = Water depth in front of the quay
- S [m] = Elevation above bottom

The mass of water is approximated as the mass under a wave peak, i.e. the mass of water under half a wavelength. This is sketched in Figure 2.4.

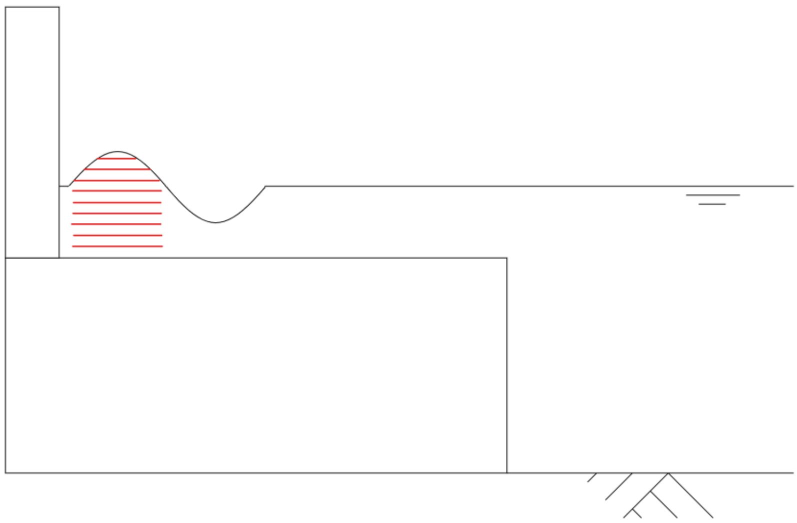

Figure 2.4: Used volume of water for force computation with the Tuin method

The wave is assumed to have a sine shape. The volume can then be computed by integrating over the sinus and adding the still water depth on top of the quay. This results in Equation 2.18.

$$V = \int_0^{\frac{L}{2}} a \sin\left(\frac{2\pi}{L} x\right) dx + \frac{L}{2} \cdot d_{w,quay} = a\left(\cos(0) - \cos\left(\frac{2\pi}{L} \cdot \frac{L}{2}\right)\right) + \frac{L}{2} \cdot d_{w,quay}$$

$$V = 2a + \frac{L}{2} \cdot d_{w,quay}$$ Equation 2.18

The total momentum is then given by Equation 2.19.

$$P = u_{x,max} \rho_w \frac{L}{2}\left(d_{w,quay} + a\right)$$ Equation 2.19

With:

- P [Ns] = Momentum
- ρ_w [kg/m^3] = Density of water
- L [m] = Wavelength

The force is then given by Equation 2.20.

$$F_{h,max} = \frac{P}{\Delta t}$$ Equation 2.20

With:

- $F_{h,max}$ [N] = Maximum horizontal force
- Δt [s] = Time step

Chen et al. (2019) found that the duration of such an impact usually lies between 0.08 and 0.18 s with the highest momenta occurring around impact durations around 0.1 s. Therefore, the duration of 0.1 s is assumed for this method.

Applicability
The conservation of momentum theory has yet to be proven accurate. It is not officially published and validated with experiments yet. However, a comparison between the formulas of Den Heijer and Tuin was made by Schalk (2023). Schalk made computations with both Tuin and Den Heijer for a retreated storm wall on top of a vertical quay with deep water waves. It was found that overall the method of Tuin generated results of similar magnitude as Den Heijer. But Den Heijer often predicted a higher force for small negative freeboards than Tuin, as Den Heijer does not take the freeboard into account at all.

Pressure-impulse theory
A mathematical model for an impact between an incompressible liquid and a solid surface has been presented by Cooker and Peregrine (1995). Their theory provides the peak pressure impulse given a fluid domain and a velocity just before impact. They showed that the pressure-impulse satisfies Laplace's equation. For a wave impact on a vertical, the use of the Laplace equation, the corresponding boundary conditions and a Fourier analysis gives the pressure impulse shown in Equation 2.21.

$$P_I(x,y) = \rho H_c \sum_{n=1}^{\infty} a_n \sin(\lambda_n y/H) \frac{\sinh[\lambda_n(b-x)/H]}{\cosh(\lambda_n b/H)} \qquad \text{Equation 2.21}$$

For -H ≤ y ≤ 0 and 0 ≤ x ≤ b and the constants a_n are:

$$a_n = 2U_0 \frac{\cos(\mu^* \lambda_n) - 1}{\lambda_n^2}$$

With:

- $P_I(x, y)$ [Pa·s] = Pressure impulse
- ρ [kg/m^3] = Density of fluid
- H_c [m] = Height of wave crest with respect to the bed
- b [m] = Width of the fluid
- λ_n [-] = (n – ½)π
- U_0 [m/s] = Velocity before impact
- μ^* [-] = Fraction of water height

The constants a_n represent the added mass that has to be slowed down in an impact.

The highest pressure impulse is obtained for b = ∞ and μ* = 1. To obtain the pressure the pressure impulse is divided by the duration of the impact as shown in Equation 2.22.

$$p = \frac{P_I}{\Delta t} \qquad \text{Equation 2.22}$$

To get the force the pressure is integrated over the water height. This includes the depth plus the wave amplitude.

The parameters which are not given are the duration of the impulse Δt and how to obtain the velocity before impact U_0. Therefore, multiple variations of this method are applied. An impulse duration of both 0.1 s and 0.05 s are used. In addition, the water velocity is computed in three different ways. First with the shallow water wave velocity, which is computed by taking the square root of gd_w. Second, using the linear wave theory as described in the conservation of momentum section before. Last, using the Stokes' 3rd order non-linear wave theory derived by Skjelbreia (1958). This yields six variations in total. The 3rd order horizontal velocity is given in Equation 2.23.

$$\frac{u}{c} = F_1 \cosh\left(\frac{2\pi S}{L}\right)\cos(\theta) + F_2 \cosh\left(\frac{4\pi S}{L}\right)\cos(2\theta) + F_3 \cosh\left(\frac{6\pi S}{L}\right)\cos(3\theta) \qquad \text{Equation 2.23}$$

With:

- F_1, F_2, F_3 [m] = constants given by:

$$F_1 = \frac{2\pi a}{L}\frac{1}{\sinh\left(\frac{2\pi d_w}{L}\right)}$$

$$F_2 = \frac{3}{4}\left(\frac{2\pi a}{L}\right)^2 \frac{1}{\left(\sinh\left(\frac{2\pi d_w}{L}\right)\right)^4}$$

$$F_3 = \frac{3}{64}\left(\frac{2\pi a}{L}\right)^3 \frac{11 - 2\cosh\left(\frac{4\pi d_w}{L}\right)}{\left(\sinh\left(\frac{2\pi d_w}{L}\right)\right)^7}$$

- θ [rad] = phase, given by:

$$\theta = \frac{2\pi}{L}(x - ct)$$

- c [m/s] = wave celerity, given by:

$$c^2 = \frac{gL}{2\pi}\tanh\left(\frac{2\pi d_w}{L}\right)\left(1 + \left(\frac{2\pi a}{L}\right)^2 \frac{\cosh\left(\frac{8\pi d_w}{L}\right) + 8}{8\left(\sinh\left(\frac{2\pi d_w}{L}\right)\right)^4}\right)$$

- a [m] = wave amplitude determined by:

$$H = 2a + 2\left(\frac{\pi}{L}\right)^2 a^3 \frac{3}{16}\frac{8\left(\cosh\left(\frac{2\pi d_w}{L}\right)\right)^6 + 1}{\left(\sinh\left(\frac{2\pi d_w}{L}\right)\right)^6}$$

The maximum velocity is found for the crest, i.e. $S = d_w + a$.

If not the whole wave breaks on the wall, the fraction of the wave which does, μ^*, is a variable as well. However, for this research, it is assumed that the whole wave breaks on the wall, as this gives the highest force.

Applicability
The pressure-impulse theory is derived for an idealized wave on a vertical wall. Made assumptions are that viscosity and surface tension are negligible and that the fluid is incompressible. The outcome is mostly influenced by the choices for Δt and U_0. The applicability therefore also depends on the assumptions where those choices are based on.

The force obtained is for a breaking wave. If breaking waves do not occur, this method might give an overestimation.

2.4 Recommended use of different fluid-structure interaction modelling tools

Depending on available resources and needed accuracy, one can choose from different modelling tools. The modelling tools considered in this paragraph are SWASH, DualSPHysics and OpenFOAM.

The most simplified model with the lowest requirement in computational resources is SWASH (Simulating WAves till SHore). This is a non-hydrostatic wave-flow model. The model has a horizontal grid whereas the vertical axis is divided in so called layers. More layers result in more accurate results, but at a certain number of layers the accuracy barely improves. The key is therefore to find the optimal number of layers to optimize accuracy and computation time. The model is based on nonlinear shallow water equations with non-hydrostatic pressure. The model does phase solving and uses the finite differences method. The results of the computations are the surface elevation, velocity and pressures over space and time.

A bit more complicated model is DualSPHysics. DualSPHysics makes use of Smoothed Particle Hydrodynamics (SPH), which is a Lagrangian method where everything consists of particles and no mesh. For the simulation of a fluid the Navier-Stokes equations are integrated locally at each of these particles using physical properties of surrounding points.

The most complex and computationally expensive model is OpenFOAM. OpenFOAM is a Computational Fluid Dynamics (CFD) tool. It uses the Navier-Stokes equation for the description of the fluid movement and the Volume of Fluid (VOF) method to track the free surface between air and water.

The main difference between SWASH and DualSPHysics / OpenFOAM is that SWASH only has one water surface layer per horizontal location. Therefore, overturning wave cannot be simulated. OpenFOAM on the other hand resolves the surface for any breaking wave shape, using many calculations. Therefore, OpenFOAM is more computationally expensive than SWASH. DualSPHysics is also more computationally expensive as it computes parameters like position and velocity for every particle in the domain. It is however still less computationally expensive than OpenFOAM.

A comparison between SWASH, DualSPHysics and OpenFOAM was done for different applications by Gruwez et al. (2020). For the application of wave impact on a vertical wall the relevant results are shown in Table 2.1. In the conclusion SWASH was recommended for the total horizontal force, if the impulse on the wall is of less importance, since it has less computational costs than OpenFOAM, while it provides relatively accurate results. But it is mentioned that SWASH is limited to hydrostatic pressure profiles regarding the impact on the wall, which might be too much of a simplification for dynamic impact events. Based on this report it seems reasonable to do the model tests for most configurations in SWASH or DualSPHysics and do a validation check using a model in the laboratory.

Table 2.1: Performance numerical models (Gruwez et al., 2020)

Performance	SWASH	DualSPHysics	OpenFOAM
Pressure	Reasonable/fair	Reasonable/fair	Good
Total horizontal force	Good	Good	Very Good
Computational time with respect to SWASH	1	18	217

Additional results regarding SWASH modelling of a horizontal wave force are provided by Van Maris (2018). The modelling was done in intermediate to deep water and SWASH appeared inaccurate for high frequencies (> 0.3 Hz) and steep irregular waves when comparing to experimental data. SWASH also underestimated the force. However, it was concluded that SWASH still was suitable for modelling to compare between different bimodal wave fields.

Chapter 3 Research methodology

In this research both physical and computational modelling is applied. The physical model is a qualitative scale model to determine which type of waves occur under certain hydraulic conditions. The results of this laboratory experiment are then used to validate the results of the computational model. This chapter describes the methodology behind the models. First, the physical model set-up is explained. Next, the theory behind the computational models, SWASH and DualSPHysics, is discussed. After that, the case study and configurations which are going to be computationally modelled are introduced. This section is followed by the model set-up. Lastly, adapted methods are introduced to compute the wave forcing on the storm wall. These methods are based on the literature from Chapter 2.

3.1 Laboratory experiment

The experiment is a qualitative scale model in a wave flume to determine which type of waves occur under certain hydraulic conditions. Here, the storm wall on top of a quay is represented by a box made of wooden panels. The set-up is supported by putting lead beams inside the structure, see Figure 3.1. The behaviour of the water is filmed so it can be analysed afterwards. Knowing the dimensions of the structure, the pixel size is determined. This then is used to determine the water depth, wavelength, and incoming wave height. What is observed is the type of wave occurring (quasi-static, slightly breaking, breaking or broken) under different values for L_{quay} / L, H / L and d_{wq} / L.

One interesting situation to investigate is when the length of the quay is 0.4 times the local peak wavelength as in this scenario broken waves instead of breaking waves are expected for vertical breakwaters (Kortenhaus & Oumeraci, 1998). Testing at around smaller and larger distances will show if for the deep water retreated storm wall scenario braking waves occur around the same point. The altering of L_{quay} / L can be done either by making the board demountable at multiple locations or by changing the wavelength of the waves. The latter is chosen as this is more practical.

The final set-up and configurations are shown in Figure 3.1 and Table 3.1 respectively. The choice for the dimensions is given in Appendix A: Experiment dimensions explanation. The structure will be made 0.235 m wide, based on the wave flume dimensions.

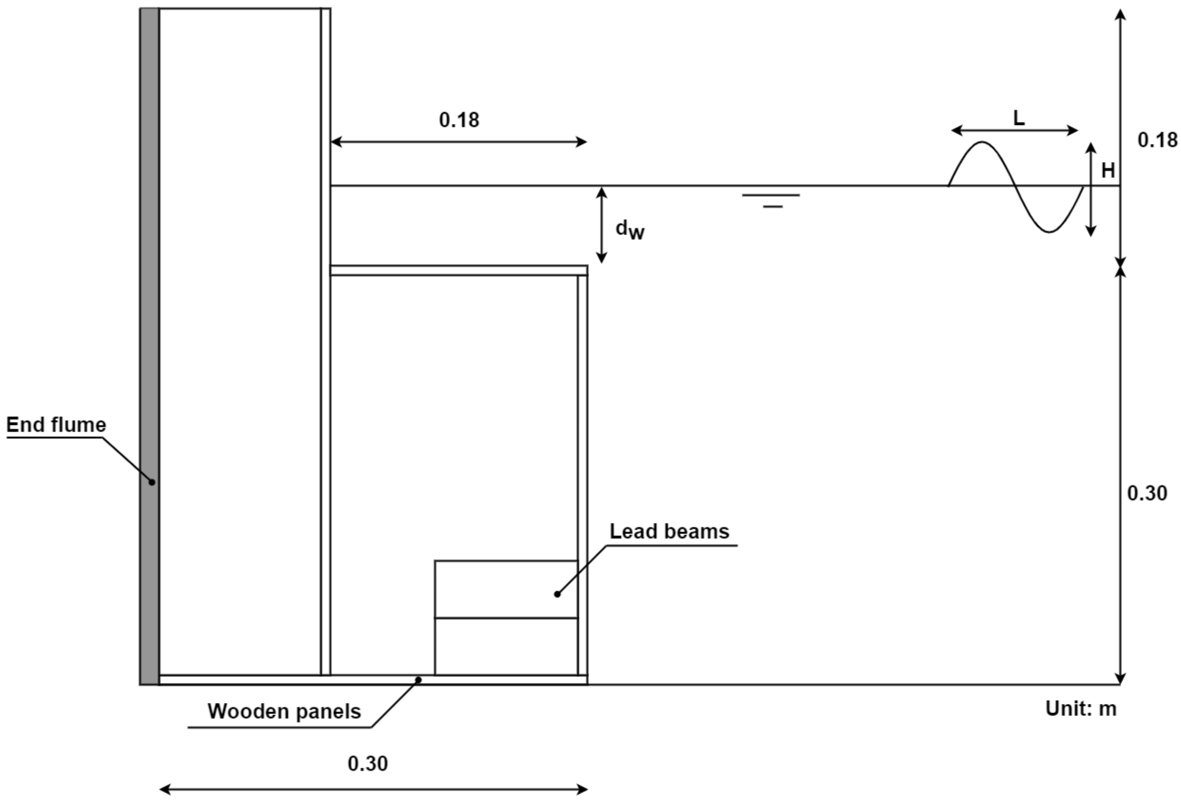

Figure 3.1: Experimental set-up

Table 3.1: Experiment configurations

Experiment number	H [cm]	T [s]	d_w [cm]	d_{wq} [cm]	L_{quay} / L	H / L	d_{wq} / L
1	4.6	0.51	30.0	0.0	0.44	0.1133	0.0000
2	5.2	0.55	30.0	0.0	0.38	0.1101	0.0000
3	6.8	0.61	29.9	-0.1	0.31	0.1170	-0.0017
4	4.2	0.51	33.1	3.1	0.44	0.1034	0.0763
5	4.5	0.51	33.3	3.3	0.44	0.1108	0.0813
6	4.9	0.56	33.4	3.4	0.37	0.1001	0.0694
7	6.3	0.56	33.4	3.4	0.37	0.1287	0.0715
8	4.3	0.51	33.7	3.7	0.44	0.1059	0.0911
9	4.8	0.55	34.2	4.2	0.38	0.1016	0.0889
10	5.3	0.55	34.4	4.4	0.38	0.1122	0.0932
11	5.2	0.61	34.7	4.7	0.31	0.0895	0.0809
12	6.9	0.62	35.0	5.0	0.30	0.1150	0.0833
13	4.7	0.56	34.5	4.5	0.37	0.0960	0.0919
14	3.5	0.51	34.9	4.9	0.44	0.0862	0.1207
15	3.5	0.61	35.0	5.0	0.31	0.0602	0.0861
16	4.9	0.55	35.3	5.3	0.38	0.1037	0.1122
17	6.8	0.62	35.7	5.7	0.30	0.1133	0.0950
18	6.9	0.61	37.2	7.2	0.31	0.1188	0.1239

3.2 Modelling methodology

For the computational modelling both SWASH and DualSPHysics are used. The reason is that these models still providing reasonable to good results with limited computation time (Gruwez et al., 2020). However, SWASH appeared unsuitable for this type of geometry and therefore the research continued with DualSPHysics.

SWASH

SWASH is a non-hydrostatic wave-flow model which is characterized by the use of layers over the vertical axis. The first model was made in SWASH, using the model of Van Maris as basis (2018). Unfortunately, this model appeared unsuitable. The recommended way to model a vertical structure is using layers with a low porosity (> 0.1). However, using porosity layers with low porosity, e.g. 0.09 showed limitations. Even though the structure height was given as input, the program takes the porosity layer over the whole vertical axis. The structure height was varied from -8 m to 14.25 m with respect to the bottom, with multiple steps in between, but the result stayed the same. The porosity layer creates a standing wave pattern in front of the quay, but on the quay a small water layer remains showing no variation in level, as seen in Figure 3.2. Other ways to model the geometry were tried as well, but they all led to unrealistic results. For an extended description of the model set-up and results, see Appendix B: SWASH.

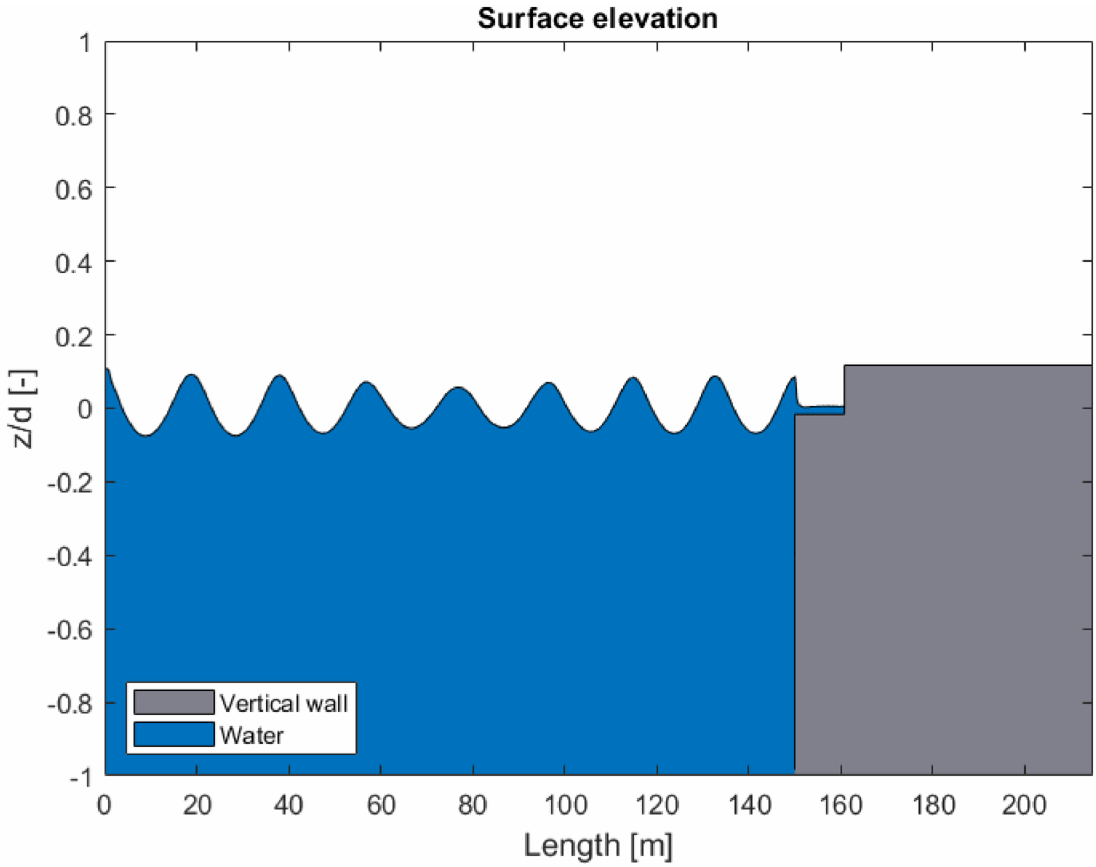

Figure 3.2: SWASH output: standing waves in front of the quay with a still water level on the quay, made with Van Maris' MATLAB code

DualSPHysics

Due to the difficulties with SWASH, the switch to DualSPHysics is made. DualSPHysics makes use of Smoothed Particle Hydrodynamics (SPH), which is a Lagrangian method where everything consists of particles and no mesh. For the simulation of a fluid the Navier-Stokes equations are integrated locally at each of these particles using physical properties of surrounding points (Domínguez Alonso et al., 2023). The Navier-Stokes equations consist of the continuity equation, given by Equation 3.1 and the conservation of momentum, given by Equations 3.2-3.3. The given equations are for a 2D flow.

$$\frac{\partial u_x}{\partial x} + \frac{\partial u_z}{\partial z} = 0 \qquad \text{Equation 3.1}$$

$$\frac{\partial u_x}{\partial t} + \frac{u_x \partial u_x}{\partial x} + \frac{u_z \partial u_x}{\partial z} = -\frac{1}{\rho}\frac{\partial p}{\partial x} + \nu\left(\frac{\partial^2 u_x}{\partial x^2} + \frac{\partial^2 u_z}{\partial z^2}\right) \qquad \text{Equation 3.2}$$

$$\frac{\partial u_z}{\partial t} + \frac{u_x \partial u_z}{\partial x} + \frac{u_z \partial u_z}{\partial z} = -\frac{1}{\rho}\frac{\partial p}{\partial z} + \nu\left(\frac{\partial^2 u_z}{\partial x^2} + \frac{\partial^2 u_x}{\partial z^2}\right) \qquad \text{Equation 3.3}$$

With:

- u_x [m/s] = Horizontal flow velocity
- u_z [m/s] = Vertical flow velocity
- ρ [kg/m^3] = Density
- v [m^2/s] = Kinematic viscosity
- x [m] = Horizontal coordinate
- z [m] = Vertical coordinate
- t [s] = Time

The neighboring particles are determined with a certain distance, called smoothing length, here denoted as h_{sl}. The smoothing length is computed using Equation 3.4.

$$h_{sl} = C_h\sqrt{dim \cdot dp^2} \qquad \text{Equation 3.4}$$

With:

- h_{sl} [m] = Smoothing length
- C_h [-] = Smoothing coefficient, 1.2 for wave propagation (DualSPHysics team, 2022)
- dim [-] = The dimension
- dp [m] = Particle distance

At every time step the new properties of each particle are computed. The particles move according to these new values.

DualSPHysics has the option to work with multiple phases, i.e. fluid and air particles. This does however increase the computational requirements like storage and simulation duration. Sato et al. (2021) found that the pressure in a violent flow field can be accurately simulated using a single-phase model as long as the density diffusion parameter is not too large. At a value of 1, pressures are underestimated. For this thesis, since computational resources are limited, a single phase model is used. The general recommended value for the density diffusion parameter of 0.1 by the DualSPHysics team is used to prevent pressure underestimation.

3.3 Introduction case study: Kop van Zuid

The case study is used to define the typical parameter range of interest, for which the wave loads on retreated walls needs to be quantified. A summary of the values of the variables at Kop van Zuid is shown in Table 3.2 and Figure 3.3. Table 3.3 shows as addition the values of the dimensionless parameters which were also used to compare the state-of-the-art in Table 1.1. The determination of these variables can be found in Appendix C: Kop van Zuid. Here the case study is simplified to Figure 3.3. Small derivations like a small bed or quay slope are disregarded.

Table 3.2: Parameter values

Parameter	Description	Unit	Kop van Zuid
d_w	Water depth	m	14.86 (averaged)
d_{wq}	Water depth on top of quay	m	0.61
d_{wq} - d_w	Height quay	m	14.25 (averaged)
L_{quay}	Length quay, i.e. distance storm wall from the edge of the quay	m	Variable
h_{sw}	Height storm wall	m	~2.28 m
Irregular waves			
H_s	Incoming significant wave height	m	1.40
T_p	Peak wave period	s	4.35
L_{op}	Peak wavelength	m	29.5
k	Wavenumber	m^{-1}	0.21
S(f)	Spectral distribution	-	JONSWAP
Regular waves			
H	Regular wave height	m	2.80
T	Regular wave period	s	3.92
L	Regular wavelength	m	24.0
k	Wavenumber	m^{-1}	0.26

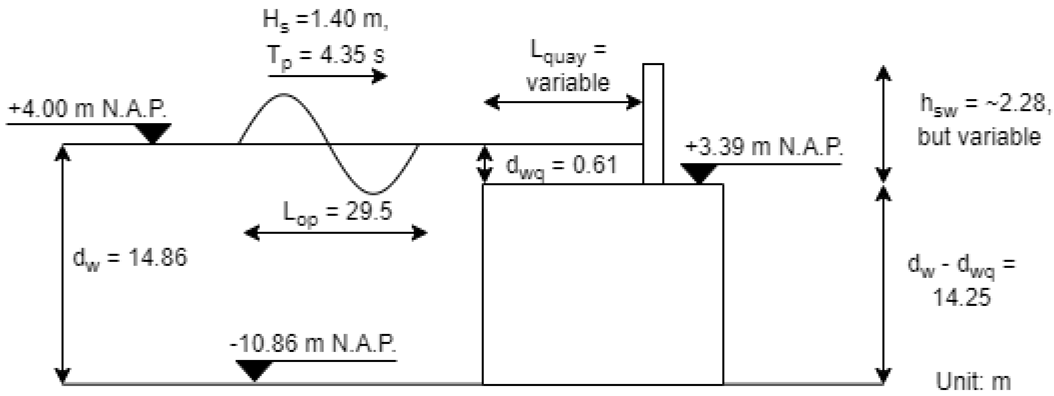

Figure 3.3: Kop van Zuid parameter values

Table 3.3: Dimensionless parameters

Parameter	Value
Irregular waves	
L_{quay} / L_{op}	Variable
h_{sw} / L_{op}	~0.066
d_{wq} / L_{op}	0.02
H_s / L_{op}	0.047
kd_w	3.12
Regular waves	
L_{quay} / L	Variable
h_{sw} / L	~0.081
d_{wq} / L	0.025
H / L	0.117
kd_w	3.86

3.4 Configurations models

The main configuration is the Kop van Zuid case. The variations in Table 3.4 and 3.5 lead to new configurations based on the main case. The parameters varied are the dimensionless parameters. Using dimensionless parameters provides the possibility to run less simulations in total, as there is one parameter less present.

The configurations consist of all the possible combinations of the variations in Table 3.4 and 3.5. These are then numbered 0 to 47 for irregular and 0 to 95 for regular waves. The values of the dimensionless parameters corresponding to the configuration numbers can be found in Appendix D: Configurations and results DualSPHysics. Irregular waves have less configurations as only the negative freeboards are considered. The reason for this is that during the simulations for the regular waves it is noticed that a zero or negative freeboard often leads to numerical instability. See Section 3.6 for a more elaborate description of numerical instabilities.

Table 3.4: Variations irregular waves

Variable parameter	Variations
L_{quay} / L_{op}	0 – 0.45 in steps of 0.15
h_{sw} / L_{op}	+/- 5%
d_{wq} / L_{op}	0.02 to +0.04 in steps of 0.02
H_s / L_{op}	2.0% and 4.7%

Table 3.5: Variations regular waves

Variable parameter	Variations
L_{quay} / L	0 – 0.45 in steps of 0.15
h_{sw} / L	+/- 5%
d_{wq} / L	-0.02 to +0.04 in steps of 0.02
H / L	5.0% and 11.7%

3.5 Model set-up

To run a DualSPHysics simulation, multiple input parameters need to be provided. This is done with a xml file. The most relevant input parameters are described in this chapter. An example of a xml file with all the parameters is shown in Appendix E: xml file example.
This chapter starts with a description of the relevant parameters. To obtain suitable values, there is looked at papers and a validation and calibration are done. The validation is done by comparing

DualSPHysics output to the laboratory experiments of Den Heijer. By tuning relevant parameters the error made by the computational model is made smaller. At the calibration model parameters are optimized to reduce computational requirements. This is done using a variance check.

3.5.1 Parameter overview

In this section an overview of the most relevant model parameters is given. The section starts with the parameters whose values are obtained using literature or follow from the Kop van Zuid schematization. These involve boundary conditions and wave absorption. Next, the parameters whose values are obtained with the validation or calibration are described. The validation and calibration are discussed in the following two sections.

Geometrical boundary conditions

The geometrical boundary conditions are based on the schematization of the kop van Zuid case study. The bed assumed flat and is therefore modelled as a flat boundary. The structure is not modeled as a boundary, like the bathymetry, but as a solid. This enables to model the fluid-structure interaction between the water and the quay with retreated storm wall.

Initial and boundary conditions

Initial conditions

As initial conditions the surface elevation and velocity are put to zero. The simulations will then be made long enough to get a steady-state solution.

Wave characteristics

For the regular waves the wave height H and wave period T are given as input. For irregular waves a unimodal Jonswap spectrum is given as input. Since the location is inside a harbor, the wind waves will play the more dominant part. Therefore, a unimodal instead of a bimodal spectrum is chosen.

Modified dynamic boundary condition (mBDC)

Because DualSPHysics works with particles both the structure and fluid are defined as particles. This condition is called the dynamic boundary condition. The contact between structure and fluid is defined as an increase in density when the particles are within 1.5 the smoothing length (h_{sl}) of the solid's boundary. This causes a repulsive force due to the pressure increase, pushing particles away from the boundary. Such a gap can disrupt the results as described by Been (2020).

A solution for this is the modified dynamic boundary condition (mDBC) from English at al. (2021). This method obtains the density of solid particles by linear interpolation from ghost points within the fluid domain. This reduces the unphysical gap. Therefore, the mDBC is used in this thesis.

Active wave absorption

The use of active wave absorption prevents that the reflected waves at the structure do not re-reflect at the wave piston. This is done by correcting the movement of the wave piston in real time. Through the velocity correction of the piston, the position in real time can be obtained. The needed absorption of the reflected free surface level is estimated by subtracting the measured free surface level in front of the piston of the target free surface level (the incoming). The measurement is done at 4 h_{sl} from the wavemaker as suggested by Altomare et al. (2017) to prevent using neighbouring particles of the piston boundary to measure.

Particle distance

Instead of a grid size, like in SWASH, DualSPHysics requires a particle distance (dp). The particles are not given a size. They are material points with attributes, like location, velocity, density, etc. Figure 3.4 shows an impression of the particles.

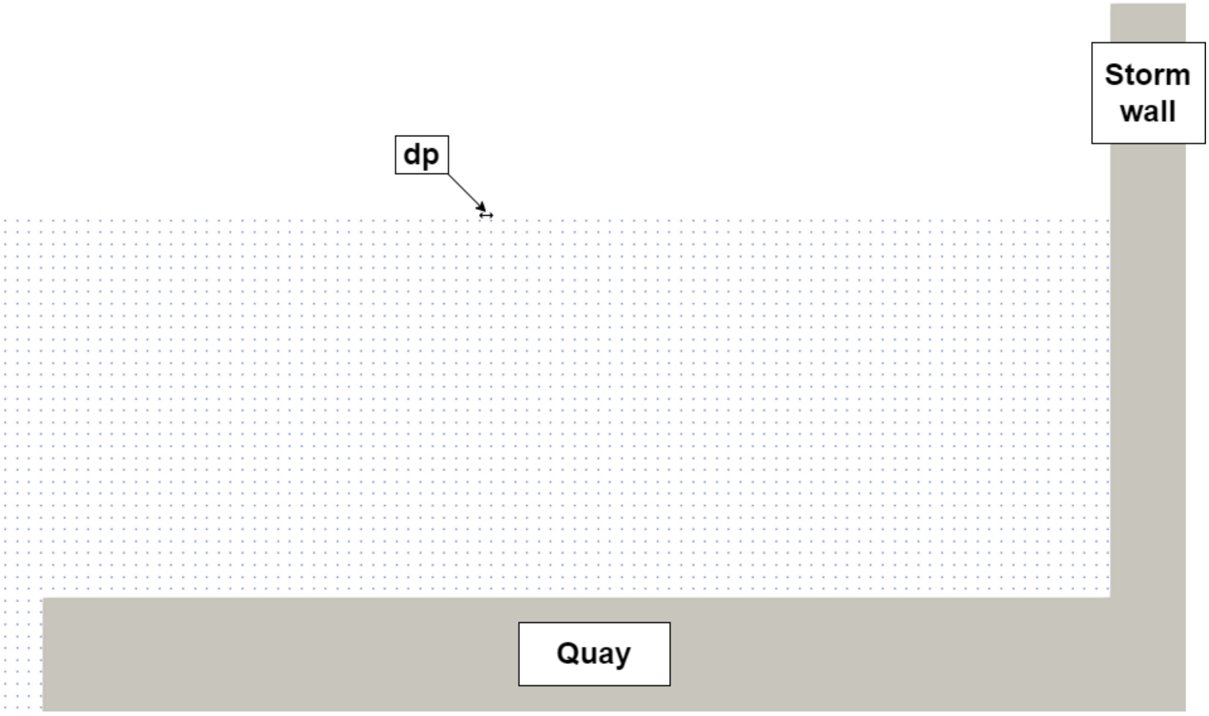

Figure 3.4: Particles at start simulation

Simulation duration
The simulation should be long enough to deliver sufficient results. A total simulation time consists of the spin-up time (15%) and the cycle time (85%). The recommended range for the cycle time is 100 to 300 waves (SWASH, 2024). The number of waves needed for irregular waves is larger than for regular waves. In an irregular wave simulation, you want sufficient high waves as these give the highest force, which is what is investigated in this research.

Pressure output
For the pressure output the measurement interval and the distance of measurement from the storm wall needs to be determined. The pressure interval determines how many pressure sensors are used over the water depth. More sensors provide a more detailed pressure profile, but also require higher storage. The pressures obtained are not exactly measured at the location of the storm wall, as the gap between the fluid particles and storm wall boundary can result in inaccurate or no results.

Basin length
A basin length is needed, as the generation of waves cannot be done close to the structure. If done anyways, this causes immediate reflection which makes it difficult to distinguish between incoming and outcoming waves.

3.5.2 Validation
To validate the DualSPHysics model and select appropriate parameters, the experiments of Den Heijer (1998) are modelled in DualSPHysics. Den Heijer performed scale experiments with a retreated storm wall on top of a vertical quay. He measured the water elevation at different locations and the pressure on the storm wall. The obtained results from the DualSPHysics model are compared with the results obtained from the laboratory experiments of Den Heijer. First, the model is validated for regular waves. After that, the model is validated for the irregular waves used in Den Heijer's experiment. The full validation can be found in Appendix F: Validation DualSPHysics.

The validation with regular waves showed that the model is very well able to model incoming waves, wave reflection and wave pressure.

The validation with irregular waves provided the optimal values for the particle distance, the simulation duration for irregular waves and the output parameters. With these optimal values the model performs well for $F_{1\%}$ and $F_{10\%}$ without requiring too much computational resources. However for F_{max} the model performed poorly. The poor prediction for F_{max} is likely due to the randomness of irregular waves and that one experiment therefore might measure a different maximum force than the other.

Particle distance
The optimal value found for smallest dimension (i.e. water depth on the quay) over the particle distance is 4. For the smallest water depth this leads to dp = 0.12 m. This equals 5 particles over the smallest water depth. For the other, larger, water depth this is 10 particles.

A balance of computation time and accuracy is found for 10 particles per wave height (H / dp = 10) by both Altomare et al. (2017) and Rota-Rosselli et al. (2018). This would indicate that for the lower water depth the accuracy might be too low. However, halving the particle distance would have more computational requirements than available. Therefore, there is continued with the values determined here.

Simulation duration (irregular waves)
An optimal ratio of duration / wave period of 556 is found in the validation. Translating to the Kop van Zuid results in a duration of 40 minutes. A duration of 40 min is however not possible due to storage limitation as explained before. A duration of 10 min appears maximum. The solution used is to do multiple simulations with different seeds to get more waves. Due to time limitations it is however only possible to get a total duration of 30 minutes.

Pressure output
For the output, the pressures on the storm wall are obtained over the storm wall height at interval heights of 1.5 dp. A smaller interval will result in similar pressures. The smaller interval is not used, as it requires additional computational resources while not providing a different (more accurate) solution. The pressured obtained are not exactly at the location of the storm wall, as the gap between the fluid particles and storm wall boundary can result in inaccurate or no results. Therefore, the measurement is done 1.5 dp from the storm wall. A larger distance from the wall gives a similar pattern, only with lower amplitude. The force is then obtained by integrating over the storm wall height using the trapezoidal rule. The trapezoidal rule is given by Equation 3.5.

$$\int_a^b f(x)dx \approx (b-a)\cdot\frac{1}{2}\big(f(a)+f(b)\big) \qquad \text{Equation 3.5}$$

With:
- x = the spatial coordinate
- f(x) = a function of the spatial coordinate
- a = lower bound of x
- b = upper bound of x

For the force on the storm wall the trapezoidal rule over the intervals results in Equation 3.6.

$$F_h = \sum_{n=0}^{N_s} \Delta z \cdot \frac{1}{2} \cdot \big(p(z = n\cdot dp) + p(z = (n+1)\cdot dp)\big) \qquad \text{Equation 3.6}$$

With:

- F_h [kN] = the horizontal force acting on the storm wall
- N_s [-] = total number of sensors along the storm wall = h_{sw} / dp + 1
- Δz [m] = vertical step size
- p [kPa] = pressure
- z [m] = vertical coordinate
- dp [m] = particle distance

3.5.3 Calibration

In the calibration the basin length, simulation duration for regular waves and water depth are determined. The calibration is done by varying one parameter at a time and observe at which value the water level variance of the stable time series stayed approximately the same. The full calibration can be found in Appendix G: Calibration DualSPHysics parameters. This resulted in a basin length of 5 wavelengths and a duration of 100 wave periods. In this thesis deep water waves are considered. To limit the needed computational time and storage, it is checked if the depth could be reduced while still maintaining similar results. This appeared not to be the case. The water depth in front of the quay will therefore remain the original quay height plus the water depth on the quay.

3.6 Model post-processing: removing outliers

The forcing obtained by DualSPHysics sometimes shows a large peak which is way larger than other peaks. An example of such a high peak is shown in Figure 3.5. Figure 3.6 on the other hand shows a simulation without such a high peak. These figures are generated by configuration 36 and 84 respectively. The only difference between these configurations is the relative quay length, as shown in Figure 3.7.

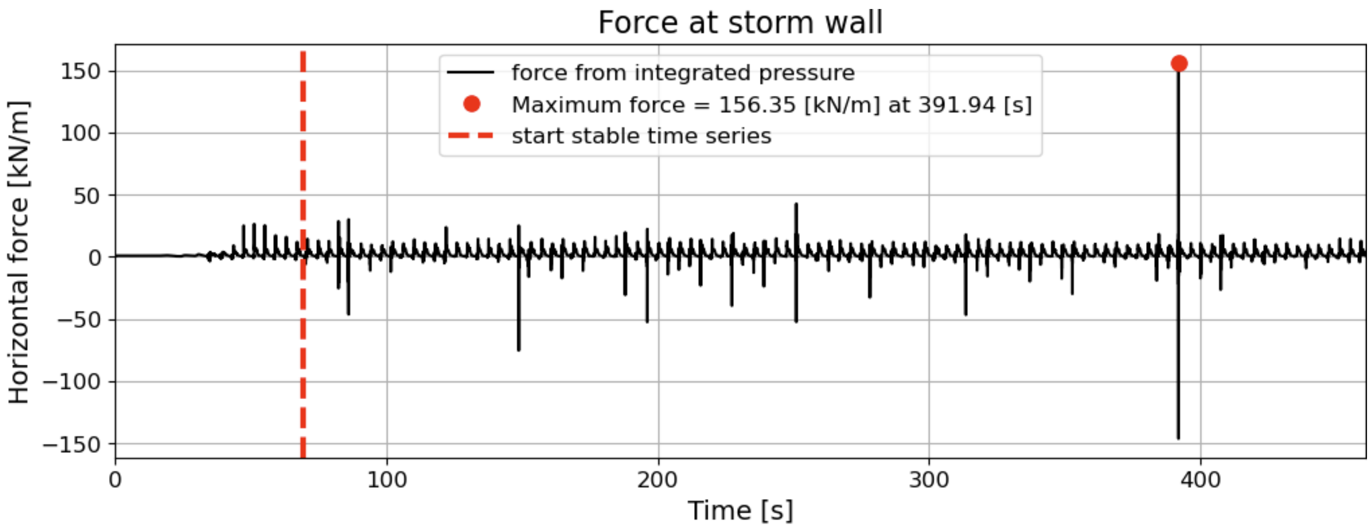

Figure 3.5: Force on storm wall over time (configuration 36, H/L = 0.05, d_{wq}/L = 0.02, L_{quay}/L = 0.15, h_{sw}/L = 0.095)

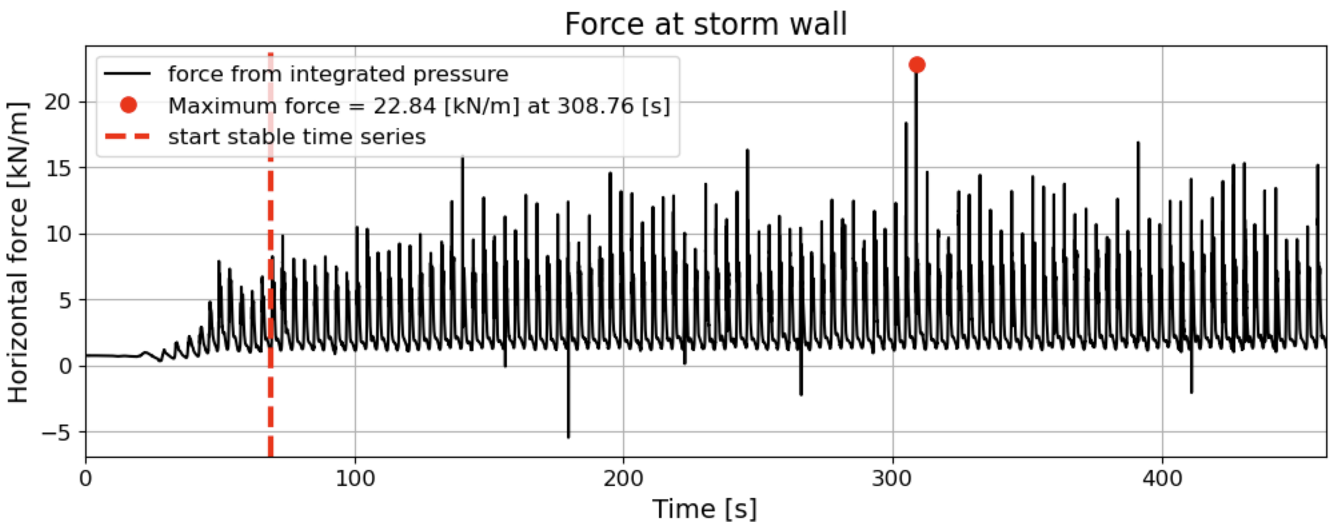

Figure 3.6: Force on storm wall over time (configuration 84, H/L = 0.05, d_{wq}/L = 0.02, L_{quay}/L = 0.45, h_{sw}/L = 0.095)

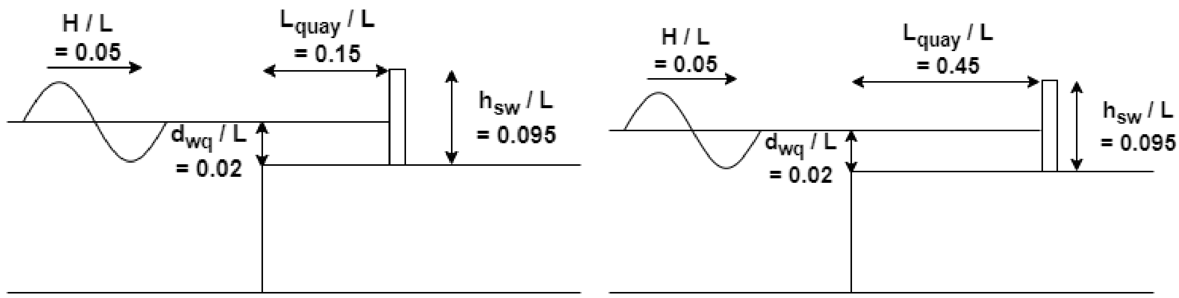

Figure 3.7: Configuration 36 (left) and configuration 84 (right)

Figure 3.8 and 3.9 show a zoom in of configuration 36, the high peak, and configuration 84, the normal peak, respectively. In Figure 3.8 the peak is very steep, only consisting of one point in time, while in Figure 3.9 the peak is wider and consists of multiple points. Making animations for the high peak in configuration 36 shows that this is caused by a numerical instability as suddenly turning particles are visible, as shown in

Figure 3.10. Due to the flowing back of water from the previous wave, only one particle depth remains in front of the bore illustrated in the figure.

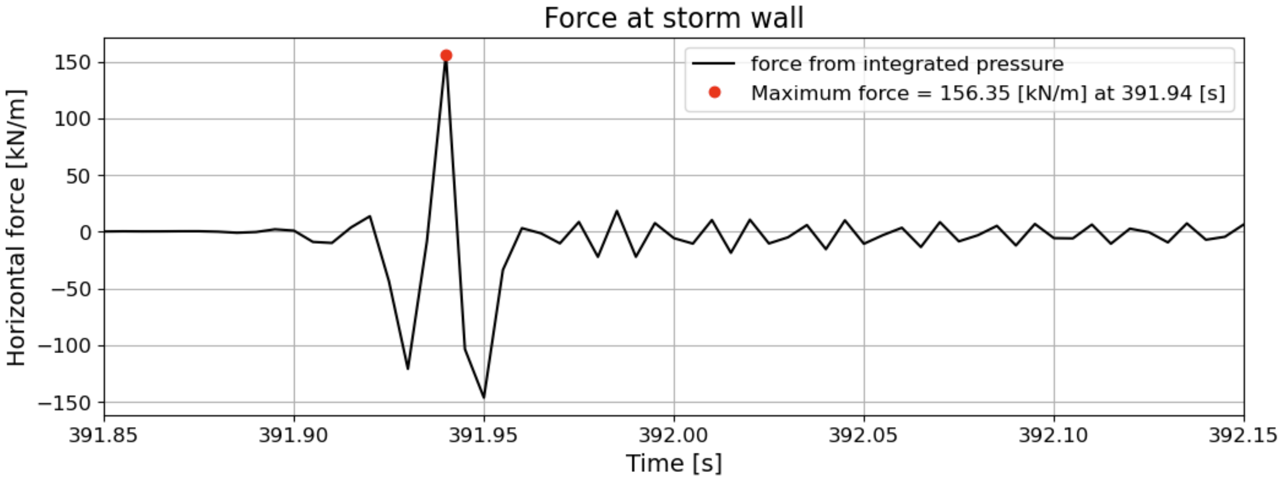

Figure 3.8: Zoom in of peak in configuration 36

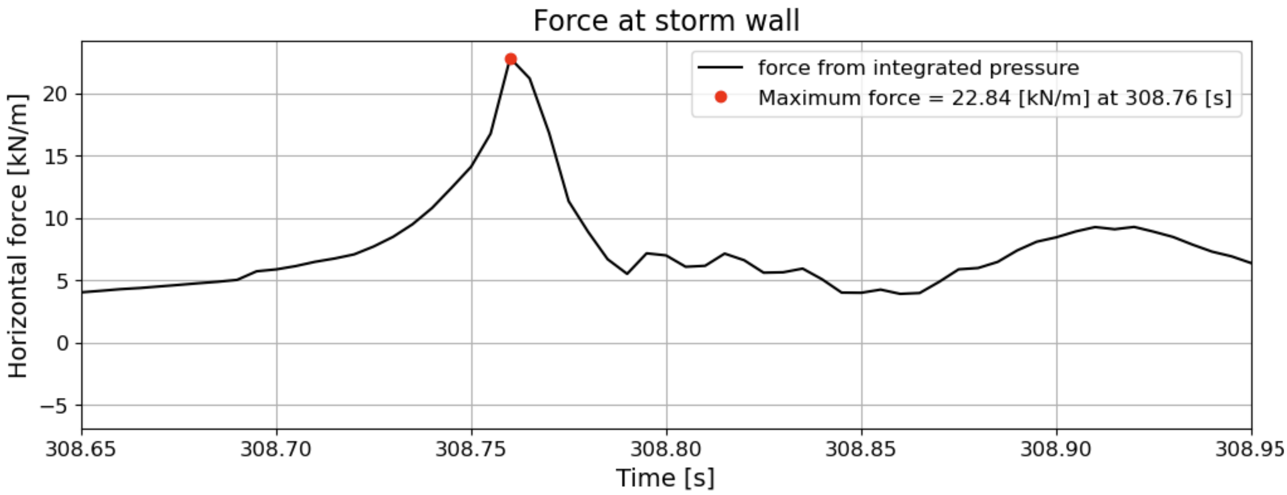

Figure 3.9: Zoom in of peak in configuration 84

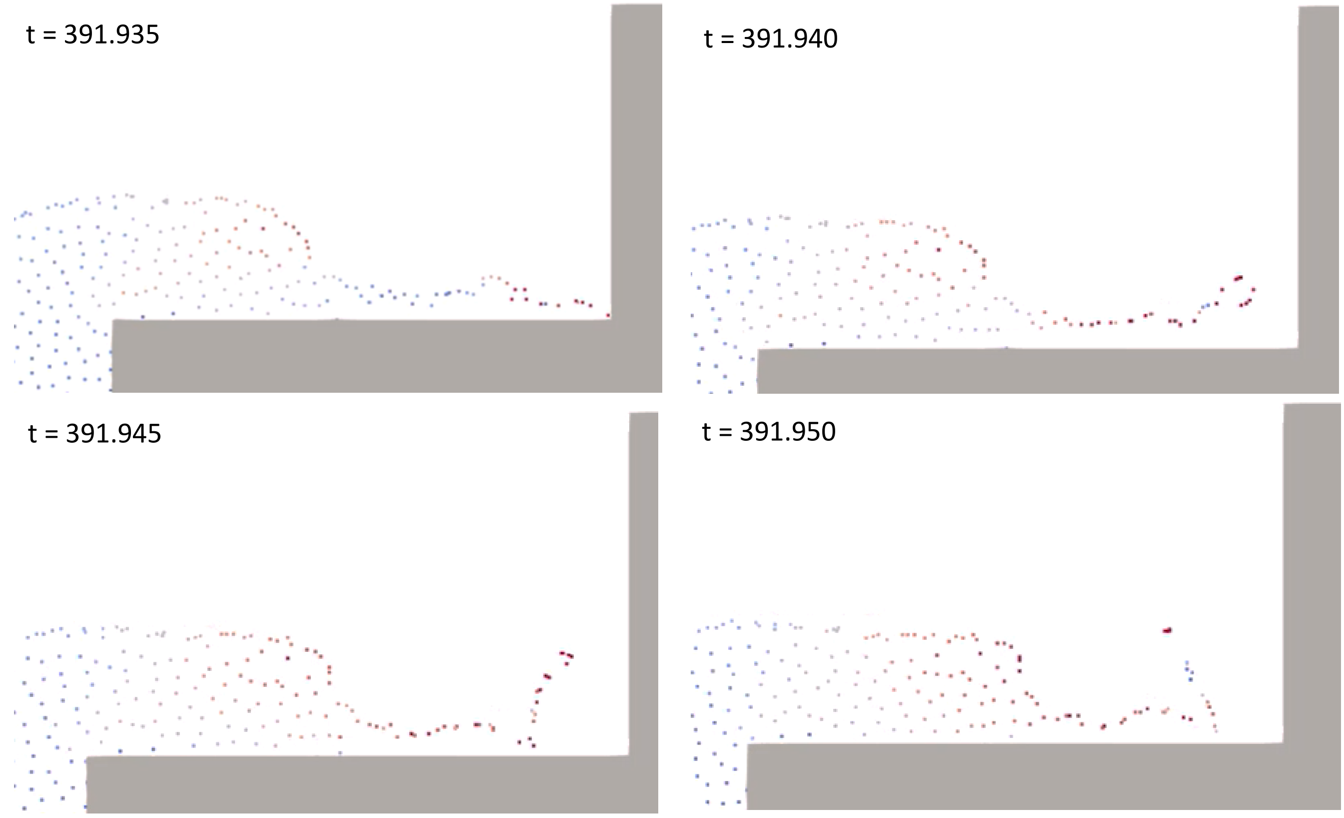

Figure 3.10: Numerical instability, turning particles (configuration 36)

For regular waves, peaks, caused by wave impacts, are expected, but peaks of similar height, not one or two way higher peaks in a long simulation. For irregular waves more variation in peak heights is expected, but they should still follow a distribution like pattern. For the two wave types two different methods are used to remove outliers and obtain more realistic results.

Regular waves
For regular waves peaks of similar heights are expected. Therefore very high peaks are removed using the z-score also known as standard score. The z-score is given by Equation 3.7.

$$z = \frac{x-\mu}{\sigma} \qquad \text{Equation 3.7}$$

With:

- x = a single sample value
- μ = mean of all samples
- σ = standard deviation of all samples

When the absolute value of the z-score is above 3, the sample is generally considered an outlier, as it is so far from the mean (Andrade, 2021).

Irregular waves
For irregular waves the z-score is less suited as a lot of variation is expected between the forces. Therefore the outliers at irregular waves are removed by looking at the histogram of the simulation. An example of such a histogram with outliers is shown in Figure 3.11.

It is expected that the histogram is not fully continuous. With a decreasing probability of occurrence it can happen that one or two bins are skipped. However, the histogram in the figure shows multiple larger gaps. The probability of this happening by most of the simulations is quite small. Based on the animations, forces after which a gap longer than three bins has occurred are considered as outliers. As an additional check an animation for the highest force is generated for every simulation. If the highest force does not appear to be caused by numerical instability, it is not removed.
The histogram method is not used for regular waves, as it is less reliable than the z-score. The z-score is a method which has been used before, while the histogram method is made up for this thesis.

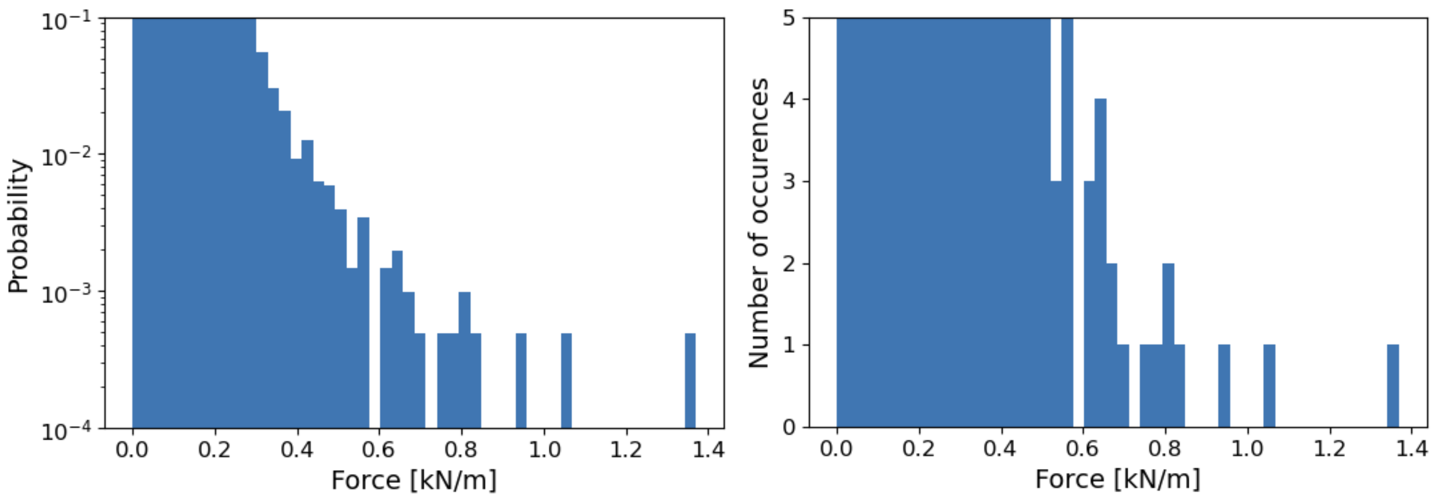

Figure 3.11: Histograms for raw force data (Den Heijer dp = 0.02 m and duration = 1500 s). Left probability, right number of occurrences in simulation.

Negative pressures
In addition to the high peak in Figure 3.5, a very low valley is visible as well. Even though some small negative pressures can be expected to occur due to wave rebound and flow separation, the strong negative peaks are unexpected. They are likely caused by tensile instability. Lyu et al. (2021) described this phenomenon and compared different possible solutions. Tensile instability is characterized by strong negative pressures, like the low point in Figure 3.5. The cause lies at the SPH gradient operator used for the fluid structure interaction. In most simulations a summation of pressure is used to discretize the pressure gradient in Navier–Stokes equations. The purpose of this is to conservate momentum. The result is however that there are no stress or strain thresholds for tensile instability. Two main phenomena which can generate tensile instability are vortex shedding (not applicable in this thesis) and added mass effects (applicable). For added mass effects, an example is a wave impact. Due to the inertia of the impact, the pressure on the fluid structure interface should be negative to prevent the structure surface to separate from the fluid.
Lyu et al. discuss three main solutions, Particle Shifting Techniques (PST), Tensile Instabilty Control (TIC) and combinations of the two. Applying one of these solutions would however come with the requirement of altering the source code of DualSPHysics, as there are no standard PST or TIC options available. This would go too much in depth for this thesis, as here the focus lies on the positive pressures. Instead, high negative pressure points are removed when they are below the mean minus three times the standard deviation of the valleys. These points are generally considered outliers (Andrade, 2021). Since the negative pressures are not contained in the high wave forcing, as those are positive, the influence on the results is limited.

3.7 Wave classification

The waves observed in the laboratory experiment and in the DualSPHysics model are both classified into five categories. In this way, the model can be validated by comparing the occurrences of different wave types. In this section it is explained when a certain configuration is assigned to a certain class.

Breaks at start quay

When the wave starts breaking immediately when entering the quay, it is assigned to 'breaks at start quay'. At the storm wall there is water pushed up, but the wave has already broken. Figure 3.12 illustrates a wave breaking at the start of the quay in both the lab and the DualSPHysics model.

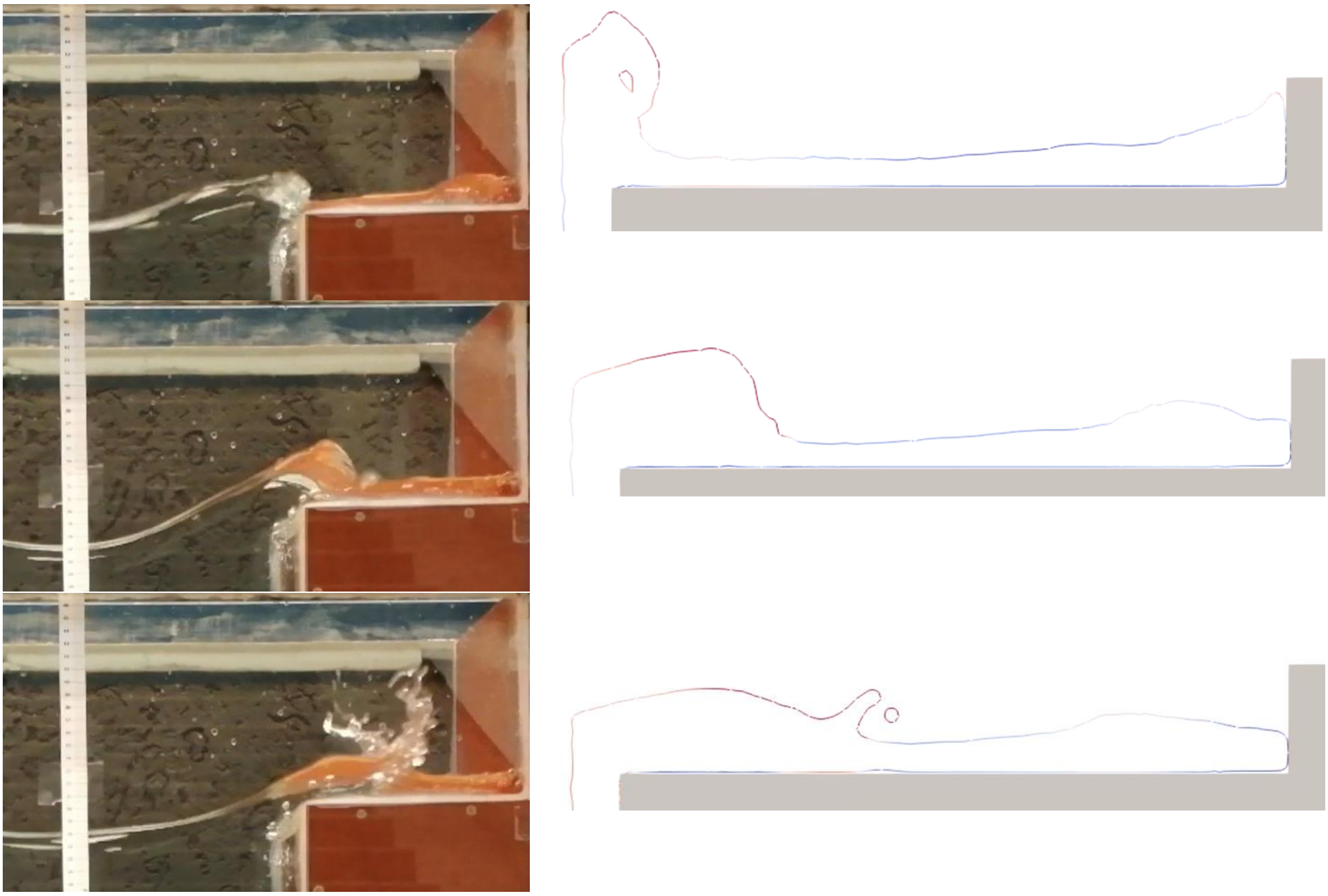

Figure 3.12: Wave breaking at the start of the quay in the lab (left) and DualSPHysics (right)

Breaks on quay

When the wave breaks after entering the quay, but it does not break on the wall, it is assigned to 'breaks on quay'. Figure 3.13 illustrates a wave breaking on the quay in both the lab and the DualSPHysics model.

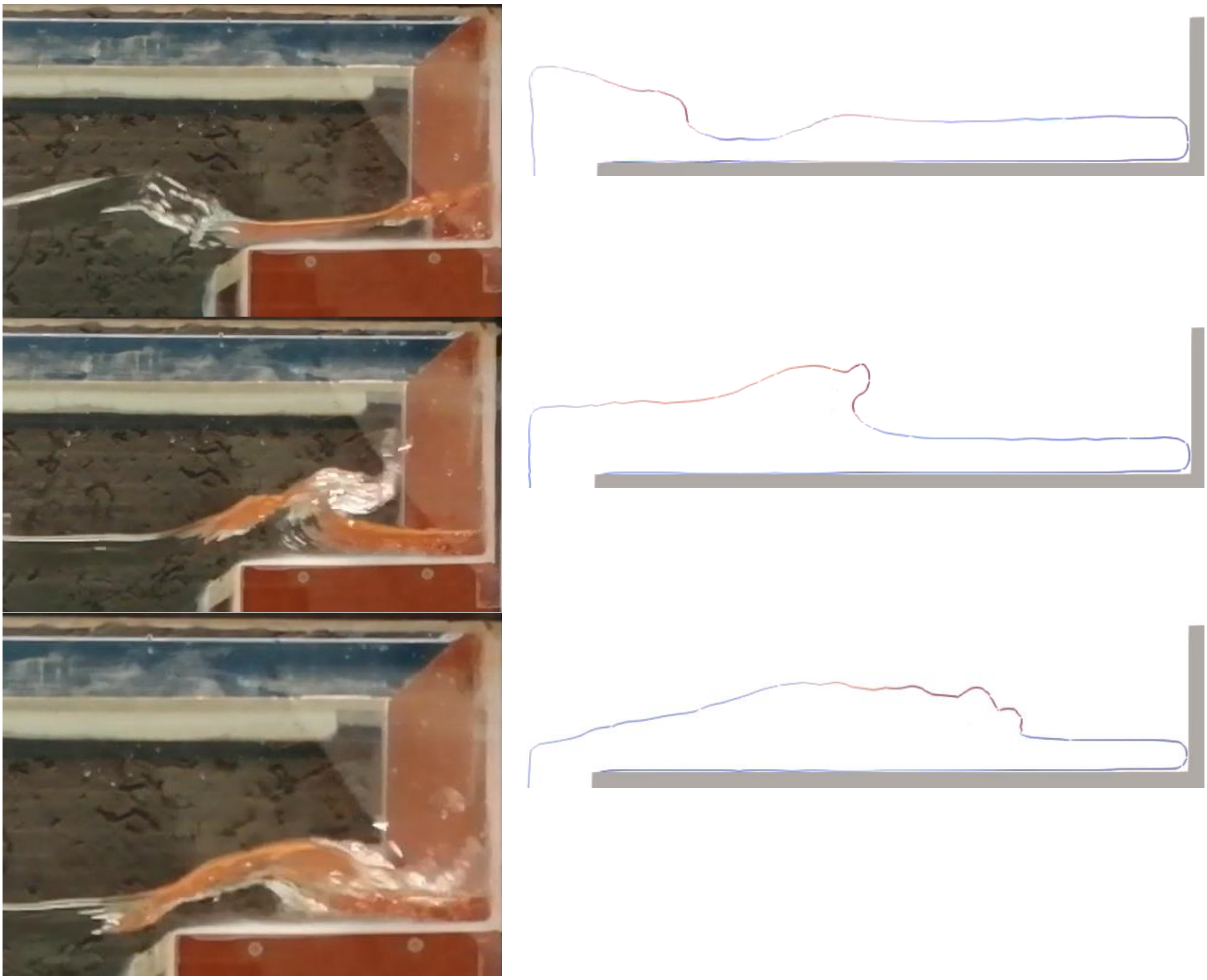

Figure 3.13: Wave breaking on the quay in the lab (left) and DualSPHysics (right)

Breaks on wall

When the overturning of the top, i.e. breaking, takes place just in front of the wall, the wave is assigned to 'breaks on wall'. Figure 3.14 illustrates a wave breaking on the wall in both the lab and the DualSPHysics model.

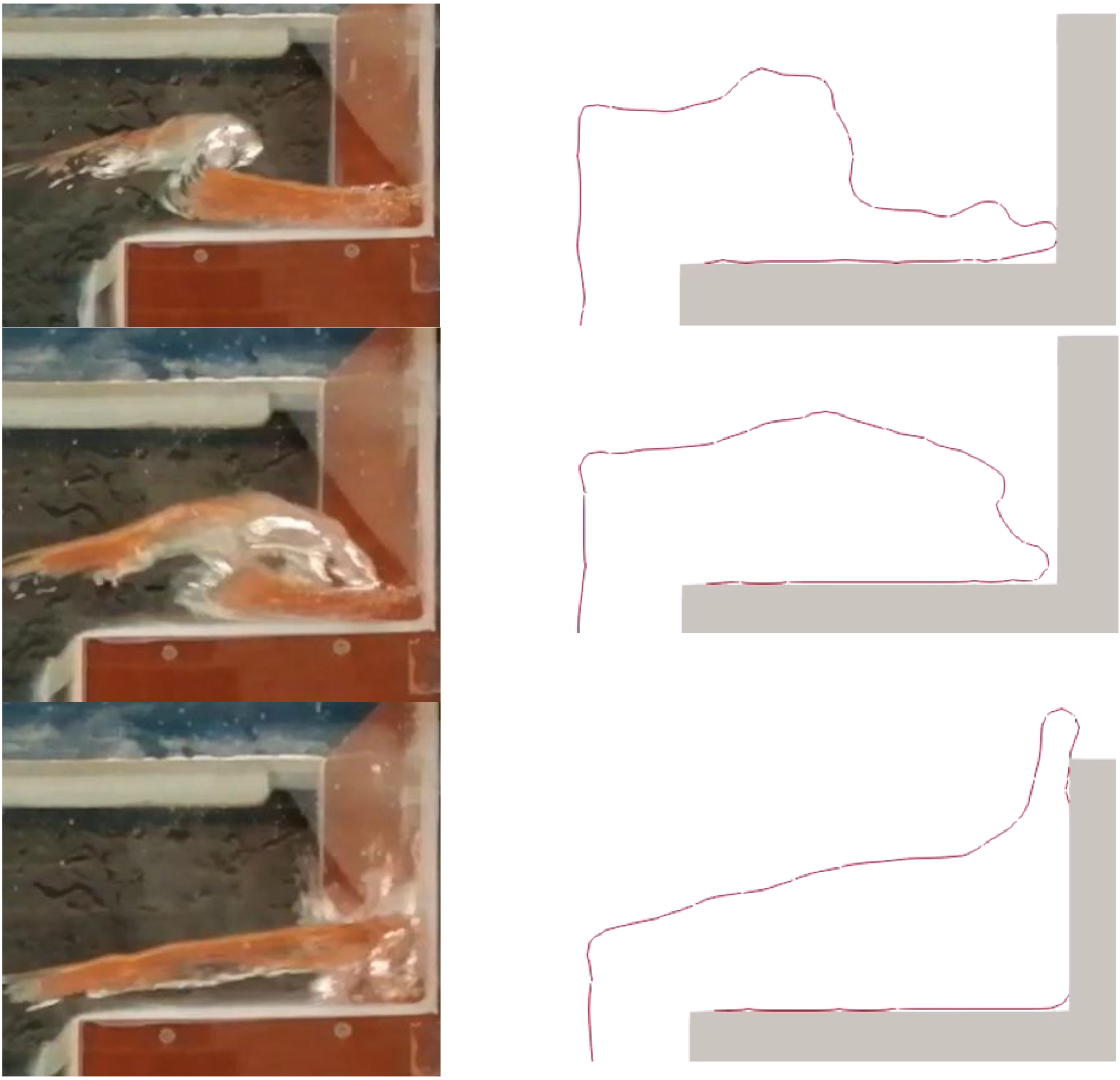

Figure 3.14: Wave breaking on the storm wall in the lab (left) and DualSPHysics (right)

Slightly breaking

When the wave has heightened, but did not overturn yet, it is assigned to 'slightly breaking'. Figure 3.15 illustrates a slightly breaking wave on the wall in both the lab and the DualSPHysics model. In the lab a slight overturning can be seen in the top photograph. Both slightly breaking waves look similar to a quasi-standing wave, but nodes and anti-nodes are not clearly visible.

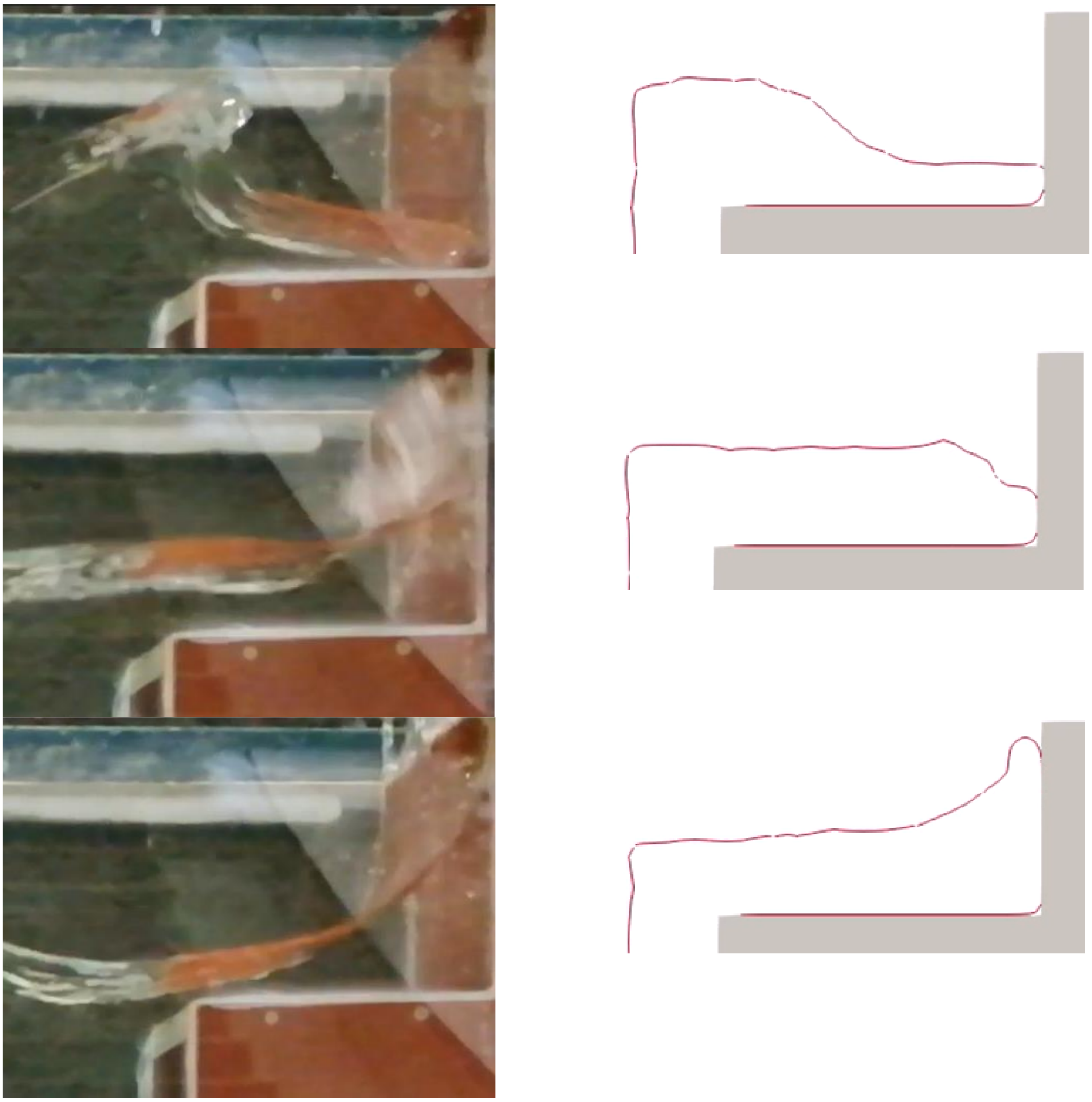

Figure 3.15: Wave slightly breaking in the lab (left) and DualSPHysics (right)

Quasi-standing

When clear nodes and antinodes are visible, with an antinode at the storm wall, the wave is assigned to ‘quasi-standing’. Figure 3.16 illustrates a quasi-standing wave on the wall in both the lab and the DualSPHysics model.

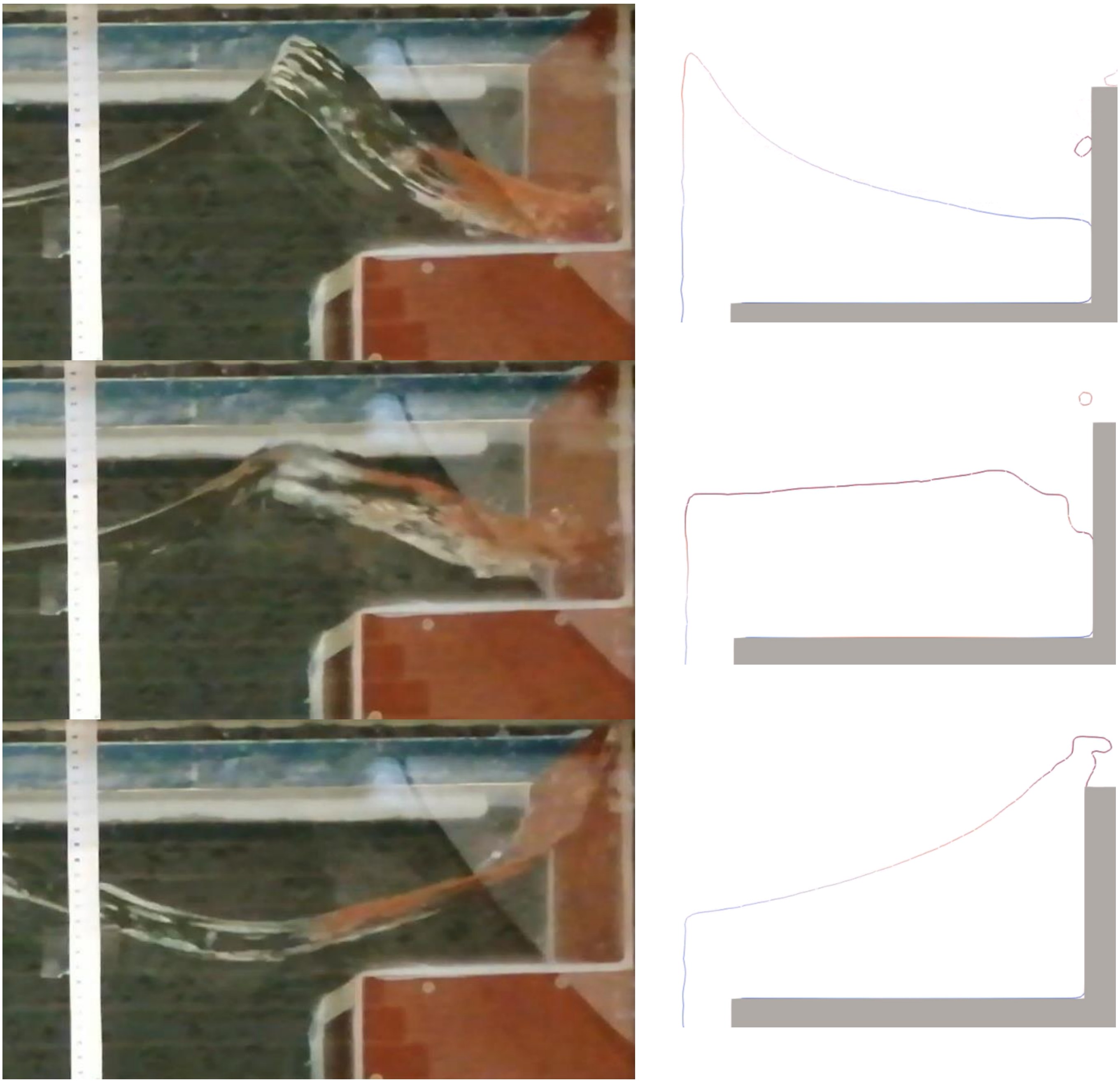

Figure 3.16: Quasi-standing wave in the lab (left) and DualSPHysics (right)

3.8 Adapted methods

To compare theoretical methods with the results of the model, two already existing theories are altered to better fit the retreated storm wall geometry. First, the implementation of the quay as a berm in the method of Goda-Takahashi is explained. After that, the method of Tuin with adaptions used in the present work is described.

Goda-Takahashi with quay as berm

In this case the quay is considered as the 'berm' because the storm wall is not placed at the edge of the quay. The pressure p_3 is therefore placed at the edge of the quay as shown in Figure 3.17.

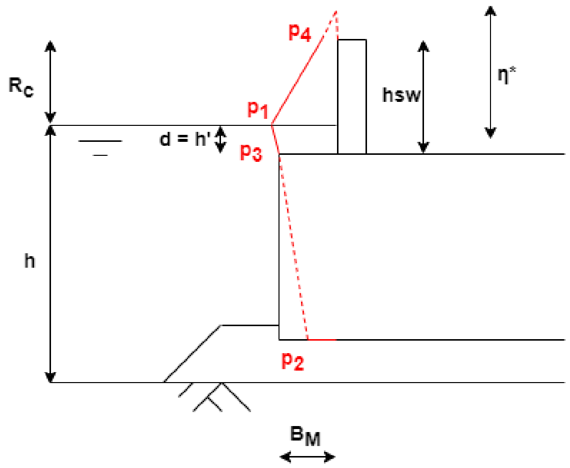

Figure 3.17: Adaption Goda-Takahashi with quay as 'berm'

Adapted conservation of momentum in the present work

In this method a few adaptions are made to the original idea of Tuin. This is done to see if and by how much more complex theories and calculations make the estimation of the force better.

To begin with, the horizontal velocity is computed with the solution of the third order Stokes non-linear wave theory derived by Skjelbreia (1958) instead of the velocity obtained from linear wave theory. The reason for this is that linear wave theory is not applicable for relatively steep waves, as seen in Figure 2.2. The shallow water wave velocity is tried as well, but this appears to give large overestimation of the force, so finally the third order non-linear velocity is chosen.

Second, a shorter impulse duration is used for waves with a high steepness (H / L = 0.117). Instead of 0.1 s, 0.05 s is used. The reason for this is that it is found that the DualSPHysics the highest impulses have an impulse duration around 0.05 s, see Figure 5.11. For irregular waves (H_s / L_{op} = 0.047) the higher impulses are found at a longer duration, so there 0.1 s is used.

Chapter 4 Results: Laboratory experiment

This chapter contains the results of the laboratory experiment. At this experiment the occurring wave types under different circumstances are observed. A wooden box with a panel on top is used as a structure. By varying the water depth, wave height and wave period, different configurations are generated.

The chapter starts with a description of the observed waves. This is followed by the observed wave type per configuration. Lastly, the visible breaking wave range is discussed.

4.1 Observed waves

In Chapter 3 five wave types are introduced: breaks at the start of the quay, breaks on the quay, breaks on the wall, slightly breaking and quasi-standing. All five wave types are observed during the experiment.

At a zero freeboard (d_{wq} = 0), the wave always starts to break at the start of the quay. An example is given in Figure 4.1. As soon as the wave comes in contact with the quay, it starts overtopping.

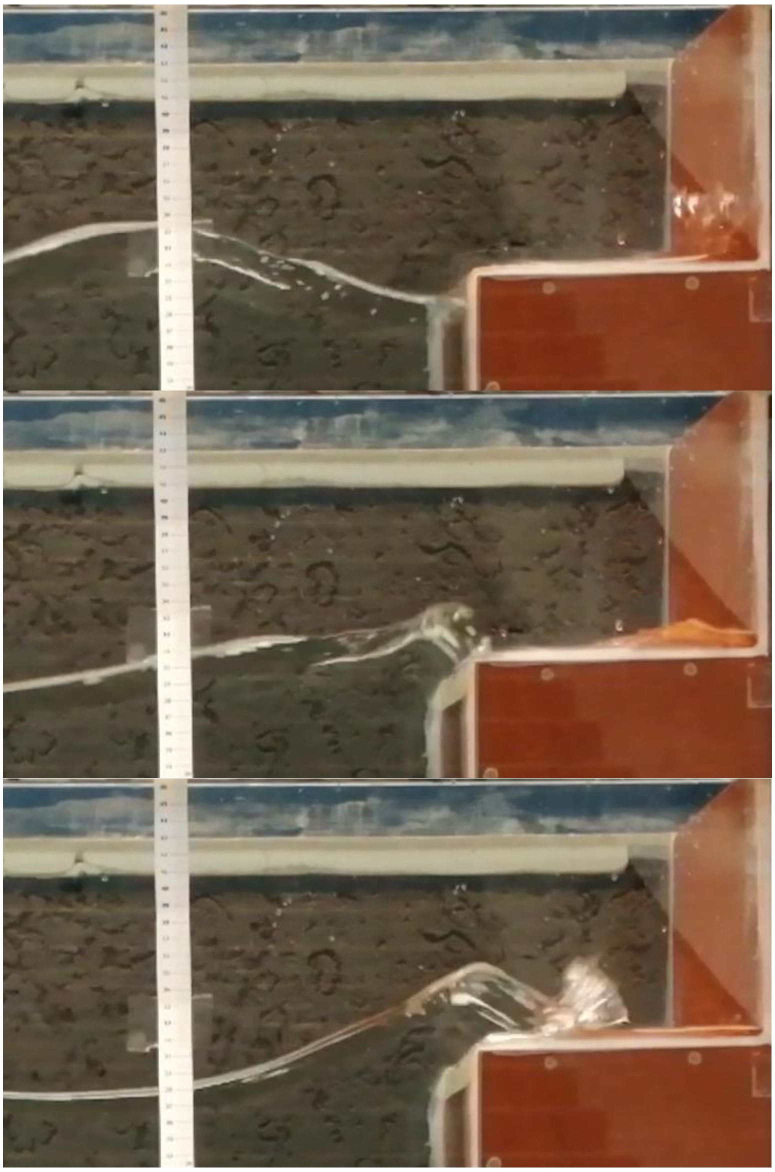

Figure 4.1: Wave breaking at the start of the quay

When a layer of water is present on the quay, the waves break later or not at all. An example of a wave which breaks on the wall is given in Figure 4.2. This type of wave occurs with the combination of a higher L_{quay} / L and d_{wq} / H value. In other words, the quay should be long enough to let the waves break and the water depth should be sufficient, so the waves do not break too early.

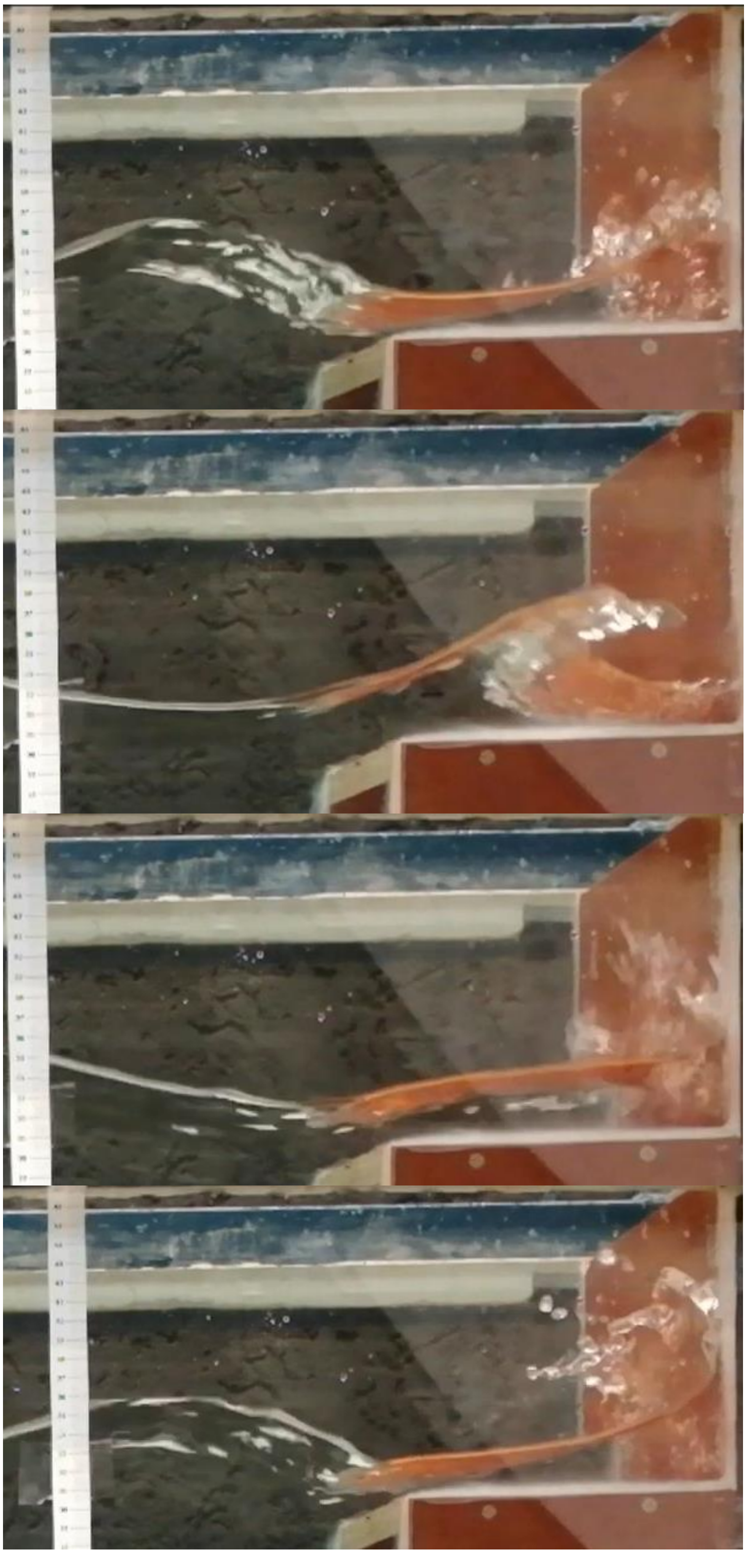

Figure 4.2: Wave breaking on storm wall

4.2 Wave type per configuration

For all the configurations in the experiment the wave type is observed. The results are shown in Table 4.1 and Figure 4.3.

Table 4.1: Results lab experiment for different values of relative quay length L_{quay}/L, wave steepness H/L and relative water depth on the quay d_{wq}/L

Experiment number	L_{quay} / L	H / L	d_{wq} / L	Wave type
1	0.44	0.1133	0.0000	breaks at start quay
2	0.38	0.1101	0.0000	breaks at start quay
3	0.31	0.1170	-0.0017	breaks at start quay
4	0.44	0.1034	0.0763	breaks on quay
5	0.44	0.1108	0.0813	breaks on quay
6	0.37	0.1001	0.0694	breaks on quay
7	0.37	0.1287	0.0715	breaks on quay
8	0.44	0.1059	0.0911	breaks on wall
9	0.38	0.1016	0.0889	breaks on wall
10	0.38	0.1122	0.0932	breaks on wall
11	0.31	0.0895	0.0809	slightly breaking
12	0.30	0.1150	0.0833	slightly breaking
13	0.37	0.0960	0.0919	breaks on wall
14	0.44	0.0862	0.1207	quasi-standing
15	0.31	0.0602	0.0861	quasi-standing
16	0.38	0.1037	0.1122	quasi-standing
17	0.30	0.1133	0.0950	slightly breaking
18	0.31	0.1188	0.1239	quasi-standing

In Figure 4.3 there are clear clusters of the type of waves occurring. L_{quay} / L does not seem to have an effect for d_{wq} / H ≤ 0 or d_{wq} / H ≥ 1, but it does have an effect in between 0 and 1. Besides the value of L_{quay} / L, the type of wave occurring in this region also depends on the value of d_{wq} / H. These types of waves are either slightly breaking (blue), breaking on the wall (magenta) or breaking on the quay (red). For d_{wq} / H ≤ 0 only breaking at the start of the quay (black) is observed, while for d_{wq} / H ≥ 1 only quasi-standing waves (green) are visible. The reason for this is that the wave cannot maintain its form if there is no water on the quay, and breaking does not occur at all if the water depth is sufficient. Therefore at low or high values of d_{wq} / H only one type of wave is observed, and L_{quay} / L does not play a role.

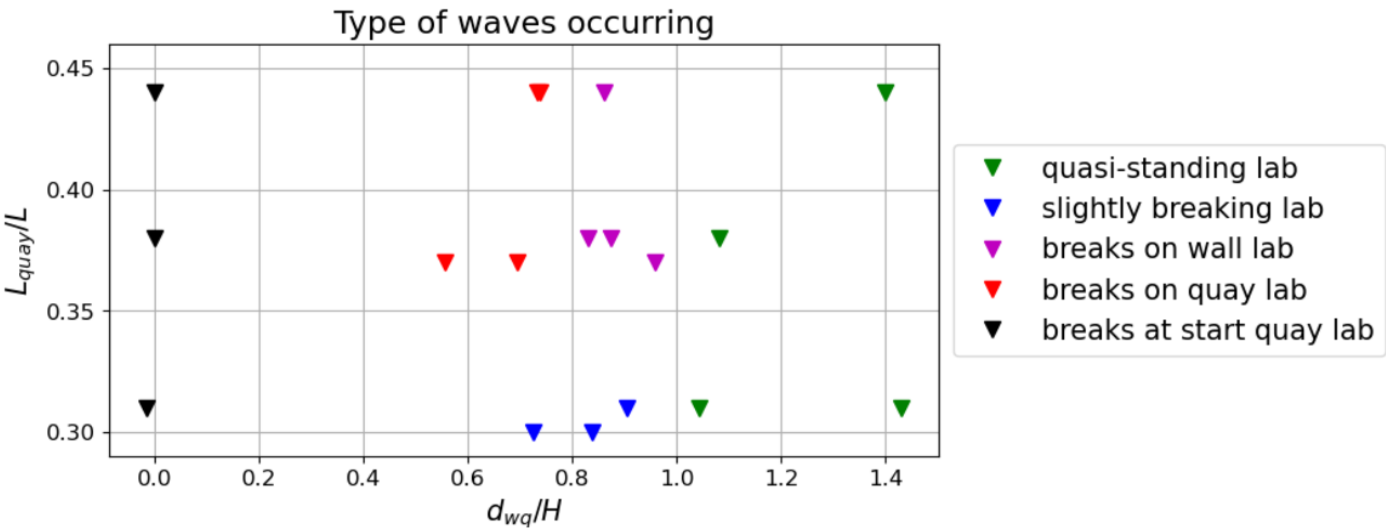

Figure 4.3: Type of waves occurring laboratory experiment

4.3 Breaking wave range

Based on the laboratory experiments a breaking wave range is estimated. This linear range is fitted using a combination of linear regression and optimization.

First, an estimate of the slope and intercept is made by fitting a line through the points which represent breaking waves at the storm wall. To get the points which present broken waves and the points which represent non-broken waves on separate sides of the line, the found slope and intercept are altered using optimization. Here, an objective function is used to minimize the number of points on the wrong side of the line. In other words, points which present broken waves are minimized to be in the non-broken waves section defined by the line and opposite. The range is then created by adding and subtracting the maximum residual, so all breaking wave points fall within the range.

Figure 4.4 shows the fit for the laboratory experiments. The breaking wave range is not optimal, as one slightly breaking wave data point falls within the range as well. Still, it provides an idea of when breaking waves can be expected.

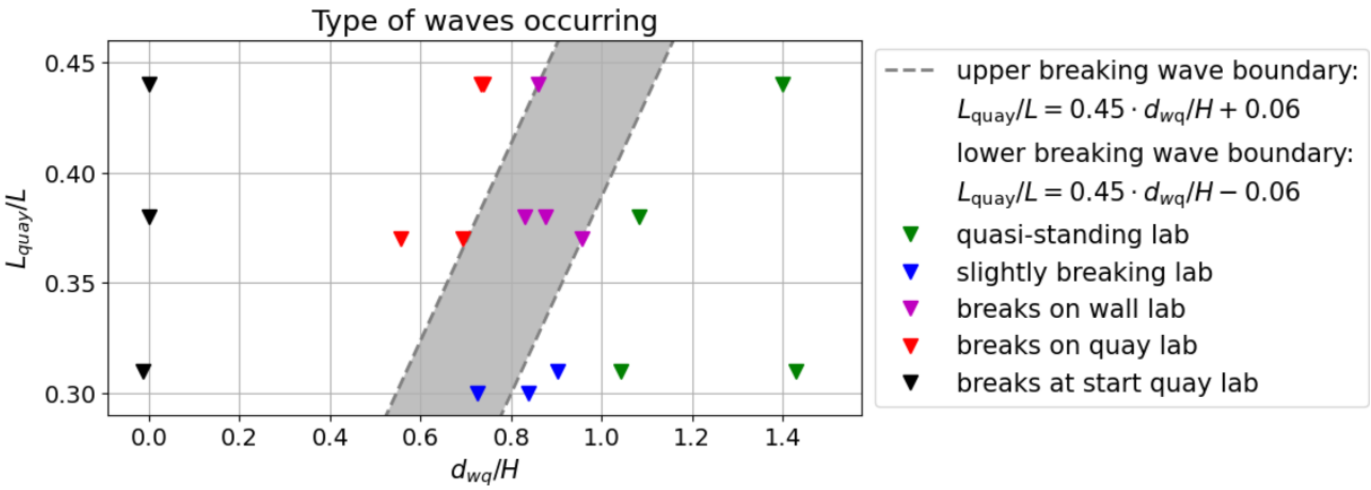

Figure 4.4: Breaking wave boundary based on lab results

Chapter 5 Results: DualSPHysics

This chapter contains the results of the DualSPHysics simulations. In DualSPHysics the Kop van Zuid case study has been modelled. By varying the geometry of the structure and the hydraulic boundary conditions different configurations are generated. Simulating these different configurations allows to see relationships between different parameters if present.

The chapter follows a similar order as Chapter 4. It starts with a description of the observed waves. This is followed by the observed wave type per configuration. After that, the visible breaking waves range is discussed. Lastly, the wave pressure and forcing results are shown.

5.1 Observed waves

In Chapter 3 five wave types are introduced: breaks at the start of the quay, breaks on the quay, breaks on the wall, slightly breaking and quasi-standing. All five wave types are observed in the simulations for both regular and irregular waves. First, the regular waves will be treated, then the irregular waves. The difference between the regular waves and irregular waves is that the regular waves only consist of one type of wave with wave height H_{max}, while the irregular waves consists of a distribution with different wave heights, also lower than H_{max}.

Regular waves

For regular waves, the exactly breaking at the wall is not often observed. Waves breaking at the start of the quay or on the quay are more common. Figure 5.1 shows the difference between a wave breaking at the start of the quay, on the quay and on the wall.

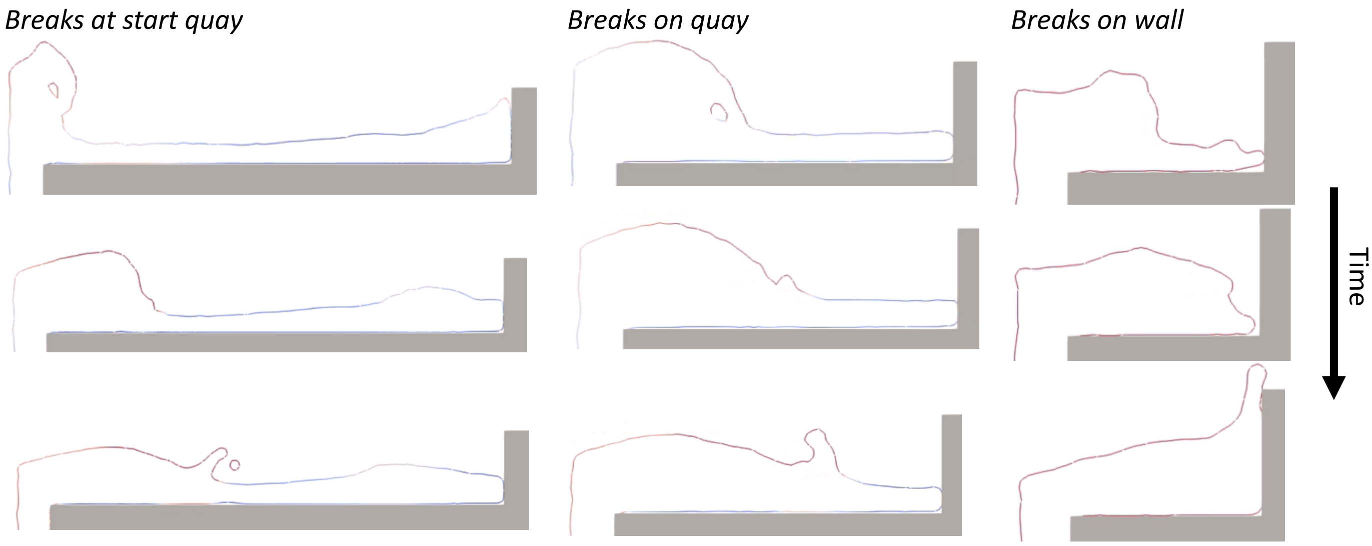

Figure 5.1: Waves breaking at different locations in DualSPHysics

In addition to the wave types, also numerical instability is observed. It is found that for positive and zero freeboard these numerical instabilities occur often. This is due to the fact that the number of particles on the quay stays limited. The resolution is therefore too coarse. Numerical instabilities appear at d_{wq} / L = 0.02 as well, for configuration 28, 36 and 44, see

Figure 3.10. Table 5.1 shows the values of the dimensionless parameters corresponding to these configurations. The only difference is the relative storm wall height. All the configurations can be found in Appendix D: Configurations and results DualSPHysics.

The peaks are removed using the z-score as explained in Chapter 3. Numerical instability is not observed for d_{wq} / L = 0.04. The boundary therefore seems to lie between d_{wq} / L = 0.02 and d_{wq} / L = 0.04 or in other words, between 5 and 10 particles per water depth on the quay.

Table 5.1: Configurations at which numerical instability occurred (regular waves)

Configuration number	**L_{quay} / L**	**h_{sw} / L**	**d_{wq} / L**	**H / L**
28	0.15	0.090281	0.02	0.05
36	0.15	0.095033	0.02	0.05
44	0.15	0.099784	0.02	0.05

Irregular waves
For irregular waves, not all wave types are observed. There are no waves observed which start breaking at the start of the quay. This is because the irregular waves have a lower wave height which makes the waves less prone to breaking. Slightly breaking waves are barely observed. Some quasi-static waves also looked a bit like slightly breaking waves due to an increase in wave height. The most common observed wave types are breaking on the quay and quasi-standing waves.

5.2 Wave type per configuration

For all the configurations made in the model, the wave type is observed. This is done for both regular and irregular waves and will be treated separately.

Regular waves
The observed wave types for regular waves are shown in Figure 5.2. The values of all the configurations can be found in Appendix D: Configurations and results DualSPHysics. In Figure 5.2 there are clear clusters of the type of waves occurring. Only the boundary between breaking at the start of the quay (black) or on the quay itself (red) is not entirely clear. At d_{wq} / H = 0.2 and L_{quay} / L = 0.30 both wave types are observed.

Similarly to the laboratory experiment, L_{quay} / L does not seem to have an effect for d_{wq} / H ≤ 0 or d_{wq} / H ≥ 1, but it does have an effect in between 0 and 1. For d_{wq} / H ≤ 0 only breaking at the start of the quay (black) is observed, while for d_{wq} / H ≥ 1 only quasi-standing waves (green) are visible.

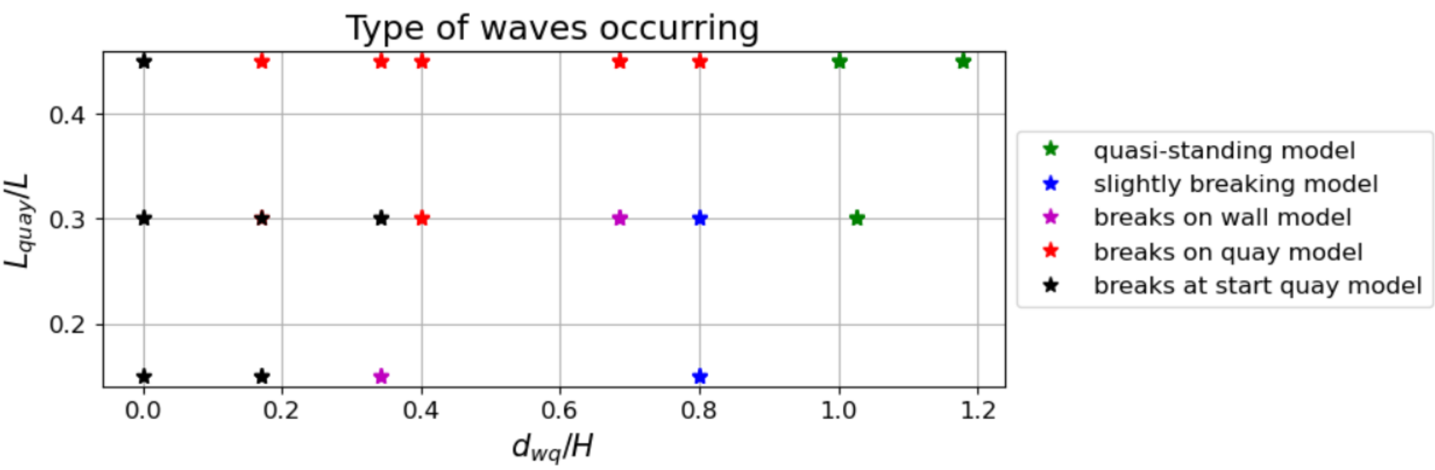

Figure 5.2: Type of regular waves occurring DualSPHysics model

Irregular waves
The observed wave types for irregular waves are shown in Figure 5.3. The values of all the configurations can be found in Appendix D: Configurations and results DualSPHysics. In Figure 5.3 there are clear clusters of the type of waves occurring, just as with regular waves in Figure 5.2. The

type of waves occurring and their frequency of occurrence in the simulations is however different. In the simulations for irregular waves, waves breaking on the quay are not present, and quasi-static waves occur the most. This is due to the fact that H_s is smaller resulting in a different ratio on the horizontal axis in Figure 5.3 (d_{wq} / H_s) than in Figure 5.2 (d_{wq} / H). The irregular waves have higher water depth on quay over wave height ratios, resulting in waves which are less likely to break.

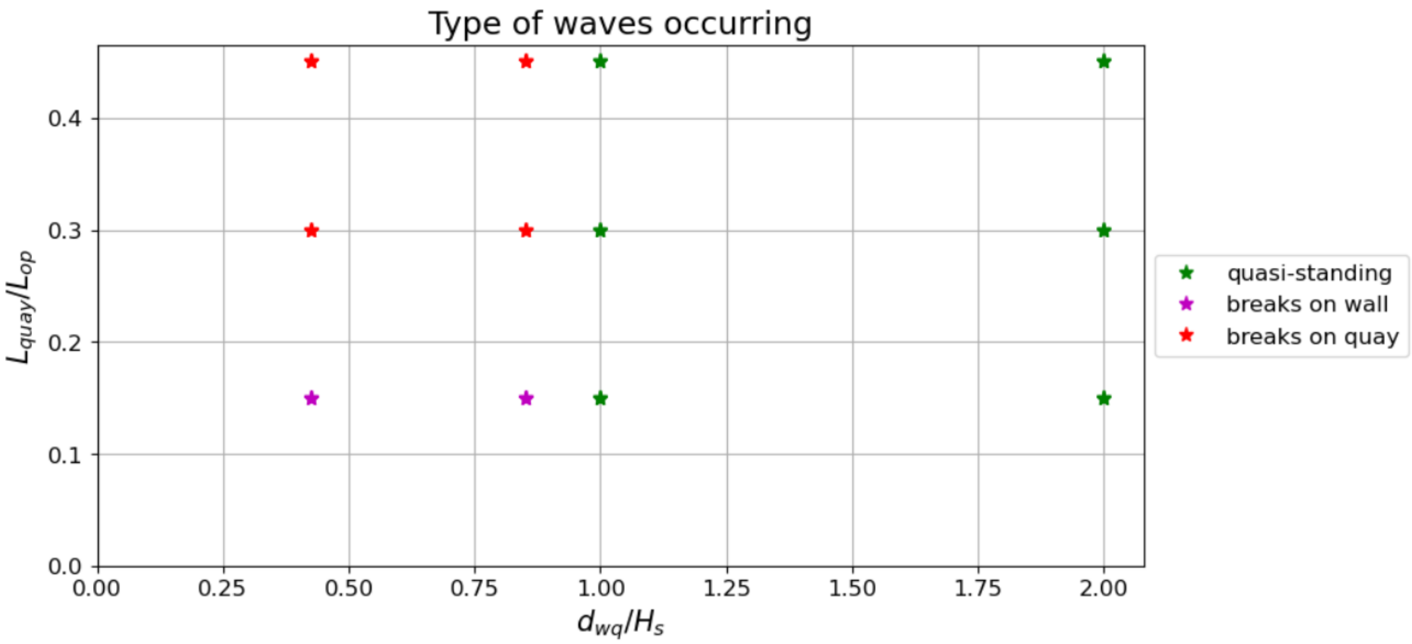

Figure 5.3: Type of irregular waves occurring DualSPHysics model

5.3 Breaking wave range

Based on the model simulations a breaking wave range is estimated. This linear range is fitted using a combination of linear regression and optimization, as explained in Chapter 4. Figure 5.4 shows the fit for breaking wave range based on the model simulations.

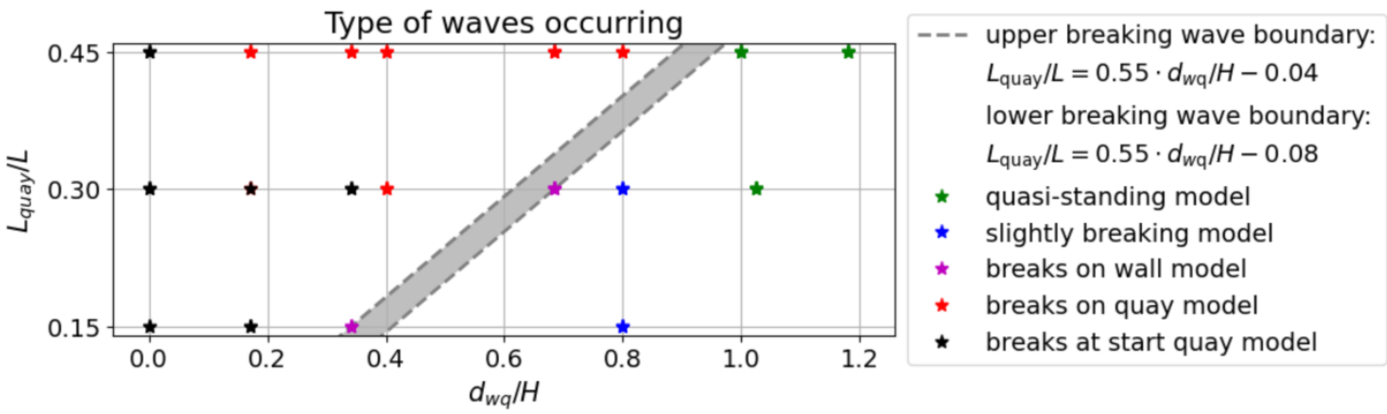

Figure 5.4: Breaking wave boundary based on DualSPHysics results regular waves

For irregular waves it is not possible to draw a breaking wave range as for regular waves. Waves breaking on the storm wall are only observed for L_{quay} / L_{op} = 0.15. As this would result in a horizontal line, it is not possible to get the breaking and non-breaking points on separate sides of the line. A breaking wave range for d_{wq} / H > 1 does not seem to be applicable, as only quasi-standing waves are observed.

5.4 Wave pressure and forcing: regular waves

Up to now only the type of waves have been discussed. This section treats the regular wave pressure and forcing and links it to the breaking wave range described in the previous section.

Wave force types used: F_{max} versus F_{peaks}

The wave force is determined by integrating the pressure profile over the storm wall height for every time step in a simulation. The maximum occurring force in a simulation consists of one value, F_{max}. For regular waves it is however more common to take the average of all peak values, F_{peaks}, since all incoming waves should be the same. Therefore when using a time series of regular waves, one would expect to have similar peak heights. However, peaks which are two times higher than the average peak occur as well. Figure 5.5 shows the time series of 100 regular waves for the configuration shown in Figure 5.6.

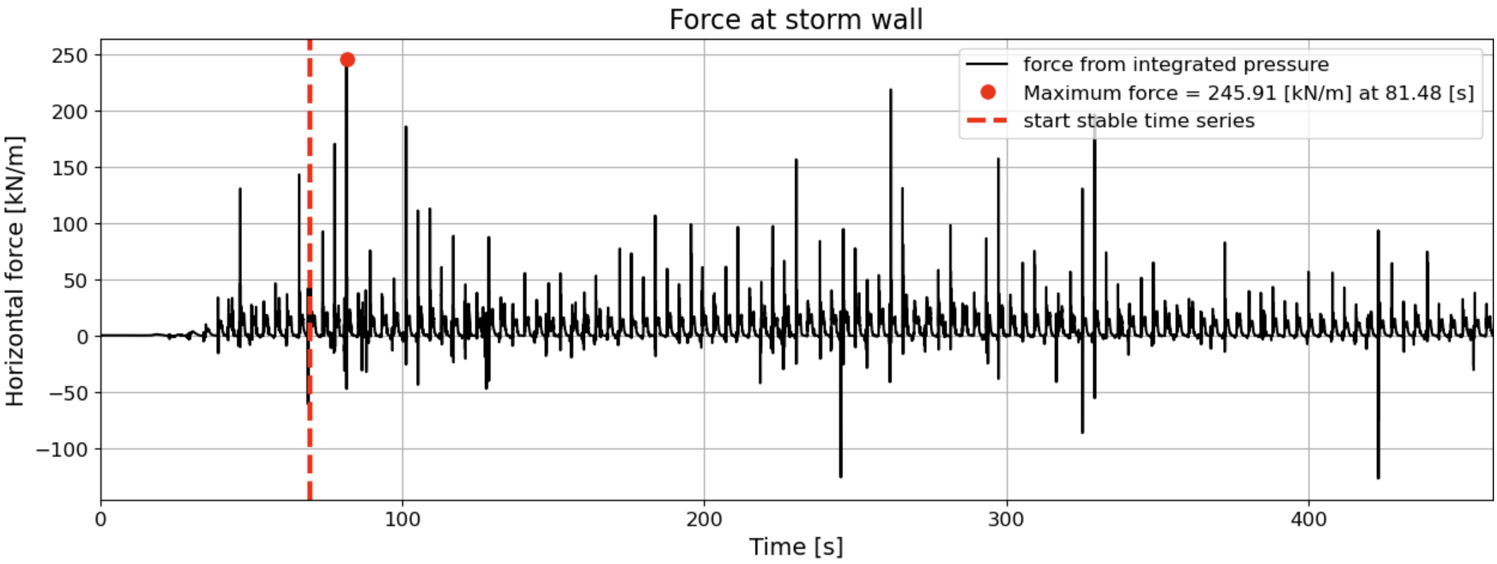

Figure 5.5: Force time series (configuration 45, H/L = 0.117, d_{wq}/L = 0.02, L_{quay}/L = 0.15, h_{sw}/L = 0.10)

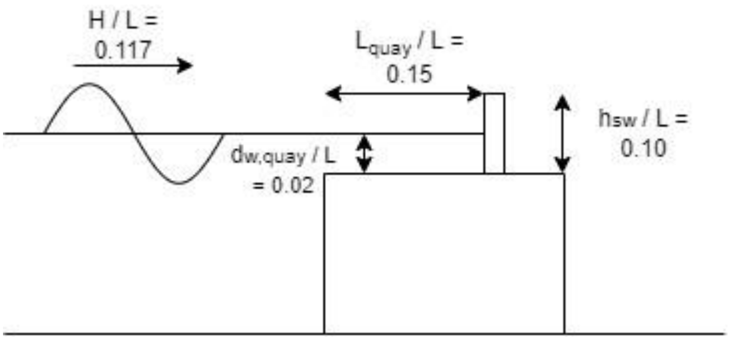

Figure 5.6: Geometry configuration 45

While most peaks are between 50 and 100 kN/m, there are also peaks visible above 100 kN/m, both around the start and end of the simulation. The simulation contains active wave absorption, so the peaks are not caused by accumulation of wave heights. Visualizing the impact around t = 81.48 s (81.23s – 81.73s), results in Figure 5.7 - Figure 5.9. This shows that the highest peak is caused by a wave which breaks just in front of the wall. The peaks in the simulation are however not all breaking just in front of the wall. Due to water flowing back and interacting with the new incoming wave, some waves will break earlier causing a lower force. An example of water flowing back is shown in

Figure 5.10. The flowing back of water is an irregular process, which causes the spread in the regular wave force. So if one is interested in high forcing, one should look at F_{max} rather than F_{peaks}.

Figure 5.7: Water surface at t = 81.23 s (configuration 45)

Figure 5.8: Water surface at t = 81.48 s (configuration 45)

Figure 5.9: Water surface at t = 81.73 s (configuration 45)

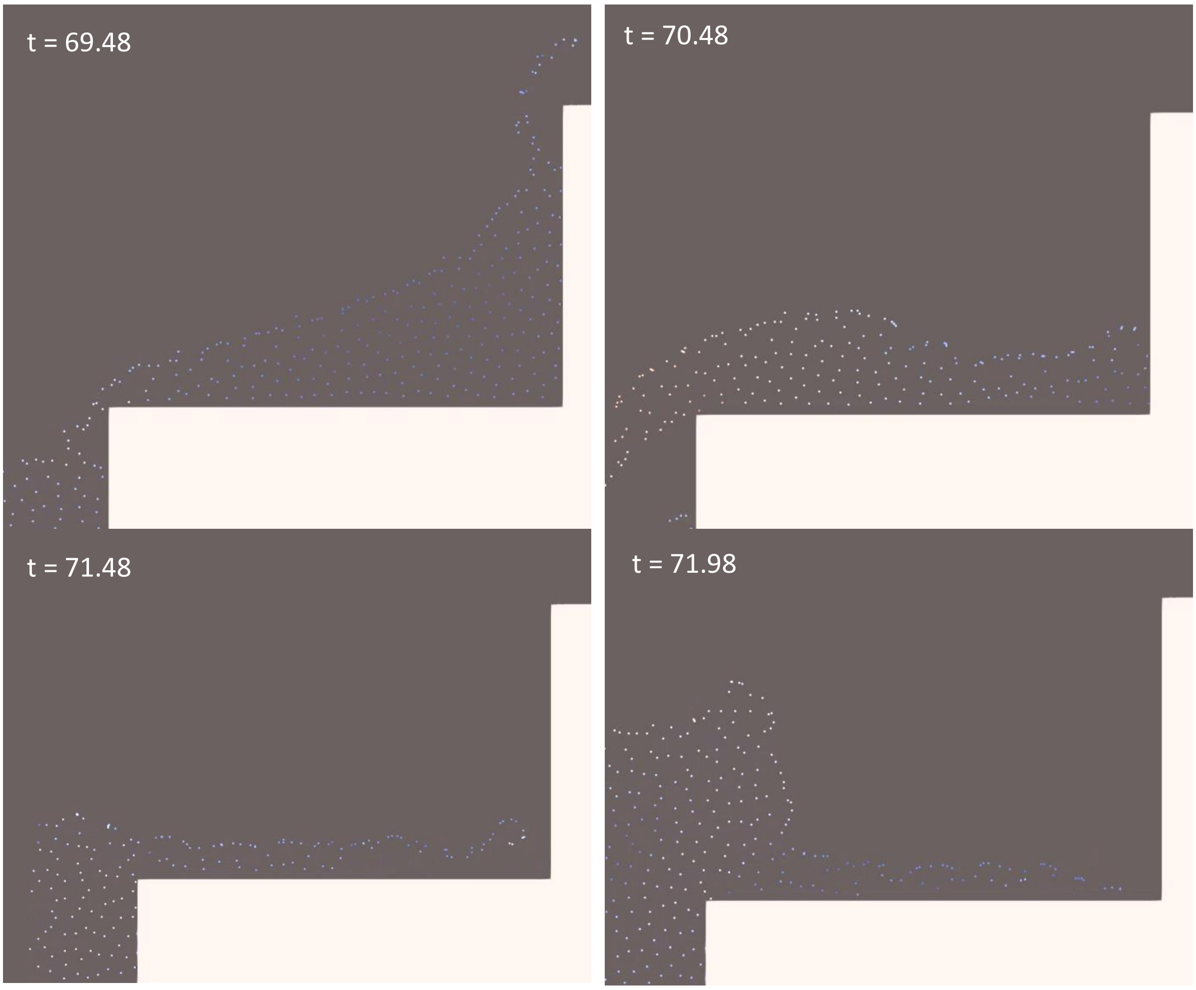

Figure 5.10: Water flowing back after impact

In the model validation for irregular waves using the experiments of Den Heijer (1998) it is concluded that the model did well with the $F_{1\%}$ and $F_{10\%}$ predictions, but rather poor with the maximum force which is most of the times overestimated. But Den Heijer measured his pressure with time intervals of 0.2 seconds. The model gives an output every 0.005 seconds. Figure 5.11 shows the duration of the impacts resulting from the model and it is visible that the impacts have a duration smaller than 0.2 seconds. Therefore, according to the model, it is possible that the experiments of Den Heijer missed these impact waves. However, it is important to note that having a higher sampling rate does not inherently validate the model's correctness. The model does not take the effect of air as a cushion into account. Therefore the actual impulse duration is probably larger than indicated by the model.

However, the need for a higher sampling resolution follows from Chen et al. (2019) who measured the impacts and their duration. The higher impacts had a duration between 0.08 – 0.18 s. The durations of those impacts are longer than the DualSPHysics model, but both are smaller than the interval which Den Heijer used to measure the pressures.

The high, unexpected, peaks are therefore not disregarded or removed like with the numerical instability discussed in Chapter 3.

Figure 5.11 shows besides a short impulse duration, also a distinction in wave steepness. A high wave steepness causes a high impulse with a short duration, while a lower steepness causes a smaller impulse with a larger duration. A possible explanation is that a wave with a high wave steepness has a higher energy concentration causing a more intense and rapid impact. A wave with a small wave steepness has its energy more spread out, causing less impact and having a longer duration.

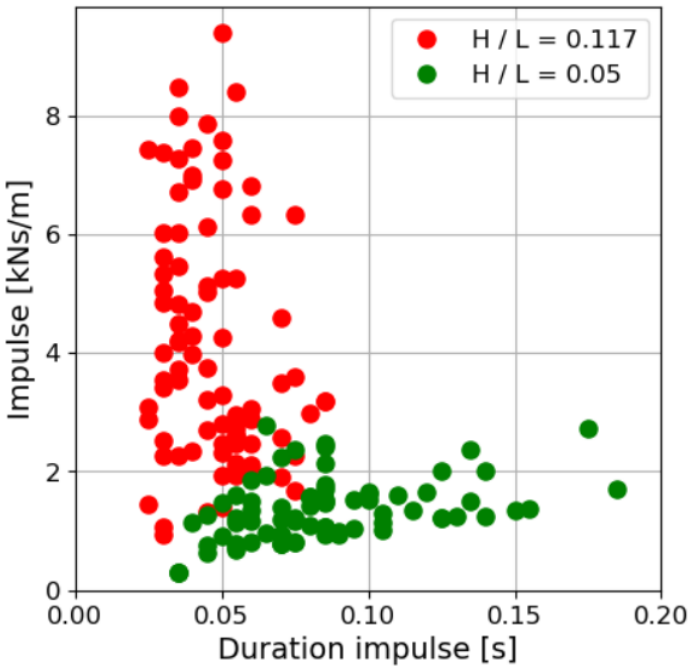

Figure 5.11: Impulse duration versus impulse magnitude

Wave pressure: results configurations

Figure 5.12 and 5.13 show the results of the model with regular incoming waves for H / L = 0.117 and H / L = 0.05 respectively. The figures show the dimensionless highest 1% pressure ($p_{1\%}$) on the storm wall, averaged over the storm wall heights. The pressure is made dimensionless using the water depth on the quay, d_{wq}. Therefore, for a d_{wq} twice as high, the force is divided by a number twice as high. An overview of values per simulation can be found in Appendix D: Configurations and results DualSPHysics. Figure 5.12 and 5.13 show the expected wave breaking range based on the laboratory experiment from Chapter 4 as well. Here, this range is used to explain the pressure behaviour. In Chapter 6 the breaking ranges of the laboratory experiment and numerical model are discussed in more detail.

The highest pressures in Figure 5.12 and 5.13 are visible around $0.15 \leq L_{quay} / L \leq 0.30$. This is because at $0.15 \leq L_{quay} / L \leq 0.30$ breaking waves on the quay or on the wall occur, which cause the higher forcing. For the lower wave steepness, in Figure 5.13, the highest pressures are caused by waves breaking on the wall, as the highest pressures fall within the breaking range. Noticeably for the higher wave steepness, in Figure 5.12, the highest forcing is caused by waves which break already on the quay. A possible explanation is that the higher waves still have a large impact after breaking, while the smaller waves do not. This is because the higher waves consist of more water and therefore also push up more water, still creating a large impact. This phenomenon is illustrated is Figure 5.14.

Besides the wave breaking range, other influences of parameters are visible. First, a higher steepness H / L results in a higher dimensionless force. Second, in both figures, simulations with a twice as high freeboard lead to a higher pressure due to the increase in hydrostatic pressure. But the pressure does not become twice times as large. Due to different wave types occurring, a breaking wave at a lower freeboard can cause pressures of similar magnitude as a just broken wave at a twice as high freeboard.

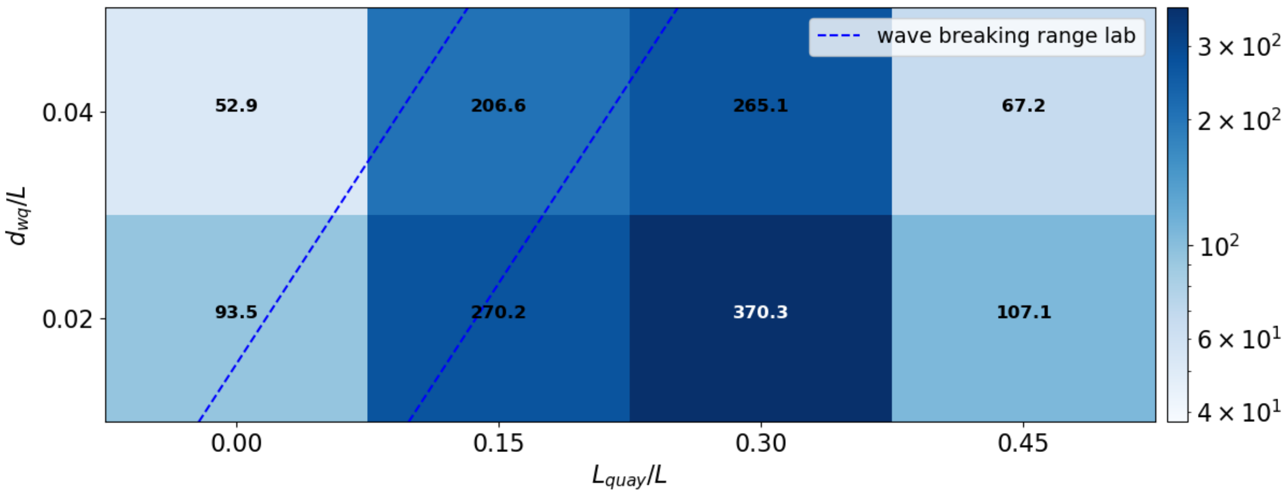

Figure 5.12: Dimensionless pressure ($p_{1\%}$ / ($\rho_w g d_{wq}$)) on storm wall for H / L = 0.117, averaged over storm wall heights

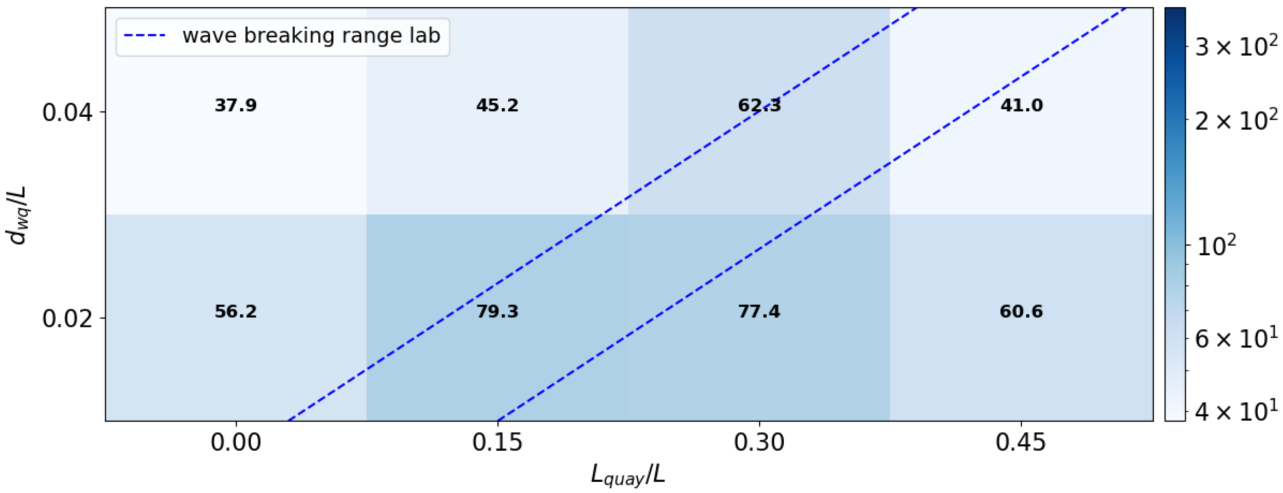

Figure 5.13: Dimensionless pressure ($p_{1\%}$ / ($\rho_w g d_{wq}$)) on storm wall for H / L = 0.05, averaged over storm wall heights

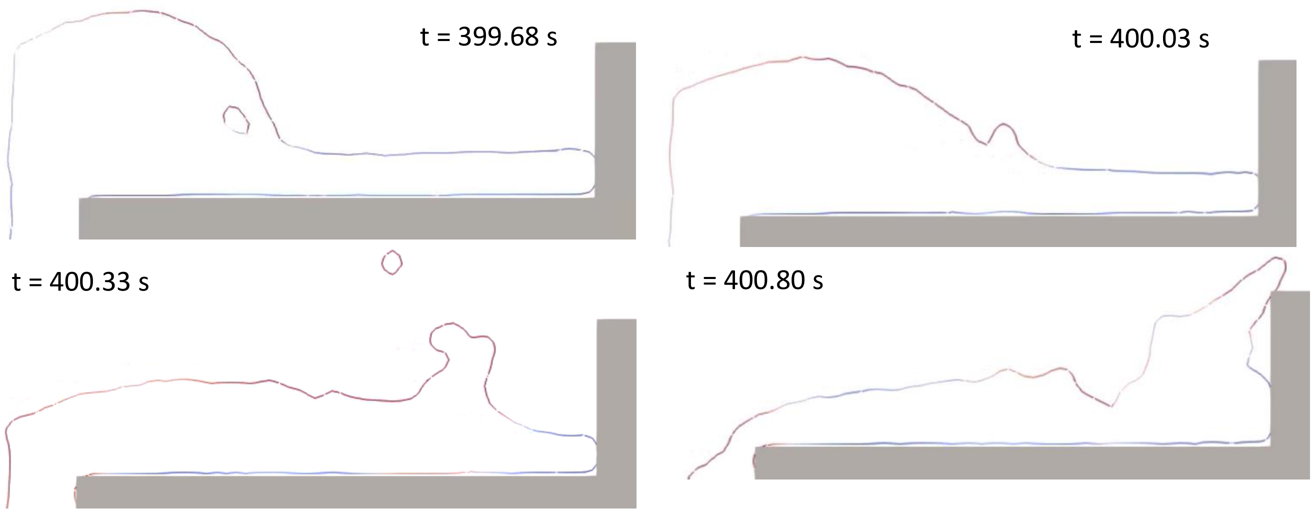

Figure 5.14: Impact after breaking wave (configuration 53, H/L = 0.117, d_{wq}/L = 0.02, L_{quay}/L = 0.30, h_{sw}/L = 0.090)

The only parameter whose influence is not entirely clear is h_{sw} / L. Figure 5.15 and 5.16 show the results of the model with regular incoming waves for H / L = 0.117 and H / L = 0.05 respectively. Here the parameter on the vertical axis is h_{sw} / L instead of d_{wq} / L. In both figures, the wave pressures stay around the same value, but in Figure 5.15 some variations up to 15% are visible for 0.15 ≤ L_{quay} / L ≤ 0.30. Wave overtopping does occur, but then a higher storm wall is expected to lead to a higher force, which is not the case in Figure 5.15, as less water overtops the wall and is included in the impact with the storm wall. The exceptions might arise from specific hydrodynamic interactions that occur at these particular relative quay lengths, where the wave behaviour (such as reflection, interference, or breaking) leads to non-intuitive results. Still, the deviations are relatively small, so it can be concluded that that the relative quay length has a larger influence than the storm wall height.

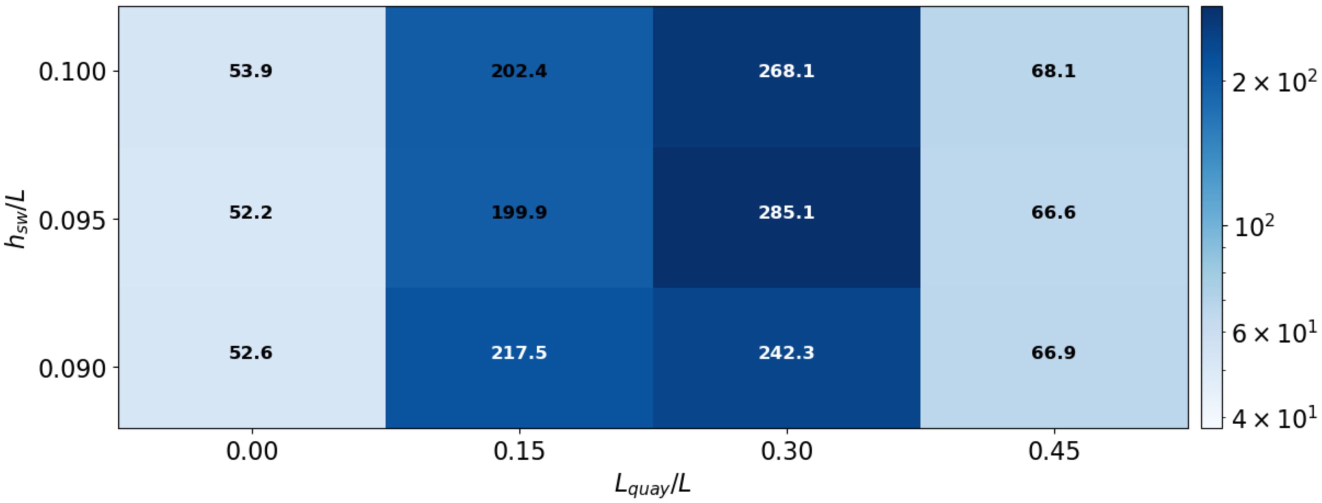

Figure 5.15: Dimensionless pressure($p_{1\%}$ / ($\rho_w g d_{wq}$)) on storm wall for H / L = 0.117, d_{wq} / L = 0.04

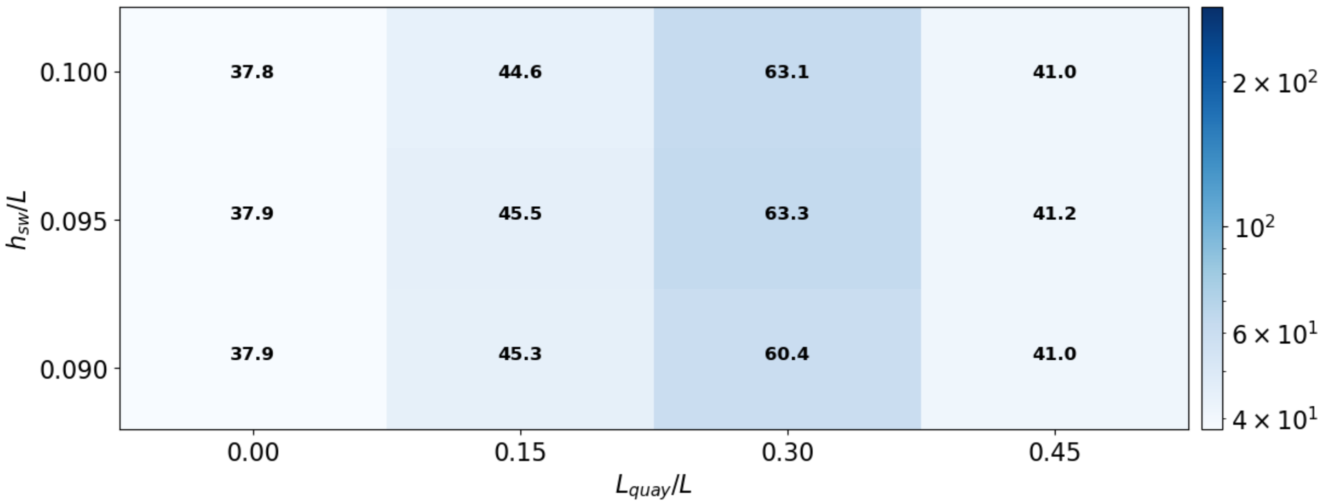

Figure 5.16: Dimensionless pressure($p_{1\%}$ / ($\rho_w g d_{wq}$)) on storm wall for H / L = 0.05, d_{wq} / L = 0.04

5.5 Wave pressure and forcing: irregular waves

This section describes the irregular wave forcing. Instead of the same incoming wave as with regular waves, here the input of wave heights and wave period differs, resulting in a larger spread in wave forcing. This section first looks at the wave height and wave force distributions and then at the wave pressure per configuration.

Wave distributions

Based on the frequency of an occurring wave height or wave force a distribution is be made. Figure 5.17 shows the distribution of wave heights and the expected distribution based on a Rayleigh distribution. The distributions seem to correspond well, but the simulation distribution is continuously above the Rayleigh distribution. This is likely due to the limited simulation duration. A longer simulation duration will provide more extreme values, causing the DualSPHysics distribution to be less steep. This can be seen by comparing Figure 5.17 with Figure 5.18 has a three times shorter simulation duration than Figure 5.17. In Figure 5.17, the deviation from the Rayleigh distribution is smaller than in Figure 5.18. In addition, the horizontal axis in Figure 5.17 has larger values, i.e. higher waves are observed.

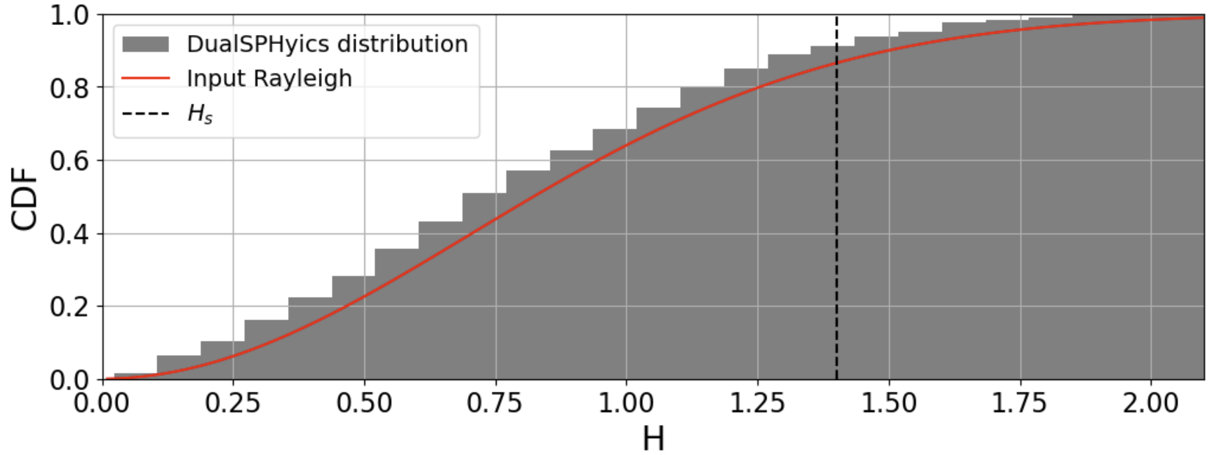

Figure 5.17: Cumulative distribution wave heights three seeds (configuration 15, H_s/L_{op} = 0.047, d_{wq}/L_{op} = 0.04, L_{quay}/L_{op} = 0.15, h_{sw}/L_{op} = 0.077)

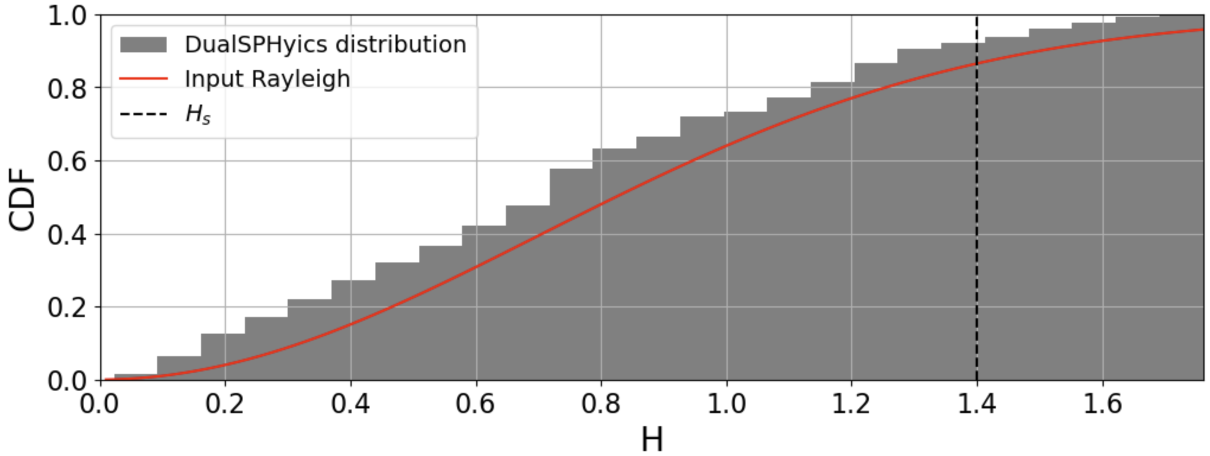

Figure 5.18: Cumulative distribution wave heights one seed (configuration 15, H_s/L_{op} = 0.047, d_{wq}/L_{op} = 0.04, L_{quay}/L_{op} = 0.15, h_{sw}/L_{op} = 0.077)

The tail of the distribution is made visible in Figure 5.19. Here the Rayleigh and DualSPHysics distributions are shown in a semi-log plot. On the vertical axis 1 divided by the probability of observing the wave height on the horizontal axis is shown. The DualSPHysics model shows a good fit for the lower waves, but some deviations occur at the larger wave heights when comparing with Rayleigh. The DualSPHysics distribution becomes steeper as the high wave heights are barely observed.

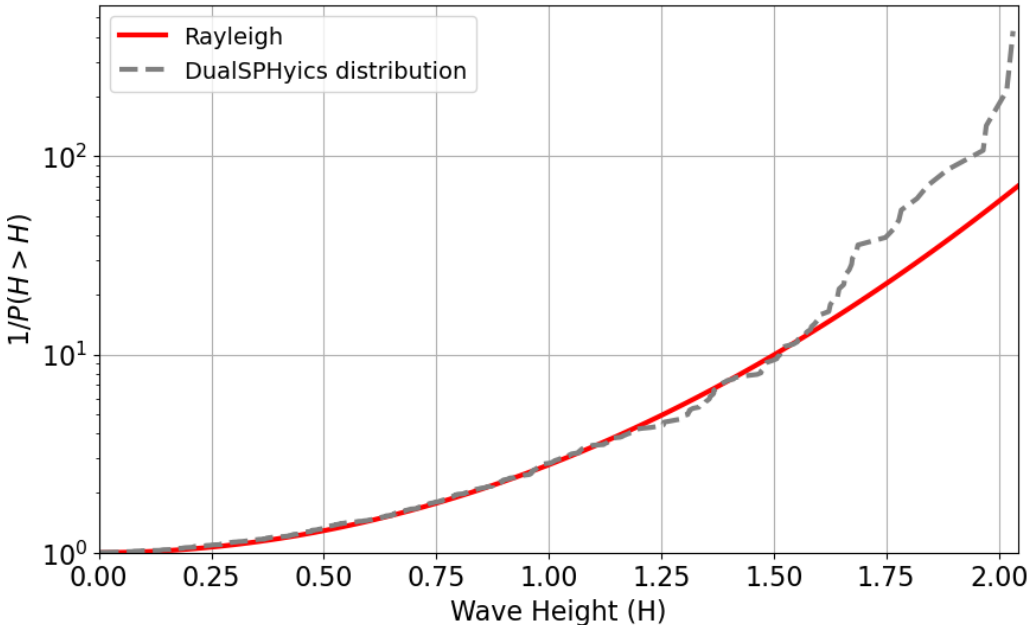

Figure 5.19: DualSPHysics and Rayleigh distributions, one divided by probability of wave height occurrence

The distribution of the dimensionless wave forcing is shown in Figure 5.20. The wave force distribution differs from the wave height distribution shape in Figure 5.17. There are more lower values in comparison with the wave height. This is because not all waves of the same wave height give the same wave force. Some might interact with water flowing back causing the wave to break earlier, causing a lower force.

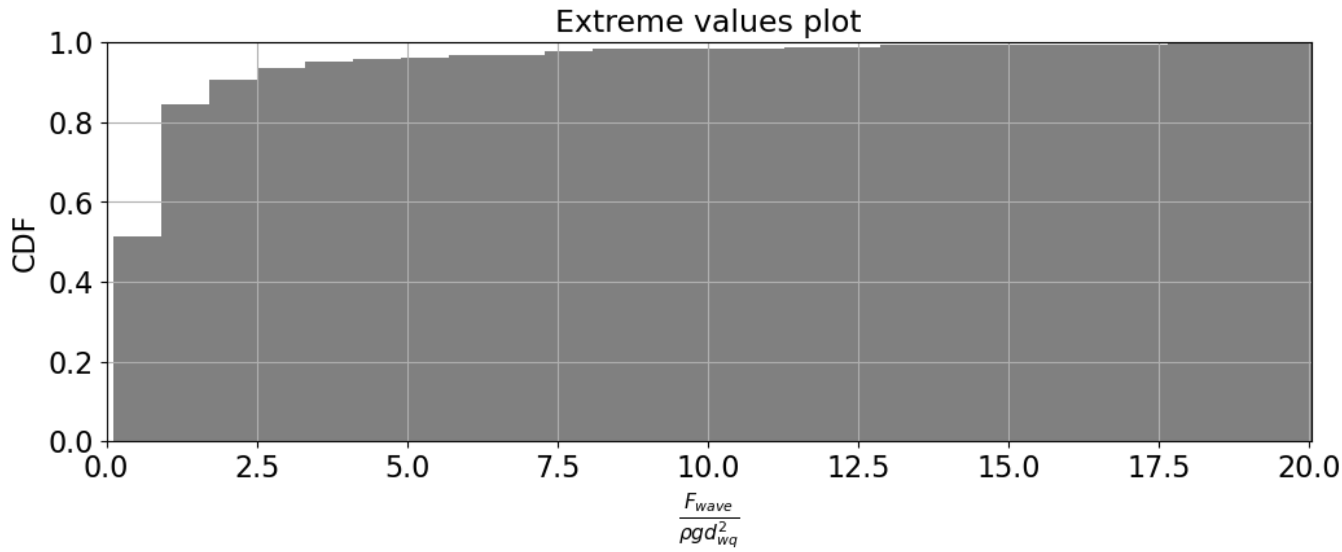

Figure 5.20: Cumulative distribution wave force two seeds seed (configuration 15, H_s/L_{op} = 0.047, d_{wq}/L_{op} = 0.04, L_{quay}/L_{op} = 0.15, h_{sw}/L_{op} = 0.077)

Wave pressure: configuration results

Figure 5.21 and 5.22 show the results of the model with regular incoming waves for H / L = 0.047 and H / L = 0.02 respectively. The figures show the dimensionless highest 1% pressure ($p_{1\%}$) on the storm wall, averaged over the storm wall heights. All the values per simulation can be found in Appendix D: Configurations and results DualSPHysics.

In Figure 5.21, H_s / L_{op} = 0.047, the highest pressure corresponds with the breaking waves observed. In Figure 5.22, H_s / L_{op} = 0.02, there are no breaking waves observed, which explains the small range in the pressure magnitude. When there are no breaking waves occurring, setting the storm wall back apparently does not lead to an increase in the pressure.

Overall, the pressure magnitude of irregular waves is about a factor 2 to 5 lower than for regular waves. The large difference is likely caused by the relative short simulation duration. The very extreme wave height is therefore not always observed. As can be seen in Figure 5.17, a wave height which is twice as large as H_s, which is the value used for H_{max} of the regular waves, is not observed. Because the pressure might not be linear to the wave height, but quadratic or exponential for example, the difference between regular and irregular wave pressure can be larger than a factor 2.

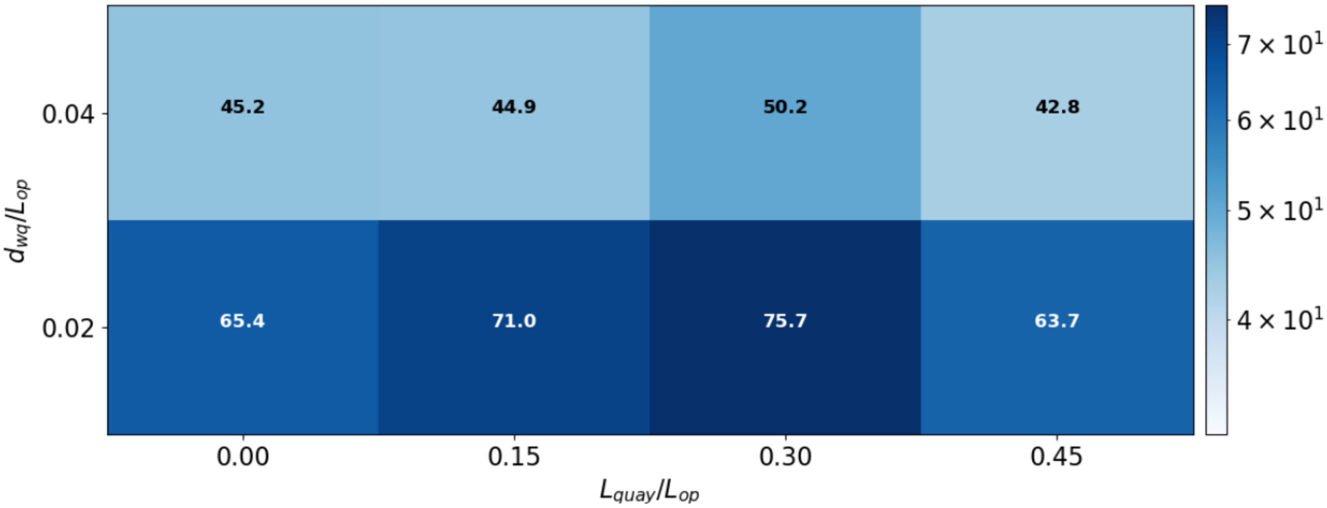

Figure 5.21: Dimensionless pressure($p_{1\%}$ / ($\rho_w g d_{wq}$)) on storm wall for H_s / L_{op} = 0.047

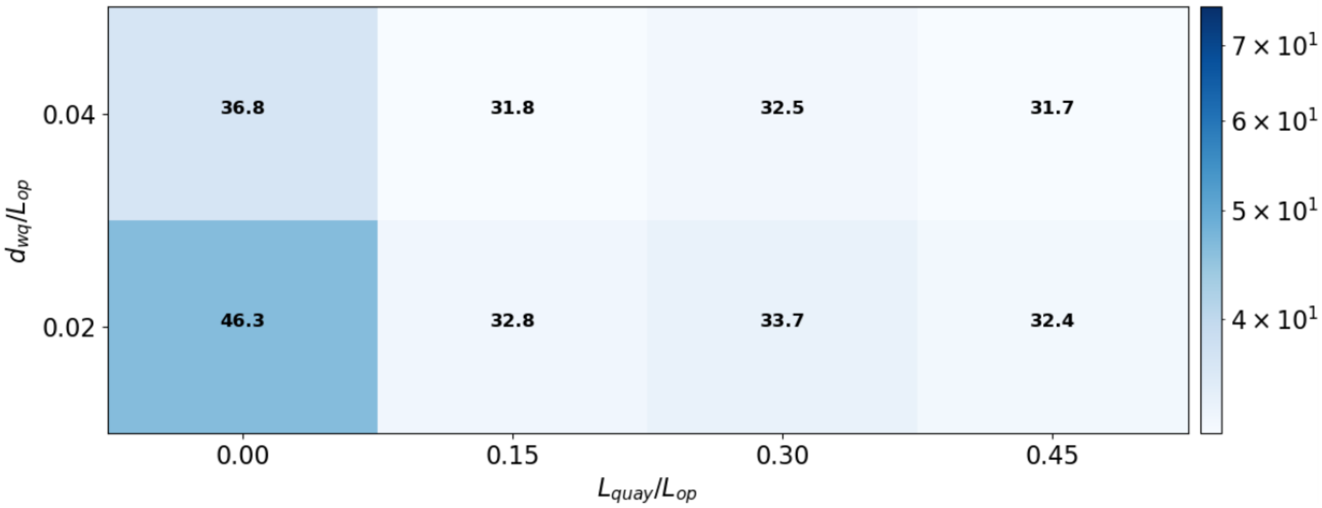

Figure 5.22: Dimensionless pressure($p_{1\%}$ / ($\rho_w g d_{wq}$)) on storm wall for H_s / L_{op} = 0.02

The influence of the height of the storm wall is shown in Figure 5.23 and 5.24 for the two different wave steepnesses. For both wave steepness, the storm wall height does not play a role. The pressure stays around the same value. Because the waves are less high, overtopping barely occurs, so an increase in storm wall height does not change the pressure.

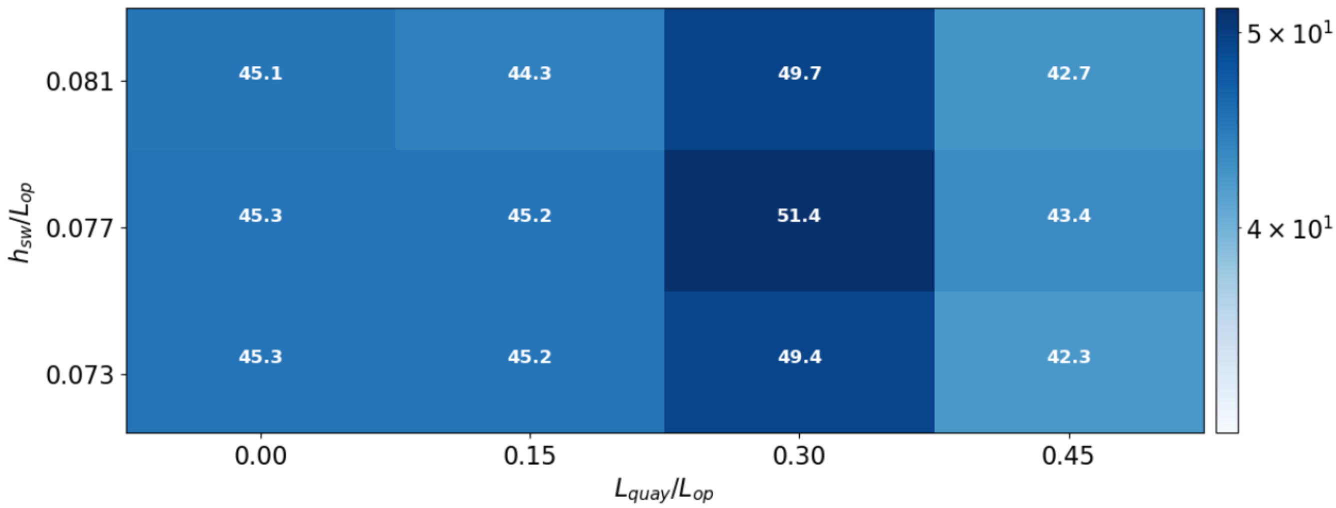

Figure 5.23: Dimensionless pressure($p_{1\%}$ / ($\rho_w g d_{wq}$)) on storm wall for H_s / L_{op} = 0.047, d_{wq} / L = 0.04

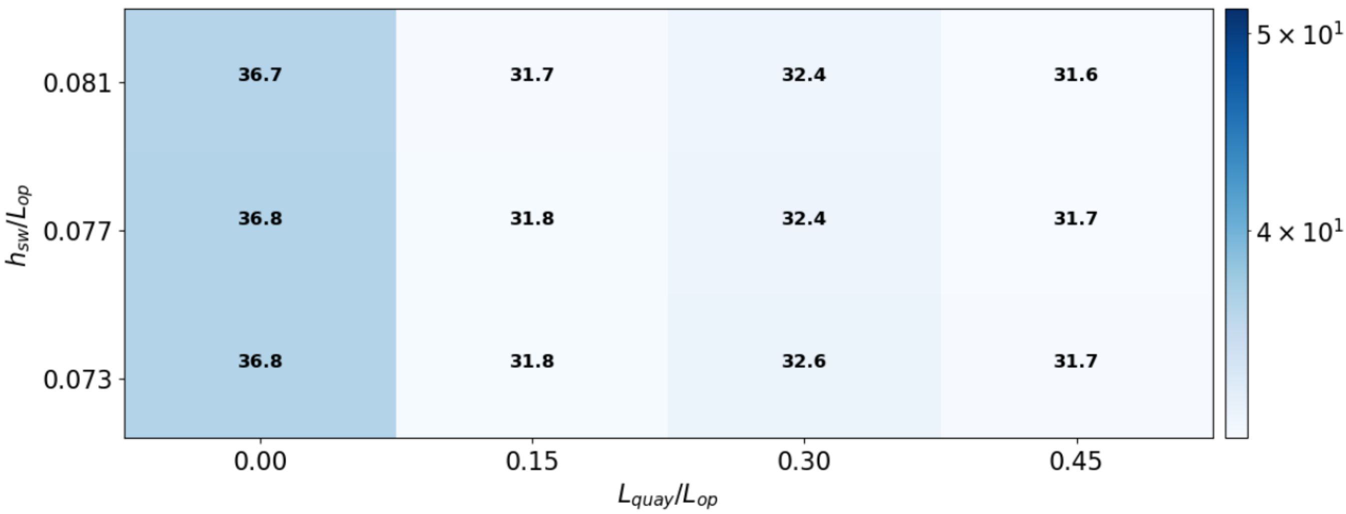

Figure 5.24: Dimensionless pressure($p_{1\%}$ / ($\rho_w g d_{wq}$)) on storm wall for Hs / Lop = 0.02, d_{wq} / L = 0.04

Chapter 6 Comparison physical and numerical model

This chapter compares the lab experiment and the DualSPHysics model, combining the previous two chapters. Since the lab experiment only contained regular waves, it is only compared to the regular wave output of the DualSPHysics model. Besides comparing, explanations are given for the differences. This chapter starts with the comparison of the occurring wave types. After that, the wave breaking boundaries are compared.

6.1 Wave types

To qualitatively verify the numerical model, a physical model is made. In both models, the type of waves occurring are observed, leading to Figure 6.1. Here, the results of the physical model are indicated with rectangles, while the numerical model results are indicated with stars. Overall the numerical model fits the laboratory results well. Only one point, indicated with a red circle and arrow, does not seem to fit the laboratory result at first sight. This point is a breaking wave, but it is expected to be a slightly breaking wave, because the closest laboratory point is a slightly breaking wave. However, if one plots the breaking wave ranges as well, as done in Figure 6.2, one sees that the point falls within the wave breaking range. Therefore, it is likely not an outlier after all.

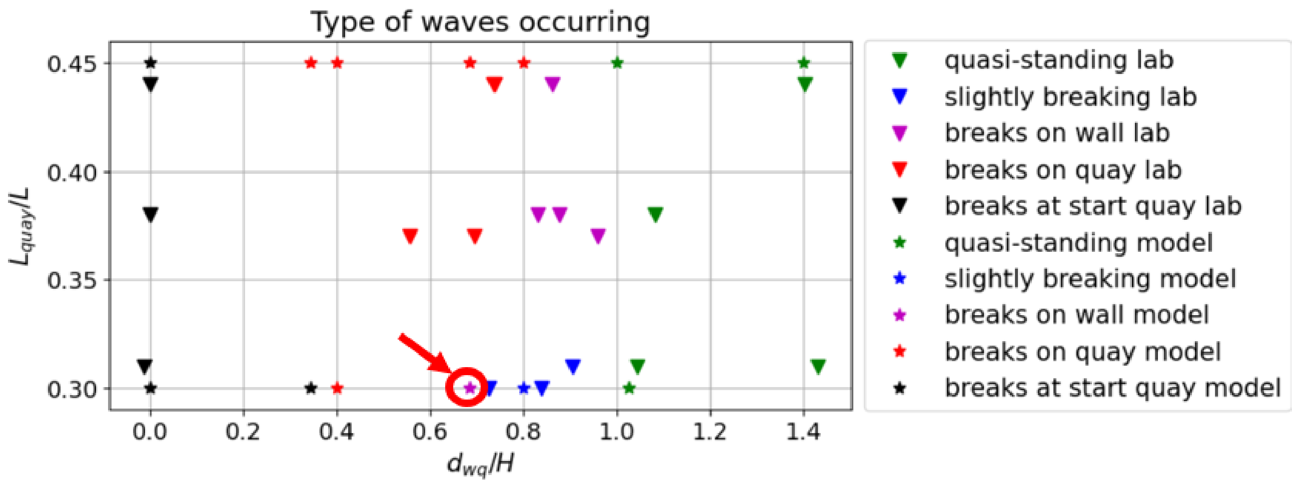

Figure 6.1: Laboratory experiment and numerical model results with one seeming outlier (indicated with red circle & arrow)

6.2 Breaking wave range

Figure 6.2 shows the breaking wave ranges of both the laboratory experiment, light grey, and the numerical model, dark grey. The range generated by the lab is wider as more breaking waves are observed in the laboratory experiments than in the numerical model. The breaking wave range generated by the model does however still fit within the wave breaking range of the lab. This indicates that the DualSPHysics model is able to correctly predict the occurring wave type.

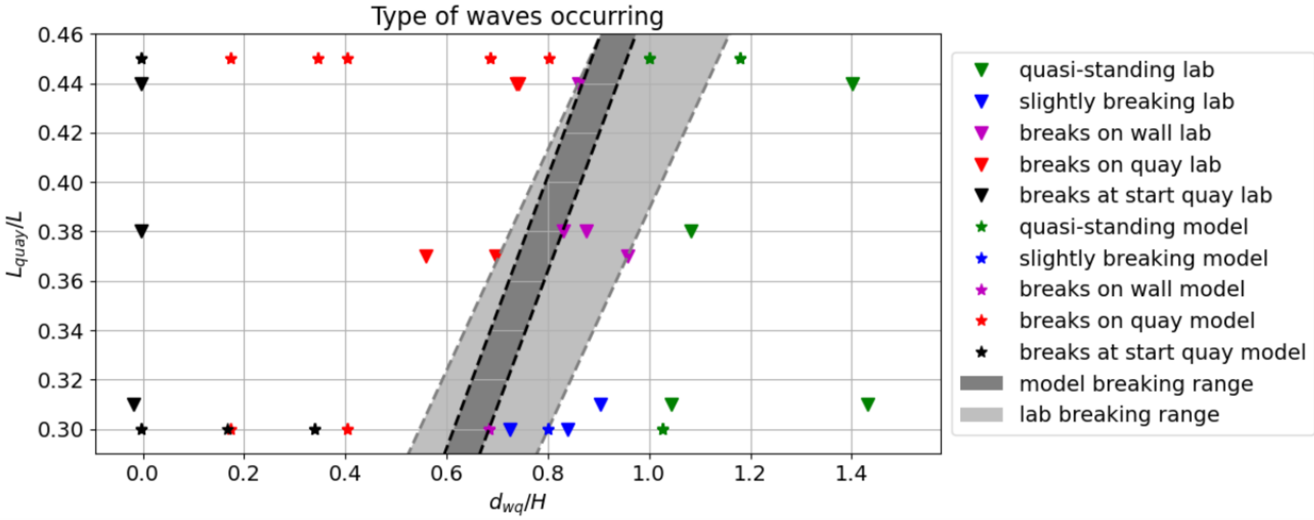

Figure 6.2: Laboratory experiment and numerical model results and breaking wave ranges

Chapter 7 Comparison results and theory

This chapter compares the results of the laboratory experiment and DualSPHysics model to expectations to the theory and new force calculating methods discussed in Chapter 2 and Chapter 3 respectively. Firstly, the wave breaking ranges are discussed. Next, the wave forcing predicted by the numerical model will be compared to the approximations given by force computation methods. Lastly, a conclusion is made which theory is best applicable for which range of parameters.

7.1 Breaking wave range

The laboratory experiment and DualSPHysics model both give a breaking wave range where waves are breaking on the storm wall. Outside of the range you have broken, slightly breaking or quasi-static waves. When a certain wave type occurs at a vertical breakwater is described by the parameter map (Kortenhaus & Oumeraci, 1998). The type of breakwater is based on the ratio of the height of the berm and the water level in front of the berm. If the quay with retreated storm wall is treated as a vertical breakwater where the quay is the berm, this research would contain high mound composite breakwaters (d_{wq} / L ≤ 0) and crown walls rubble mound breakwaters (d_{wq} / L > 0), see Figure 7.1.

The parameter map predicts only broken waves for zero or positive freeboard. This is both observed at the laboratory experiment and the DualSPHysics model. For the negative freeboard the parameter map indicates the type of waves occurring with the ratio of the wave height and the water depth in front of the berm. The waves in this research are deep water waves and therefore all small waves according to the parameter map in Figure 7.1. The parameter map only predicts slightly breaking waves in this case, while breaking and broken waves are observed in the models as well. This difference is likely caused by the fact that the breakwaters have a sloping berm, while the quay is vertical. The waves in the models suddenly enter shallow water while the waves considered in the parameter map experience a gradually decreasing depth. The waves in the models therefore are suddenly very high waves in comparison with the water depth on the quay which causes them to break. Therefore, the numbers in the parameter map for vertical breakwater do not seem to be applicable for a vertical quay with a retreated wall. However, the pattern of wave types occurring is similar. For smaller waves (larger d_{wq} / H) only slightly breaking and quasi-standing waves are observed independent of the quay length. For larger waves the type of waves occurring depends on the width of the berm, where a narrow berm is more likely to cause slightly breaking waves and a wider berm is more likely to cause broken waves.

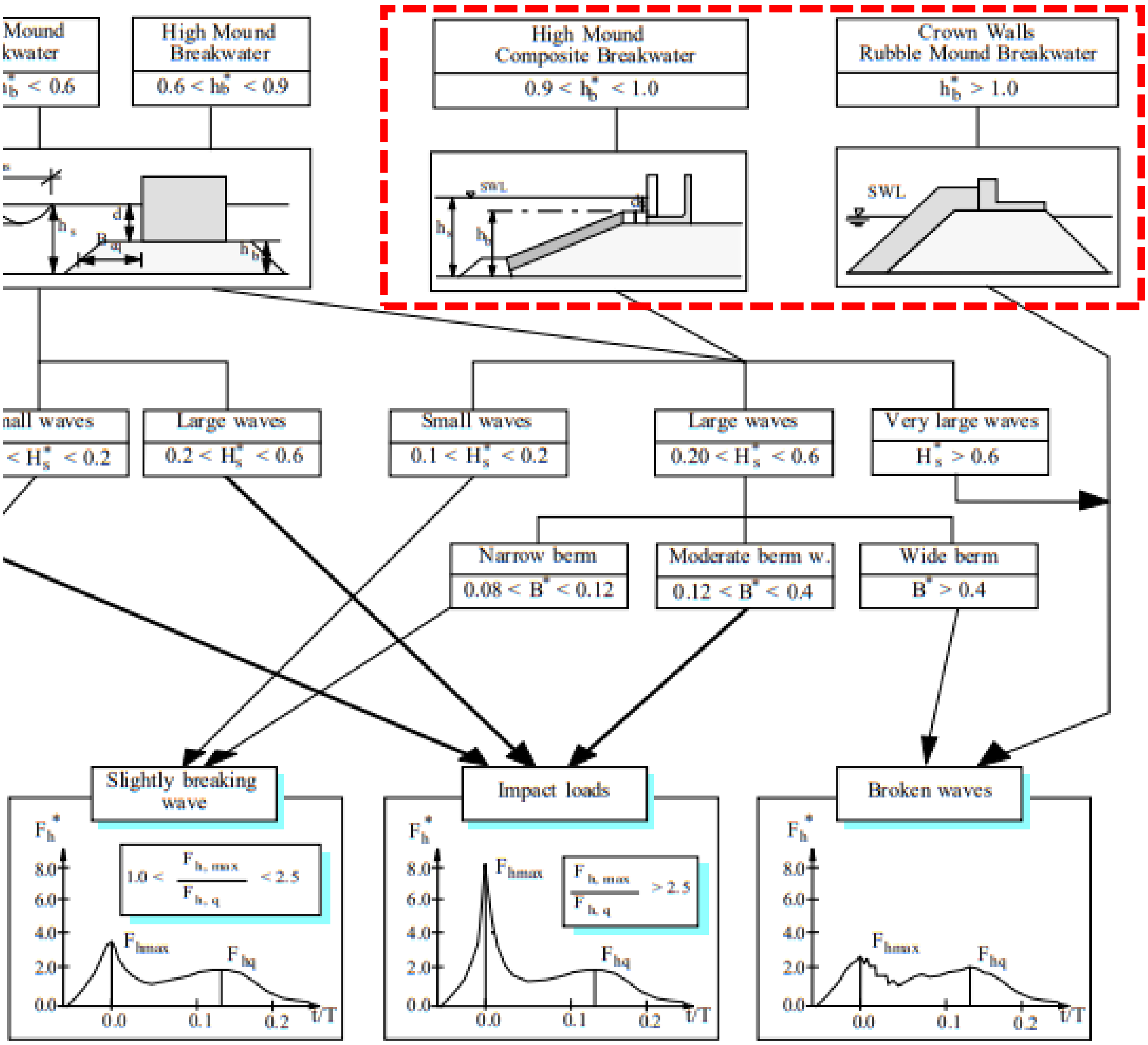

$$\text{with } h_b^* = \frac{h_b}{h_s};\; H_s^* = \frac{H_s}{h_s};\; B^* = \frac{B_{eq}}{L};\; F_h^* = \frac{F_h}{\rho \cdot g \cdot H_b^2}$$

Figure 7.1: Right side parameter map, Kortenhaus & Oumeraci (1998)

7.2 Wave forcing: regular waves

The wave forcing obtained from the numerical model is compared with five theories. These theories consist of existing theories (Tuin, Den Heijer, Cooker-Peregrine) and adaptions of existing theories (adapted Tuin, Goda with quay as berm). Figure 7.2 and 7.3 show the relative root mean squared error (RMSE) and the relative error respectively. The values are shown in Table 7.1 and 7.2. Here only the results for d_{wq} / L > 0 are shown, as lower values often led to numerical errors in the model. In addition only the results for L_{quay} / L > 0 are shown, as standing waves, occurring at L_{quay} / L = 0, are not interesting for the maximum wave force. In Appendix H: Wave forcing computed with theories, the results for L_{quay} / L = 0 are shown as well, showing that the linear standing wave theory performs best as expected. The linear standing wave is not treated here, as the previous results already have shown that these do not occur for the highest forcing.

For 0.15 ≤ L_{quay} / L ≤ 0.30 the highest impacts are observed. The formulas which are based on an impact force on the storm wall, i.e. Den Heijer, Tuin, adapted Tuin and Cooker-Peregrine, perform the best. For Cooker-Peregrine multiple versions are tried as explained in Chapter 2. It appeared that

using the shallow water approximation for the velocity and an impulse duration of 0.05 s gave the best result. This is the brown line shown in Figure 7.2 and 7.3.
For L_{quay} / L = 0.45 broken waves are observed. The Tuin and adapted Tuin formulas appear not suitable for this situation, overestimating the force. The other methods provide more accurate estimations.

With regard to computing impact waves ($0.15 \leq L_{quay} / L \leq 0.30$) only the adapted Tuin formula gives an overestimation, while the other methods give underestimations. For Tuin and Den Heijer the underestimations are the smallest. This is expected, as these methods are all specifically made for the scenario of a retreated storm wall on a vertical quay, while the others (Goda and Cooker-Peregrine) are not.

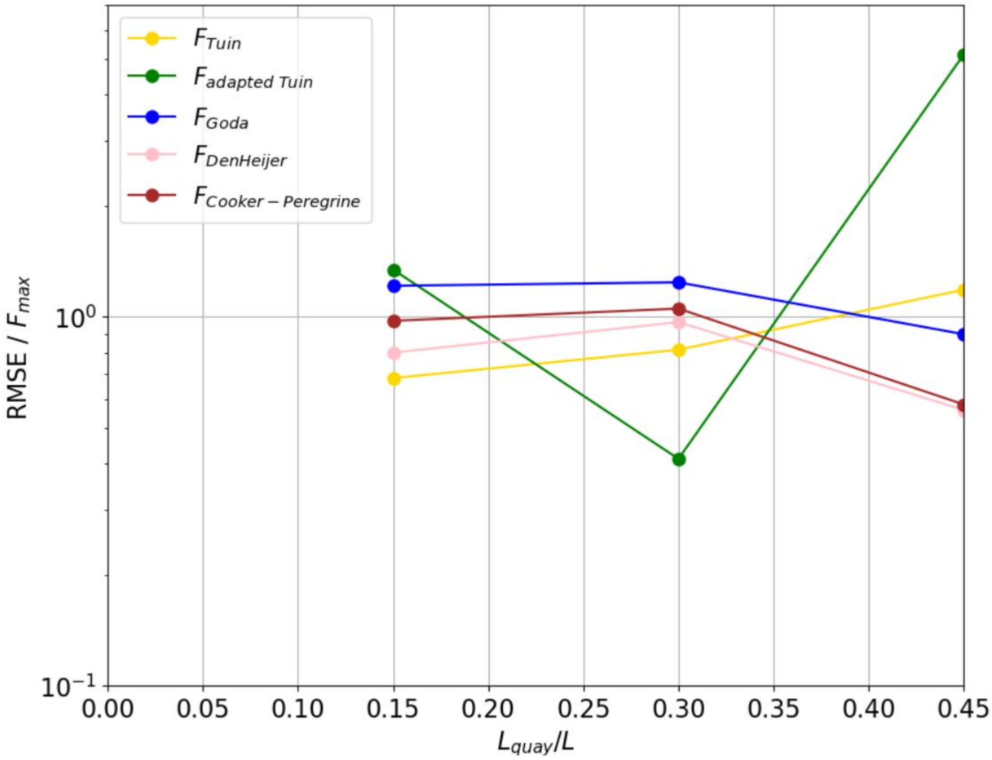

Figure 7.2: RMSE theories with respect to maximum regular wave horizontal force in DualSPHysics per relative quay length

Table 7.1: RMSE theories with respect to maximum regular wave horizontal force in DualSPHysics per relative quay length

L_{quay} / L	0.15	0.30	0.45
F_{Tuin}	0.68	0.82	1.19
$F_{adapted\ Tuin}$	1.34	0.41	5.15
F_{Goda}	1.22	1.24	0.90
$F_{DenHeijer}$	0.80	0.97	0.56
$F_{Cooker-Peregrine}$	0.97	1.05	0.89

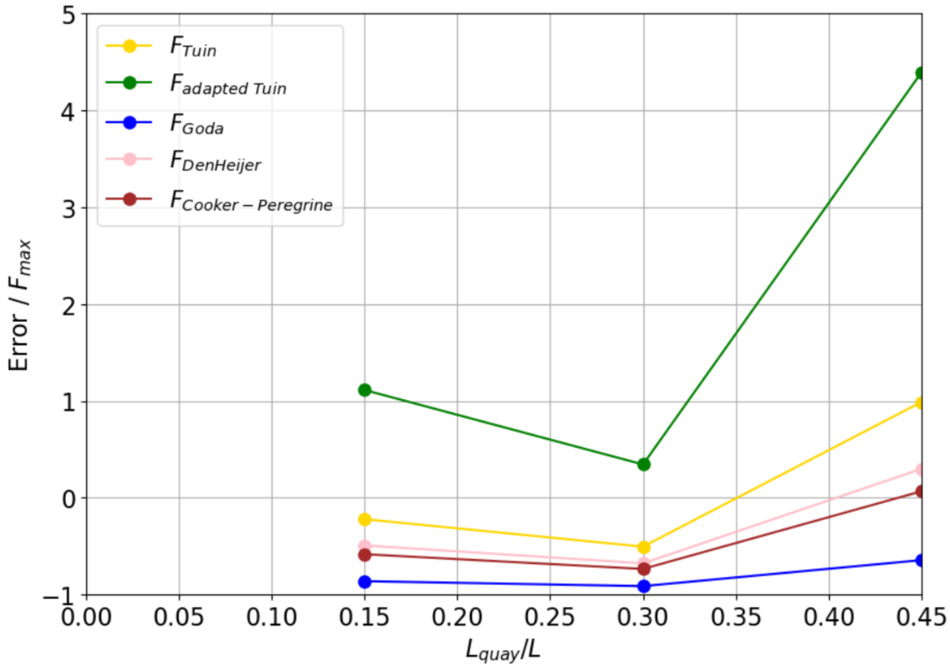

Figure 7.3: Error theories (theory - F_{max}) with respect to maximum regular wave horizontal force in DualSPHysics per relative quay length

Table 7.2: Error theories (theory - F_{max}) with respect to maximum regular wave horizontal force in DualSPHysics per relative quay length

L_{quay} / L	0.15	0.30	0.45
F_{Tuin}	-0.22	-0.50	0.99
$F_{adapted\ Tuin}$	1.11	0.34	4.39
F_{Goda}	-0.86	-0.91	-0.64
$F_{DenHeijer}$	-0.49	-0.68	0.30
$F_{Cooker-Peregrine}$	-0.58	-0.73	0.07

When looking at other parameters, similar patterns are visible. Figure 7.4 and 7.5 show the relative root mean squared error (RSME) and the relative error respectively with the relative depth (d_{wq} / H) on the horizontal axis instead of the relative quay length. The values can be found in Table 7.3 and 7.4.

Here for lower d_{wq} / H, where broken or breaking waves are expected, the formulas which are based on an impact force on the storm wall again perform the best. With higher values of d_{wq} / H slightly breaking and quasi-standing waves occur more often and these formulas perform worse. Again the adapted Tuin method is the only method which continuously gives an overestimation. For the region where impact waves are expected (d_{wq} / H < 0.35) the Tuin and Den Heijer method again give the smallest underestimation.

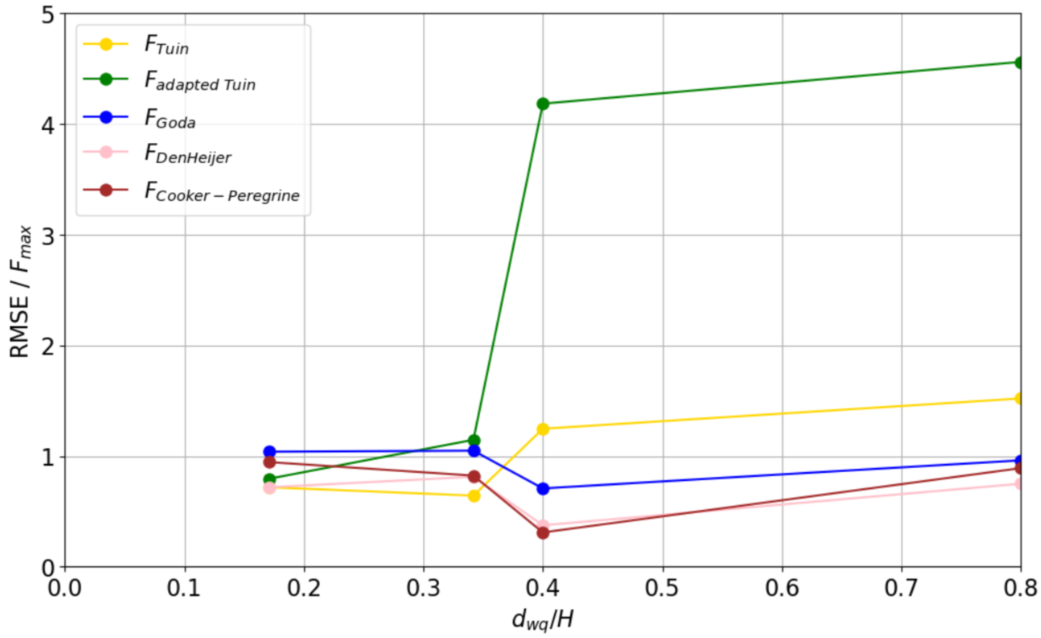

Figure 7.4: RMSE theories with respect to maximum regular wave horizontal force in DualSPHysics per relative quay water depth

Table 7.3: RMSE theories with respect to maximum regular wave horizontal force in DualSPHysics per relative quay water depth

d_{wq} / H	0.17	0.34	0.40	0.80
F_{Tuin}	0.72	0.64	1.25	1.52
$F_{adapted\ Tuin}$	0.79	1.15	4.18	4.56
F_{Goda}	1.04	1.05	0.70	0.96
$F_{DenHeijer}$	0.72	-0.81	0.37	0.75
$F_{Cooker-Peregrine}$	0.95	0.82	0.31	0.89

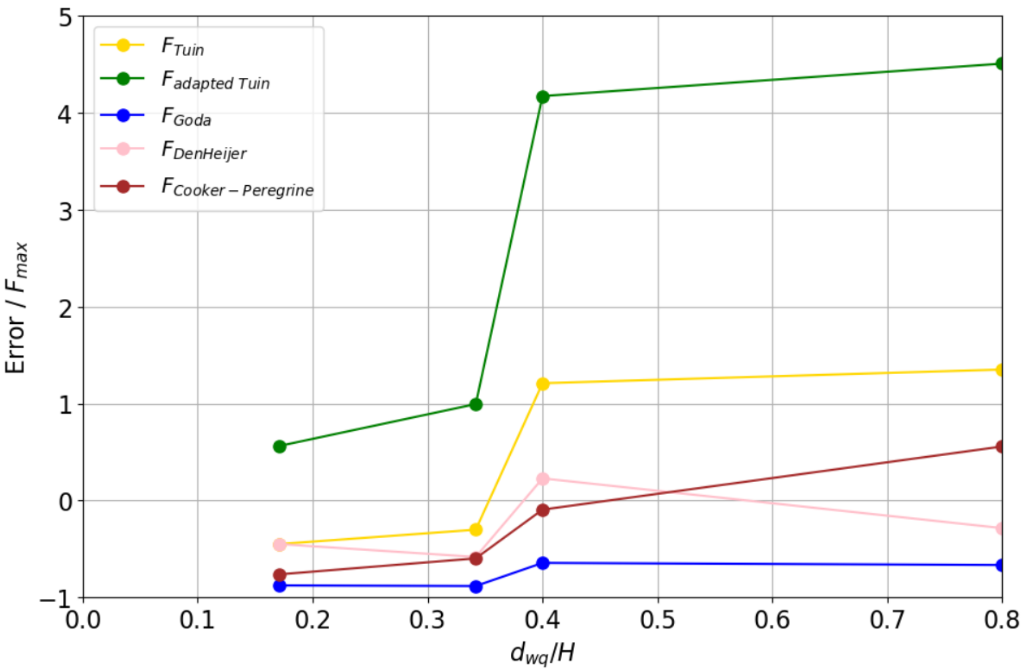

Figure 7.5: Error theories (theory - F_{max}) with respect to maximum regular wave horizontal force in DualSPHysics per relative quay water depth

Table 7.4: Error theories (theory - F_{max}) with respect to maximum regular wave horizontal force in DualSPHysics per relative quay water depth

d_{wq} / H	0.17	0.34	0.40	0.80
F_{Tuin}	-0.45	-0.30	1.21	1.35
$F_{adapted\ Tuin}$	0.56	0.99	4.17	4.51
F_{Goda}	-0.88	-0.88	-0.64	-0.66
$F_{DenHeijer}$	-0.45	-0.58	0.23	-0.28
$F_{Cooker\text{-}Peregrine}$	-0.76	-0.60	-0.09	0.56

7.3 Wave forcing: irregular waves

For the irregular waves, the same five theories as for the regular waves are used. Instead of H and L, the values for H_s and L_{op} are used respectively. Figure 7.6 and 7.7 show the relative root mean squared error (RSME) and the relative error respectively. The values are shown in Table 7.5 and 7.6.

For 0.15 ≤ L_{quay} / L ≤ 0.30 the highest impacts are observed. The formulas which are based on an impact force on the storm wall, i.e. Den Heijer, Tuin, adapted Tuin and Cooker-Peregrine, perform the best. But, with respect to regular waves the Tuin and adapted Tuin formulae perform worse for L_{quay} / L = 0.15. Tuin now consequently overestimates the force, just as adapted Tuin. For Cooker-Peregrine multiple versions are tried as explained in Chapter 2. It appeared that using the shallow water approximation for the velocity and an impulse duration of 0.05 s gave the best result, same as for regular waves.

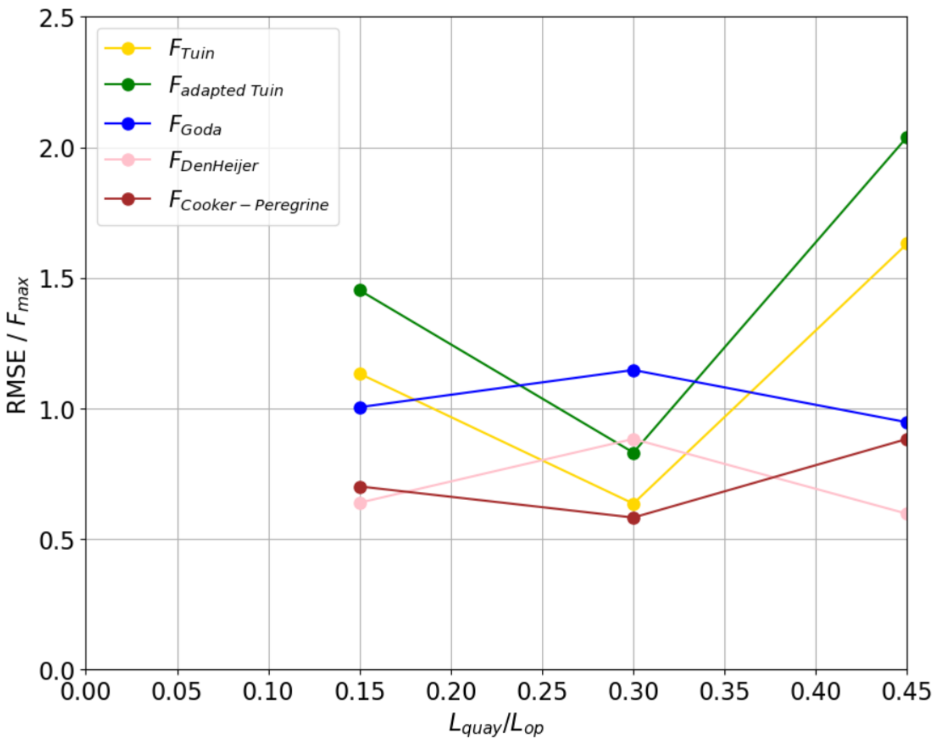

Figure 7.6: RMSE theories with respect to maximum irregular wave horizontal force in DualSPHysics per relative quay length

Table 7.5: RMSE theories with respect to maximum irregular wave horizontal force in DualSPHysics per relative quay length

L_{quay} / L_{op}	0.15	0.30	0.45
F_{Tuin}	1.13	0.63	1.63
$F_{adapted\ Tuin}$	1.45	0.83	2.04
F_{Goda}	1.00	1.14	0.95
$F_{DenHeijer}$	0.64	0.88	0.60
$F_{Cooker\text{-}Peregrine}$	0.70	0.58	0.88

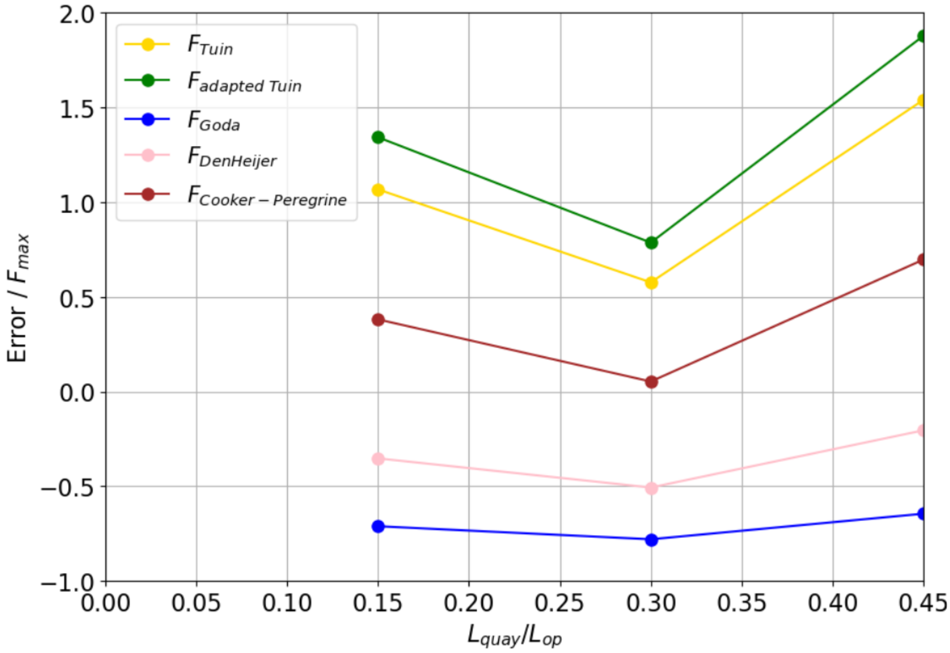

Figure 7.7: Error theories (theory - F_{max}) with respect to maximum irregular wave horizontal force in DualSPHysics per relative quay length

Table 7.6: Error theories (theory - F_{max}) with respect to maximum irregular wave horizontal force in DualSPHysics per relative quay length

L_{quay} / L_{op}	0.15	0.30	0.45
F_{Tuin}	1.07	0.58	1.54
$F_{adapted\ Tuin}$	1.34	0.79	1.88
F_{Goda}	-0.71	-0.78	-0.64
$F_{DenHeijer}$	-0.35	-0.50	-0.20
$F_{Cooker-Peregrine}$	0.38	0.05	0.70

When looking at other parameters, similar patterns are visible. Figure 7.8 and 7.9 show the relative root mean squared error (RSME) and the relative error respectively with the relative depth (d_{wq} / H) on the horizontal axis instead of the relative quay length. The values can be found in Table 7.7 and 7.8.

Here for lower d_{wq} / H, where broken or breaking waves are expected. The formulas which are based on an impact force on the storm wall again perform the best. With higher values of d_{wq} / H quasi-standing waves occur more often and these formulas perform worse. Again Tuin consequently gives an overestimation.

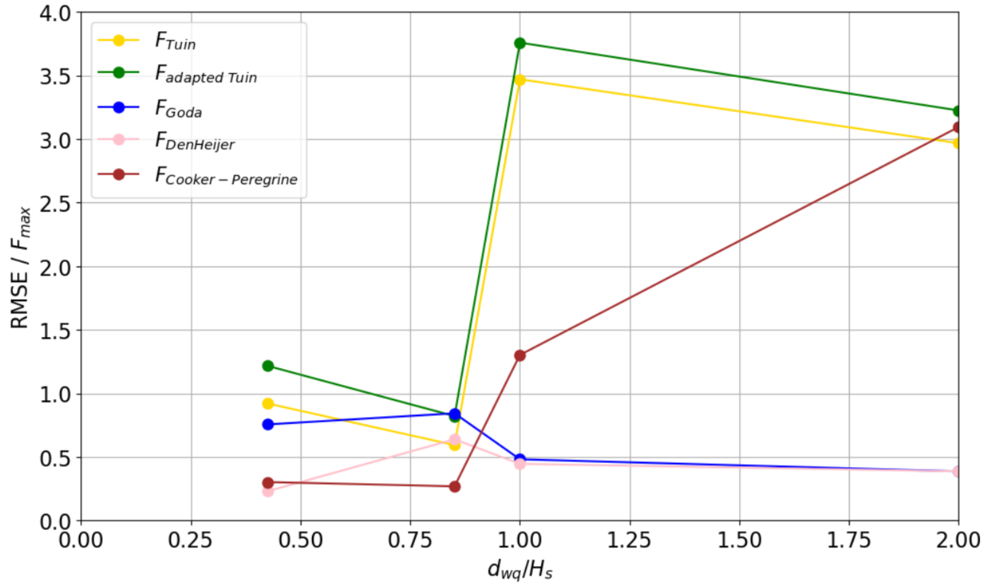

Figure 7.8: RMSE theories with respect to maximum irregular wave horizontal force in DualSPHysics per relative quay water depth

Table 7.7: RMSE theories with respect to maximum irregular wave horizontal force in DualSPHysics per relative quay water depth

d_{wq} / H_s	**0.43**	**0.85**	**1.0**	**2.0**
F_{Tuin}	0.92	0.59	3.47	2.97
$F_{adapted\ Tuin}$	1.22	0.82	3.76	3.23
F_{Goda}	0.76	0.84	0.48	0.38
$F_{DenHeijer}$	0.23	0.64	0.45	0.39
$F_{Cooker\text{-}Peregrine}$	0.30	0.27	1.30	3.10

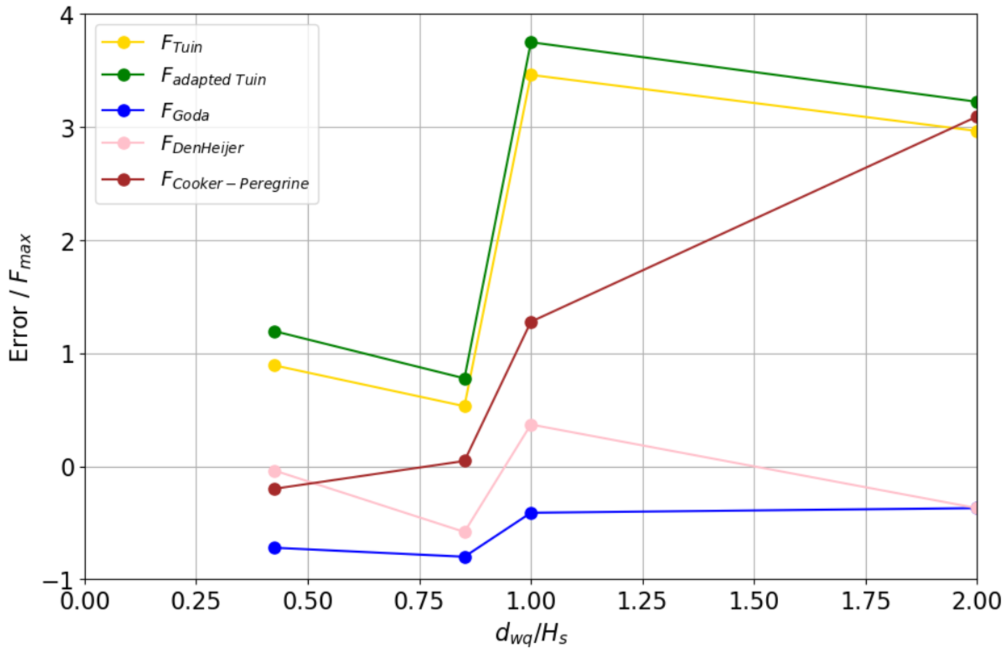

Figure 7.9: Error theories (theory - F_{max}) with respect to maximum irregular wave horizontal force in DualSPHysics per relative quay water depth

Table 7.8: Error theories (theory - F_{max}) with respect to maximum irregular wave horizontal force in DualSPHysics per relative quay water depth

d_{wq} / H_s	0.43	0.85	1.0	2.0
F_{Tuin}	0.89	0.53	3.46	2.97
$F_{adapted\ Tuin}$	1.19	0.78	3.75	3.22
F_{Goda}	-0.72	-0.80	-0.41	-0.37
$F_{DenHeijer}$	-0.04	-0.58	0.37	-0.37
$F_{Cooker-Peregrine}$	-0.20	0.05	1.28	3.09

7.4 Best fitting theories

In the regions where impact waves are expected, the Den Heijer, Tuin, adapted Tuin and Cooker-Peregrine formula perform the best. On average the Tuin formula performs the best out of these four for regular waves and Cooker-Peregrine for irregular waves. So noticeably, the adapted Tuin formula does not show a clear improvement with respect to the Tuin formula. The adapted Tuin formula computed the velocity of the impacting water based on Stokes' 3rd order non-linear wave theory, while the Tuin formula uses linear wave theory. The fact that the adapted Tuin formula does not show an improvement, indicates that the largest contributor to the error made by the Tuin formula is not the velocity of the water.

When looking at broken, breaking and slightly breaking wave types in general, the Den Heijer and Cooker-Peregrine formulae seem to fit the best. Even though the Tuin methods makes a smaller error for regular impact waves, it makes a relatively large overestimation for the slightly breaking waves. It also makes consequently an overestimation for irregular waves. Den Heijer and Cooker-Peregrine on the other hand still perform relatively well with slightly breaking waves and irregular waves. However, it should be kept in mind that the irregular wave simulations might be too short. Larger wave forces might occur in a longer simulation, making Tuin better fitting.

To conclude, Den Heijer and cooker-Peregrine provide in general the most accurate force prediction. Note, if impact waves are expected, Tuin might be a better option, as the overestimation provides an estimation on the safer side.

Chapter 8 Fitting

In this chapter formulas will be fitted to the results of the DualSPHysics model. Since the most forcing occurs at $0.15 \leq L_{quay} / L \leq 0.30$, the fitting will be done for this region. The fitting will be done in two ways. First, a simple formula is fitted based on the visible relationship of the points (e.g. exponential, parabolic, etc.). After that, a formula is fitted based on the formulas of Tuin, Den Heijer and Cooker-Peregrine. Lastly, a conclusion will be made which fit is the most suitable.

8.1 Fitting using mathematical relationships

When plotting the dimensionless force against a combination of the dimensionless parameters, one can try to fit a line. There are different combinations possible on the axes (adding, multiplying etc. of dimensionless parameters) and different possible lines to fit (linear, exponential, etc.). Figure 8.1 and 8.2 show the best fits, using an exponential relationship for regular and irregular waves respectively. The other tried methods are a power, a parabola, a fraction, and a logarithmic fit, see Appendix I: Mathematical fits. The exponential however performed the best. The force is made dimensionless using the water depth on top of the quay. The horizontal axis shows a combination of four different ratios.

First, when the quay length is large with respect to the wavelength, the waves are likely to have already broken before reaching the quay, therefore causing a low force. Second, when the storm wall is large, more water can interact with the wall and therefore the force becomes larger. Third, when the water depth on the quay with respect to the wave height is large, the waves are less likely to break, therefore causing a lower force. Last, if the waves wave a high steepness, they are more likely to break therefore causing a higher force.

The relative residuals in Figure 8.1 show that the fit does perform similar for low and high values of the x-axis, but in Figure 8.2 the fit performs worse for low values of the x-axis. Also note that the fit has a complex axis, which makes it difficult to interpret and visualize. Therefore, an attempt with the formulas based on theory is also made.

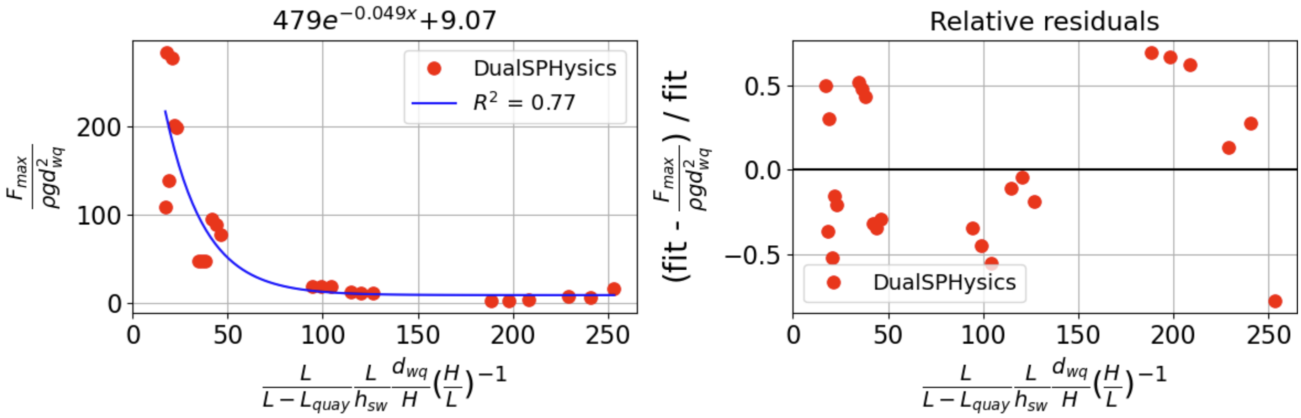

Figure 8.1: Exponential fit (left) and corresponding relative residuals (right), regular waves

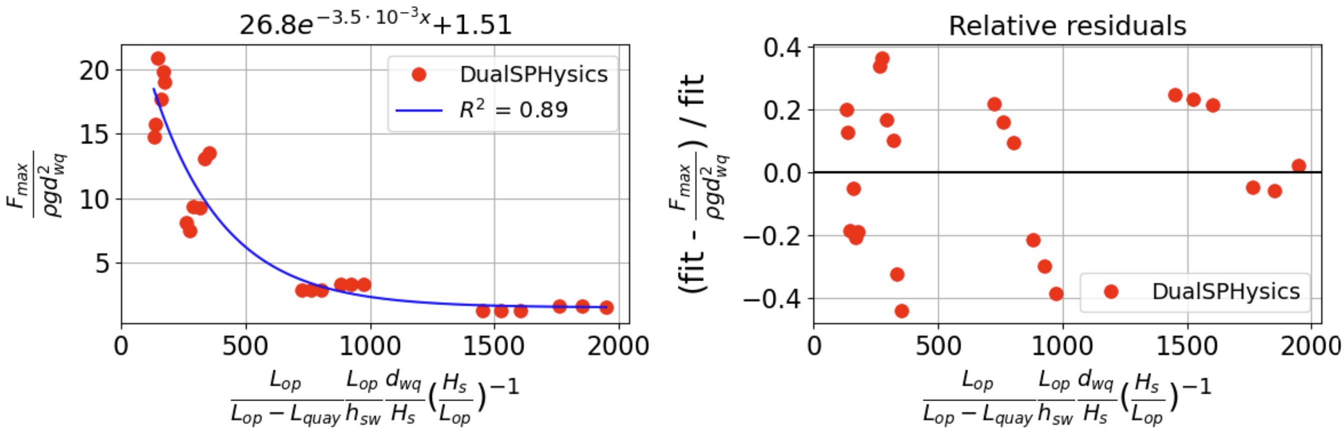

Figure 8.2: Exponential fit (left) and corresponding relative residuals (right), irregular waves

8.2 Fitting using formulas based on theory

In this section the formulas of Tuin, Den Heijer (DH) and Cooker-Peregrine (CP) are fitted to the DualSPHysics data. This is done by multiplying with a coefficient and adding a coefficient. The results are shown in Figure 8.3 and 8.5 for regular and irregular waves respectively. The fits of the three theories and the exponential fit are shown. The legend also shows the Willmott's refined index of agreement, d_r (2012). This is an index to evaluate a model's performance. This index is also used for the validation, see Appendix F: Validation DualSPHysics. The index ranges from -1 to 1, where a value below 0.5 is considered a poor model performance. All methods score above 0.7 for regular waves, which indicates a fairly good fit. For irregular waves the scores are a bit lower, around 0.65.

The Cooker-Peregrine method scores the best out of the theories. Especially in the region 100 – 150 (regular) and 700 – 1300 (irregular) on the horizontal axis the method performs better than others.

The exponential fit does good for both regular and irregular waves. It performs better for irregular waves, while the theories perform worse for irregular waves.

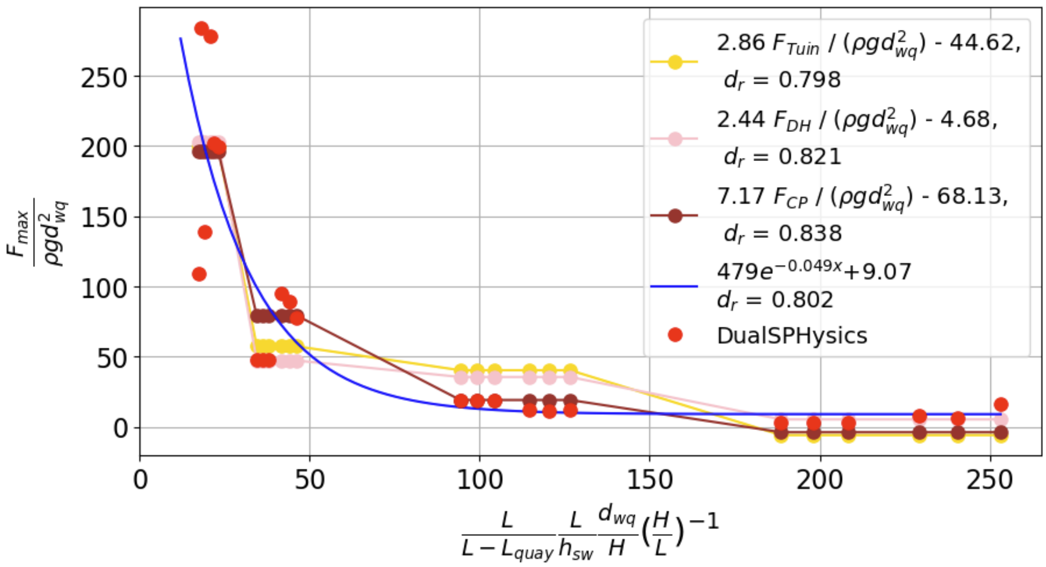

Figure 8.3: Different fits with Willmott's refined index of agreement, regular waves

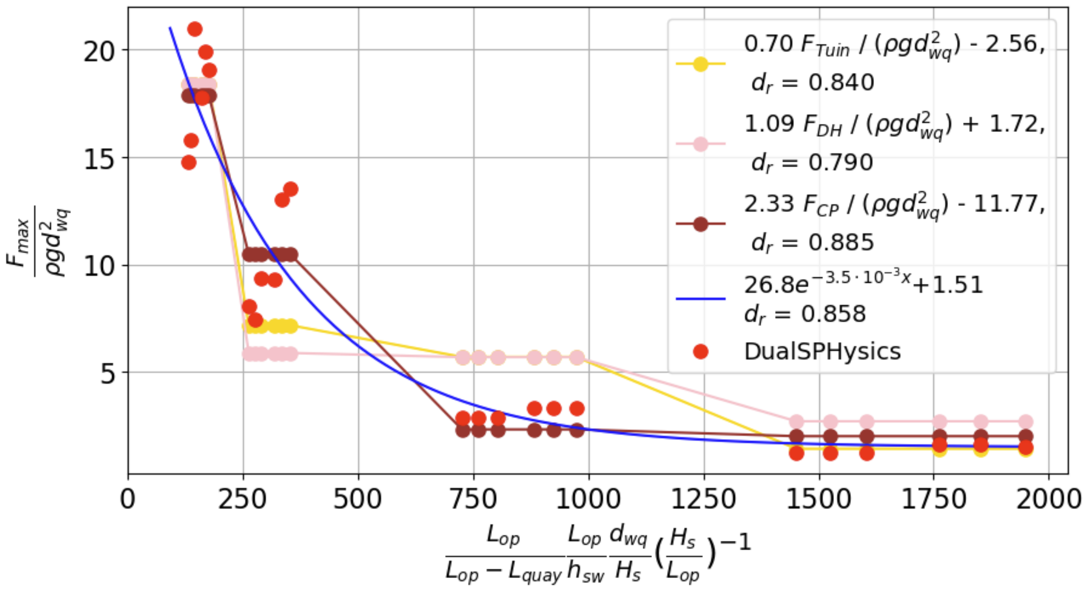

Figure 8.4: Different fits with Willmott's refined index of agreement, irregular waves

8.3 Most suitable fits

In this chapter, fits with mathematical relationships and formulas based on theory were done. The most suitable fits were the exponential fit and the Cooker-Peregrine formula for the two different methods respectively. The methods fit the data fairly good, but they do deviate more for higher forcing. The fits only provide a first rough estimate. Therefore, it is not recommended to use them for the final design without the use of additional safety factors.

Chapter 9 Discussion

This chapter presents a discussion on the study's approaches, highlighting areas for improvement and offering potential solutions. Initially, the limitations of the model are examined, including aspects such as resolution, handling outliers, simulation duration, and the exclusion of air. Subsequently, the applicability of the derived formulas is addressed. Lastly, the laboratory experiment is discussed.

Model resolution

In this study the wave forcing is determined with DualSPHysics. This software makes use of particles representing the water body. The resolution is characterized by the particle distance. With the used particle distance, the number of particles in the smallest layer of water on the quay is 5. This appeared the maximum number of particles per water layer which could be modeled with the available computational resources. This resolution is however likely too coarse. For positive freeboard, less than five particles appear on the quay, often resulting in numerical instability. Numerical instability sometimes also occurs for the negative freeboard with five particles, but these are not frequent and could be removed. For a large negative freeboard with 10 particles on the quay, numerical instability did not occur at all. The needed resolution therefore likely lies between 5 and 10 particles per water depth on the quay.

In this study deep water waves are considered, requiring a large depth in front of the quay, limiting the number of particles which can be used. An attempt was made to reduce the depth in front of the quay, but this appeared to have too much influence on the results. Another solution would be using multi-resolution SPH. DualSPHysics only allows for one particle distance as input, but some other SPH models like SPHinXsys allow for different particle distances in different regions. The particle distance for particles on the quay can then be reduced, creating a better resolution without increasing the computational resources significantly.

Another possible solution is the use of an irregular quay surface. This has been tested for negative and positive freeboard with the same resolution as used throughout the thesis. For negative freeboard, the numerical instability peaks disappear. For positive freeboard they remain, but they are less frequent. See Appendix J: Irregular quay surface, for a more detailed description of this method.

Removing outliers

For every simulation an animation for the largest force is generated. Based on this animation it can be determined if the high peak is caused by a numerical instability or not. If the peak is an outlier caused by numerical instability it is removed. Peaks of similar height are removed as well using the methods described in Chapter 3. The method for regular waves, i.e. removing above the mean plus 3 standard deviations, is commonly used as these points are generally considered as outliers (Andrade, 2021). This method is however not applied for irregular waves. For irregular waves there is a large spread in wave forcing, so the mean plus 3 standard deviations as limit would also remove valid peaks. Instead, the peaks are removed based on large gaps occurring in the tail of the histogram. The method is made up for this research and is not a validated and widely used method. In the irregular waves simulations for the Kop van Zuid case, this histogram method only is applied for one simulation, as others did not show numerical instability. But the histogram method is more often applied for the validation, see Appendix F: Validation DualSPHysics. Therefore, especially the validation should be taken with care. To solve this problem, it is recommended to increase the resolution, for example using a SPH model which allows multi-resolution, to prevent numerical instabilities from occurring at all.

Irregular waves simulation duration
To observe the maximum wave height in an irregular wave simulation, the duration of the simulation should be sufficient. A shorter duration makes the probability of observing the maximum wave height ($2H_s$), which is used for the regular waves simulations, smaller. Due to limited available time and computational resources, the simulations for irregular waves are made shorter than found in the validation. In fact, the simulations are likely too short, as the magnitude of the regular and irregular wave forcing differs with a factor 10. The solution used to overcome storage problems is to run the irregular wave simulations with different seeds. However, due to the limited time left, not as many seeds could be run as desired. It should therefore be taken into account that the irregular wave forcing by the DualSPHysics is likely to give an underestimation of the maximum wave force occurring in the design storm. The solution would be to run more simulations with more seeds for the irregular waves.

Impulse duration: absence of air
DualSPHysics has the option to work with multiple phases, i.e. fluid and air particles. This does however increase the computational requirements like storage and simulation duration. Sato et al. (2021) found that the pressure in a violent flow field can be accurately simulated using a single-phase model as long as the density diffusion parameter is not too large. Because the deep water irregular waves already require large computational resources and a violent flow field should be able to be modeled with a single phase model, a single phase model is used. When looking at the impulse however, small durations are observed with respect to durations observed in another research (Chen et al., 2019; Den Heijer, 1998). Because there is no air to act like a cushion, the impulse duration is likely larger. To validate this, the simulations should be run with the multiple phases option.

Applicability formulas
To estimate the maximum wave force occurring, this study provides formulas. Examples are an exponential fit or the Cooker-Peregrine method with two additional coefficients. Even though the fit of the formulas is fairly good, the fit is made to the model predictions, which contain inaccuracies themselves. Therefore, the methods are only recommended for a rough first estimation of the wave force. Use the wave height according to the standards applicable in the project's country in the formulas for an estimation of the wave force in the conceptual design. For the follow-up designs laboratory experiments or CFD models are recommended for a better force estimation.

Also, the methods are only recommended to use within the values of the dimensionless parameters used in this study. To name a few, the approaching waves should be deep water waves, the water depth on the quay should at least be 0.02 the wavelength and the quay length should be between 0.15 and 0.45 wavelength. All the ranges are shown in Table 3.4 and 3.5.

Accuracy and precision laboratory experiment
For the laboratory experiment, waves are measured using a smartphone camera. Consequently, the wave height and wavelength measurements are limited by the camera's pixel resolution. The pixel size used is 0.66 mm, which is considered sufficient for the used wave heights which are in the order of cm. However, the determination of the pixel size and the location of the water level also contain inaccuracies. More measurements, which are also more precise, can be obtained using wave sensors, if one desired to determine a more precise wave breaking range.

Chapter 10 Conclusions & Recommendations

In this research the wave forcing on retreated storm walls on top of quays is investigated, using a laboratory experiment, empirical and analytical formulae, and the numerical models SWASH and DualSPHysics. The main research question is “What is the influence of the geometry of a retreated storm wall on top of a quay wall on the wave forcing exerted on the storm wall?”

This chapter goes through the results in this report to answer the main research question. After that, recommendations for follow-up research are given.

10.1 Conclusions

In this study both a laboratory experiment as well as a numerical model are used to answer the research questions. This section will go through the sub-questions one by one to finally arrive at the answer to the main research question.

10.1.1 Breaking wave range

First of all it is determined when breaking waves on retreated storm wall are expected, as they give the largest forces. In both the lab experiment as the DualSPHysics model clear clusters of wave types occurring are observed. A linear relationship between the relative quay length (L_{quay} / L) and relative water depth (d_{wq} / H) is found creating a breaking wave range. Above the range, waves which already break at the start of the quay or on the quay are observed, while below the range slightly breaking and quasi-standing waves are observed. The relationship found by the laboratory experiment is described by:

$$upper\ limit: \frac{L_{quay}}{L} = 0.45\frac{d_{wq}}{H} + 0.06 \qquad \text{Equation 10.1}$$

$$lower\ limit: \frac{L_{quay}}{L} = 0.45\frac{d_{wq}}{H} - 0.06 \qquad \text{Equation 10.2}$$

With:

- L_{quay} [m] = Quay length
- L [m] = Wavelength
- d_{wq} [m] = Water depth on top of the quay
- H [m] = Wave height

For the ranges 0.15 ≤ L_{quay} / L ≤ 0.45 and 0.0 ≤ d_{wq} / H ≤ 1.4. Within this range, waves breaking at the storm wall are observed. It is observed that these breaking waves generally lead to the highest forcing. Only for high wave steepnesses (H / L = 0.117) the broken waves can lead to higher forcing, as a lot of water is pushed up, which creates a bore-like water mass, which causes an impact on the storm wall.

10.1.2 Suitability SWASH and DualSPHysics

In this study two numerical models are used, SWASH and DualSPHysics. This suitability of these models is investigated, as they need to be used to obtain credible wave forcing.

SWASH is a non-hydrostatic flow model. It makes uses a grid in the horizontal direction and vertical layers in the vertical direction. This model appears however unsuitable for this research.

Therefore, the main model used this research is DualSPHysics. This is a Smoothed Particle Hydrodynamics model (SPH), which uses particles moving in time and space instead of a grid. The model appears well suitable to simulate different wave types (broken, breaking, slightly breaking and quasi-static) when comparing with the results of lab experiment. In the validation, model parameters are determined and the ability of predicting forces is evaluated by comparing force simulations to measured values in the laboratory experiments of Den Heijer. It appears that the model does well in predicting the highest 1% and 10% forcing of an irregular wave field ($F_{1\%}$ and $F_{10\%}$). The error predicted by the two finest used resolutions did not differ more than 5%pt, with an error magnitude of around 10% and 5% for $F_{1\%}$ and $F_{10\%}$ respectively. However, the maximum wave force is in the validation often overestimated. The poor prediction for the maximum force is likely due to the randomness of irregular waves (sampling error). In addition, the experiments used for the validation contained a relatively coarse measuring frequency which can cause the omission of high peaks in the forcing. Furthermore, the impact duration modelled by the numerical model is thought to be very short, when comparing to impact durations found by Chen et al. (2019). These short impact durations cause a higher force as, the same impulse gives a lower force with a longer duration. Lastly, some high peaks simulated by the numerical model are caused by numerical instability. These are mostly manually removed, but some might have been missed, causing an overestimation of the maximum wave force.

The DualSPHysics model is not able to model positive freeboard, because this often leads to numerical instability, as explained in Chapter 9. A higher resolution is needed to prevent this. Which leads to the last point, namely that the model is computationally expensive. To use it, enough time and storage space are necessary. A GPU is also preferred to speed up the computations.

10.1.3 Differences numerical and physical model

The laboratory experiment is used to validate the type of waves occurring in the numerical model. Thirteen configurations are compared and only one is different. So, the numerical model and the experiment show large correspondence. The laboratory experiment and numerical model do however show differences when generating a breaking wave range. The breaking wave range from the numerical model has a steeper slope and is narrower. The narrowness is caused by the lower number of waves breaking on the wall observed in the simulations than in the experiments. The wave breaking range from the numerical model does however fit in the wave breaking range of the laboratory experiments.

10.1.4 Effect on storm wall height and quay length on wave forcing

To determine the effect of the geometry on the wave forcing, the influence of the quay length and storm wall height on the wave forcing is investigated. Based on the DualSPHysics results, the quay length has a clearer effect on the wave force than the storm wall height. Using a quay length of 0.15 to 0.30 times the wavelength can increase the wave force by approximately a factor 10 in comparison with no quay length, i.e. when the storm wall is placed at the edge of the quay. This increase is caused due the occurrence of breaking waves. This follows from Equation 10.1 and 10.2 for the range of d_w/H simulated. A quay length of 0.45 still causes an increase, but only of around a factor of 2. Here broken waves are observed instead of breaking waves.

The storm wall height did not have a clear influence on the wave forcing. In most cases the effect in changing the storm wall height is negligible. But in some cases, especially with higher waves a different storm wall height leads to a different wave force, changing with a factor 1.2 to 2. How the force changes is not entirely clear. An increase in wall height does not necessary lead to an increase in force. Wave overtopping does occur, but then a higher storm wall is expected to lead to a higher force, as less water overtops the wall and is included in the impact with the storm wall. The differences in patterns likely arise from specific hydrodynamic interactions that occur at particular relative quay lengths, where the wave behaviour (such as reflection, interference, or breaking) leads to non-intuitive results.

10.1.5 Influence freeboard

In this research the influence of a zero and negative freeboard (i.e. a submerged quay) is investigated, as the magnitude of the freeboard can have an influence on the wave breaking and therefore also the wave force. This indeed appears to be the case.

Both the lab experiment and the DualSPHysics model showed that a zero freeboard leads to waves breaking at the start of the quay, while a freeboard larger than the wave height results in quasi-standing waves. Freeboards in between lead to broken, breaking or slightly breaking waves, dependent on the wave height and quay length.

In the DualSPHysics model, a simulation with a twice as high freeboard leads to a higher pressure due to the increase in hydrostatic pressure. But the pressure does not become twice as large. Due to different wave types occurring, a breaking wave at a lower freeboard can cause pressures of similar magnitude as a just broken wave at a twice as high freeboard.

10.1.6 Differences results and simplified methods from literature

To see if there is correspondence with previous found results, the results of this thesis are compared with methods from literature.

The wave forcing is compared to four already existing theories and two adaptations of existing theories. Some of these theories include Den Heijer, which is an empirical fit through small scale lab data, Cooker-Peregrine, which is a field solution for an idealized wave impact which provides the pressure impulse and Tuin (unpublished), which estimates the force based on the conservation of momentum.

When looking at broken, breaking and slightly breaking wave types in general, the Den Heijer and Cooker-Peregrine formulae seem to fit the best. Even though the Tuin methods makes a smaller error for regular impact waves, it makes a relatively large overestimation for the slightly breaking waves. It also makes consequently an overestimation for irregular waves. Den Heijer and Cooker-Peregrine on the other hand still performs relatively well with slightly breaking waves and irregular waves. However, it should be kept in mind that the irregular wave simulations might be too short. Larger wave forces might occur in a longer simulation, making Tuin better fitting. The overall difference between the methods and the model predictions are however still large. The best fitting methods still have differences between 5 and 35%.

Therefore, coefficients are added to the best fitting methods for impact waves, Den Heijer, Tuin and Cooker-Peregrine. When adding coefficients to the different methods the Cooker-Peregrine method becomes the best fitting method. One can also fit a simple formula is fitted based on the visible relationship of the points (e.g. exponential, parabolic, etc.). Here the exponential fit performs the best, but it does not show a significant increase in accuracy compared to the Cooker-Peregrine method with added coefficients.

10.1.7 Main conclusion

The geometry of a retreated storm wall on top of a quay wall is characterized by the quay length and the storm wall height. The quay length appears to have the largest influence as this determines which types of waves occur. When having a quay length of 0.15 to 0.30 times the wavelength a significant increase in wave pressure of around a factor 5 can be expected, due to breaking waves. Making the quay longer leads to broken waves occurring more often with only an increase in wave pressure of a factor 1.1. The exact increase also depends on the relative depth on top of the quay and the wave steepness, as these also influence the type of waves occurring.

The formulas which come closest to the forcing found by DualSPHysics are the Cooker-Peregrine formula with added coefficients and the exponential fit. It should be taken into account that the numerical model itself contains inaccuracies and that the formulas can only be used for a rough first estimation.

10.2 Recommendations

Based on the discussion and conclusions recommendations for follow-up research arise.

First of all, it is recommended to validate the wave forcing with either a full scale laboratory experiment or with a model which allows a higher resolution without requiring a significant increase in computational resources. This can be for example be done by using a model which allows different resolutions in different regions. The use of a multi-phase model would be recommended as well.

Second, it would be interesting to further investigate the coefficients for the Cooker-Peregrine method. This method is fully based on physics and appears the most accurate. The coefficients are now only based on the numerical model simulations which contain uncertainties. Therefore, they are not recommended to be used for designs after the conceptual design. In addition, the Cooker-Peregrine method does not contain the factor L_{quay} / L yet, as the water column length is assumed infinite for this research. The effect of the factor L_{quay} / L is now present in the coefficient. The investigation can be done by simulating more configurations with smaller intervals of the dimensionless parameters and / or a wider range of the dimensionless parameters. This will also provide more precise coefficients and/or a more precise for formula which might be used after the conceptual design.

Third, the influence of positive freeboard on the wave forcing is recommended to investigate. With the used resolution it is not possible to accurately investigate it with DualSPHysics, but a higher resolution, other numerical models or a physical model might be able to provide new insights.

Fourth and last, the influence of the storm wall height is recommended to investigate further. The influence of the storm wall height is less than the other parameters, but its influence is the least intuitive one. The influence can be researched by doing more simulations with smaller intervals between the values of h_{sw} / L.

References

Actueel Hoogtebestand Nederland. (n.d.). *AHN Viewer*. Retrieved 4 January, 2024, from https://ahn.arcgisonline.nl/ahnviewer/

Altomare, C., Domínguez, J.M., Crespo, A.J.C., González-Cao, J., Suzuki, T., Gómez-Gesteir, M. & Troch, P. (2017). Long-crested wave generation and absorption for SPH-based DualSPHysics model. *Coastal Engineering, 127,* 37-54. https://doi.org/10.1016/j.coastaleng.2017.06.004

Amini, M. & Memari, A. M. (2023). CFD Evaluation of Regular and Irregular Breaking Waves on Elevated Coastal Buildings. *International Journal of Civil Engineering*. https://doi.org/10.1007/s40999-023-00898-2

Andrade C. (2021). Z Scores, Standard Scores, and Composite Test Scores Explained. *Indian Journal of Psychological Medicine*, 43(6):555-557. doi:10.1177/02537176211046525

Artes. (2024). Artist impression of automated storm wall in Antwerp [Image]. https://artesgroup.be/werven/mobiele-waterkering-antwerpen

Been, S. (2020). *Smoothed Particle Hydrodynamic Modelling of Wave Impact Title*. Delft: TU Delft, Faculty of Civil Engineering and Geosciences. https://repository.tudelft.nl/islandora/object/uuid:da456924-c5e4-4e93-8780-cc0853850ddc?collection=education

Chen, X., Hofland, B., Molenaar, W., Capel, A., Van Gent, M. R. A. (2019). Use of impulses to determine the reaction force of a hydraulic structure with an overhang due to wave impact. *Coastal Engineering*, 147 (75-88). https://doi.org/10.1016/j.coastaleng.2019.02.003

Cumberbatch, E. (1959). *The impact of a water wedge on a wall*. Department of Mathematics, University of Manchester.

Den Heijer, F. (1998). *Golfoverslag en krachten op verticale waterkeringsconstructies*. Delft Hydraulics. https://repository.tudelft.nl/islandora/object/uuid%3Aeabd2a30-ec31-4c18-b8b6-68bfaf43e6d6

Domínguez Alonso, J. M., Crespo, A. J. C., Gesteira, M. G., Rogers, B. D., Fourtakas, G., Stansby, P., Vacondio, R., Altomare, C., Tafuni, A., Garcia Feal, O., Martinez Estevez, I., O'Connor, J., English, A., Gonzalez Cao, J., Canelas, R., Mokos, A., Longshaw, S. & Barreiro, A. (2023). *SPH formulation*. Github. Retrieved 4 June, 2023, from https://github.com/DualSPHysics/DualSPHysics/wiki/3.-SPH-formulation

DualSPHysics team. (2022). *XML Guide for DualSPHysics*. https://dual.sphysics.org/

Duits, M., Kuijper, B., Rongen, G., Waterman, R., Ansink, J., De Waal, H., Tanis, H., Slomp R. & Van Walsem, T. (2020). *Hydra-NL* (Version 2.8.2) [Computer Software]. https://iplo.nl/thema/water/applicaties-modellen/waterveiligheidsmodellen/hydra-nl/

English, A., Domínguez, J.M., Vacondio, R. Crespo, A. J. C., Stansby, P. K., Lind, S. J., Chiapponi, L. & Gómez-Gesteira, M. (2022). Modified dynamic boundary conditions (mDBC) for general-purpose smoothed particle hydrodynamics (SPH): application to tank sloshing, dam break and fish pass problems. Comp. Part. Mech. 9, 1–15. https://doi.org/10.1007/s40571-021-00403-3

EurOtop, 2018. Manual on wave overtopping of sea defences and related structures. An overtopping manual largely based on European research, but for worldwide application. Van der Meer, J.W., Allsop, N.W.H., Bruce, T., De Rouck, J., Kortenhaus, A., Pullen, T., Schüttrumpf, H., Troch, P. and Zanuttigh, B., www.overtopping-manual.com.

Goda, Y. (1974). New wave pressure formulae for composite breakwater. Proceedings of 14th conference on Coastal Engineering, Copenhagen, Denmark, ASCE, 1702-1720.

Google. (2014). Historical pier San Francisco. Retrieved 6 February 2024 from https://www.google.nl/maps/@37.8037252,-122.3974828,3a,75y,241.47h,98.51t/data=!3m6!1e1!3m4!1sEX8GkKoz0BADMpvMt-BuUQ!2e0!7i13312!8i6656?entry=ttu

Gruwez, V., Altomare, C., Suzuki, T., Streicher, M., Cappietti, L., Kortenhaus, A. & Torch, P. (2020). An Inter-Model Comparison for Wave Interactions with Sea Dikes on Shallow Foreshores. *Journal of Marine Science and Engineering, 8,* 985-1022. doi:10.3390/jmse8120985

Hasselmann, K., T. P. Barnett, E. Bouws, H. Carlson, D. E. Cartwright, K. Enke, J. A. Ewing, H. Gienapp, D. E. Hasselmann, P. Kruseman, A. Meerburg, P. Muller, D. J. Olbers, K. Richter, W. Sell, and H. Walden. (1973). Measurements of Wind-Wave Growth and Swell Decay during the Joint North Sea Wave Project (JONSWAP). *Ergnzungsheft zur Deutschen Hydrographischen Zeitschrift Reihe*, A(8)(8 0):p.95.

Higuera, P. Lara, J. L. & Losada, I. J. (2013). Realistic wave generation and active wave absorption for Navier–Stokes models: Application to OpenFOAM®. *Coastal Engineering, 71*, 102-118. https://doi.org/10.1016/j.coastaleng.2012.07.002

IPCC, 2023: Summary for Policymakers. In: Climate Change 2023: Synthesis Report. Contribution of Working Groups I, II and III to the Sixth Assessment Report of the Intergovernmental Panel on Climate Change [Core Writing Team, H. Lee and J. Romero (eds.)]. IPCC, Geneva, Switzerland, pp. 1-34, doi: 10.59327/IPCC/AR6-9789291691647.001

Kortenhaus, A.; Oumeraci, H. (1998). Classification of wave loading on monolithic coastal structures. Proceedings International Conference Coastal Engineering (ICCE), ASCE, Copenhagen, Denmark, no. 26, 14 pp.

Le Méhauté, B. (1976). *An Introduction to Hydrodynamics and Water Waves*. Berlin: Springer-Verlag.

Lyu, H., Sun, P., Huang, X., Chen, S. & Zhang, A. (2021). On removing the numerical instability induced by negative pressures in SPH simulations of typical fluid–structure interaction problems in ocean engineering. *Applied Ocean Research*, *117*, 102938, ISSN 0141-1187, https://doi.org/10.1016/j.apor.2021.102938.

Mansard, E.P.D. & Funke, E.R. (1980). The Measurement of Incident and Reflected Spectra Using a Least Squares Method. *Coastal Engineering*, 154-172. https://doi.org/10.1061/9780872622647.008

Meinen, N. E., Maria, R. D. J., Hofland, B., & Jonkman, S. N. (2020). Applicability of the goda–takahashi wave load formula for vertical slender hydraulic structures. Journal of Marine Science and Engineering, 8(11), 1-31. Article 868. https://doi.org/10.3390/jmse8110868

Omnetech. (2019). *coefficient of friction between concrete and soil*. Retrieved 28 September, 2023, from https://omnetech.com/mDTubhGK/coefficient-of-friction-between-concrete-and-soil

OpenFOAM. (2023). *Chapter 1 Introduction*. Retrieved 7 December, 2023, from https://www.openfoam.com/documentation/user-guide/1-introduction

Pierson, W. J. and L. Moskowitz. (1964). A proposed spectral form for fully developed wind seas based on the similarity theory of S. A. Kitaigorodskii. *Journal of Geophysical Research1*, 69 (December): 5181–5190.

Port of Rotterdam. (2023). *mcs nap.* Retrieved 14 December, 2023, from https://gis.portofrotterdam.com/apps/mcs_nap/

Rijkswaterstaat Waterinfo. (2023). *Waterhoogte oppervlaktewater Rotterdam*. Retrieved 14 December, 2023, from https://waterinfo.rws.nl/#/thema/Waterveiligheid

Romano, A. & Bellotti, G. (2023). Wave forces on vertical caissons with retreated wall: A first experimental insight. *Coastal Engineering 186*. https://doi.org/10.1016/j.coastaleng.2023.104396

Rota-Rosselli, R. A., Vernengo, G., Altomare, C., Brizzolara, S., Bonfiglio, L., Guercio, R. (2018). Ensuring numerical stability of wave propagation by tuning model parameters using genetic algorithms and response surface methods. *Environmental modelling & software, 103,* 62-73. https://doi.org/10.1016/j.envsoft.2018.02.003

Sato, K., Kawasaki, K., Watanabe, K., & Koshimura, S. (2021). Validation of the applicability of the particle-based open-source software DualSPHysics to violent flow fields. *Coastal Engineering Journal*, 63(4), 545–572. https://doi.org/10.1080/21664250.2021.1991608

Schalk, A.E. (2023). *Decrease wave overtopping at vertical quay walls.* TU Delft.

Skjelbreia, L. (1958). *Gravity waves Stokes' third order approximation tables of functions*. Council on wave research the engineering foundation. https://babel.hathitrust.org/cgi/pt?id=mdp.39015002017724&seq=9

Stolte, W., Baart, F., Muis, S., Hijma M.P., Taal, M., Le Bars, D. & Drijfhout, S. (2023). *Zeespiegelmonitor 2022*. Deltares. https://pub.kennisbank.deltares.nl/Details/fullCatalogue/1000021208

Takahashi, S. (2002). *DESIGN OF VERTICAL BREAKWATERS*. PORT and AIRPORT RESEARCH INSTITUTE, JAPAN. https://citeseerx.ist.psu.edu/document?repid=rep1&type=pdf&doi=bab3715070c06a6daf4f93b7101c755d92d05cd3

The SWASH Team. (2017). SWASH User manual. Delft: TU Delft, Faculty of Civil Engineering and Geosciences.

The SWASH Team. (2024). *SWASH User Manual. SWASH version 10.01.* Delft: TU Delft, Faculty of Civil Engineering and Geosciences. https://swash.sourceforge.io/download/zip/swashuse.pdf

Tuin, H. G. (2016). *Calculation 20 Wave forces on retaining wall*. [Unpublished]. OpenIJ.

Tuin, H. G., Hofland, B., Voortman, H. & De Almeida, E. (2022). Evaluation and validation of the spectral linear wave theory and 'traditional' formulae for pulsating wave loads for unimodal and bimodal seas. *Journal of coastal and hydraulic structures, 2,* 21. https://journals.open.tudelft.nl/jchs/article/view/6538/5510

Tuin, H. G. (2024). Wave impact on retreated storm wall on top of a vertical structure [Image].

Tuin, H. G. (n.d.). Lock door Ijmuiden [Image].

Van Doorslaer, K., Romano, A., Bellotti, G., Altomare, Cáceres, C., I., De Rouck, J., Franco, L. & Van der Meer, J. (2015). Force measurements on storm walls due to overtopping waves: a middle-scale model experiment. *Conference: Coastal Structures 2015*. https://www.researchgate.net/publication/283515041_Force_measurements_on_storm_walls_due_to_overtopping_waves_a_middle-scale_model_experiment

Van Maris, B. (2018). *Wave loads on vertical walls. Validation of design methods for non-breaking waves of bimodal spectra.* Delft: TU Delft, Faculty of Civil Engineering and Geosciences. https://repository.tudelft.nl/islandora/object/uuid%3Afe306bcf-2125-4151-8f1f-ebbe036941c6

Volman, R. (n.d.). Location Kop van Zuid [Image]. https://www.planviewer.nl/imro/files/NL.IMRO.0599.BP1107KopvanZuid-on02/t_NL.IMRO.0599.BP1107KopvanZuid-on02.html

Willmott, C.J., Robeson, S.M. & Matsuura, K. (2012). A refined index of model performance. *Int. J. Clim*, *32*, 2088–2094. https://doi.org/10.1002/joc.2419

Zijlema, M., Stelling, G. & Smit, P. (2011). SWASH: An operational public domain code for simulating wave fields and rapidly varied flows in coastal waters. *Coastal Engineering, 58,* 992-1012. https://doi.org/10.1016/j.coastaleng.2011.05.015

Appendix A: Experiment dimensions explanation

This appendix explains how the dimensions and configurations for the laboratory experiment are determined.

Wave height and wavelength

The wave parameters are chosen with respect to the maximum wave height in the wave field, as this wave is the most interesting. This wave height is about twice as high as the significant wave height. For the case van Kop van Zuid:

$H_{max}/L \approx 2 \cdot 1.4 / 24.0 \approx 0.12$

To see the influence of the wave steepness, there will also be tested for lower and higher steepness.

Water depth

The ratio d_w over d_{wq} in the case of Kop van Zuid is relatively large (~24), which makes it difficult to scale. However, for deepwater waves the bottom barely has any effect on the wave reshaping as the distance between the water surface and bed bottom is relatively large. Therefore, an experiment with a different d_w / d_{wq} can be used, as long the waves are deep water waves (d_w / L_{op} > 0.5). For example, take a scaled water depth of 35 cm. This leads to a maximum allowable wavelength of 35 / 0.5 = 70 cm. Using the ratio H/L mentioned above, the maximum allowable wave height in the experiment becomes 8 cm.

To exactly represent the case of Kop van Zuid this would lead to a d_{wq} of 1.5 cm. Such a small dimension is however likely to cause too many scale effects. Instead there is chosen to use a d_{wq} of around 5 cm and also use this in the models. Multiple variations would be modelled anyway, so these then become the variations which can be used to verify the model.

Configurations

Since it is easier to change the waves than the structure, the waves are modified during the experiment. The final set-up of the experiment and the dimensions of the structure are shown in Figure A.1 and A.2 respectively. Table A.1 shows the different scenarios which are going to be tested.

The hole seen in the back view provides the ability to place lead beams in de box for additional stability. The wooden panel at the left side provides additional stability as well. Lastly, the wooden panel at the bottom is extended to prevent overturning.

The box is placed at the end of the flume. This panel of the flume prevents sliding of the structure.

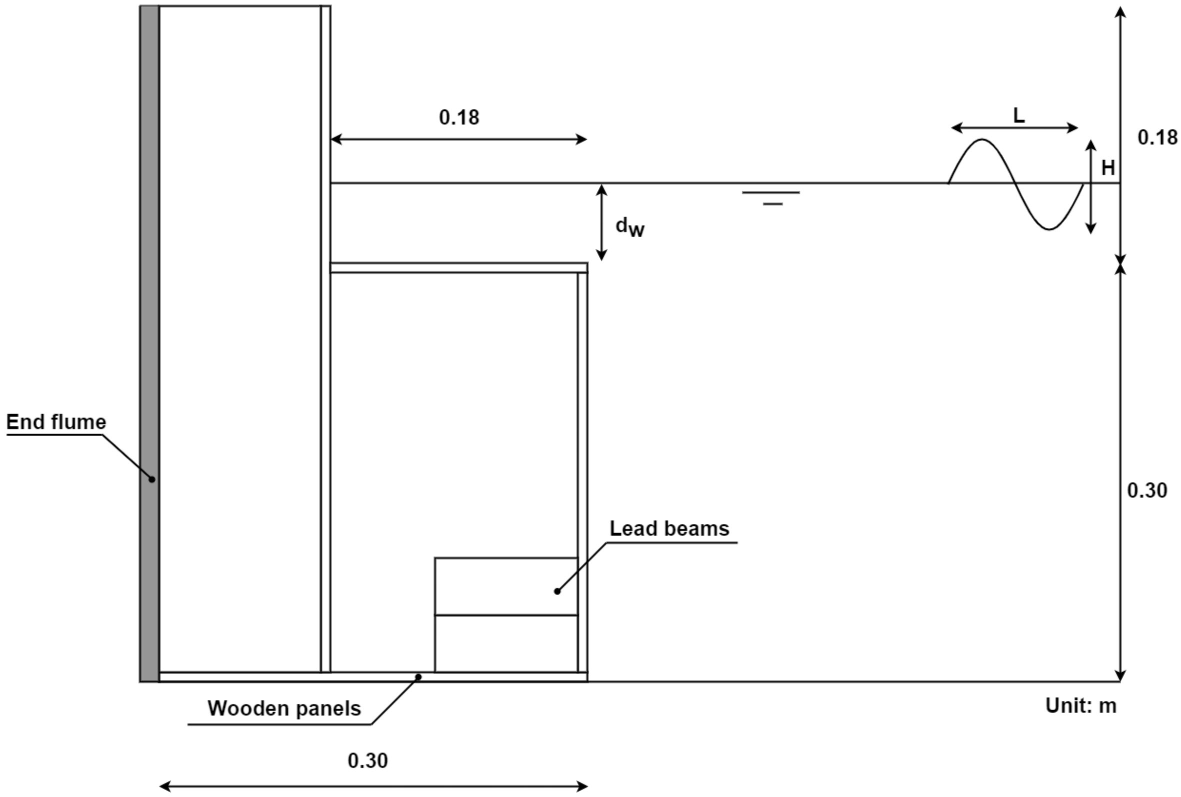

Figure A.1: Experimental set-up

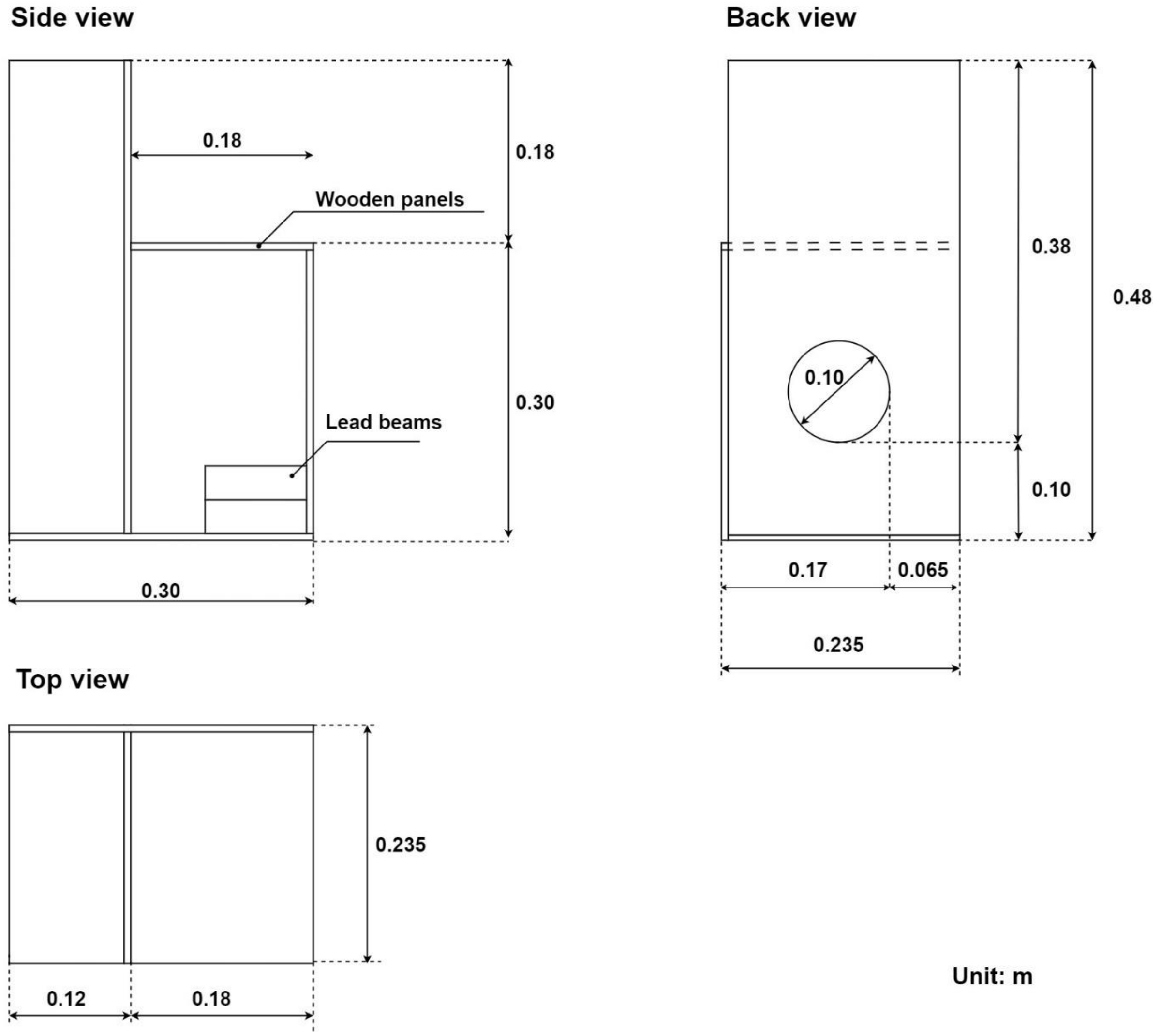

Figure A.2: Structure dimensions

Table A.1: Experiment configurations

Experiment number	H [cm]	T [s]	d_w [cm]	d_{wq} [cm]	L_{quay} / L	H / L	d_{wq} / L
1	4.6	0.51	30.0	0.0	0.44	0.1133	0.0000
2	5.2	0.55	30.0	0.0	0.38	0.1101	0.0000
3	6.8	0.61	29.9	-0.1	0.31	0.1170	-0.0017
4	4.2	0.51	33.1	3.1	0.44	0.1034	0.0763
5	4.5	0.51	33.3	3.3	0.44	0.1108	0.0813
6	4.9	0.56	33.4	3.4	0.37	0.1001	0.0694
7	6.3	0.56	33.4	3.4	0.37	0.1287	0.0715
8	4.3	0.51	33.7	3.7	0.44	0.1059	0.0911
9	4.8	0.55	34.2	4.2	0.38	0.1016	0.0889
10	5.3	0.55	34.4	4.4	0.38	0.1122	0.0932
11	5.2	0.61	34.7	4.7	0.31	0.0895	0.0809
12	6.9	0.62	35.0	5.0	0.30	0.1150	0.0833
13	4.7	0.56	34.5	4.5	0.37	0.0960	0.0919
14	3.5	0.51	34.9	4.9	0.44	0.0862	0.1207
15	3.5	0.61	35.0	5.0	0.31	0.0602	0.0861
16	4.9	0.55	35.3	5.3	0.38	0.1037	0.1122
17	6.8	0.62	35.7	5.7	0.30	0.1133	0.0950
18	6.9	0.61	37.2	7.2	0.31	0.1188	0.1239

Structure length
The length of the structure is chosen 18 cm to get practical wavelengths with the chosen values for L_{quay} / L. The wavelength is then chosen such that the structure width corresponds to 0.45 L, 0.40 L, 0.30 L. Values below 0.3 L are not chosen because 0.3 L is the smallest value measurable with deep water waves. The value 0.40 L is chosen because then broken waves instead of breaking waves are expected. The value 0.45 L is chosen, because the 0.40 L might not be a very strict boundary. To ensure observing broken waves as well, 0.45 L is chosen. In addition, 0.30 L and 0.45 L are also modelled in SWASH for the Kop van Zuid case and can therefore be compared with results of the SWASH model.

Wall height
Since the wall height is not easily adaptable, it is chosen to only use one wall height. The influence of the wall height on the waves will therefore not be investigated. The wall height is chosen as the top of the flume, i.e. 18 cm. This corresponds to one time the maximum water depth with 1.85 times the maximum wave height.

Wave flume characteristics
The characteristics of the wave flume are shown in Table A.2.

Table A.2: Wave flume characteristics

Parameter	Value	Unit
Effective length	4.00	m
Width	0.24	m
Height	0.48	m

Appendix B: SWASH

This appendix describes the methodology behind SWASH (Simulating Waves till SHore), the model set-up and the applicability of SWASH for this study.

Methodology

SWASH is an open-source non-hydrostatic wave-flow model. The model has a horizontal grid whereas the vertical axis is divided in so called layers. More layers result in more accurate results, but at a certain number of layers the accuracy barely improves. The key is therefore to find the optimal number of layers to optimize accuracy and computation time.

The model is based on nonlinear shallow water equations with non-hydrostatic pressure. The nonlinear shallow water equations in flux form are given by Equations B.1-B.3.

$$\frac{\partial d_w}{\partial t} + \nabla \boldsymbol{q} = 0 \qquad \text{Equation B.1}$$

$$\frac{\partial d_w \boldsymbol{u}}{\partial t} + \nabla(\boldsymbol{q} \otimes \boldsymbol{u}) = -g d_w \nabla \zeta \qquad \text{Equation B.2}$$

$$\boldsymbol{u}(\boldsymbol{x}, t) = \frac{1}{d_w} \int_{z=-d}^{z=\zeta} \boldsymbol{v}(\boldsymbol{x}, z, t) dz \qquad \text{Equation B.3}$$

With:

- d_w [m] = water depth
- t [s] = time
- **q** [m^2/s] = mass flux = d_w**u**
- **u** [m/s] = depth averages flow velocity vector, containing the components u(**x**, t) and v(**x**, t) along the horizontal and vertical axis respectively
- ∇ [-] = two-dimensional gradient operator = (∂_x, ∂_y)
- g [m/s^2] = gravitational acceleration = 9.81
- ζ [m] = free surface
- z [m] = vertical coordinate
- -d [m] = vertical coordinate of the bottom

The model does phase solving and uses the finite differences method. The results are the surface elevation, velocity and pressures over space and time.

A model for a vertical structure is already made by a previous student for the lock of IJmuiden (Van Maris, 2018). This model is used as a starting point. One of the conclusions drawn from this model was that Goda-Takahashi underestimates the wave force in the range of $0.5 \lesssim kd_w \lesssim 2.5$. This conclusion was validated by laboratory experiments by Tuin et al. (2022).

Model set-up

The SWASH simulation is started with an input file where the model parameters are defined. These parameters are related to grids, initial and boundary conditions, numerical computations, physics, and the output format. The input parameters used, and the explanation why are discussed below.

Computational grid

The computational grid defines the resolution in space and the extent in the space of the computations. It needs to be defined in the horizontal and vertical direction separately, as the horizontal direction uses grid cells, whereas the vertical direction uses layers. The extent of the grid needs to be defined as well.

Horizontal direction
In the horizontal direction the resolution needs to be defined in terms of the grid cell width. The recommended spatial resolution for the horizontal direction depends on the type of waves. For low waves 50 grid cells per peak wavelength are sufficient. However, for relatively high waves at least 100 grid cells per wavelength are recommended. In the Kop van Zuid case H_s / $d_w \approx 0.1$, which is not considered high, but also not very low. To be on the safe side, 100 grid cells are recommended by the SWASH manual. Therefore, 100 grid cells are used in this study. With an irregular wavelength of 29.5 m this leads to a rounded grid size Δx of 0.30 m. For regular waves a rounded grid size Δx of 0.20 m is used as the wavelength is shorter.

Vertical direction
In the vertical direction, the grid is defined in a fixed number of layers. The number of layers depends on the application type: vertical flow structures and wave transformation. In this study waves are transferring from deep water to a small layer of water on a quay or an almost dry quay. Therefore, wave transformation is the governing process.

For wave transformation the governing parameter in this study is the peak wave frequency. High frequencies may propagate too slow for too few layers. Table B.1 shows the maximum frequency [Hz] for which the celerity of the waves can still be modeled correctly as function of still water depth [m] and number of layers K.

Table B.1: Maximum frequency [Hz] (The SWASH Team, 2024)

d (m)	K = 1	K = 2	K = 3
1	0.82	1.37	2.00
5	0.37	0.61	0.89
10	0.26	0.43	0.63
15	0.21	0.35	0.52
20	0.18	0.31	0.45
25	0.16	0.27	0.40
30	0.15	0.25	0.36
35	0.14	0.23	0.34
40	0.13	0.22	0.32
45	0.12	0.20	0.30
50	0.12	0.19	0.28
100	0.08	0.14	0.20

Preferably the maximum frequency is 1.5 to 2 times the peak frequency. In the case of Kop van Zuid this will lead to:

$$f_{max} = 1.5 - 2 \cdot \frac{1}{T_p} = 1.5 - 2 \cdot \frac{1}{4.35} = 0.34 - 0.46\ [Hz]$$

For a water depth of around 15 m, this leads to a requirement of 3 layers. Due to unrealistic output, as described later in this appendix, 4 layers were also applied.

Grid domain (horizontal plane)
The grid domain is the horizontal distance from the location where the waves are generated to the back of the structure. The boundary of this domain should at least be two wave lengths away from the area of interest. Since the waves in front of the quay are at the boundary of deep water and the bottom is flat, the bottom is not expected to have a significant influence on the wave characteristics.

However, to be on the safe side the boundary is placed at 2.5 peak wave lengths of the quay, i.e. 75 m. Adding the maximum occurring quay length (0.5 L_{op} ≈ 15 m) and the storm wall thickness (an estimation of 1 m to get a number divisible by the grid size 0.3) leads to a maximum length of interest of 91 m. For smaller quay lengths, the length of interest will also be smaller.

Behind the storm wall a sponge layer will be placed to adsorb the wave energy from the waves which penetrate through the wall. More about this follows in the section about the input grid below. The sponge layer also needs to be added to the grid domain. A sponge layer of 1 to 3 times the wavelength is recommended. Therefore, using a sponge layer of 1.5 L_{op} ≈ 44 m, this leads to a maximum total domain of 135 m. For smaller quay lengths, the domain will also be smaller.

Input grid: bathymetry
SWASH has the option to load in grids from separate files. For the application in this thesis the bathymetry is the only input grid. The bed is modelled flat. The quay wall and storm wall are modelled as porosity layers with a low porosity (n = 0.1) as this is the best method regarding stability. The wave energy which penetrates through these porosity layers is adsorbed by the sponge layer behind them.

Initial and boundary conditions
Initial conditions
As initial conditions the surface elevation and velocity are put to zero. The simulations will then be made long enough to get a steady-state solution.

Wave characteristics
For the regular waves the wave height H and wave period T are given as input. For irregular waves a unimodal Jonswap spectrum file is given as input. Since the location is inside a harbor, the wind waves will play the more dominant part. Therefore, a unimodal instead of a bimodal spectrum is chosen.

Boundary reflection
To prevent waves reflecting at the wave generating boundary a weakly reflective condition is adopted.

Numerical parameters
Simulation duration
The total simulation time consists of the spin-up time (15%) and the cycle time (85%). The recommended range for the cycle time is 100 to 300 waves.

For regular waves, 300 waves with a wave period of 3.92 seconds leads to a computation time of 20 minutes. This requires then a simulation duration of 23 minutes. The higher bound of 300 waves is chosen, due to unrealistic output as described later in this appendix.

For irregular waves, sufficient waves with at least the significant wave height are desired. The probability of exceedance of H_s corresponds to 0.135. Choosing at least 100 waves higher than H_s, 100 / 0.135 = 741 waves are needed. The frequency range of the waves ranges from half the peak frequency to three times the peak frequency, i.e. 0.11 Hz to 0.69 Hz. So, the longest wave period is 9 seconds. This results in a required simulation time of 2 hours and 10 minutes.

Time step
Since SWASH uses explicit time integration the time step should satisfy the so-called CFL condition. In this condition the Courant number is computed. The time step is dynamically changed by SWASH to be in the user specified range. The minimum value of the Courant number is usually 0.2 and the maximum value for waves interacting with steep structures (e.g. a quay or wall) a value of 0.5 is

recommended. Therefore, the Courant range used in this study is [0.2; 0.5]. The initial time step is put at 0.0001 s, as SWASH automatically adjusts the value to one which satisfies the CFL condition.

Vertical pressure gradient
The location of the grid points for the non-hydrostatic pressure can be either at the cell center or at the layer interface. The first is called the standard lay-out while the second is called the box lay-out. In this study the standard layout is used, as this is recommended when vertical structures are important (The SWASH Team, 2017).

Physical parameters: wave breaking
SWASH is not able to model breaking waves due to wave steepness, but it is able to account for depth-induced wave breaking. In case of a low number of layers (1 - 3) this needs to be explicitly specified as the progress needs a higher resolution. Since in this study 3 or 4 layers are used, and depth-induced wave breaking is expected due to the quay, this option is turned on.

Output
To store all the output for surface elevation, velocity, and pressure for every grid point for every time step would require a lot of storage space. Therefore, the decision is made to store the time series for surface elevation, velocity, and pressure only at one specific location. This is done for the grid point two points away from the storm wall, as the grid point right in front of the wall can suffer from numerical influence of the wall, reaching excessive values (Van Maris, 2018). Only the water level is stored for the whole domain at all time steps.

Applicability

Schematization quay wall and storm wall
SWASH has three options to model structures:
- including the structure in the bathymetry
- using porosity layers with a low porosity (< 0.1)
- a combination of the two

Based on the results, including the structure in the bathymetry is not recommended. The model quickly becomes instable and errors like water levels below bottom levels may occur. Besides, the working model for a structure in the bathymetry showed no reflection of the waves at the quay or storm wall. However, reflection at a vertical structure may be expected, creating a standing wave like pattern.

Using porosity layers with low porosity, e.g. 0.09 also showed limitations. Even though the structure height was given as input, the program takes the porosity layer over the whole vertical axis. The structure height was varied from -8 m to 14.25 with multiple steps in between, but the result stayed the same. The porosity layer creates a standing wave pattern in front of the quay, but on the quay a small water layer remains showing no variation in level, as seen in Figure B.1. When taking a porosity higher then 0.1, e.g. 0.11, it is visible that some water flows through the structure, treating it as a porous structure instead of an impermeable structure, as seen in Figure B.2.

The last option tested was a combination of the two. Half of the quay height was modeled with the bathymetry. The other half was modeled by placing a porous structure on top. This showed the same results as only using a porosity layer. A standing wave appeared in front of the quay, but the water on top of the quay stayed still.

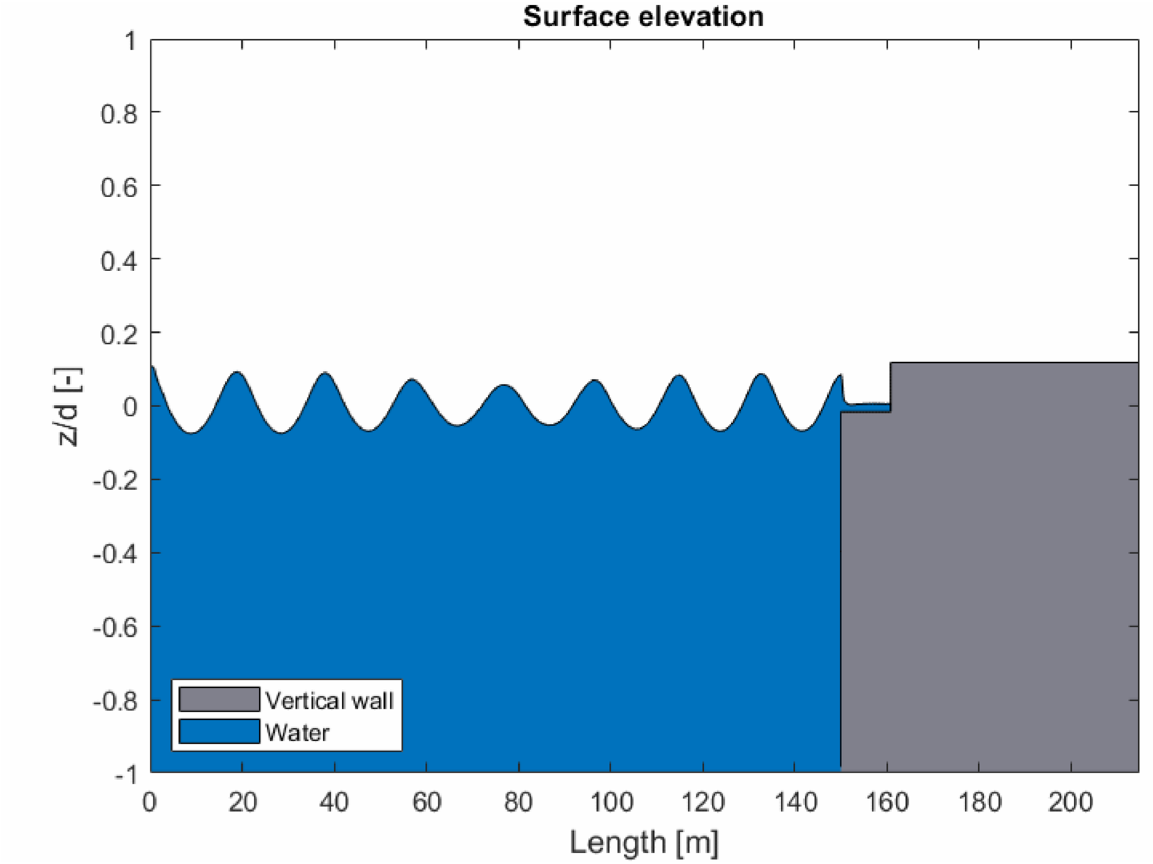

Figure B.1: SWASH output: standing waves in front of the quay with a still water level on the quay, made with B. Maris' MATLAB code

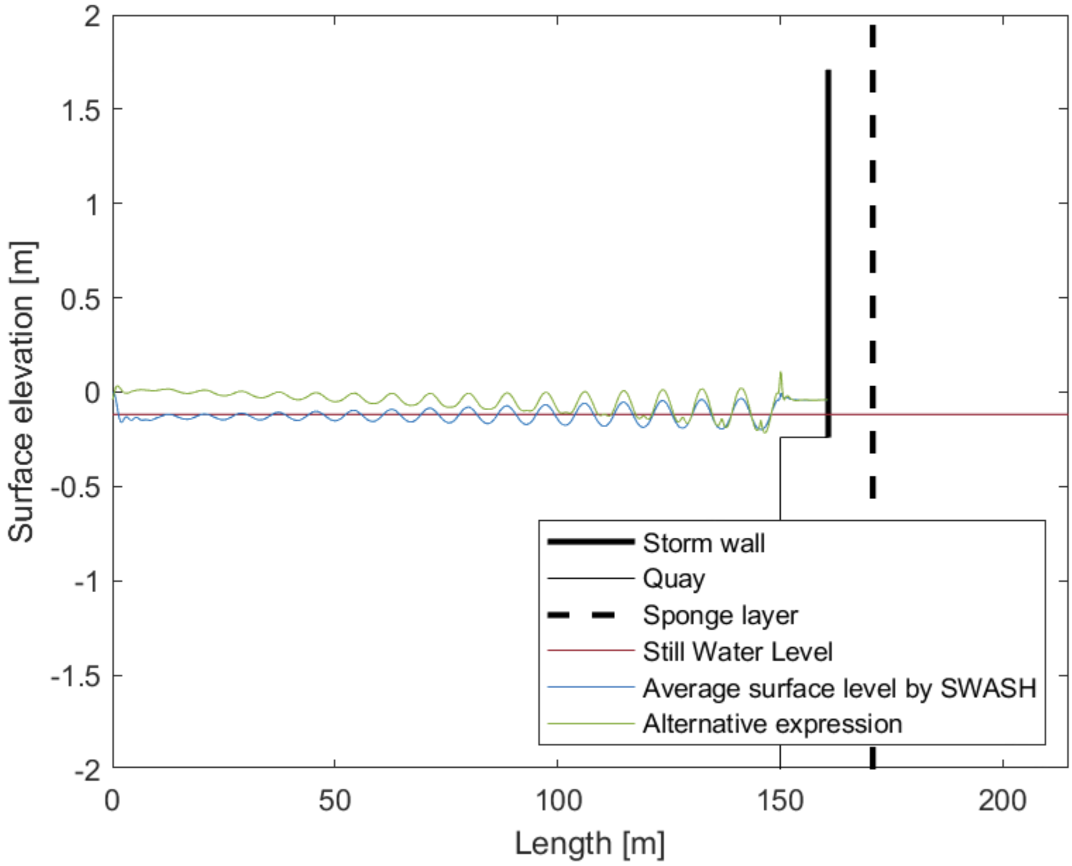

Figure B.2: SWASH output: porosity of quay = 0.11, made with B. Maris' MATLAB code

Influence of other parameters
The options for the schematization of the quay were tried with different parameters, but in the end, results were similar and the way the structure is defined played the most important role for the result.

The other parameters which had some influences were the number of layers, the layer thicknesses, the type of vertical hydraulic gradient scheme and the grid size. These parameters played a role when schematizing the structure with the bathymetry. This option would only give an output for coarse resolutions, i.e. low number of vertical layers, no low thicknesses of layers and high grid size. In most cases only the standard layout would give an output while the box layout gave errors. Even though the result does not look very odd, because the grids are way coarser than recommended and no reflection is visible, it is likely that the results are not trustworthy.

Conclusion
The current version of SWASH (10.01) is not able to model waves going over a submerged impermeable structure accurately. For a vertical wall where no overtopping waterflow is expected, it might still be suitable.

Appendix C: Kop van Zuid

This appendix contains how the information regarding the Kop van Zuid case is obtained. This includes the geometry at the Kop van Zuid and the hydraulic loading conditions. At the end of the appendix an overview is given of all the determined parameters.

Elevation quay

The elevation of the present quay is obtained by AHN viewer (Actueel Hoogtebestand Nederland, n.d.) resulting in Figure C.1. The starting point of the elevation profile in Figure C.1 is at (92769.4753; 435484.6177) and the end point is at (93063.9571; 435725.1244).

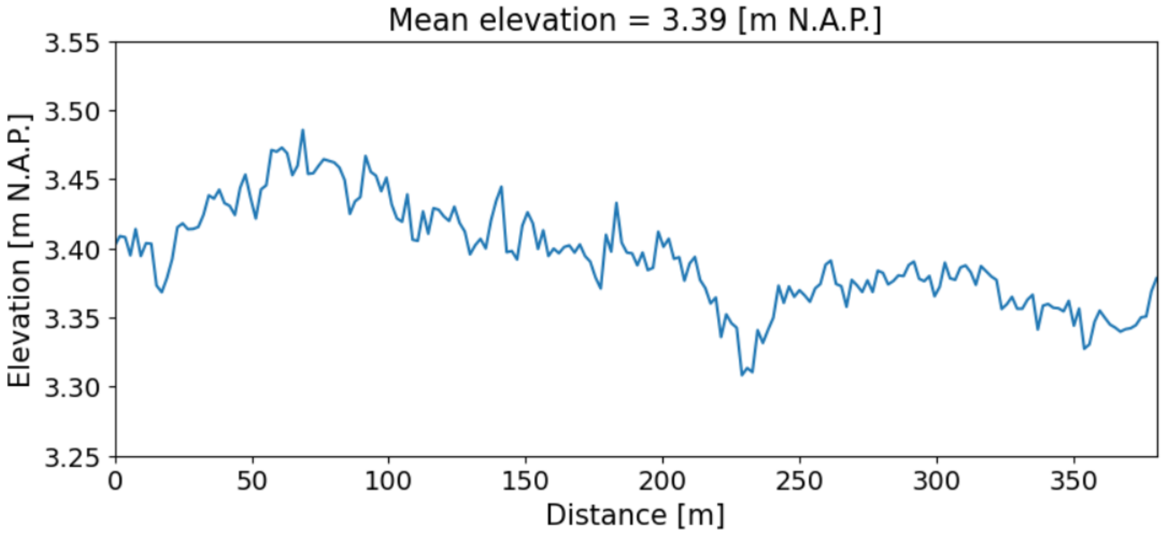

Figure C.1: Elevation profile AHN

Hydraulic loading

HydraNL is used to compute the hydraulic boundary conditions for different return periods. For dike section 14-2, at Kop van Zuid, this leads to the values in Table C.1 for target year 2100.

Table C.1: Values for hydraulic loadings for target year 2100 for dike section 14-2

Return period	Water level [m N.A.P.]	Water level Europoortkering open [m N.A.P.]	Significant wave height [m]	Peak period [s]	Spectral period [s]
100	3.14	2.78	1.04	3.82	3.47
1,000	3.30	3.11	1.21	4.10	3.73
10,000	3.68	4.00	1.40	4.35	3.95
100,000	4.26	4.47	1.60	4.60	4.18

The translation to regular waves is made for the return period of 10,000 years. Looking at the maximum wave height, as this gives the highest impact, the regular wave height becomes

$$H = 2H_s = 2 \cdot 1.40 = 2.80\ [m]$$

based on a rule of thumb. The period is based on a rule of thumb as well. Assuming a wave period of 10% less than the peak period the wave period T becomes 3.92 s.

For the water level the worst case scenario is used where the Europoortkering is open. An additional benefit of using this water depth is that the smallest dimension in the model (the water depth on the quay) can be modelled with a lower resolution, since the water depth on the quay is higher. This saves computation time.

Bed level
To determine the water depth in m, the bed level is required. Using the website of the Port of Rotterdam and Rijkswaterstaat Waterinfo simultaneously, the current water depth [m] and the current water level [m N.A.P.] can be determined, giving the bed level (2023). This gives a bed level between -10.6 and -11.1 m N.A.P.

Wavelength
Based on the peak wave period the peak deep water wavelength can be obtained using Equation C.1.

$$L_{op} = \frac{gT_p^2}{2\pi} \qquad \text{Equation C.1}$$

With:

- g $[m/s^2]$ = gravitational acceleration = 9.81
- T_p [s] = peak wave period
- d_w [m] = water depth
- L_{op} [m] = peak deep water wavelength

This results in the values for peak deep water wavelength shown in Table C.2.

Wave number
The wave numbers in Table C.2 are computed with Equation C.2.

$$k = \frac{2\pi}{L} \qquad \text{Equation C.2}$$

With:

- k [rad/m] = wave number
- L [m] = wavelength

Storm wall height
To get an estimation of a likely storm wall height the EurOtop Overtopping Manual (2018) is used. The needed formula is defined by impulsive or non-impulsive conditions and the presence of an influencing foreshore. When the water depth is 4 times larger than $H_{m0,deep}$, there is no influencing foreshore and Equation C.3 can be used.

$$\frac{q}{\sqrt{g \cdot H_{m0}^3}} = 0.054 \cdot \exp\left(-\left(2.12\frac{R_c}{H_{m0}}\right)^{1.3}\right) \qquad \text{Equation C.3}$$

With:

- R_c [m] = Freeboard
- H_{m0} [m] = Spectral significant wave height ≈ H_s
- q $[m^3/s/m]$ = Wave overtopping discharge

For the cases study this is indeed the case. Assuming a maximum allowable wave overtopping discharge of 10 L/s/m (EurOtop, 2018), the minimum required freeboard is 1.67 m. With a water depth on the quay of 0.61 m, this leads to a required storm wall height of 2.28 m.

Results

Table C.2 shows the results for the parameter values. Table C.3 shows as addition the values of the dimensionless parameters which were also used to compare the state-of-the-art in Table 1.1.

Table C.2: Parameter values

Parameter symbol	Description	Unit	Kop van Zuid
d_w	Water depth	m	14.86 (averaged)
d_{wq}	Water depth on top of quay	m	0.61
d_{wq} - d_w	Height quay	m	14.25 (averaged)
L_{quay}	Length quay, i.e. distance storm wall from the edge of the quay	m	Variable
h_{sw}	Height storm wall	m	Around 2.28 m
Irregular waves			
H_s	Significant wave height	m	1.40
T_p	Peak wave period	s	4.35
L_{op}	Peak wavelength	m	29.5
k	Wavenumber	m^{-1}	0.21
Regular waves			
H	Regular wave height	m	2.80
T	Regular wave period	s	3.92
L	Regular wavelength	m	24.0
k	Wavenumber	m^{-1}	0.26

Table C.3: Dimensionless parameters

Parameter	Value
Irregular waves	
L_{quay} / L_{op}	Variable
h_{sw} / L_{op}	Around 0.066
d_{wq} / L_{op}	0.02
H_s / L_{op}	0.05
kd_w	3.12
Regular waves	
L_{quay} / L	Variable
h_{sw} / L	Around 0.081
d_{wq} / L	0.025
H / L	0.12
kd_w	3.86

Appendix D: Configurations and results DualSPHysics

This appendix contains all the results of the DualSPHysics model. Table D.1 – D.5 contain the results of the regular waves and Table D.6 – D.10 for the irregular waves. The tables go in the order of configurations, DualSPHysics force, theory force, Cooker-Peregrine force, observed wave type.

Regular waves

Table D.1: Values dimensionless parameters configurations regular waves

Configuration	L_{quay} / L	h_{sw} / L	d_{wq} / L	H / L
0	0	0.090281	-0.02	0.05
1	0	0.090281	-0.02	0.117
2	0	0.090281	0	0.05
3	0	0.090281	0	0.117
4	0	0.090281	0.02	0.05
5	0	0.090281	0.02	0.117
6	0	0.090281	0.04	0.05
7	0	0.090281	0.04	0.117
8	0	0.095033	-0.02	0.05
9	0	0.095033	-0.02	0.117
10	0	0.095033	0	0.05
11	0	0.095033	0	0.117
12	0	0.095033	0.02	0.05
13	0	0.095033	0.02	0.117
14	0	0.095033	0.04	0.05
15	0	0.095033	0.04	0.117
16	0	0.099784	-0.02	0.05
17	0	0.099784	-0.02	0.117
18	0	0.099784	0	0.05
19	0	0.099784	0	0.117
20	0	0.099784	0.02	0.05
21	0	0.099784	0.02	0.117
22	0	0.099784	0.04	0.05
23	0	0.099784	0.04	0.117
24	0.15	0.090281	-0.02	0.05
25	0.15	0.090281	-0.02	0.117
26	0.15	0.090281	0	0.05
27	0.15	0.090281	0	0.117
28	0.15	0.090281	0.02	0.05
29	0.15	0.090281	0.02	0.117
30	0.15	0.090281	0.04	0.05
31	0.15	0.090281	0.04	0.117
32	0.15	0.095033	-0.02	0.05
33	0.15	0.095033	-0.02	0.117
34	0.15	0.095033	0	0.05
35	0.15	0.095033	0	0.117
36	0.15	0.095033	0.02	0.05
37	0.15	0.095033	0.02	0.117
38	0.15	0.095033	0.04	0.05
39	0.15	0.095033	0.04	0.117
40	0.15	0.099784	-0.02	0.05
41	0.15	0.099784	-0.02	0.117
42	0.15	0.099784	0	0.05
43	0.15	0.099784	0	0.117
44	0.15	0.099784	0.02	0.05

45	0.15	0.099784	0.02	0.117
46	0.15	0.099784	0.04	0.05
47	0.15	0.099784	0.04	0.117
48	0.3	0.090281	-0.02	0.05
49	0.3	0.090281	-0.02	0.117
50	0.3	0.090281	0	0.05
51	0.3	0.090281	0	0.117
52	0.3	0.090281	0.02	0.05
53	0.3	0.090281	0.02	0.117
54	0.3	0.090281	0.04	0.05
55	0.3	0.090281	0.04	0.117
56	0.3	0.095033	-0.02	0.05
57	0.3	0.095033	-0.02	0.117
58	0.3	0.095033	0	0.05
59	0.3	0.095033	0	0.117
60	0.3	0.095033	0.02	0.05
61	0.3	0.095033	0.02	0.117
62	0.3	0.095033	0.04	0.05
63	0.3	0.095033	0.04	0.117
64	0.3	0.099784	-0.02	0.05
65	0.3	0.099784	-0.02	0.117
66	0.3	0.099784	0	0.05
67	0.3	0.099784	0	0.117
68	0.3	0.099784	0.02	0.05
69	0.3	0.099784	0.02	0.117
70	0.3	0.099784	0.04	0.05
71	0.3	0.099784	0.04	0.117
72	0.45	0.090281	-0.02	0.05
73	0.45	0.090281	-0.02	0.117
74	0.45	0.090281	0	0.05
75	0.45	0.090281	0	0.117
76	0.45	0.090281	0.02	0.05
77	0.45	0.090281	0.02	0.117
78	0.45	0.090281	0.04	0.05
79	0.45	0.090281	0.04	0.117
80	0.45	0.095033	-0.02	0.05
81	0.45	0.095033	-0.02	0.117
82	0.45	0.095033	0	0.05
83	0.45	0.095033	0	0.117
84	0.45	0.095033	0.02	0.05
85	0.45	0.095033	0.02	0.117
86	0.45	0.095033	0.04	0.05
87	0.45	0.095033	0.04	0.117
88	0.45	0.099784	-0.02	0.05
89	0.45	0.099784	-0.02	0.117
90	0.45	0.099784	0	0.05
91	0.45	0.099784	0	0.117
92	0.45	0.099784	0.02	0.05
93	0.45	0.099784	0.02	0.117
94	0.45	0.099784	0.04	0.05
95	0.45	0.099784	0.04	0.117

Table D.2: Computed regular wave forces using DualSPHysics

Configuration	F_{max} [kN/m]	F_{peaks} [kN/m]
0	1.286684	0.943544
1	38.3862	10.23385
2	3.974334	3.357549
3	38.30218	15.31709
4	8.844598	7.76302
5	81.64652	24.86723
6	15.08723	13.83262
7	59.98047	25.40829
8	1.286684	0.943544
9	28.36339	9.656146
10	3.974334	3.357549
11	60.97455	16.57379
12	8.844598	7.76302
13	43.71595	21.15797
14	15.02923	13.81023
15	73.4551	26.4445
16	1.286684	0.943544
17	42.36106	11.12735
18	3.974334	3.357549
19	131.2267	18.45896
20	8.844598	7.76302
21	55.89697	22.41182
22	15.04616	13.76357
23	88.353	30.68063
24	173.647	13.57813
25	151.7951	30.58211
26	166.6044	22.31506
27	247.0034	48.07359
28	42.58086	12.88621
29	313.0142	59.00691
30	30.97144	18.75169
31	429.6623	137.2219
32	259.6553	16.46607
33	253.4094	34.61603
34	291.498	26.95451
35	353.5527	54.62007
36	42.58086	12.88621
37	641.4446	66.70761
38	27.12691	19.03683
39	432.5981	117.8901
40	119.6744	8.539376
41	147.2641	34.07206
42	67.8983	14.77166
43	141.6392	44.0521
44	42.58086	12.88621
45	245.912	64.01163
46	24.77032	18.62719
47	430.2513	131.5298
48	70.67271	6.445966
49	54.33197	18.8741
50	296.0658	11.50996
51	281.6046	47.92144

52	27.15246	13.84104
53	450.1093	106.1068
54	145.682	32.59854
55	701.1315	174.451
56	218.5618	8.656278
57	61.30528	19.94851
58	106.5334	10.19904
59	274.8036	47.87071
60	24.6852	14.81885
61	455.2579	130.1059
62	59.26018	32.81355
63	802.0798	224.4354
64	70.26987	6.299336
65	79.25287	20.56755
66	77.44064	9.921908
67	219.7337	43.95262
68	27.30348	14.59051
69	627.505	140.566
70	71.03793	33.79296
71	856.9114	212.4152
72	110.2848	5.370765
73	45.54179	13.50902
74	19.29185	1.763325
75	42.90775	17.17524
76	20.0669	11.17976
77	149.05	27.07427
78	37.5524	20.65312
79	93.79692	36.78647
80	34.63216	2.381093
81	73.06043	13.37929
82	19.29185	1.763325
83	48.7924	18.61599
84	22.83802	11.53691
85	63.40948	22.96593
86	37.74764	20.42748
87	208.4662	38.48161
88	138.9643	5.185262
89	49.10234	12.53881
90	19.29185	1.763325
91	43.41375	18.86676
92	22.83802	11.53945
93	191.0162	26.80807
94	34.03301	20.87825
95	178.9187	39.65631

Table D.3: Computed regular wave forces using theories

Configuration	F_{Tuin} [kN/m]	$F_{adapted\ Tuin}$ [kN/m]	F_{Goda} [kN/m]	$F_{Den\ Heijer}$ [kN/m]	F_{max} linear standing wave χ=1 [kN/m]	F_{max} linear standing wave χ=0 [kN/m]
0	20.80364	48.5017064	3.419024	37.23876	2.542752	0.070632
1	84.49872	235.0634039	27.15362	192.276	26.40067	4.151592
2	11.55379	26.82920646	6.29935	37.23876	7.0632	1.7658
3	62.90395	172.9456633	34.47647	192.276	38.4552	9.6138
4	66.97574	156.710888	10.82481	37.23876	13.8143	5.706404

5	192.2127	522.6657687	43.52879	192.276	52.70094	17.30173
6	122.3764	283.7792595	17.45221	37.23876	22.65253	11.82069
7	321.4737	780.3208643	54.47213	192.276	68.80303	27.04794
8	20.80364	48.5017064	3.419005	37.23876	2.542752	0.070632
9	84.49872	235.0634039	27.15358	192.276	26.40067	4.151592
10	11.55379	26.82920646	6.29892	37.23876	7.0632	1.7658
11	62.90395	172.9456633	34.47551	192.276	38.4552	9.6138
12	66.97574	156.710888	10.82489	37.23876	13.8143	5.706404
13	192.2127	537.5961493	43.52886	192.276	52.70094	17.30173
14	122.3764	290.345011	17.45239	37.23876	22.65253	11.82069
15	321.4737	795.4017712	54.47232	192.276	68.80303	27.04794
16	20.80364	48.5017064	3.419013	37.23876	2.542752	0.070632
17	84.49872	235.0634039	27.15362	192.276	26.40067	4.151592
18	11.55379	26.82920646	6.298473	37.23876	7.0632	1.7658
19	62.90395	172.9456633	34.4746	192.276	38.4552	9.6138
20	66.97574	156.710888	10.82477	37.23876	13.8143	5.706404
21	192.2127	544.9390815	43.52871	192.276	52.70094	17.30173
22	122.3764	293.6296366	17.45228	37.23876	22.65253	11.82069
23	321.4737	809.9067791	54.47219	192.276	68.80303	27.04794
24	20.80364	48.5017064	3.419024	37.23876	2.542752	0.070632
25	84.49872	235.0634039	27.15362	192.276	26.40067	4.151592
26	11.55379	26.82920646	6.29935	37.23876	7.0632	1.7658
27	62.90395	172.9456633	34.47647	192.276	38.4552	9.6138
28	66.97574	156.710888	10.82481	37.23876	13.8143	5.706404
29	192.2127	522.6657687	43.52879	192.276	52.70094	17.30173
30	122.3764	283.7792595	17.45221	37.23876	22.65253	11.82069
31	321.4737	780.3208643	54.47213	192.276	68.80303	27.04794
32	20.80364	48.5017064	3.419005	37.23876	2.542752	0.070632
33	84.49872	235.0634039	27.15358	192.276	26.40067	4.151592
34	11.55379	26.82920646	6.29892	37.23876	7.0632	1.7658
35	62.90395	172.9456633	34.47551	192.276	38.4552	9.6138
36	66.97574	156.710888	10.82489	37.23876	13.8143	5.706404
37	192.2127	537.5961493	43.52886	192.276	52.70094	17.30173
38	122.3764	290.345011	17.45239	37.23876	22.65253	11.82069
39	321.4737	795.4017712	54.47232	192.276	68.80303	27.04794
40	20.80364	48.5017064	3.419013	37.23876	2.542752	0.070632
41	84.49872	235.0634039	27.15362	192.276	26.40067	4.151592
42	11.55379	26.82920646	6.298473	37.23876	7.0632	1.7658
43	62.90395	172.9456633	34.4746	192.276	38.4552	9.6138
44	66.97574	156.710888	10.82477	37.23876	13.8143	5.706404
45	192.2127	544.9390815	43.52871	192.276	52.70094	17.30173
46	122.3764	293.6296366	17.45228	37.23876	22.65253	11.82069
47	321.4737	809.9067791	54.47219	192.276	68.80303	27.04794
48	20.80364	48.5017064	3.419024	37.23876	2.542752	0.070632
49	84.49872	235.0634039	27.15362	192.276	26.40067	4.151592
50	11.55379	26.82920646	6.29935	37.23876	7.0632	1.7658
51	62.90395	172.9456633	34.47647	192.276	38.4552	9.6138
52	66.97574	156.710888	10.82481	37.23876	13.8143	5.706404
53	192.2127	522.6657687	43.52879	192.276	52.70094	17.30173
54	122.3764	283.7792595	17.45221	37.23876	22.65253	11.82069
55	321.4737	780.3208643	54.47213	192.276	68.80303	27.04794
56	20.80364	48.5017064	3.419005	37.23876	2.542752	0.070632
57	84.49872	235.0634039	27.15358	192.276	26.40067	4.151592
58	11.55379	26.82920646	6.29892	37.23876	7.0632	1.7658

59	62.90395	172.9456633	34.47551	192.276	38.4552	9.6138
60	66.97574	156.710888	10.82489	37.23876	13.8143	5.706404
61	192.2127	537.5961493	43.52886	192.276	52.70094	17.30173
62	122.3764	290.345011	17.45239	37.23876	22.65253	11.82069
63	321.4737	795.4017712	54.47232	192.276	68.80303	27.04794
64	20.80364	48.5017064	3.419013	37.23876	2.542752	0.070632
65	84.49872	235.0634039	27.15362	192.276	26.40067	4.151592
66	11.55379	26.82920646	6.298473	37.23876	7.0632	1.7658
67	62.90395	172.9456633	34.4746	192.276	38.4552	9.6138
68	66.97574	156.710888	10.82477	37.23876	13.8143	5.706404
69	192.2127	544.9390815	43.52871	192.276	52.70094	17.30173
70	122.3764	293.6296366	17.45228	37.23876	22.65253	11.82069
71	321.4737	809.9067791	54.47219	192.276	68.80303	27.04794
72	20.80364	48.5017064	3.419024	37.23876	2.542752	0.070632
73	84.49872	235.0634039	27.15362	192.276	26.40067	4.151592
74	11.55379	26.82920646	6.29935	37.23876	7.0632	1.7658
75	62.90395	172.9456633	34.47647	192.276	38.4552	9.6138
76	66.97574	156.710888	10.82481	37.23876	13.8143	5.706404
77	192.2127	522.6657687	43.52879	192.276	52.70094	17.30173
78	122.3764	283.7792595	17.45221	37.23876	22.65253	11.82069
79	321.4737	780.3208643	54.47213	192.276	68.80303	27.04794
80	20.80364	48.5017064	3.419005	37.23876	2.542752	0.070632
81	84.49872	235.0634039	27.15358	192.276	26.40067	4.151592
82	11.55379	26.82920646	6.29892	37.23876	7.0632	1.7658
83	62.90395	172.9456633	34.47551	192.276	38.4552	9.6138
84	66.97574	156.710888	10.82489	37.23876	13.8143	5.706404
85	192.2127	537.5961493	43.52886	192.276	52.70094	17.30173
86	122.3764	290.345011	17.45239	37.23876	22.65253	11.82069
87	321.4737	795.4017712	54.47232	192.276	68.80303	27.04794
88	20.80364	48.5017064	3.419013	37.23876	2.542752	0.070632
89	84.49872	235.0634039	27.15362	192.276	26.40067	4.151592
90	11.55379	26.82920646	6.298473	37.23876	7.0632	1.7658
91	62.90395	172.9456633	34.4746	192.276	38.4552	9.6138
92	66.97574	156.710888	10.82477	37.23876	13.8143	5.706404
93	192.2127	544.9390815	43.52871	192.276	52.70094	17.30173
94	122.3764	293.6296366	17.45228	37.23876	22.65253	11.82069
95	321.4737	809.9067791	54.47219	192.276	68.80303	27.04794

Table D.4: Computed regular wave forces using Cooker-Peregrine with different velocities (u_{lwt} & u_{3rd}) and impulse durations (dt)

Configuration	$F_{Cooker-Pperegrine}$, dt=0.05, u_{lwt} [kN/m]	$F_{Cooker-Peregrine}$, dt=0.1, u_{lwt} [kN/m]	$F_{Cooker-Peregrine}$, dt=0.05, u_{3rd} [kN/m]	$F_{Cooker-Peregrine}$, dt=0.1, u_{3rd} [kN/m]	$F_{Cooker-Peregrine}$, dt=0.05, $u_{shallow}$ [kN/m]	$F_{Cooker-Peregrine}$, dt=0.1, $u_{shallow}$ [kN/m]
0	0.513985611	0.256992805	0.602195123	0.301097561	-	-
1	54.13919447	27.06959723	77.87772412	38.93886206	-	-
2	10.75041262	5.37520631	12.5961067	6.298053351	0	0
3	113.5174433	56.75872165	163.2848	81.64240001	0	0
4	31.14563908	15.57281954	36.49453754	18.24726877	27.47466289	13.73733145
5	195.6249647	97.81248233	281.3800501	140.690025	83.25312802	41.62656401
6	59.96328807	29.98164404	70.2637271	35.13186355	81.06792481	40.5339624
7	284.036929	142.0184645	408.5384222	204.2692111	185.5341527	92.76707635
8	0.513985611	0.256992805	0.602195123	0.301097561	-	-
9	54.13919447	27.06959723	77.87772412	38.93886206	-	-
10	10.75041262	5.37520631	12.5961067	6.298053351	0	0

11	113.5174433	56.75872165	163.2848	81.64240001	0	0
12	31.14563908	15.57281954	36.49453754	18.24726877	27.47466289	13.73733145
13	195.6249647	97.81248233	281.3800501	140.690025	83.25312802	41.62656401
14	59.96328807	29.98164404	70.2637271	35.13186355	81.06792481	40.5339624
15	286.5922441	143.2961221	412.2138049	206.1069024	185.5341527	92.76707635
16	0.513985611	0.256992805	0.602195123	0.301097561	-	-
17	54.13919447	27.06959723	77.87772412	38.93886206	-	-
18	10.75041262	5.37520631	12.5961067	6.298053351	0	0
19	113.5174433	56.75872165	163.2848	81.64240001	0	0
20	31.14563908	15.57281954	36.49453754	18.24726877	27.47466289	13.73733145
21	195.6249647	97.81248233	281.3800501	140.690025	83.25312802	41.62656401
22	59.96328807	29.98164404	70.2637271	35.13186355	81.06792481	40.5339624
23	287.5066274	143.7533137	413.5289884	206.7644942	185.5341527	92.76707635
24	0.176385959	0.08819298	0.150548953	0.075274476	-	-
25	29.70086845	14.85043423	20.64751007	10.32375504	-	-
26	4.408456618	2.204228309	3.762490172	1.881245086	0	0
27	68.7525622	34.3762811	47.79756033	23.89878017	0	0
28	14.28039692	7.140198459	12.18736058	6.093680292	27.47466289	13.73733145
29	123.9434726	61.97173628	86.16971043	43.08485522	83.25312802	41.62656401
30	29.79003273	14.89501636	25.42290863	12.71145431	81.06792481	40.5339624
31	195.2697319	97.63486595	135.7615636	67.88078179	185.5341527	92.76707635
32	0.176385959	0.08819298	0.150548953	0.075274476	-	-
33	29.70086845	14.85043423	20.64751007	10.32375504	-	-
34	4.408456618	2.204228309	3.762490172	1.881245086	0	0
35	68.7525622	34.3762811	47.79756033	23.89878017	0	0
36	14.28039692	7.140198459	12.18736058	6.093680292	27.47466289	13.73733145
37	123.9434726	61.97173628	86.16971043	43.08485522	83.25312802	41.62656401
38	29.79003273	14.89501636	25.42290863	12.71145431	81.06792481	40.5339624
39	195.2697319	97.63486595	135.7615636	67.88078179	185.5341527	92.76707635
40	0.176385959	0.08819298	0.150548953	0.075274476	-	-
41	29.70086845	14.85043423	20.64751007	10.32375504	-	-
42	4.408456618	2.204228309	3.762490172	1.881245086	0	0
43	68.7525622	34.3762811	47.79756033	23.89878017	0	0
44	14.28039692	7.140198459	12.18736058	6.093680292	27.47466289	13.73733145
45	123.9434726	61.97173628	86.16971043	43.08485522	83.25312802	41.62656401
46	29.79003273	14.89501636	25.42290863	12.71145431	81.06792481	40.5339624
47	195.2697319	97.63486595	135.7615636	67.88078179	185.5341527	92.76707635
48	0.176385959	0.08819298	0.150548953	0.075274476	-	-
49	29.70086845	14.85043423	20.64751007	10.32375504	-	-
50	4.408456618	2.204228309	3.762490172	1.881245086	0	0
51	68.7525622	34.3762811	47.79756033	23.89878017	0	0
52	14.28039692	7.140198459	12.18736058	6.093680292	27.47466289	13.73733145
53	123.9434726	61.97173628	86.16971043	43.08485522	83.25312802	41.62656401
54	29.79003273	14.89501636	25.42290863	12.71145431	81.06792481	40.5339624
55	195.2697319	97.63486595	135.7615636	67.88078179	185.5341527	92.76707635
56	0.176385959	0.08819298	0.150548953	0.075274476	-	-
57	29.70086845	14.85043423	20.64751007	10.32375504	-	-
58	4.408456618	2.204228309	3.762490172	1.881245086	0	0
59	68.7525622	34.3762811	47.79756033	23.89878017	0	0
60	14.28039692	7.140198459	12.18736058	6.093680292	27.47466289	13.73733145
61	123.9434726	61.97173628	86.16971043	43.08485522	83.25312802	41.62656401
62	29.79003273	14.89501636	25.42290863	12.71145431	81.06792481	40.5339624
63	195.2697319	97.63486595	135.7615636	67.88078179	185.5341527	92.76707635
64	0.176385959	0.08819298	0.150548953	0.075274476	-	-

65	29.70086845	14.85043423	20.64751007	10.32375504	-	-
66	4.408456618	2.204228309	3.762490172	1.881245086	0	0
67	68.7525622	34.3762811	47.79756033	23.89878017	0	0
68	14.28039692	7.140198459	12.18736058	6.093680292	27.47466289	13.73733145
69	123.9434726	61.97173628	86.16971043	43.08485522	83.25312802	41.62656401
70	29.79003273	14.89501636	25.42290863	12.71145431	81.06792481	40.5339624
71	195.2697319	97.63486595	135.7615636	67.88078179	185.5341527	92.76707635
72	0.176385959	0.08819298	0.150548953	0.075274476	-	-
73	29.70086845	14.85043423	20.64751007	10.32375504	-	-
74	4.408456618	2.204228309	3.762490172	1.881245086	0	0
75	68.7525622	34.3762811	47.79756033	23.89878017	0	0
76	14.28039692	7.140198459	12.18736058	6.093680292	27.47466289	13.73733145
77	123.9434726	61.97173628	86.16971043	43.08485522	83.25312802	41.62656401
78	29.79003273	14.89501636	25.42290863	12.71145431	81.06792481	40.5339624
79	195.2697319	97.63486595	135.7615636	67.88078179	185.5341527	92.76707635
80	0.176385959	0.08819298	0.150548953	0.075274476	-	-
81	29.70086845	14.85043423	20.64751007	10.32375504	-	-
82	4.408456618	2.204228309	3.762490172	1.881245086	0	0
83	68.7525622	34.3762811	47.79756033	23.89878017	0	0
84	14.28039692	7.140198459	12.18736058	6.093680292	27.47466289	13.73733145
85	123.9434726	61.97173628	86.16971043	43.08485522	83.25312802	41.62656401
86	29.79003273	14.89501636	25.42290863	12.71145431	81.06792481	40.5339624
87	195.2697319	97.63486595	135.7615636	67.88078179	185.5341527	92.76707635
88	0.176385959	0.08819298	0.150548953	0.075274476	-	-
89	29.70086845	14.85043423	20.64751007	10.32375504	-	-
90	4.408456618	2.204228309	3.762490172	1.881245086	0	0
91	68.7525622	34.3762811	47.79756033	23.89878017	0	0
92	14.28039692	7.140198459	12.18736058	6.093680292	27.47466289	13.73733145
93	123.9434726	61.97173628	86.16971043	43.08485522	83.25312802	41.62656401
94	29.79003273	14.89501636	25.42290863	12.71145431	81.06792481	40.5339624
95	195.2697319	97.63486595	135.7615636	67.88078179	185.5341527	92.76707635

Table D.5: Observed wave types, regular waves (L_{quay} / L > 0)

Configuration	L_{quay} / L	h_{sw} / L	d_{wq} / L	H / L	Very high peak in data?	Observed wave type
24	0.15	0.090281	-0.02	0.05	Yes	*Data lost
25	0.15	0.090281	-0.02	0.117	No, multiple high peaks, no very high	Particles flying away. Numerical instability.
26	0.15	0.090281	0	0.05	No, multiple high peaks, no very high	*Data lost
27	0.15	0.090281	0	0.117	Yes	Breaks at start quay
28	0.15	0.090281	0.02	0.05	Yes	Particles suddenly turning. Numerical instability.
29	0.15	0.090281	0.02	0.117	One peak 1.5 times higher than other peaks	Breaks at start quay, but impact located just in front of wall.
30	0.15	0.090281	0.04	0.05	Yes	Slightly breaking
31	0.15	0.090281	0.04	0.117	No	Breaks on wall
32	0.15	0.095033	-0.02	0.05	Yes, two	Bouncing particles. Numerical instability.
33	0.15	0.095033	-0.02	0.117	Yes	Particles flying away. Numerical instability.
34	0.15	0.095033	0	0.05	One peak 1.5 times higher than other peaks	Breaks at start quay.

35	0.15	0.095033	0	0.117	One peak 1.5 times higher than other peaks	Particles suddenly turning. Numerical instability.
36	0.15	0.095033	0.02	0.05	Yes	Particles suddenly turning. Numerical instability.
37	0.15	0.095033	0.02	0.117	Yes	Breaks at start quay, but impact located just in front of wall.
38	0.15	0.095033	0.04	0.05	No	Quasi-static / slightly breaking
39	0.15	0.095033	0.04	0.117	One peak 1.5 times higher than other peaks	Wave breaks on the quay, just in front of wall
40	0.15	0.099784	-0.02	0.05	Yes	Bouncing particles. Numerical instability.
41	0.15	0.099784	-0.02	0.117	No	Particles suddenly turning. Numerical instability.
42	0.15	0.099784	0	0.05	No	Particles suddenly turning. Numerical instability.
43	0.15	0.099784	0	0.117	No	Particles flying away. Numerical instability.
44	0.15	0.099784	0.02	0.05	Yes	Particles suddenly turning. Numerical instability.
45	0.15	0.099784	0.02	0.117	No	Breaks at start quay, but impact located just in front of wall.
46	0.15	0.099784	0.04	0.05	No	Quasi-static / slightly breaking
47	0.15	0.099784	0.04	0.117	No	Breaks on wall.
48	0.3	0.090281	-0.02	0.05	Yes, multiple high peaks	Bouncing particles. Numerical instability.
49	0.3	0.090281	-0.02	0.117	No	Breaks at start quay.
50	0.3	0.090281	0	0.05	Yes	Particles flying away. Numerical instability.
51	0.3	0.090281	0	0.117	Yes	Breaks at start quay.
52	0.3	0.090281	0.02	0.05	One peak 1.5 times higher than other peaks	Breaks on quay.
53	0.3	0.090281	0.02	0.117	Yes, multiple towards end simulation	Breaks on quay.
54	0.3	0.090281	0.04	0.05	Yes	Slightly breaking.
55	0.3	0.090281	0.04	0.117	No	Breaks at start quay.
56	0.3	0.095033	-0.02	0.05	Yes	Bouncing particles. Numerical instability.
57	0.3	0.095033	-0.02	0.117	No	Breaks on quay.
58	0.3	0.095033	0	0.05	Yes	Particles suddenly turning. Numerical instability.
59	0.3	0.095033	0	0.117	One peak 1.5 times higher than other peaks	Breaks at start quay.
60	0.3	0.095033	0.02	0.05	No	Breaks on quay.
61	0.3	0.095033	0.02	0.117	One peak 1.5 times higher than other peaks	Breaks on quay.

62	0.3	0.095033	0.04	0.05	No	Slightly breaking.
63	0.3	0.095033	0.04	0.117	No	Breaks at start quay.
64	0.3	0.099784	-0.02	0.05	Multiple at the start	Bouncing particles. Numerical instability.
65	0.3	0.099784	-0.02	0.117	One peak 1.5 times higher than other peaks	Breaks on quay.
66	0.3	0.099784	0	0.05	Yes	Particles suddenly turning. Numerical instability.
67	0.3	0.099784	0	0.117	One peak 2 times higher than other peaks	Breaks at start quay.
68	0.3	0.099784	0.02	0.05	No	Breaks on quay.
69	0.3	0.099784	0.02	0.117	Multiple towards end simulation	Breaks at start quay.
70	0.3	0.099784	0.04	0.05	No	Slightly breaking.
71	0.3	0.099784	0.04	0.117	Yes	Breaks at start quay.
72	0.45	0.090281	-0.02	0.05	Yes	Bouncing particles. Numerical instability.
73	0.45	0.090281	-0.02	0.117	Higher peaks towards the end	Breaks at start quay.
74	0.45	0.090281	0	0.05	Yes	Sloshing water.
75	0.45	0.090281	0	0.117	No	Breaks at start quay.
76	0.45	0.090281	0.02	0.05	No	Breaks on quay.
77	0.45	0.090281	0.02	0.117	Yes	Breaks on quay.
78	0.45	0.090281	0.04	0.05	A couple (4) high peaks	Breaks on quay.
79	0.45	0.090281	0.04	0.117	No	Breaks on quay.
80	0.45	0.095033	-0.02	0.05	Multiple at start simulation	Bouncing particles. Numerical instability.
81	0.45	0.095033	-0.02	0.117	One peak 1.5 times higher than other peaks	Breaks on quay.
82	0.45	0.095033	0	0.05	Yes	Sloshing water.
83	0.45	0.095033	0	0.117	No	Breaks at start quay.
84	0.45	0.095033	0.02	0.05	One peak 1.5 times higher than other peaks	Breaks on quay.
85	0.45	0.095033	0.02	0.117	No	Breaks on quay.
86	0.45	0.095033	0.04	0.05	No	Breaks on quay.
87	0.45	0.095033	0.04	0.117	Yes	Breaks on quay.
88	0.45	0.099784	-0.02	0.05	Yes	Bouncing particles. Numerical instability.
89	0.45	0.099784	-0.02	0.117	No	Breaks on wall.
90	0.45	0.099784	0	0.05	Yes	Sloshing water.
91	0.45	0.099784	0	0.117	No	Breaks at start quay.
92	0.45	0.099784	0.02	0.05	One peak 1.5 times higher than other peaks	Slightly breaking
93	0.45	0.099784	0.02	0.117	Yes, 2	Breaks on quay.
94	0.45	0.099784	0.04	0.05	No	Breaks on quay.
95	0.45	0.099784	0.04	0.117	Yes	Breaks on quay.
96	0.30	-	0.08	0.117	-	Breaks on wall.
97	0.45	-	0.08	0.117	-	Breaks on quay.
98	0.30	-	0.12	0.117	-	Quasi-standing.

99	0.45	-	0.117	0.117	-	Quasi-standing.
100	0.45	-	0.1638	0.117	-	Quasi-standing.

* 96-100 are additional runs to compare with lab experiment data

Irregular waves

Table D.6: Values dimensionless parameters configurations irregular waves

Configuration	L_{quay} / L_{op}	h_{sw} / L_{op}	d_{wq} / L_{op}	H_s / L_{op}
0	0.0	0.073314656	0.02	0.02
1	0.0	0.073314656	0.02	0.047
2	0.0	0.073314656	0.04	0.02
3	0.0	0.073314656	0.04	0.047
4	0.0	0.077173322	0.02	0.02
5	0.0	0.077173322	0.02	0.047
6	0.0	0.077173322	0.04	0.02
7	0.0	0.077173322	0.04	0.047
8	0.0	0.081031988	0.02	0.02
9	0.0	0.081031988	0.02	0.047
10	0.0	0.081031988	0.04	0.02
11	0.0	0.081031988	0.04	0.047
12	0.15	0.073314656	0.02	0.02
13	0.15	0.073314656	0.02	0.047
14	0.15	0.073314656	0.04	0.02
15	0.15	0.073314656	0.04	0.047
16	0.15	0.077173322	0.02	0.02
17	0.15	0.077173322	0.02	0.047
18	0.15	0.077173322	0.04	0.02
19	0.15	0.077173322	0.04	0.047
20	0.15	0.081031988	0.02	0.02
21	0.15	0.081031988	0.02	0.047
22	0.15	0.081031988	0.04	0.02
23	0.15	0.081031988	0.04	0.047
24	0.3	0.073314656	0.02	0.02
25	0.3	0.073314656	0.02	0.047
26	0.3	0.073314656	0.04	0.02
27	0.3	0.073314656	0.04	0.047
28	0.3	0.077173322	0.02	0.02
29	0.3	0.077173322	0.02	0.047
30	0.3	0.077173322	0.04	0.02
31	0.3	0.077173322	0.04	0.047
32	0.3	0.081031988	0.02	0.02
33	0.3	0.081031988	0.02	0.047
34	0.3	0.081031988	0.04	0.02
35	0.3	0.081031988	0.04	0.047
36	0.45	0.073314656	0.02	0.02
37	0.45	0.073314656	0.02	0.047
38	0.45	0.073314656	0.04	0.02
39	0.45	0.073314656	0.04	0.047
40	0.45	0.077173322	0.02	0.02
41	0.45	0.077173322	0.02	0.047
42	0.45	0.077173322	0.04	0.02
43	0.45	0.077173322	0.04	0.047
44	0.45	0.081031988	0.02	0.02
45	0.45	0.081031988	0.02	0.047
46	0.45	0.081031988	0.04	0.02

47	0.45	0.081031988	0.04	0.047

Table D.7: Computed irregular wave forces using DualSPHysics

Configuration	F_{max} [kN/m]	$F_{0.1\%}$ [kN/m]
0	6.381395	6.264361
1	15.465176	15.147546
2	13.864329	13.691057
3	24.026578	23.698034
4	6.381395	6.264361
5	15.473272	15.149936
6	13.864329	13.691057
7	24.160539	23.828309
8	6.381395	6.264361
9	15.509387	15.173199
10	13.864329	13.691057
11	24.470873	24.122187
12	9.779130	6.784893
13	71.709698	26.858582
14	17.239093	13.418243
15	128.271512	42.606028
16	9.779130	6.784893
17	54.023008	23.937066
18	17.239093	13.361536
19	102.068201	40.344387
20	9.779130	6.784893
21	50.559052	24.493449
22	17.239093	13.453494
23	110.785433	41.057374
24	11.448573	6.333902
25	65.255112	26.668107
26	20.599599	14.330228
27	184.871415	49.929794
28	11.448573	6.333902
29	68.033945	27.005928
30	22.461047	14.946051
31	178.673792	48.186266
32	11.448573	6.333902
33	60.731072	26.076815
34	22.396112	14.680920
35	127.288925	52.693322
36	6.013402	5.226592
37	35.019559	21.175893
38	18.849810	14.015908
39	85.767142	37.383195
40	6.013402	5.226592
41	39.710662	21.166792
42	19.324563	13.880856
43	106.857250	37.704557
44	6.013402	5.233276
45	43.285545	21.024196
46	22.494566	14.081221
47	47 97.761485	40.766034

Table D.8: Computed irregular wave forces using theories

Configuration	F_{Tuin} [kN/m]	$F_{adapted\ Tuin}$ [kN/m]	F_{Goda} [kN/m]	$F_{Den\ Heijer}$ [kN/m]	F_{max} linear standing wave χ=1 [kN/m]	F_{max} linear standing wave χ=0 [kN/m]
0	40.51271	43.1374	5.344053	12.43285	6.927859	3.876195
1	102.6478	119.0768	15.13919	52.19147	19.38203	8.14128
2	78.35292	83.45787	12.44048	12.43285	15.39878	10.6728
3	190.935	221.6468	24.8671	52.19147	32.31779	17.17031
4	40.51271	43.1374	5.343882	12.43285	6.927859	3.876195
5	102.6478	119.0768	15.13912	52.19147	19.38203	8.14128
6	78.35292	83.45787	12.44044	12.43285	15.39878	10.6728
7	190.935	221.6468	24.86703	52.19147	32.31779	17.17031
8	40.51271	43.1374	5.34398	12.43285	6.927859	3.876195
9	102.6478	119.0768	15.13911	52.19147	19.38203	8.14128
10	78.35292	83.45787	12.44043	12.43285	15.39878	10.6728
11	190.935	221.6468	24.86702	52.19147	32.31779	17.17031
12	40.51271	43.1374	5.344053	12.43285	6.927859	3.876195
13	102.6478	119.0768	15.13919	52.19147	19.38203	8.14128
14	78.35292	83.45787	12.44048	12.43285	15.39878	10.6728
15	190.935	221.6468	24.8671	52.19147	32.31779	17.17031
16	40.51271	43.1374	5.343882	12.43285	6.927859	3.876195
17	102.6478	119.0768	15.13912	52.19147	19.38203	8.14128
18	78.35292	83.45787	12.44044	12.43285	15.39878	10.6728
19	190.935	221.6468	24.86703	52.19147	32.31779	17.17031
20	40.51271	43.1374	5.34398	12.43285	6.927859	3.876195
21	102.6478	119.0768	15.13911	52.19147	19.38203	8.14128
22	78.35292	83.45787	12.44043	12.43285	15.39878	10.6728
23	190.935	221.6468	24.86702	52.19147	32.31779	17.17031
24	40.51271	43.1374	5.344053	12.43285	6.927859	3.876195
25	102.6478	119.0768	15.13919	52.19147	19.38203	8.14128
26	78.35292	83.45787	12.44048	12.43285	15.39878	10.6728
27	190.935	221.6468	24.8671	52.19147	32.31779	17.17031
28	40.51271	43.1374	5.343882	12.43285	6.927859	3.876195
29	102.6478	119.0768	15.13912	52.19147	19.38203	8.14128
30	78.35292	83.45787	12.44044	12.43285	15.39878	10.6728
31	190.935	221.6468	24.86703	52.19147	32.31779	17.17031
32	40.51271	43.1374	5.34398	12.43285	6.927859	3.876195
33	102.6478	119.0768	15.13911	52.19147	19.38203	8.14128
34	78.35292	83.45787	12.44043	12.43285	15.39878	10.6728
35	190.935	221.6468	24.86702	52.19147	32.31779	17.17031
36	40.51271	43.1374	5.344053	12.43285	6.927859	3.876195
37	102.6478	119.0768	15.13919	52.19147	19.38203	8.14128
38	78.35292	83.45787	12.44048	12.43285	15.39878	10.6728
39	190.935	221.6468	24.8671	52.19147	32.31779	17.17031
40	40.51271	43.1374	5.343882	12.43285	6.927859	3.876195
41	102.6478	119.0768	15.13912	52.19147	19.38203	8.14128
42	78.35292	83.45787	12.44044	12.43285	15.39878	10.6728
43	190.935	221.6468	24.86703	52.19147	32.31779	17.17031
44	40.51271	43.1374	5.34398	12.43285	6.927859	3.876195
45	102.6478	119.0768	15.13911	52.19147	19.38203	8.14128
46	78.35292	83.45787	12.44043	12.43285	15.39878	10.6728
47	190.935	221.6468	24.86702	52.19147	32.31779	17.17031

Table D.9: Computed irregular wave forces using Cooker-Peregrine with different velocities (u_{lwt} & u_{3rd}) and impulse durations (dt)

Configuration	$F_{Cooker-Pperegrine}$, dt=0.05, u_{lwt} [kN/m]	$F_{Cooker-Peregrine}$, dt=0.1, u_{lwt} [kN/m]	$F_{Cooker-Peregrine}$, dt=0.05, u_{3rd} [kN/m]	$F_{Cooker-Peregrine}$, dt=0.1, u_{3rd} [kN/m]	$F_{Cooker-Peregrine}$, dt=0.05, $u_{shallow}$ [kN/m]	$F_{Cooker-Peregrine}$, dt=0.1, $u_{shallow}$ [kN/m]
0	3.98201989	1.991009945	3.739360876	1.869680438	20.6857019	10.34285095
1	21.28871116	10.64435558	18.33046881	9.165234406	43.45799336	21.72899668
2	11.00589956	5.502949779	10.33215873	5.166079363	80.89630349	40.44815174
3	45.18582154	22.59291077	38.90094239	19.45047119	130.533188	65.26659401
4	3.98201989	1.991009945	3.739360876	1.869680438	20.6857019	10.34285095
5	21.28871116	10.64435558	18.33046881	9.165234406	43.45799336	21.72899668
6	11.00589956	5.502949779	10.33215873	5.166079363	80.89630349	40.44815174
7	45.18582154	22.59291077	38.90094239	19.45047119	130.533188	65.26659401
8	3.98201989	1.991009945	3.739360876	1.869680438	20.6857019	10.34285095
9	21.28871116	10.64435558	18.33046881	9.165234406	43.45799336	21.72899668
10	11.00589956	5.502949779	10.33215873	5.166079363	80.89630349	40.44815174
11	45.18582154	22.59291077	38.90094239	19.45047119	130.533188	65.26659401
12	3.98201989	1.991009945	3.739360876	1.869680438	20.6857019	10.34285095
13	21.28871116	10.64435558	18.33046881	9.165234406	43.45799336	21.72899668
14	11.00589956	5.502949779	10.33215873	5.166079363	80.89630349	40.44815174
15	45.18582154	22.59291077	38.90094239	19.45047119	130.533188	65.26659401
16	3.98201989	1.991009945	3.739360876	1.869680438	20.6857019	10.34285095
17	21.28871116	10.64435558	18.33046881	9.165234406	43.45799336	21.72899668
18	11.00589956	5.502949779	10.33215873	5.166079363	80.89630349	40.44815174
19	45.18582154	22.59291077	38.90094239	19.45047119	130.533188	65.26659401
20	3.98201989	1.991009945	3.739360876	1.869680438	20.6857019	10.34285095
21	21.28871116	10.64435558	18.33046881	9.165234406	43.45799336	21.72899668
22	11.00589956	5.502949779	10.33215873	5.166079363	80.89630349	40.44815174
23	45.18582154	22.59291077	38.90094239	19.45047119	130.533188	65.26659401
24	3.98201989	1.991009945	3.739360876	1.869680438	20.6857019	10.34285095
25	21.28871116	10.64435558	18.33046881	9.165234406	43.45799336	21.72899668
26	11.00589956	5.502949779	10.33215873	5.166079363	80.89630349	40.44815174
27	45.18582154	22.59291077	38.90094239	19.45047119	130.533188	65.26659401
28	3.98201989	1.991009945	3.739360876	1.869680438	20.6857019	10.34285095
29	21.28871116	10.64435558	18.33046881	9.165234406	43.45799336	21.72899668
30	11.00589956	5.502949779	10.33215873	5.166079363	80.89630349	40.44815174
31	45.18582154	22.59291077	38.90094239	19.45047119	130.533188	65.26659401
32	3.98201989	1.991009945	3.739360876	1.869680438	20.6857019	10.34285095
33	21.28871116	10.64435558	18.33046881	9.165234406	43.45799336	21.72899668
34	11.00589956	5.502949779	10.33215873	5.166079363	80.89630349	40.44815174
35	45.18582154	22.59291077	38.90094239	19.45047119	130.533188	65.26659401
36	3.98201989	1.991009945	3.739360876	1.869680438	20.6857019	10.34285095
37	21.28871116	10.64435558	18.33046881	9.165234406	43.45799336	21.72899668
38	11.00589956	5.502949779	10.33215873	5.166079363	80.89630349	40.44815174
39	45.18582154	22.59291077	38.90094239	19.45047119	130.533188	65.26659401
40	3.98201989	1.991009945	3.739360876	1.869680438	20.6857019	10.34285095
41	21.28871116	10.64435558	18.33046881	9.165234406	43.45799336	21.72899668
42	11.00589956	5.502949779	10.33215873	5.166079363	80.89630349	40.44815174
43	45.18582154	22.59291077	38.90094239	19.45047119	130.533188	65.26659401
44	3.98201989	1.991009945	3.739360876	1.869680438	20.6857019	10.34285095
45	21.28871116	10.64435558	18.33046881	9.165234406	43.45799336	21.72899668
46	11.00589956	5.502949779	10.33215873	5.166079363	80.89630349	40.44815174
47	45.18582154	22.59291077	38.90094239	19.45047119	130.533188	65.26659401

Table D.10: Observed wave types, irregular waves (L_{quay} / L > 0)

Configuration	L_{quay} / L_{op}	h_{sw} / L_{op}	d_{wq} / L_{op}	H_s / L_{op}	Very high peak in data? Seed 1 / 2	Observed wave type (seed 1 / 2 / 3)
12	0.15	0.073314656	0.02	0.02	No / No / Yes	Quasi-standing* / Slightly breaking (all)
13	0.15	0.073314656	0.02	0.047	No / Yes / Yes (twice as high)	Breaks on wall (all)
14	0.15	0.073314656	0.04	0.02	At odd location / No / Yes	Quasi-standing (all)
15	0.15	0.073314656	0.04	0.047	Yes / Yes / Yes, two	Breaks on wall (all)
16	0.15	0.077173322	0.02	0.02	No / No / Yes	Quasi-standing* (1/2) / Slightly breaking (1/2)/ Numerical instability (3)
17	0.15	0.077173322	0.02	0.047	No / No / No	Breaks on wall (all)
18	0.15	0.077173322	0.04	0.02	At odd location / No / No	Quasi-standing (all)
19	0.15	0.077173322	0.04	0.047	No / Yes / Yes, a couple	Breaks on wall (1/2) / Bouncing of wall > Numerical instability (3)
20	0.15	0.081031988	0.02	0.02	No / No / Yes	Quasi-standing* (1/2) / Numerical instability (3)
21	0.15	0.081031988	0.02	0.047	No / Yes / No	Breaks on wall (all)
22	0.15	0.081031988	0.04	0.02	At odd location / No / No	Quasi-standing (all)
23	0.15	0.081031988	0.04	0.047	Yes / Yes / Yes, a couple	Breaks on wall (all)
24	0.3	0.073314656	0.02	0.02	No / No / No	Quasi-standing* (all)
25	0.3	0.073314656	0.02	0.047	1.5 times higher than others / No / No	Breaks on quay (all)
26	0.3	0.073314656	0.04	0.02	No / No / No	Quasi-standing* (all)
27	0.3	0.073314656	0.04	0.047	Yes / Yes, a couple / Yes	Breaks on quay (all)
28	0.3	0.077173322	0.02	0.02	No / No / No	Quasi-standing* (all)
29	0.3	0.077173322	0.02	0.047	No / Yes / Yes (twice as high)	Breaks on quay (1,3) / Numerical instability (2)
30	0.3	0.077173322	0.04	0.02	Yes / No / No	Quasi-standing (1/3) / Breaks on quay (2)
31	0.3	0.077173322	0.04	0.047	Yes / Yes / No	Breaks on quay (all)
32	0.3	0.081031988	0.02	0.02	No / No / No	Quasi-standing* (all)
33	0.3	0.081031988	0.02	0.047	No / No / No	Breaks on quay (all)
34	0.3	0.081031988	0.04	0.02	No / No / No	Quasi-standing (all)
35	0.3	0.081031988	0.04	0.047	No / Yes / No	Breaks on quay (all)
36	0.45	0.073314656	0.02	0.02	No / No / No	Quasi-standing* (all)
37	0.45	0.073314656	0.02	0.047	Yes / No / No	Breaks on quay (all)
38	0.45	0.073314656	0.04	0.02	No / No / No	Quasi-standing* (all)
39	0.45	0.073314656	0.04	0.047	Yes, multiple/ Yes / Yes, a couple	Breaks on quay (all)
40	0.45	0.077173322	0.02	0.02	No / No / No	Quasi-standing* (all)
41	0.45	0.077173322	0.02	0.047	Yes, a couple / Yes, a couple / No	Breaks on quay (all)
42	0.45	0.077173322	0.04	0.02	No / No / No	Quasi-standing* (all)
43	0.45	0.077173322	0.04	0.047	Yes, a couple / Yes / Yes	Breaks on quay (all)
44	0.45	0.081031988	0.02	0.02	No / No / No	Quasi-standing* (all)
45	0.45	0.081031988	0.02	0.047	Yes / No / No	Breaks on quay (all)
46	0.45	0.081031988	0.04	0.02	No / No / 1.5 times higher than others	Quasi-standing* (all)
47	0.45	0.081031988	0.04	0.047	No / Yes / No	Breaks on quay (all)

*Quasi-standing pattern in front of quay, on quay more like a small propagating wave which gets reflected

Appendix E: xml file example

The example below shows the xml file of configuration 85 with the values shown in Table E.1.

Table E.1: Dimensionless parameter values configuration 85

Parameter	Value
L_{quay} / L	0.45
h_{sw} / L	0.095
d_{wq} / L	0.02
H / L	0.117


```xml
<case>
  <casedef>
    <constantsdef>
      <gravity x="0" y="0" z="-9.81" comment="Gravitational acceleration"
units_comment="m/s^2" />
      <rhop0 value="1000" comment="Reference density of the fluid" units_comment="kg/m^3" />
      <rhopgradient value="2" comment="Initial density gradient 1:Rhop0, 2:Water column, 3:Max.
water height (default=2)" />
      <hswl value="0" auto="true" comment="Maximum still water level to calculate speedofsound
using coefsound" units_comment="metres (m)" />
      <gamma value="7" comment="Polytropic constant for water used in the state equation" />
      <speedsystem value="0" auto="true" comment="Maximum system speed (by default the
dam-break propagation is used)" />
      <coefsound value="20" comment="Coefficient to multiply speedsystem" />
      <speedsound value="0" auto="true" comment="Speed of sound to use in the simulation (by
default speedofsound=coefsound*speedsystem)" />
      <coefh value="1.2" comment="Coefficient to calculate the smoothing length
(h=coefh*sqrt(3*dp^2) in 3D)" />
      <cflnumber value="0.2" comment="Coefficient to multiply dt" />
    </constantsdef>
    <mkconfig boundcount="230" fluidcount="9">
      <mkorientfluid mk="0" orient="Xyz" />
    </mkconfig>
    <geometry>
      <definition dp="0.12">
        <pointref x="0" y="0" z="0" />
        <pointmin x="-10" y="0" z="-0.6" />
        <pointmax x="162.8" y="0" z="30.53" />
      </definition>
      <commands>
        <list name="GeometryForNormals">
          <setactive drawpoints="0" drawshapes="1" />
          <setshapemode>actual | bound</setshapemode>
                                        <setmkbound mk="0" />
                                        <drawextrude closed="false">
                                                <extrude x="0" y="2" z="0" />
            <point x="#Tankx0" y="-1" z="#Tankz0" />
            <point x="#Tankx1" y="-1" z="#Tankz1" />
            <point x="#Tankx2" y="-1" z="#Tankz2" />
            <layers vdp="0.5" />
```

```
    </drawextrude>

            <setnormalinvert invert="false" />
                                        <setmkbound mk="1" />
    <drawbox>
      <boxfill>solid</boxfill>
      <point x="#Quayx1" y="-1" z="#Tankz1" />
      <endpoint x="#Quayx2" y="1" z="#Quayz2" />
      <layers vdp="0.5" />
    </drawbox>

                                        <setmkbound mk="2" />
    <drawbox>
      <boxfill>solid</boxfill>
      <point x="#Storm_wallx1" y="-1" z="#Quayz2" />
      <endpoint x="#Quayx2" y="1" z="#Storm_wallz2" />
      <layers vdp="0.5" />
    </drawbox>
    <shapeout file="hdp" />
    <resetdraw />
  </list>
  <mainlist>

    <newvar Tankx0="-10" Tankz0="0" />
    <newvar Tankx1="162.8" Tankz1="0" />
    <newvar Tankx2="162.8" Tankz2="30.53" />
    <newvar Hdp="Dp/2" />
            <newvar Quayx1="144" Quayx2="162.8" />
    <newvar Quayz2="14.25" />
            <newvar Storm_wallx1="154.8" />
            <newvar Storm_wallz2="16.53" />
                                        <exportvar vars="Hdp" />

    <runlist name="GeometryForNormals" />

    <setshapemode>actual | bound</setshapemode>
    <setdrawmode mode="full" />

    <setmkbound mk="10" />
    <drawbox>
      <boxfill>solid</boxfill>
      <point x="#-Dp*3" y="-1" z="#Tankz0" />
      <size x="#Dp*3" y="2" z="#(Storm_wallz2-Tankz0)*2" />
    </drawbox>

    <setmkbound mk="0" />
                                        <setfrdrawmode auto="true" />
                                        <drawextrude closed="false">
                                                <extrude x="0" y="2" z="0" />
      <point x="#Tankx0" y="-1" z="#Tankz0" />
      <point x="#Tankx1" y="-1" z="#Tankz1" />
```

```
                <point x="#Tankx2" y="-1" z="#Tankz2" />
                <layers vdp="0,-1,-2" />
            </drawextrude>
                                        <setfrdrawmode auto="false" />

                    <setmkbound mk="1" />
            <drawbox>
                <boxfill>solid</boxfill>
                <point x="#Quayx1" y="-1" z="#Tankz1" />
                <endpoint x="#Quayx2" y="1" z="#Quayz2" />
            </drawbox>

                    <setmkbound mk="2" />
            <drawbox>
                <boxfill>solid</boxfill>
                <point x="#Storm_wallx1" y="-1" z="#Quayz2" />
                <endpoint x="#Quayx2" y="1" z="#Storm_wallz2" />
            </drawbox>

            <setmkfluid mk="0" />
            <fillbox x="0.5" y="0" z="0.12">
                <modefill>void</modefill>
                <point x="0" y="-1" z="0" />
                <size x="154.8" y="2" z="14.73" />
            </fillbox>
            <shapeout file="" />
          </mainlist>
        </commands>
      </geometry>
      <normals>
                          <distanceh value="2.0" comment="Maximum distance (H*distanceh) to
compute normals data (default=2)" />
                          <geometryfile file="[CaseName]_hdp_Actual.vtk" comment="File with
boundary geometry (VTK format)" />
      </normals>
      <motion>
        <objreal ref="10">
          <begin mov="1" start="0" />
          <mvnull id="1" />
        </objreal>
      </motion>
    </casedef>
    <execution>
      <special>
        <initialize>
          <boundnormal_plane mkbound="10">
                                        <point auto="true" comment="Point is calculated
automatically accoding to normal configuration." />
            <normal x="1" y="0" z="0" />
                                        <maxdisth v="0" comment="Maximum distance to boundary
limit. It uses H*maxdisth (default=2)" />
```

```
            </boundnormal_plane>
        </initialize>
        <wavepaddles>
            <piston>
                <mkbound value="10" comment="Mk-Bound of selected particles" />
                <waveorder value="2" comment="Order wave generation 1:1st order, 2:2nd order
(def=1)" />
                <start value="0" comment="Start time (def=0)" />
                <duration value="0" comment="Movement duration, Zero is the end of simulation
(def=0)" />
                <depth value="14.73" comment="Fluid depth (def=0)" />
                <pistondir x="1" y="0" z="0" comment="Movement direction (def=(1,0,0))" />
                <waveheight value="2.8" comment="Wave height" />
                <waveperiod value="3.92" comment="Wave period" />
                <phase value="0" comment="Initial wave phase in function of PI (def=0)" />
                <ramp value="1" comment="Periods of ramp (def=0)" />
                <savemotion xpos="5.0" zpos="-0.26" comment="Saves motion data. xpos and zpos are
optional. zpos=-depth of the measuring point" />
                <awas_zsurf>
                    <startawas value="12.0" comment="Time to start AWAS correction
(def=ramp*waveperiod)" />
                    <swl value="14.73" comment="Still water level (free-surface water)" />
                    <elevation value="2" comment="Order wave to calculate elevation 1:1st order, 2:2nd
order (def=2)" />
                    <gaugex valueh="4" comment="Position in X from piston to measure free-surface
water (def=5*Dp)" />
                    <gaugey value="0" comment="Position in Y to measure free-surface water" />
                    <gaugezmin value="0.2" comment="Minimum position in Z to measure free-surface
water, it must be in water (def=domain limits)" />
                    <gaugezmax value="21.73" comment="Maximum position in Z to measure free-surface
water (def=domain limits)" />
                    <gaugedp value="0.25" comment="Resolution to measure free-surface water, it uses
Dp*gaugedp (def=0.1)" />
                    <coefmasslimit value="0.4" comment="Coefficient to calculate mass of free-surface
(def=0.5 on 3D and 0.4 on 2D)" />
                    <savedata value="1" comment="Saves CSV with information 1:by part, 2:more info
3:by step (def=0)" />
                    <limitace value="2" comment="Factor to limit maximum value of acceleration, with 0
disabled (def=2)" />
                    <_correction coefstroke="1.8" coefperiod="1" powerfunc="3" comment="Drift
correction configuration (def=no applied)" />
                </awas_zsurf>
            </piston>
        </wavepaddles>
    </special>
    <parameters>
        <parameter key="SavePosDouble" value="0" comment="Saves particle position using double
precision (default=0)" />
        <parameter key="Boundary" value="2" comment="Boundary method 1:DBC, 2:mDBC
(default=1)" />
```

```xml
        <parameter key="StepAlgorithm" value="2" comment="Step Algorithm 1:Verlet, 2:Symplectic (default=1)" />
        <parameter key="VerletSteps" value="40" comment="Verlet only: Number of steps to apply Euler timestepping (default=40)" />
        <parameter key="Kernel" value="2" comment="Interaction Kernel 1:Cubic Spline, 2:Wendland (default=2)" />
        <parameter key="ViscoTreatment" value="1" comment="Viscosity formulation 1:Artificial, 2:Laminar+SPS (default=1)" />
        <parameter key="Visco" value="0.01" comment="Viscosity value" />
        <parameter key="ViscoBoundFactor" value="0" comment="Multiply viscosity value with boundary (default=1)" />
        <parameter key="DensityDT" value="3" comment="Density Diffusion Term 0:None, 1:Molteni, 2:Fourtakas, 3:Fourtakas(full) (default=0)" />
        <parameter key="DensityDTvalue" value="0.1" comment="DDT value (default=0.1)" />
        <parameter key="Shifting" value="0" comment="Shifting mode 0:None, 1:Ignore bound, 2:Ignore fixed, 3:Full (default=0)" />
        <parameter key="ShiftCoef" value="-2" comment="Coefficient for shifting computation (default=-2)" />
        <parameter key="ShiftTFS" value="0" comment="Threshold to detect free surface. Typically 1.5 for 2D and 2.75 for 3D (default=0)" />
        <parameter key="RigidAlgorithm" value="1" comment="Rigid Algorithm 0:collision-free, 1:SPH, 2:DEM, 3:Chrono (default=1)" />
        <parameter key="FtPause" value="0.0" comment="Time to freeze the floatings at simulation start (warmup) (default=0)" units_comment="seconds" />
        <parameter key="CoefDtMin" value="0.05" comment="Coefficient to calculate minimum time step dtmin=coefdtmin*h/speedsound (default=0.05)" />
        <parameter key="DtIni" value="0" comment="Initial time step. Use 0 to defult use (default=h/speedsound)" units_comment="seconds" />
        <parameter key="DtMin" value="0" comment="Minimum time step. Use 0 to defult use (default=coefdtmin*h/speedsound)" units_comment="seconds" />
        <parameter key="DtFixed" value="0" comment="Fixed Dt value. Use 0 to disable (default=disabled)" units_comment="seconds" />
        <parameter key="DtFixedFile" value="NONE" comment="Dt values are loaded from file. Use NONE to disable (default=disabled)" units_comment="milliseconds (ms)" />
        <parameter key="DtAllParticles" value="0" comment="Velocity of particles used to calculate DT. 1:All, 0:Only fluid/floating (default=0)" />
        <parameter key="TimeMax" value="461" comment="Time of simulation" units_comment="seconds" />
        <parameter key="TimeOut" value="0.02" comment="Time out data" units_comment="seconds" />
        <parameter key="PartsOutMax" value="1" comment="%/100 of fluid particles allowed to be excluded from domain (default=1)" units_comment="decimal" />
        <parameter key="RhopOutMin" value="700" comment="Minimum rhop valid (default=700)" units_comment="kg/m^3" />
        <parameter key="RhopOutMax" value="1300" comment="Maximum rhop valid (default=1300)" units_comment="kg/m^3" />
        <simulationdomain comment="Defines domain of simulation (default=Uses minimun and maximum position of the generated particles)">
            <posmin x="default" y="default" z="default" comment="e.g.: x=0.5, y=default-1, z=default-10%" />
            <posmax x="default" y="default" z="30.53" />
```

```
        </simulationdomain>
      </parameters>
    </execution>
  </case>
```

Appendix F: Validation DualSPHysics

To validate the DualSPHysics model and select appropriate parameters, the experiments of Den Heijer (1998) are modelled in DualSPHysics. The obtained results are than compared with the results obtained from the laboratory experiments of Den Heijer. This appendix starts with a short description of Den Heijer's experiments. Next, the DualSPHysics model is validated for regular waves. After that, the model is validated for the irregular waves, using the same parameters Den Heijer's experiment.

Den Heijer laboratory experiment

The laboratory experiment of Den Heijer contained several configurations of a vertical wall. Examples are a breakwater, berm or slope in front or a bullnose on the storm wall. Only six contained a vertical wall on a vertical quay as shown in Figure F.1. These six tests are used to compare, as these have a similar geometry as the Kop van Zuid case study.

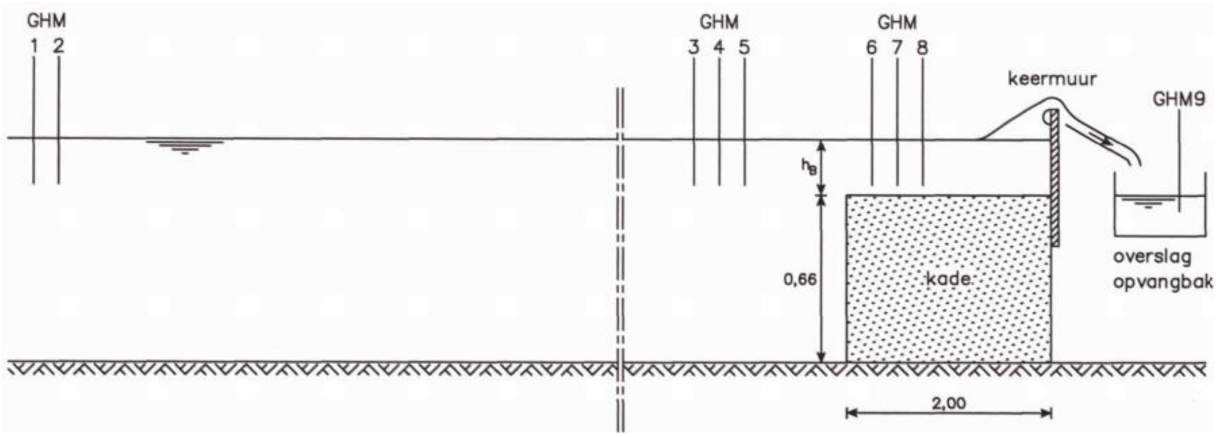

Figure F.1: Experimental set-up experiments 3001-3006 (measurements in m) (Den Heijer, 1998)

The flume used is the DualSPHysics model is 26 m long at the location of GHM 1 and 2 in Figure F.1. The measured waves at GHM 1 and 2 are used as input waves for the DualSPHysics model. For the DualSPHysics model the geometry is chosen the same as the Den Heijer laboratory experiment, but the overtopping catchment container is left out for simplicity reasons. Instead of being catched in a container, the overtopping particles will go out of the domain of the simulation.

Regular waves

This section of the appendix validates the model for wave generation, wave reflection and wave pressure using regular waves. Regular waves are used for this, as the expected behaviour of regular waves is known, whereas irregular waves make the investigation of the previous mentioned parameters unnecessary complex.

Wave generation

To check if the wave piston correctly generates waves and if the waves are correctly reflected, a simplified scenario is used with regular waves and a single vertical wall, without a storm wall on top. Given the significant wave height and peak period used as a regular wave input H = 0.206 m and T = 1.84 s resulted in the output shown in Figure F.2.

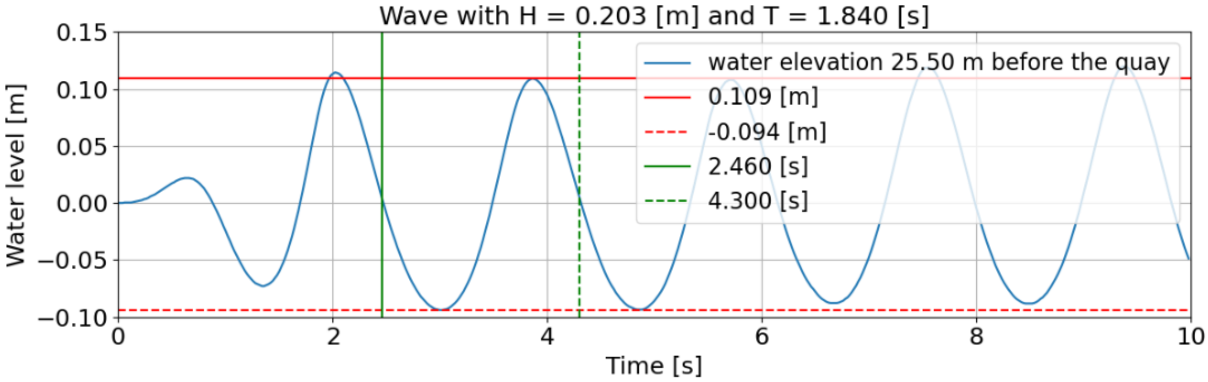

Figure F.2: Measured water elevation 0.5 m after wave piston

The produced wave height comes close to the input wave height (99%). The small decrease might be due to the effect of the bottom, as these are not deep water waves, and the wave height is measured 0.5 m away from the piston.

Wave reflection

The incoming and reflected wave spectrum are determined with the three gauge method of Mansard and Funke (1980). The method relies on the assumption that irregular waves can be seen as a linear superposition of an infinite number of discrete components with their own frequency, phase and amplitude. Knowing the water level at three locations at the same time and the distance between the locations, the phase relationships can be computed. With this information the incoming and reflected wave spectrum are then obtained. A step-by-step guide is provided by Mansard and Funke in their paper. The spectra results of the DualSPHysics model are shown in Figure F.3.

The highest peak is located close at the input frequency (0.54 Hz). The reflection coefficient is around 1 for the peak frequency, as expected. It starts varying more for higher frequencies, but the higher frequencies are not reliable as here the coherency factor, as seen in Figure F.4, decreases while the frequency increases (Mansard & Funke, 1980).

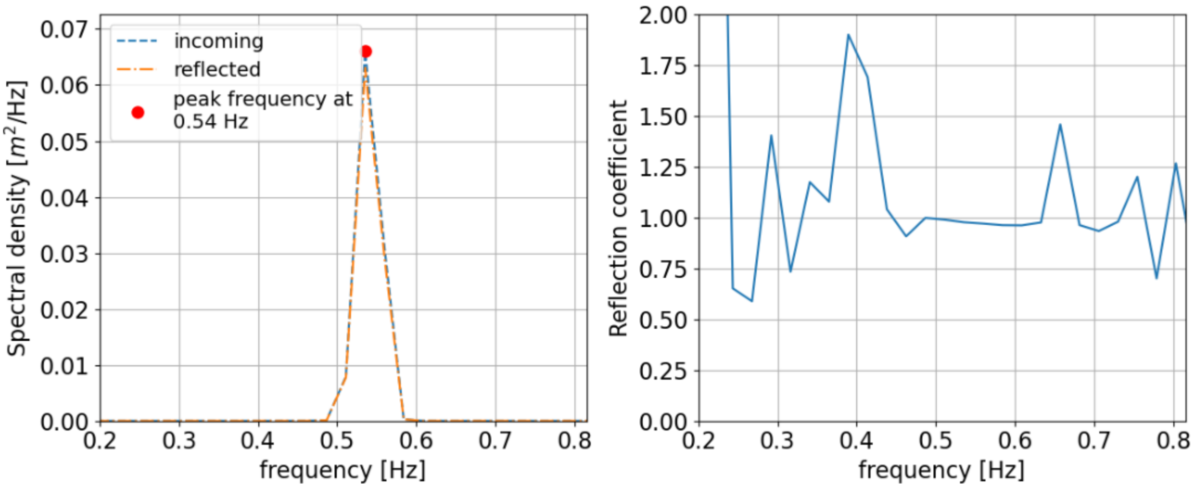

Figure F.3: Incoming and reflected wave spectra (left) and reflection coefficient (right) for regular waves

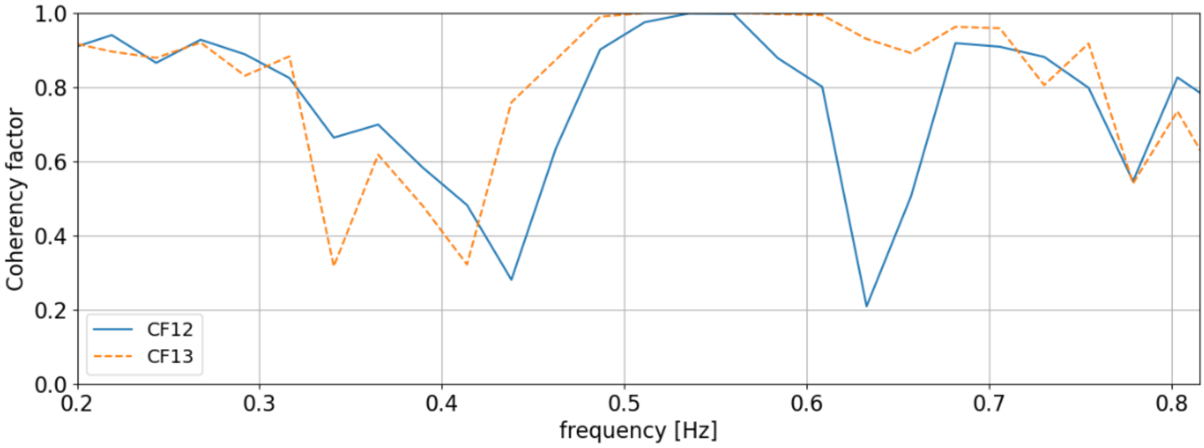

Figure F.4: Coherency factor between sensor 1 and 2 and sensor 1 and 3 regular waves

Wave pressure

As additional check the wave pressure under a wave is also plotted, resulting in Figure F.5. First, a linear part for the part above the still water level is obtained and then an exponential decrease, as expected from linear wave theory. Only the pressure starts at a higher value at the linear part than one would expect from linear wave theory. This can be explained by the second order effect, which is taken into account by DualSPHysics, but not by linear wave theory. The waves in DualSPHysics do not have a sinusoidal form, but a steeper crests and wider bases. The comparison with Goda is also made. Based on the research of Tuin et al. (2022) for a kd_w value of around 1, which is the case for this Den Heijer experiment, Goda is expected to underestimate by a factor of 1.25, as seen in Figure F.6, with respect to linear wave theory which indeed appears to be the case. In conclusion, regular waves in DualSPHysics behave closely as expected.

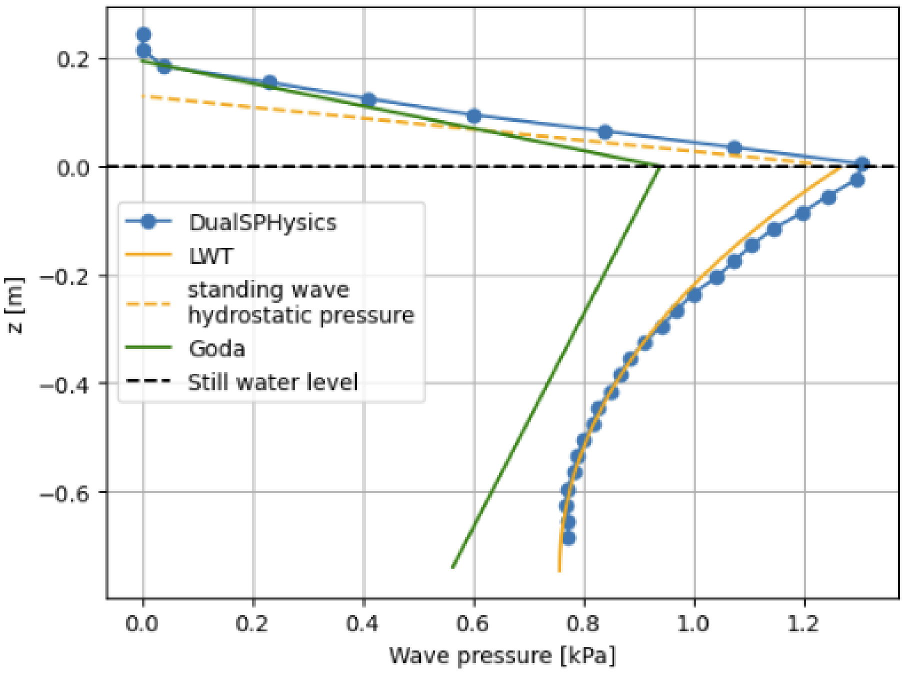

Figure F.5: Wave pressure standing wave

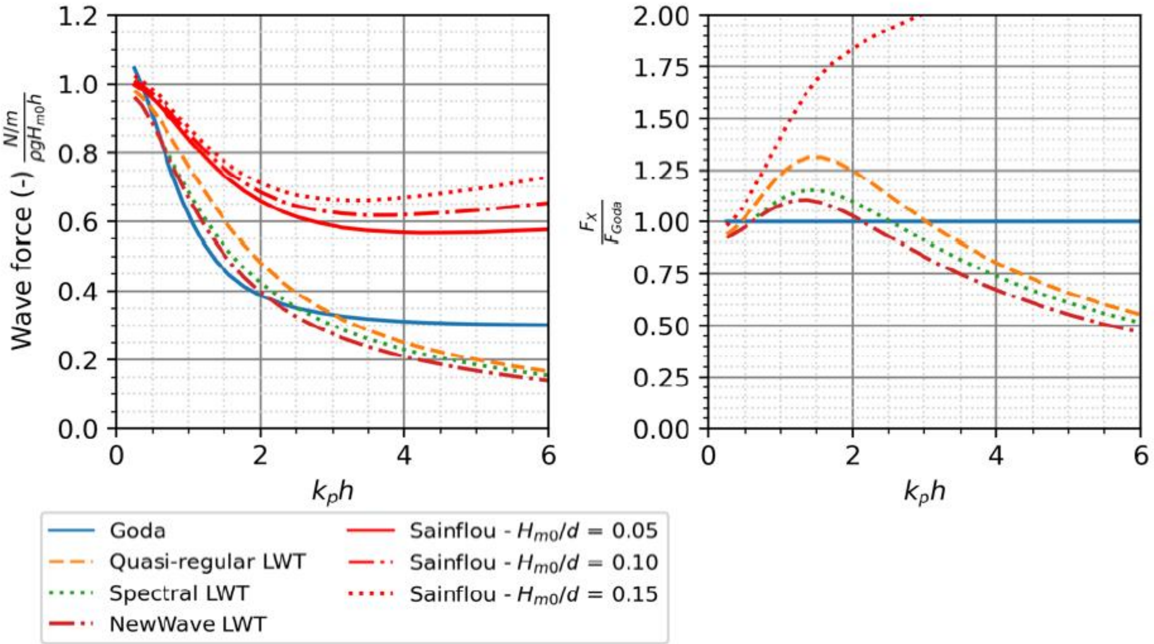

Figure F.6: Comparison between wave force formulae below SWL for 100% reflection. NOTE: results of spectral LWT and New Wave LWT are dependent on the shape of the spectrum. (Tuin et al., 2022)

Irregular waves

Den Heijer used irregular waves in his experiment and reported the values for F_{max}, $F_{1\%}$ and $F_{10\%}$ for all his configurations. For a few configurations he also provided the wave spectra of the incoming and reflected wave together with the reflection coefficient. These results are in this section used to optimize the particle distance, the simulation duration for irregular waves and the output parameters of the DualSPHysics model. Last, the overall model performance is evaluated using Willmott's refined index of agreement.

Pressure measuring

To validate if the pressure is measured accurately enough, the following parameters are altered:

- Location sensor in front of the storm wall
- Interval height of the sensors over the vertical axis
- Output time step

The pressure is measured 1.5 dp in front of the storm wall with intervals of 0.03 m over the vertical axis. To verify these dimensions the pressure is also measured at a larger distance (4 h_{sl}) and with smaller intervals (0.01 m). Measuring at a larger distance gives peaks at approximately the same locations, the overall magnitude is just smaller. Measuring with smaller intervals gives a small decrease in the maximum force in the order of hundredths. Figure F.7 shows an example of the measured force on the storm wall using the initial (and final) model measurement parameters. Figure F.8 and F.9 show the same measured from a larger distance and with smaller intervals respectively.

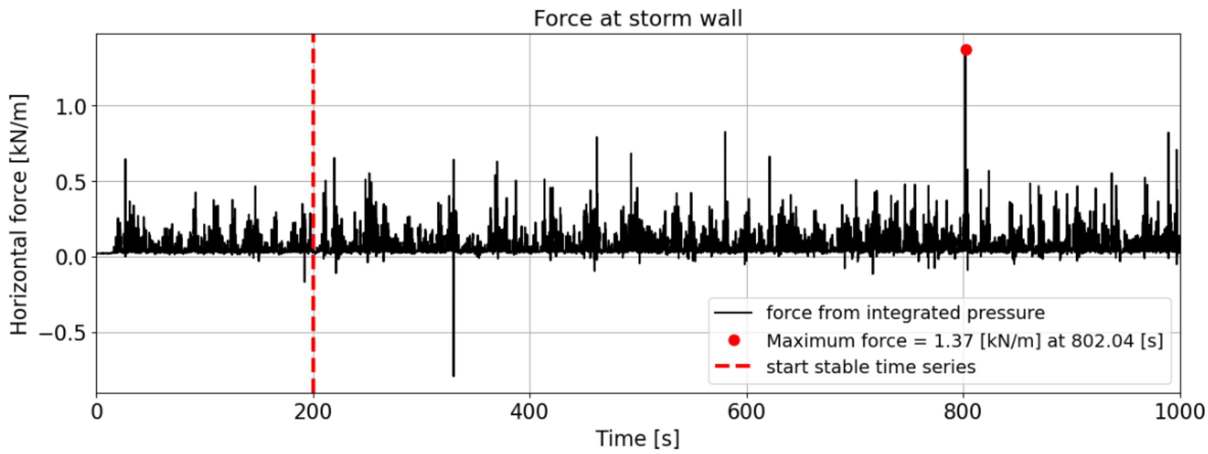

Figure F.7: Force on storm wall measured at -1.5 dp m with intervals of 0.03 m over the vertical

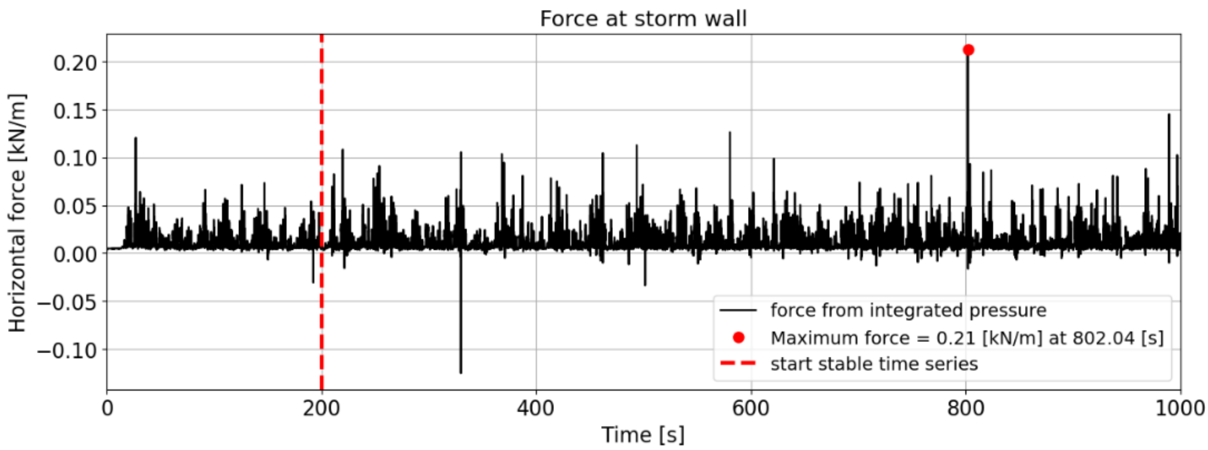

Figure F.8: Force on storm wall measured at 4 hsl m with intervals of 0.03 m over the vertical

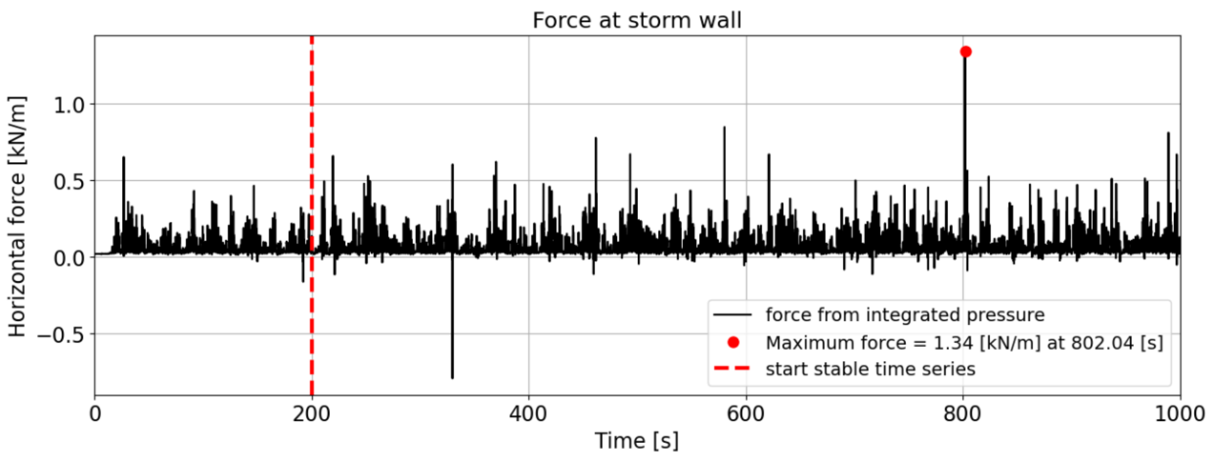

Figure F.9: Force on storm wall measured at -1.5 dp m with intervals of 0.01 m over the vertical

Lastly, Figure F.10 shows the output for a smaller time step output (0.01 s instead of 0.02 s). This output looks quite different. The peak is lower and at a different location. This might indicate that the time step taken before is not small enough to adequately capture the waves.

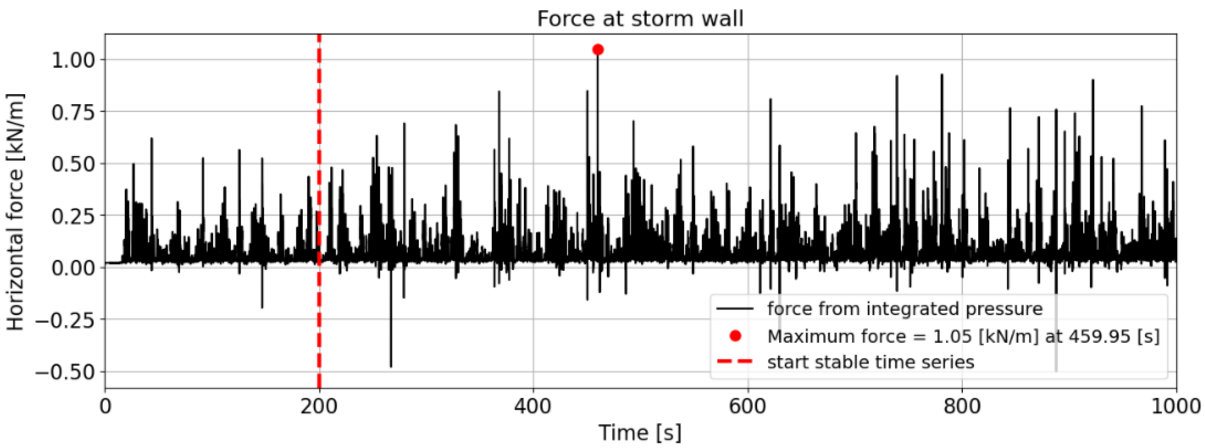

Figure F.10: Force on storm wall measured with time step = 0.01 s

In Figure F.11 one can see that the peak only consists of one point when an output step of 0.02 s is used. One might expect that a point in between might lie higher. However, in Figure F.12 one can see the peak sampled with multiple points (time step 0.005 s) and the peak lies lower. Still even though the peak value decreased with approximately 55%, the impulse, computed by integrating the area under the peak, only decreased with 22%.

The results for the optimum model parameters are still considered valid, as $F_{1\%}$ and $F_{10\%}$ lie close to the values of Den Heijer. In addition, Den Heijer's experiment were performed with the same measurement frequency as used in the previous runs. However, for the Kop van Zuid case studies a smaller time step (0.005) will be used to prevent numerical errors and missing wave impacts.

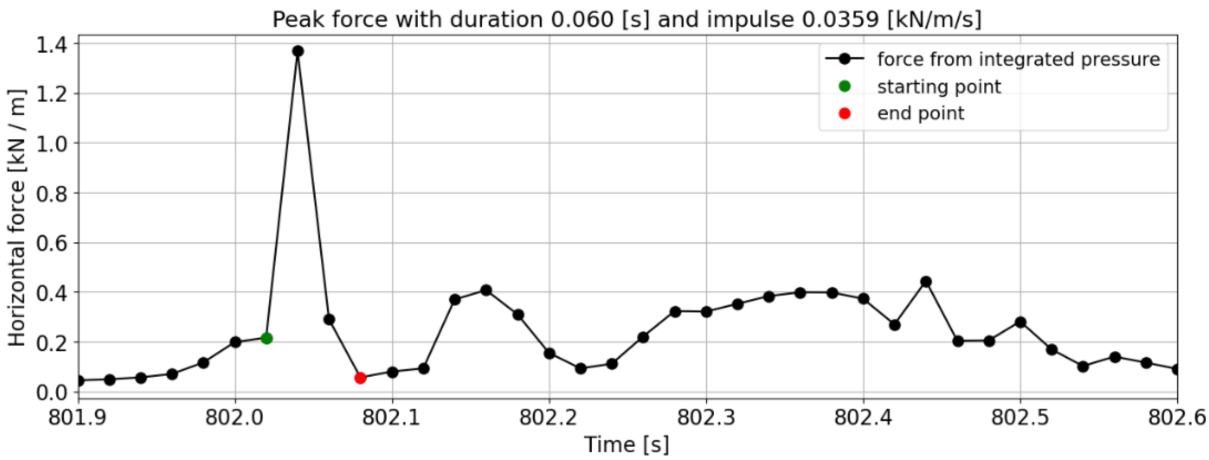

Figure F.11: Peak force on storm wall measured with time step = 0.02 s

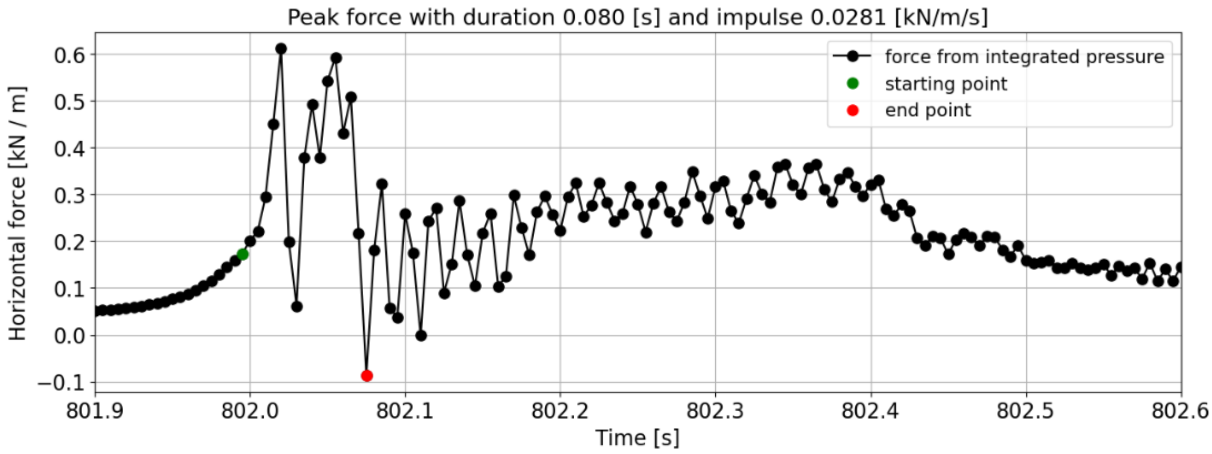

Figure F.12: Peak force on storm wall measured with time step = 0.005 s

Forcing

The first experiment, number 3001, is modelled and optimized in DualSPHysics. With the obtained optimized parameters, the model is also run for the other experiment numbers 3002 till 3006.

The optimized parameters are determined by computing the values for F_{max}, $F_{1\%}$ and $F_{10\%}$ predicted by the model and comparing them with the values of Den Heijer as done in Table F.1 and Figure F.13. Figure F.13 shows the performance of the model for different dp and simulation duration. Table F.1 shows all the exact values from Figure F.13, sorted by increasing sum of absolute errors.

Table F.1: Absolute error in percentages made by the model for different forcing types, ordered by sum of errors

	F_max [kN/m]	F_1% [kN/m]	F_10% [kN/m]	dp [m]	duration [s]	outliers removed
DualSPHysics, raw, dp = 0.025 [m], duration = 1500.0 [s]	194.330087	6.866492	17.431548	0.025	1500	False
DualSPHysics, outliers removed, dp = 0.025 [m], duration = 1500.0 [s]	21.632924	5.829674	17.209192	0.025	1500	True
DualSPHysics, raw, dp = 0.025 [m], duration = 1000.0 [s]	48.861454	1.873411	13.125196	0.025	1000	False
DualSPHysics, outliers removed, dp = 0.025 [m], duration = 1000.0 [s]	1.114925	1.412857	13.019008	0.025	1000	True
DualSPHysics, raw, dp = 0.02 [m], duration = 1500.0 [s]	104.674122	10.924936	2.436955	0.020	1500	False
DualSPHysics, outliers removed, dp = 0.02 [m], duration = 1500.0 [s]	23.21159	12.081759	2.686809	0.020	1500	True
DualSPHysics, raw, dp = 0.02 [m], duration = 1000.0 [s]	104.674122	9.931563	3.130507	0.020	1000	False
DualSPHysics, outliers removed, dp = 0.02 [m], duration = 1000.0 [s]	23.21159	10.6723	3.28634	0.020	1000	True
DualSPHysics, raw, dp = 0.015 [m], duration = 1500.0 [s]	39.770269	10.705722	7.738326	0.015	1500	False
DualSPHysics, outliers removed, dp = 0.015 [m], duration = 1500.0 [s]	19.446321	11.592475	7.93804	0.015	1500	True
DualSPHysics, raw, dp = 0.015 [m], duration = 1000.0 [s]	39.770269	9.251595	8.007347	0.015	1000	False
DualSPHysics, outliers removed, dp = 0.015 [m], duration = 1000.0 [s]	21.782792	10.575794	8.305797	0.015	1000	True

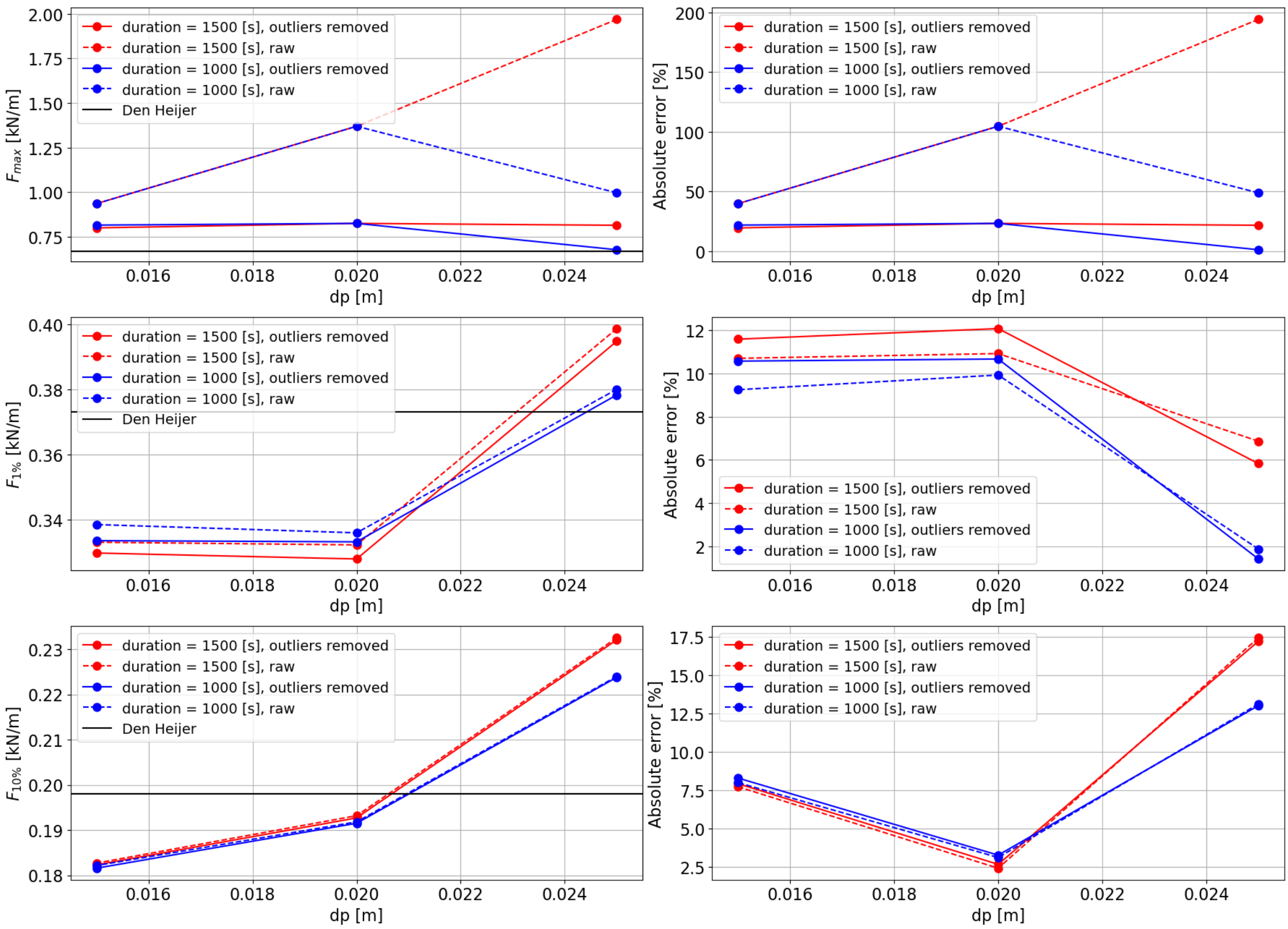

Figure F.13: Predicted and observed values (left) and the absolute error in percentages (left)

Figure F.13 and Table F.1 also show the results with outliers removed. When computing the force and plotting a histogram, some outliers can be detected as discussed in Chapter 3. It is expected that the histogram is not fully continuous. With a decreasing probability of occurrence it can happen that one or two bins are skipped. However, the histograms show multiple larger gaps. The probability of this happening by most of the simulations is quite small. Based on the animations, forces after which a gap longer than three bins has occurred are considered as outliers.
The analysis is done with both the original computed forces (raw) and a version with outliers removed. This application is visible for the maximum force and $F_{1\%}$, but barely has any influence on $F_{10\%}$ as the latter is based on more values. The order of models in Table F.1 shows that removing outliers has a positive effect on the accuracy of the model regarding the maximum force. However, the model tends to underestimate $F_{1\%}$ and $F_{10\%}$ for dp < 0.25. Not removing out high peaks will increase the predicted values for $F_{1\%}$ and $F_{10\%}$ and therefore make the predictions closer to the measurements.

$F_{1\%}$ is mainly influenced by a couple of high peaks and F_{max} by only one. Due to the randomness of an irregular wave field it is logical that the model cannot exactly reproduce the values obtained by Den Heijer and that the errors for more extreme values are larger. Figure F.14 and F.15 show the values which influence $F_{1\%}$ both for the raw and outliers removed dataset.

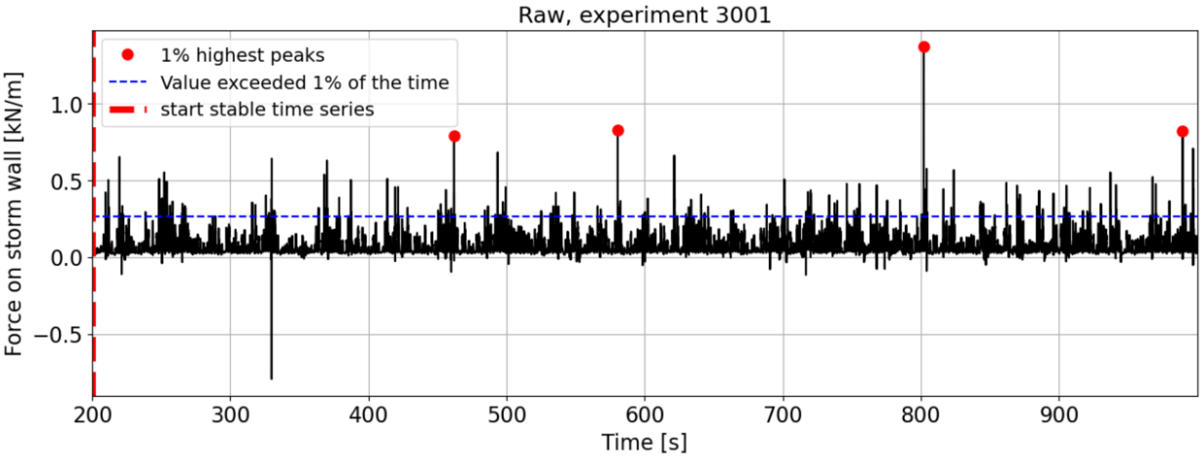

Figure F.14: 1% peaks in raw data

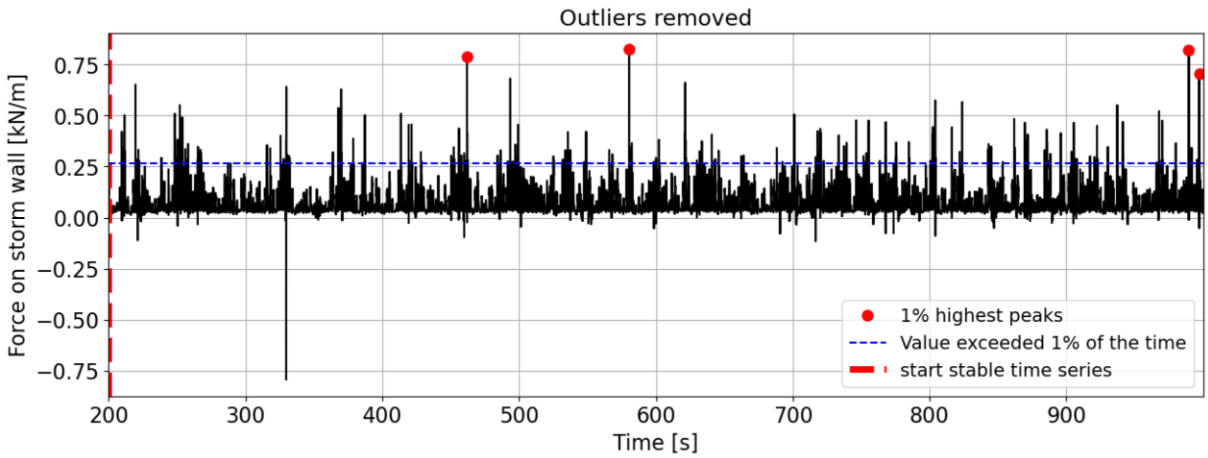

Figure F.15: 1% peaks in data with outliers removed

Figure F.14 and F.15 also show an odd low point a bit past 300 seconds. This is likely caused by tensile instability. Lyu et al. (2021) described this phenomenon and compared different possible solutions. Tensile instability is characterized by strong negative pressures, like the low point in Figure F.14 and F.15. The cause lies at the SPH gradient operator used for the fluid structure interaction. In most simulations a summation of pressure is used to discretize the pressure gradient in Navier–Stokes equations. The purpose of this is to conservate momentum. The result is however that there are no stress or strain thresholds for tensile instability. Two main phenomena which can generate tensile instability are vortex shedding (not applicable in this thesis) and added mass effects (applicable). For added mass effects, an example is a wave impact. Due to the inertia of the impact, the pressure on the fluid structure interface should be negative to prevent the structure surface to separate from the fluid.
Lyu et al. discuss three main solutions, Particle Shifting Techniques (PST), Tensile Instabilty Control (TIC) and combinations of the two. Applying one of these solutions would however come with the requirement of altering the source code of DualSPHysics, as there are no standard PST or TIC options available. This would go too much in depth for this thesis, as here the focus lies on the positive pressures. Instead, high negative pressure points are removed when they are below the mean minus three times the standard deviation of the valleys. These points are generally considered outliers (Andrade, 2021).

Distance particles

Due to large requirements in storage space, a particle distance of 0.01 m could only be simulated for 100 seconds, which is why it is not added to Figure F.12. Figure F.16 and F.17 show the simulation with dp = 0.01 and 0.02 m respectively. It can be seen that peaks are at the same locations, but the height varies. On average, the peaks for dp = 0.02 m are 24% lower. The highest peak is higher, but the highest peaks are not the same peak in time in the simulations. The underestimation of $F_{1\%}$ and $F_{10\%}$ and the overestimation of F_{max} might be reduced by using a smaller particle distance, but due to high storage requirements this is unfeasible for this thesis. Therefore, the results should be considered with care, knowing that the magnitude of the force might differ.

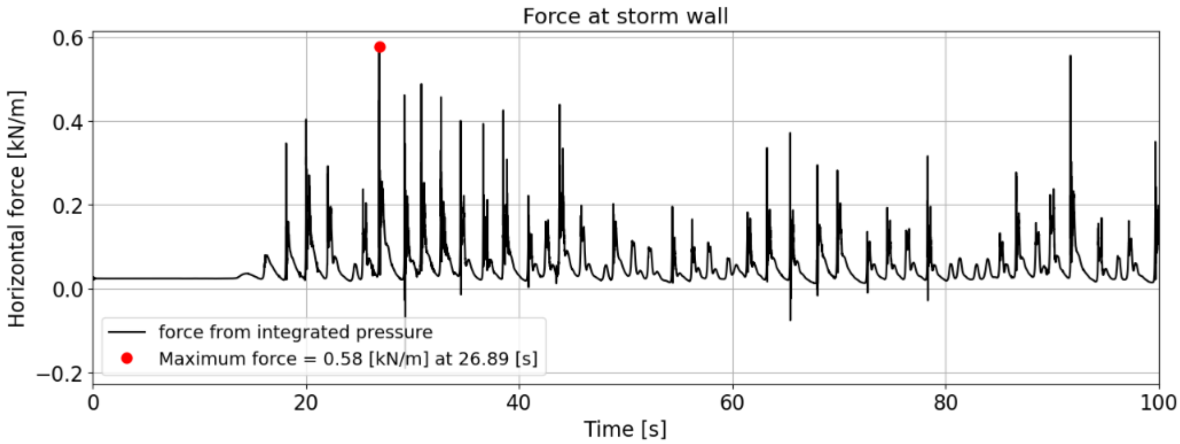

Figure F.16: Simulation Den Heijer experiment 3001 with dp = 0.01 m

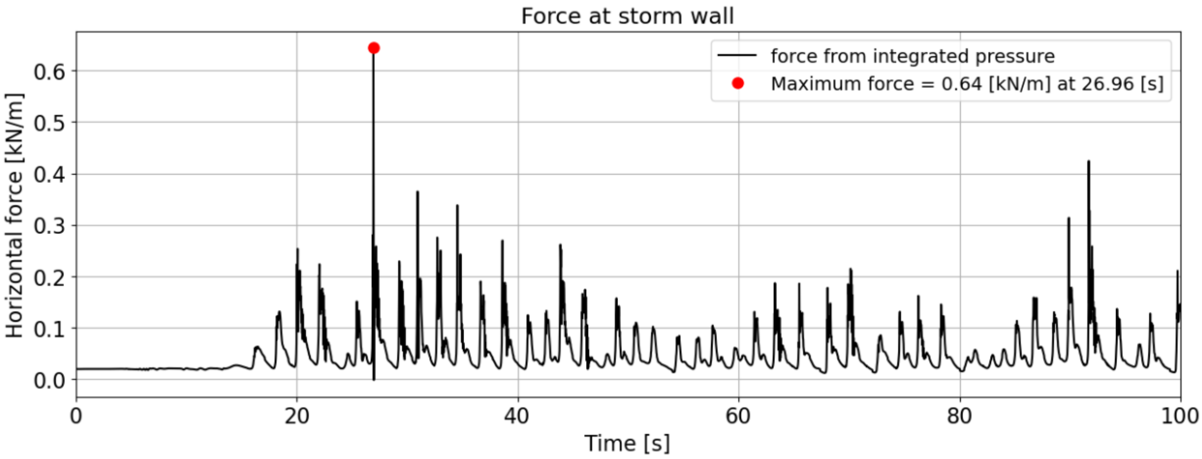

Figure F.17: Simulation Den Heijer experiment 3001 with dp = 0.02 m

Wave spectrum

For the experiment number 3001 Den Heijer provided the incoming and outcoming wave spectra at different locations together with the reflection coefficient, shown in Figure F.18. Figure F.19 shows the obtained wave spectra and reflection coefficient of the model. Both wave spectra have their differences with the wave spectra of Den Heijer. First of all, the magnitudes of the spectra are smaller than the spectra of Den Heijer. Second, the dips of the reflection coefficients are a factor 2 to 3 lower than the reflection coefficients of Den Heijer. However, the location of the peaks / dips in the plots seem to be at the same frequencies.

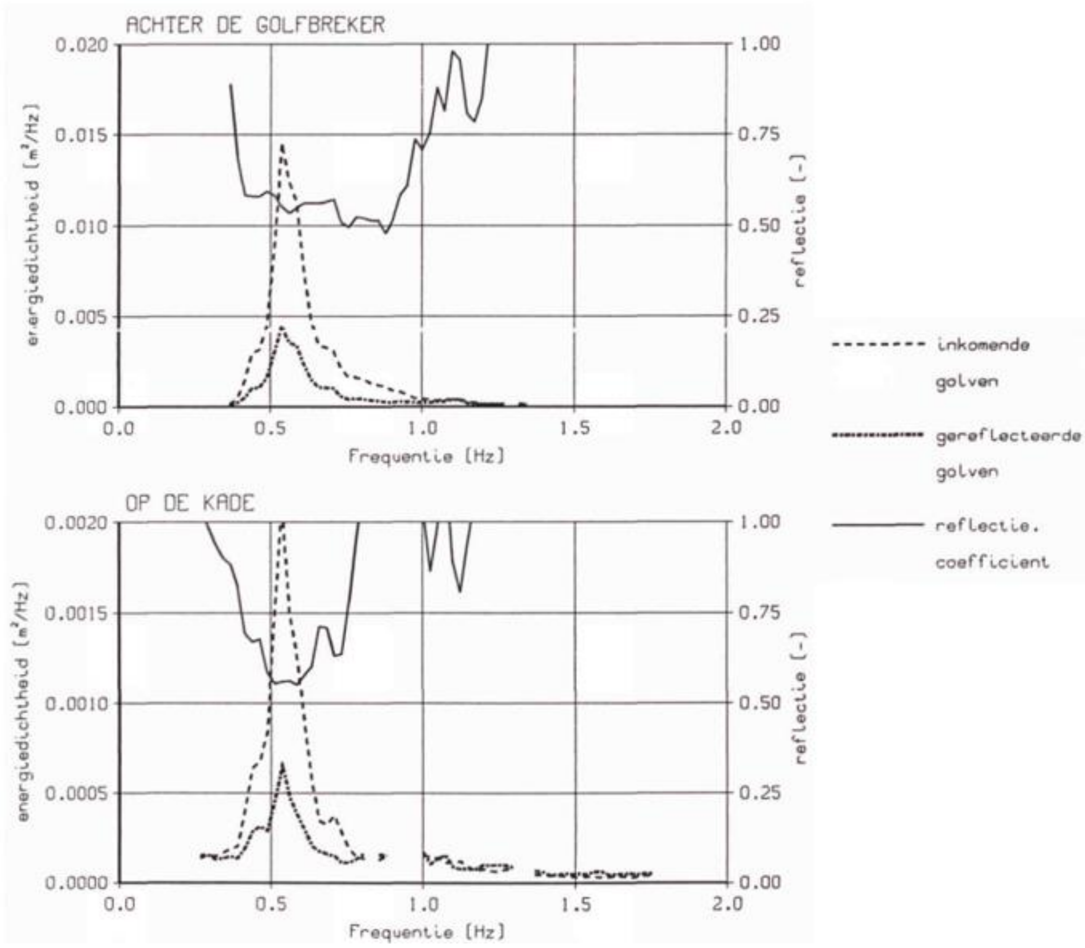

Figure F.18: Wave spectra experiment 3001, 5 m in front of the quay (top) and 1 m in front of the storm wall (bottom) (Den Heijer, 1998)

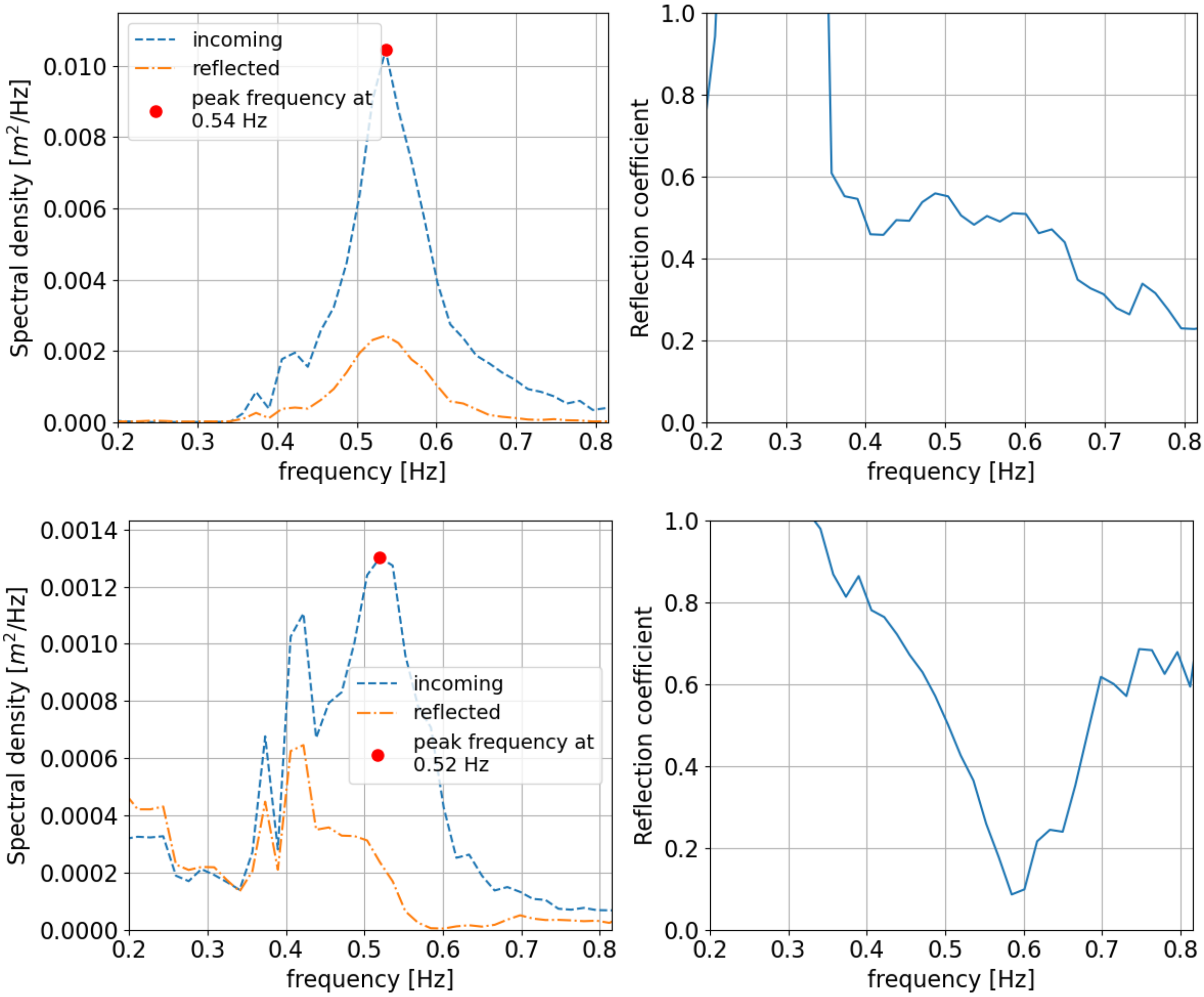

Figure F.19: Wave spectra DualSPHysics 3001, 5 m in front of the quay (top) and 1 m in front of the storm wall (bottom)

Wave propagation

Den Heijer provided the incoming significant wave height at different locations in the flume. These values are compared to the values obtained from the model in Table F.2.

Table F.2: Wave propagation Den Heijer and DualSPHysics

Location	Experiment number	Den Heijer		DualSPHysics	
		H_{si} [m]	T_p [s]	H_{si} [m]	T_p [s]
5 m in front of quay	3001	0.196	1.800	0.153	2.078
1 m in front of storm wall	3001	0.080	-	0.079	-
5 m in front of quay	3002	0.195	1.800	0.151	2.047
1 m in front of storm wall	3002	0.076	-	0.071	-
5 m in front of quay	3003	0.148	2.120	0.136	2.248
1 m in front of storm wall	3003	0.115	-	0.137	-
5 m in front of quay	3004	0.203	1.800	0.155	1.989
1 m in front of storm wall	3004	0.119	-	0.111	-
5 m in front of quay	3005	0.147	2.160	0.136	2.248
1 m in front of storm wall	3005	0.114	-	0.136	-
5 m in front of quay	3006	0.203	1.790	0.155	2.078
1 m in front of storm wall	3006	0.116	-	0.111	

The largest differences are in the magnitude of the incoming wave height. Especially the wave heights in front of the quay wall are always underestimated. The underestimation varies from 8-

24%. The model does capture the change in incoming wave height. A higher wave height for an experiment leads also to a higher value in the model. For the incoming wave height in front of the storm wall the model seems to perform better for shorter peak periods.

There are also some differences in the peak wave period. A higher peak period observed in Den Heijer's experiments also results in a higher predicted peak wave period by DualSPHysics. Still the model tends to overestimate the wave periods, especially for the smaller wave periods.

Evaluation of model performance

The model is evaluated using Willmott's refined index of agreement (2012), given by Equation F.1.

$$d_r = \begin{cases} 1 - \frac{MAE}{C \cdot MAD}, MAE \ \leq C \cdot MAD \\ \frac{C \cdot MAD}{MAE} - 1, MAE > C \cdot MAD \end{cases} \quad \text{Equation F.1}$$

Where the index d_r is bounded by [-1, 1], C is a scaling factor, here taken to 2, MAE is the mean absolute error defined by Equation F.2 and MAD is the mean absolute deviation defined by Equation F.3.

$$MAE = \frac{1}{N}\sum_{i=1}^{N}|P_i - O_i| \quad \text{Equation F.2}$$

$$MAD = \frac{1}{N}\sum_{i=1}^{N}|O_i - \bar{O}| \quad \text{Equation F.3}$$

With:

- N = The number of observed samples
- P_i = Sample from predicted series
- O_i = Sample from observed series
- $\bar{O}$ = The mean of the observed series

When the value of $d_r < 0.5$, the model's performance is considered to be poor. While a value of 1 indicates the perfect model.

The optimized DualSPHysics model is evaluated using the values of F_{max}, $F_{1\%}$ and $F_{10\%}$ of Den Heijer's experiments, leading to three d_r values, shown in Table F.3.

Table F.3: Willmott's refined index of agreement for the DualSPHysics model with Den Heijer's experiments

Force	F_{max}	$F_{1\%}$	$F_{10\%}$
d_r raw data	-0.014	0.715	0.694
d_r outliers removed	-0.728	0.719	0.691

This indicates that the model preforms reasonable / good for $F_{1\%}$ and $F_{10\%}$, but rather poor for F_{max}. The poor prediction for F_{max} is likely due to the randomness of irregular waves and that one experiment therefore might measure a different maximum force than the other. Noticeable between Den Heijer's experiments, is experiment 3004. This configuration had the highest significant wave height and highest wall among the 1.8 s peak periods. However the values for F_{max}, $F_{1\%}$ and $F_{10\%}$ are not the highest. The model does however predict a higher force, like one would expect. Removing experiment 3004 leads to the Willmott's indices in Table F.4. Which indicates a very good performance for $F_{1\%}$ and $F_{10\%}$. However the performance for F_{max} stays poor.

Table F.4: Willmott's refined index of agreement for the DualSPHysics model with Den Heijer's experiments without experiment number 3004

Force	F_{max}	$F_{1\%}$	$F_{10\%}$
d_r raw data	0.032	0.813	0.877
d_r outliers removed	-0.728	0.828	0.876

Translation to case study

The smallest dimension in Den Heijer is the water depth on the quay, with 0.08 m as minimum. The ratio smallest dimension / dp is then 4. The time duration of 1000 seconds with a wave period of approximately 1.8 s has a ratio of duration / period = 556.

Translating these model parameter values for the Kop van Zuid results in dp = 0.12 m and a duration of 40 minutes for irregular waves. A duration of 40 min is however not possible due to storage limitation. A duration of 10 min appears maximum. The solution used is to do multiple simulations with different seeds to get more waves. Due to time limitations it is however only possible to get a total duration of 30 minutes.

The experiment of Den Heijer uses a wave flume of approximately 6 peak wave lengths in front of the quay. This is because for some configurations a breakwater was placed in the flume as well. Since for the Kop van Zuid a breakwater is not present the model is optimized by decreasing the basin length just before the model becomes unstable, see Appendix G: Calibration DualSPHysics parameters. This led to a basin length of 5 wave lengths.

Appendix G: Calibration DualSPHysics parameters

This appendix describes the calibration of simulation duration for regular waves, the basin length and the water depth.

The calibration is done by varying one parameter at the time and observe at which value the water level variance and / or the horizontal force variance of the stable time series stayed approximately the same. The spin-up time would be approximately 15%, but 20% is taken to be on the safer side, i.e. only the last 80% of the time series are considered. The calibration is done using regular waves for the scenario which lies closest to the Kop Van Zuid case. The fixed parameters are shown in Table G.1.

Table G.1: Values parameters used scenario for calibration

Parameter	Value
L_{quay} / L	0.45
h_{sw} / L	0.081
d_{wq} / L	0.01
H / L	0.117

Number of waves

The calibration is started using the minimum value of the recommended waves by the SWASH team (2024) of 100 waves and then increased and decreased. Figure G.1 shows the variation in water level at the storm wall for the stable part of the simulation for different numbers of waves, while Figure G.2 shows the variance in total horizontal force. A decrease in steepness in the curves can be observed starting from 90 to 100 waves. There is still a decrease in variance, but this is because some particles splash over the wall and are not refilled. Therefore, the longer the simulation the less particles are present, so on average a lower water level and force. To stay within the recommended range of the SWASH team, 100 waves are used for the final runs.

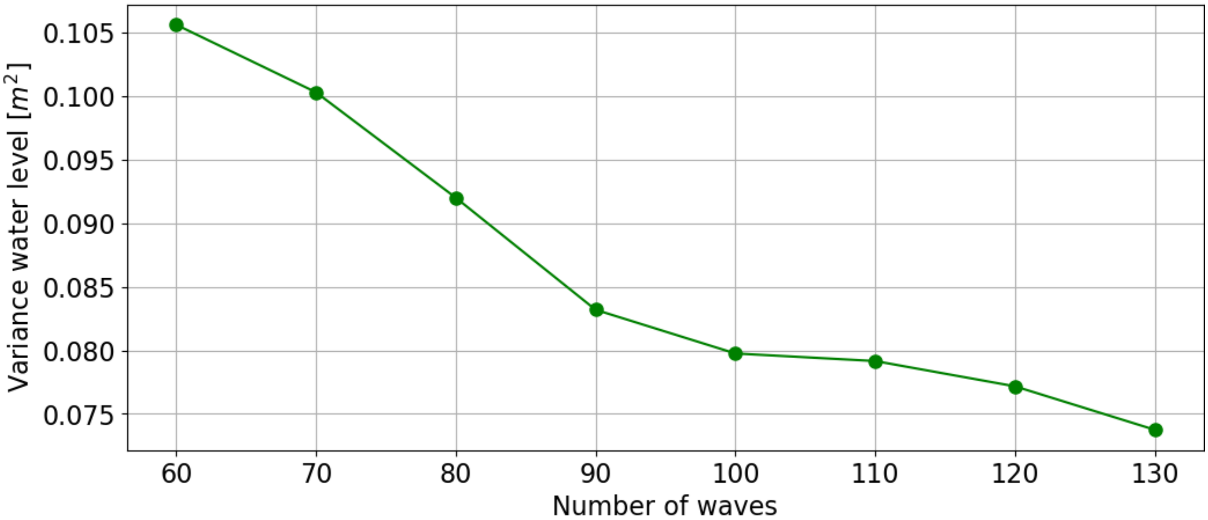

Figure G.1: Variance of water level at storm wall for different numbers of waves

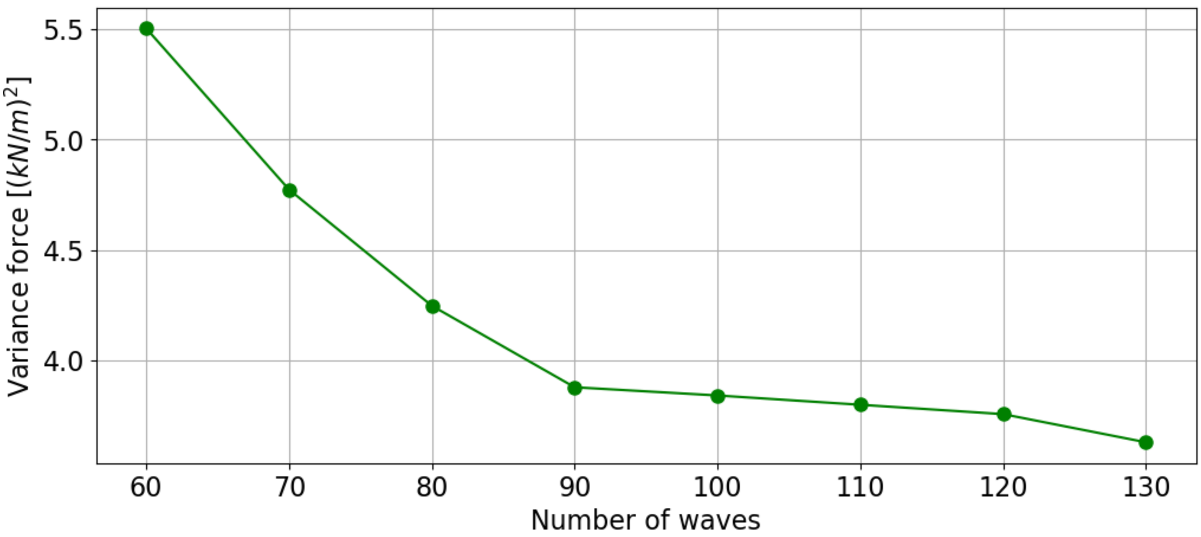

Figure G.2: Variance of total horizontal force at storm wall for different numbers of waves

Basin length
The first basin length used is six wave lengths based on the experiment of Den Heijer (1998). Then the basin length is reduced until unstableness in the variance is observed. This can be seen in Figure G.3 and G.4 for the water level and force respectively. A basin length of 5 – 6 wavelengths appears to be stable, as the smaller wavelength deviate more. The smallest stable basin length, 5 wavelengths, is therefore used in the simulations.

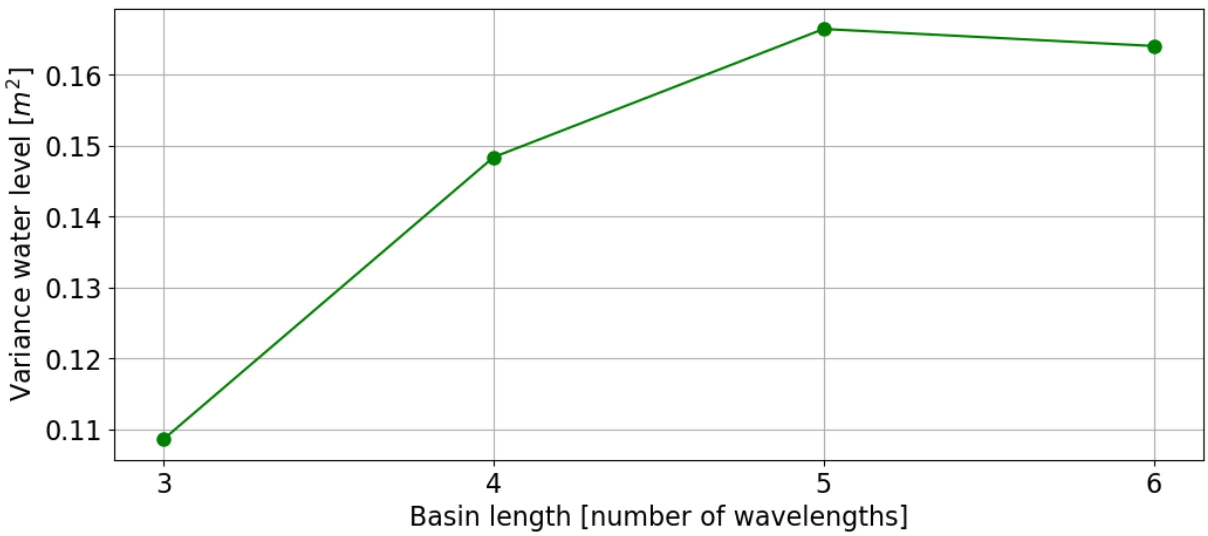

Figure G.3: Variance of water level at storm wall for different basin lengths

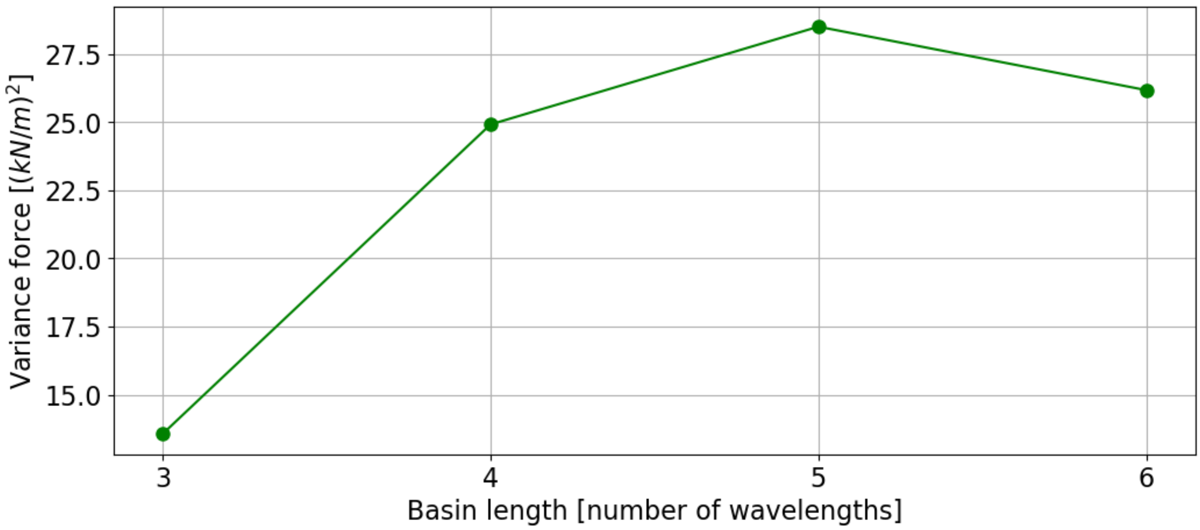

Figure G.4: Variance of total horizontal force at storm wall for different basin lengths

Water depth

In this thesis deep water waves are considered. To limit the needed computational time and storage, it is checked if the depth could be reduced while still maintaining similar results. Figure G.5 shows the wave forcing with the original depth for case 39, while Figure G.6 shows the wave forcing with a 25% reduced depth. The reduction on the depth clearly influences the wave forcing on the storm wall. The peaks for the reduced depth are higher and at different moments in time.

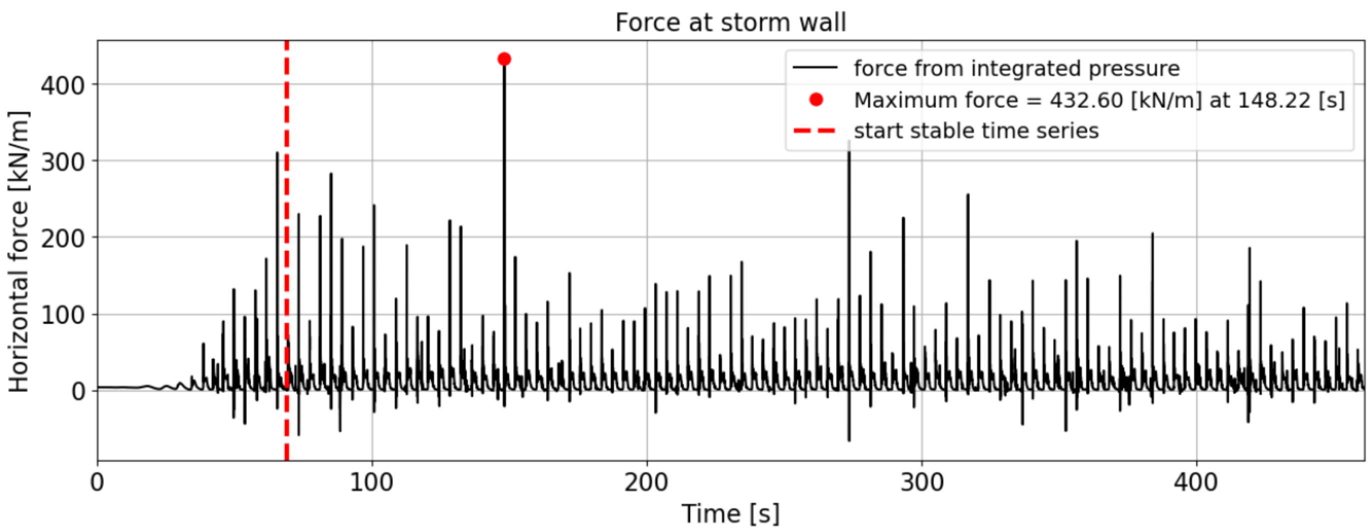

Figure G.5: Original water depth configuration 39 (H/L = 0.117, d_{wq}/L = 0.04, L_{quay}/L = 0.15, h_{sw}/L = 0.095)

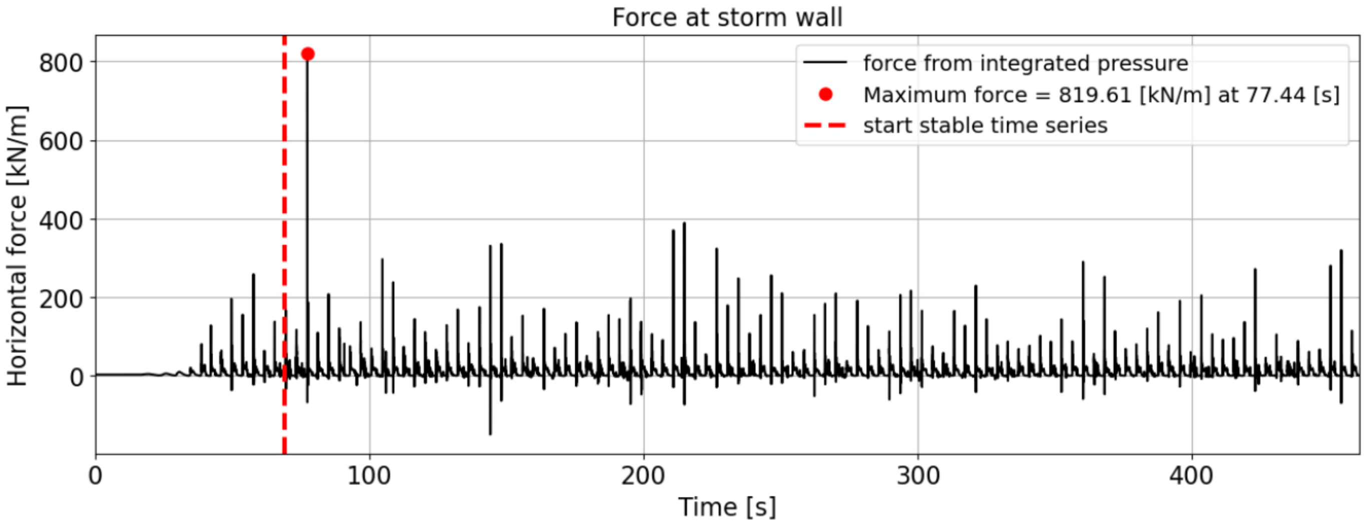

Figure G.6: 25% reduced water depth configuration 39 (H/L = 0.117, d_{wq}/L = 0.04, L_{quay}/L = 0.15, h_{sw}/L = 0.095)

Appendix H: Wave forcing computed with theories

This appendix contains the wave forcing theories analysis for both regular and irregular waves. The difference with the main report is that here L_{quay} / L = 0 and the linear standing wave theory are treated as well.

Regular waves

The wave forcing obtained from the numerical model is compared with six theories. These theories consist of existing theories (linear standing wave , Tuin, Den Heijer, Cooker-Peregrine) and adaptions of existing theories (adapted Tuin, Goda with quay as berm). For the linear standing wave both full reflection (χ = 1) and no reflection (χ = 0) are used.

Figure H.1 and H.2 show the relative root mean squared error (RMSE) and the relative error respectively. The values are shown in Table H.1 and H.2. Here only the results for d_{wq} / L > 0 are shown, as lower values often led to numerical errors in the model. When the storm wall is located at the edge of the quay, i.e. L_{quay} / L = 0, a standing wave with reflection is observed. So indeed the linear standing wave theory preforms the best. For 0.15 ≤ L_{quay} / L ≤ 0.30 the highest impacts are observed. The formulas which are based on an impact force on the storm wall, i.e. Den Heijer, Tuin, adapted Tuin and Cooker-Peregrine, perform the best. For L_{quay} / L = 0.45 broken waves are observed. The Tuin and adapted Tuin formulas appear not suitable for this situation, overestimating the force. The other methods provide more accurate estimations.

With regard to computing impact waves (0.15 ≤ L_{quay} / L ≤ 0.30) only the adapted Tuin formula gives an overestimation, while the other methods give underestimations. For Tuin and Den Heijer the underestimations are the smallest. This is expected, as these methods are all specifically made for the scenario of a retreated storm wall on a vertical quay, while the others (Goda, Cooker-Peregrine and linear standing wave) are not.

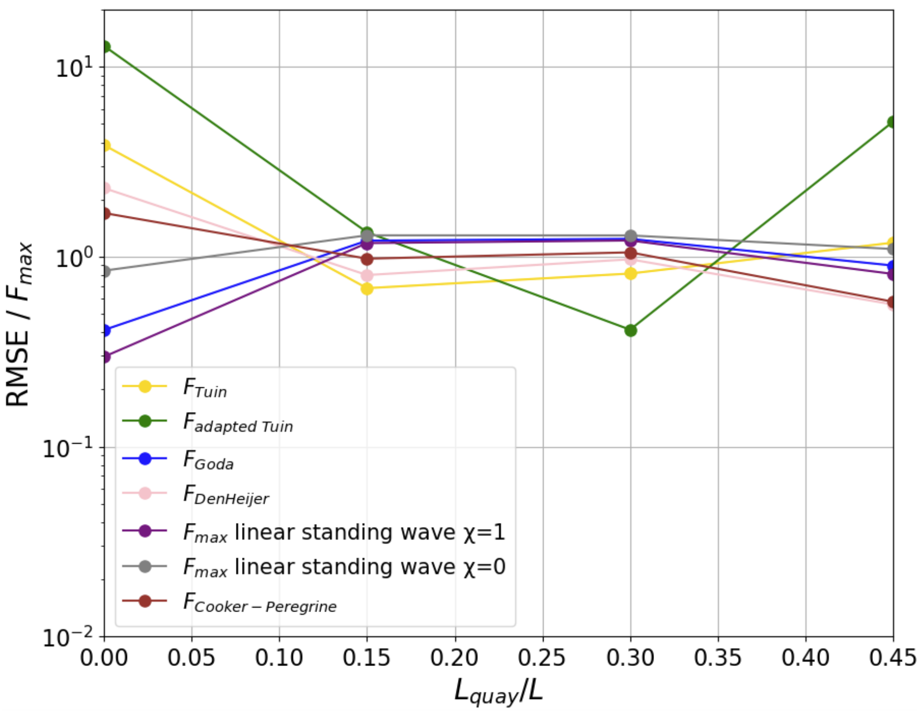

Figure H.1: RMSE theories with respect to maximum regular wave horizontal force in DualSPHysics per relative quay length

Table H.1: RMSE theories with respect to maximum regular wave horizontal force in DualSPHysics per relative quay length

L_{quay} / L	0.0	0.15	0.30	0.45
F_{Tuin}	3.87	0.68	0.82	1.19
$F_{adapted\ Tuin}$	12.90	1.34	0.41	5.15
F_{Goda}	0.41	1.22	1.24	0.90
$F_{DenHeijer}$	2.30	0.80	0.97	0.56
F_{max} linear standing wave χ = 1	0.30	1.18	1.22	0.81
F_{max} linear standing wave χ = 0	0.84	1.30	1.29	1.10
$F_{Cooker\text{-}Peregrine}$	1.70	0.97	1.05	0.89

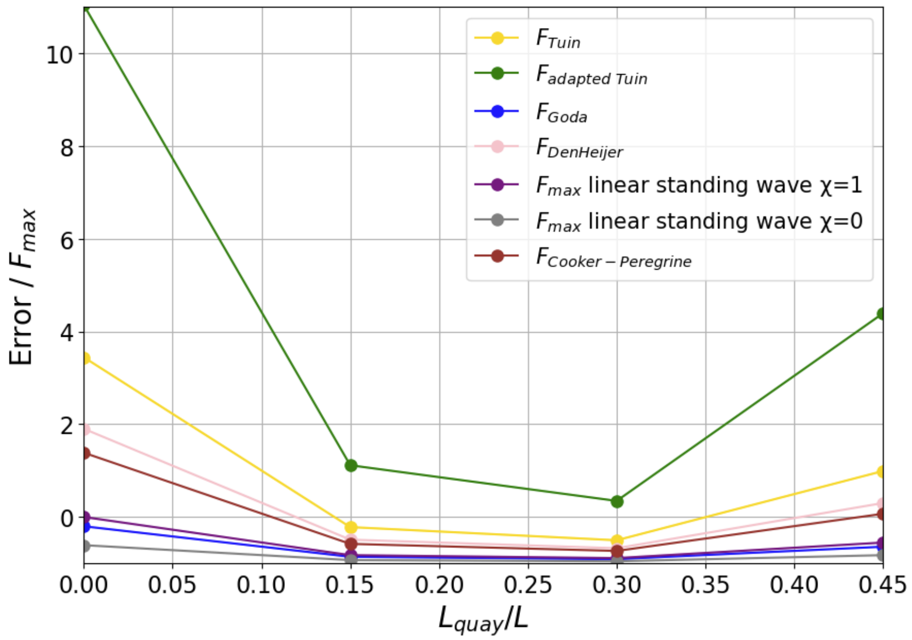

Figure H.2: Error theories (theory - F_{max}) with respect to maximum regular wave horizontal force in DualSPHysics per relative quay length

Table H.2: Error theories (theory - F_{max}) with respect to maximum regular wave horizontal force in DualSPHysics per relative quay length

L_{quay} / L	0.0	0.15	0.30	0.45
F_{Tuin}	3.44	-0.22	-0.50	0.99
$F_{adapted\ Tuin}$	11.04	1.11	0.34	4.39
F_{Goda}	-0.20	-0.86	-0.91	-0.64
$F_{DenHeijer}$	1.90	-0.49	-0.68	0.30
F_{max} linear standing wave χ = 1	$-1.75 \cdot 10^{-3}$	-0.82	-0.89	-0.55
F_{max} linear standing wave χ = 0	-0.61	-0.93	-0.96	-0.82
$F_{Cooker\text{-}Peregrine}$	1.38	-0.58	-0.73	0.07

When looking at other parameters, similar patterns are visible. Figure H.3 and H.4 show the relative root mean squared error (RSME) and the relative error respectively with the relative depth (d_{wq} / H) on the horizontal axis instead of the relative quay length. The values can be found in Table H.3 and H.4. Here only the results for L_{quay} / L > 0 are shown, as standing waves, occurring at L_{quay} / L = 0, are not interesting for the maximum wave force.

Here for lower d_{wq} / H, where broken or breaking waves are expected, the formulas which are based on an impact force on the storm wall again perform the best. With higher values of d_{wq} / H slightly breaking and quasi-standing waves occur more often and these formulas perform worse. Again the adapted Tuin method is the only method which continuously gives an overestimation. For the region where impact waves are expected (d_{wq} / H < 0.35) the Tuin and Den Heijer method again give the smallest underestimation.

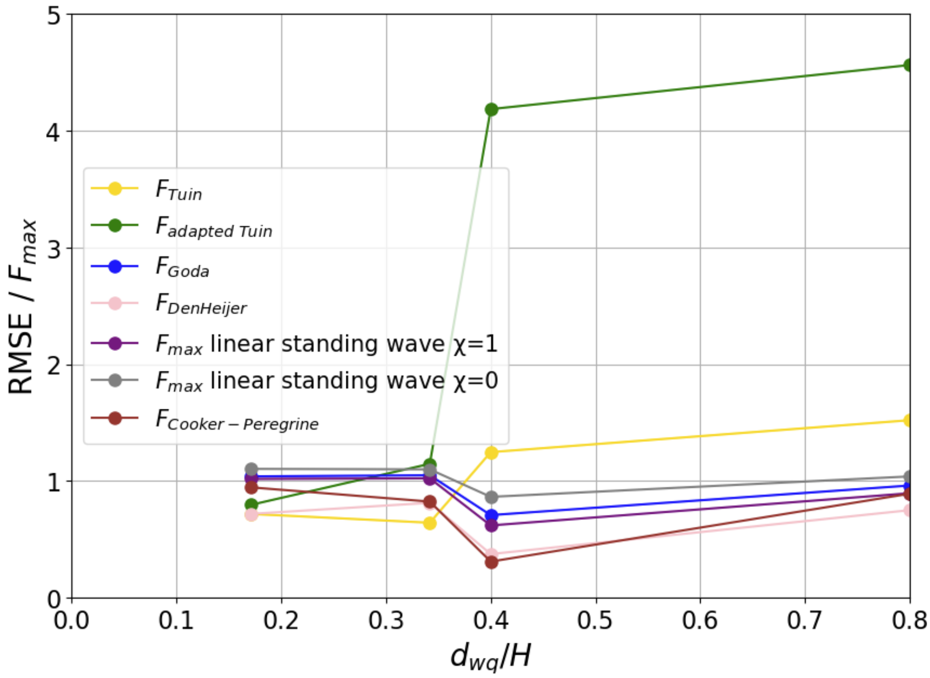

Figure H.3: RMSE theories with respect to maximum regular wave horizontal force in DualSPHysics per relative quay water depth

Table H.3: RMSE theories with respect to maximum regular wave horizontal force in DualSPHysics per relative quay water depth

d_{wq} / H	0.17	0.34	0.40	0.80
F_{Tuin}	0.72	0.64	1.25	1.52
$F_{adapted\ Tuin}$	0.79	1.15	4.18	4.56
F_{Goda}	1.04	1.05	0.70	0.96
$F_{DenHeijer}$	0.72	-0.81	0.37	0.75
F_{max} linear standing wave χ = 1	1.02	1.02	0.62	0.89
F_{max} linear standing wave χ = 0	1.10	1.10	0.86	1.04
$F_{Cooker-Peregrine}$	0.95	0.82	0.31	0.89

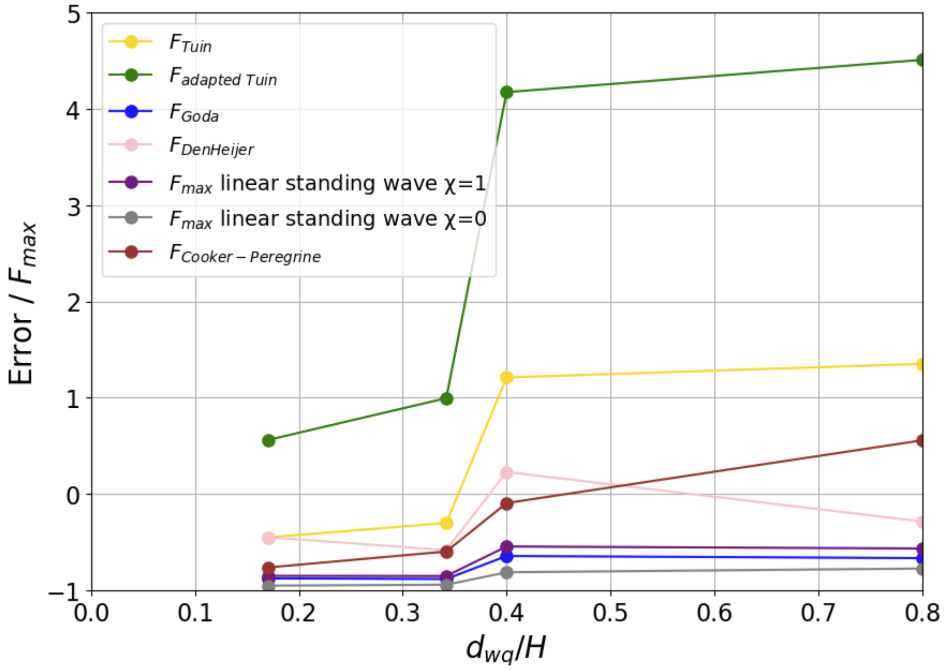

Figure H.4: Error theories (theory - F_{max}) with respect to maximum regular wave horizontal force in DualSPHysics per relative quay water depth

Table H.4: Error theories (theory - F_{max}) with respect to maximum regular wave horizontal force in DualSPHysics per relative quay water depth

d_{wq} / H	0.17	0.34	0.40	0.80
F_{Tuin}	-0.45	-0.30	1.21	1.35
$F_{adapted\ Tuin}$	0.56	0.99	4.17	4.51
F_{Goda}	-0.88	-0.88	-0.64	-0.66
$F_{DenHeijer}$	-0.45	-0.58	0.23	-0.28
F_{max} linear standing wave χ = 1	-0.85	-0.85	-0.54	-0.57
F_{max} linear standing wave χ = 0	-0.95	-0.94	-0.81	-0.77
$F_{Cooker-Peregrine}$	-0.76	-0.60	-0.09	0.56

Irregular waves

For the irregular waves, the same six theories as for the regular waves are used. Instead of H and L, the values for H_s and L_{op} are used respectively. Figure H.5 and H.6 show the relative root mean squared error (RSME) and the relative error respectively. The values are shown in Table H.5 and H.6.

When the storm wall is located at the edge of the quay, i.e. L_{quay} / L = 0, Goda performs the best. The reason that a linear standing wave estimation performs worse, is because there is no standing wave observed. The reason is because for an irregular wave field, the waves have different wave periods and heights, so there is less reflection than with the same incoming waves.

For 0.15 ≤ L_{quay} / L ≤ 0.30 the highest impacts are observed. The formulas which are based on an impact force on the storm wall, i.e. Den Heijer, Tuin, adapted Tuin and Cooker-Peregrine, perform the best. But, with respect to regular waves the Tuin and adapted Tuin formulae perform worse for L_{quay} / L = 0.15. Tuin now consequently overestimates the force, just as adapted Tuin.

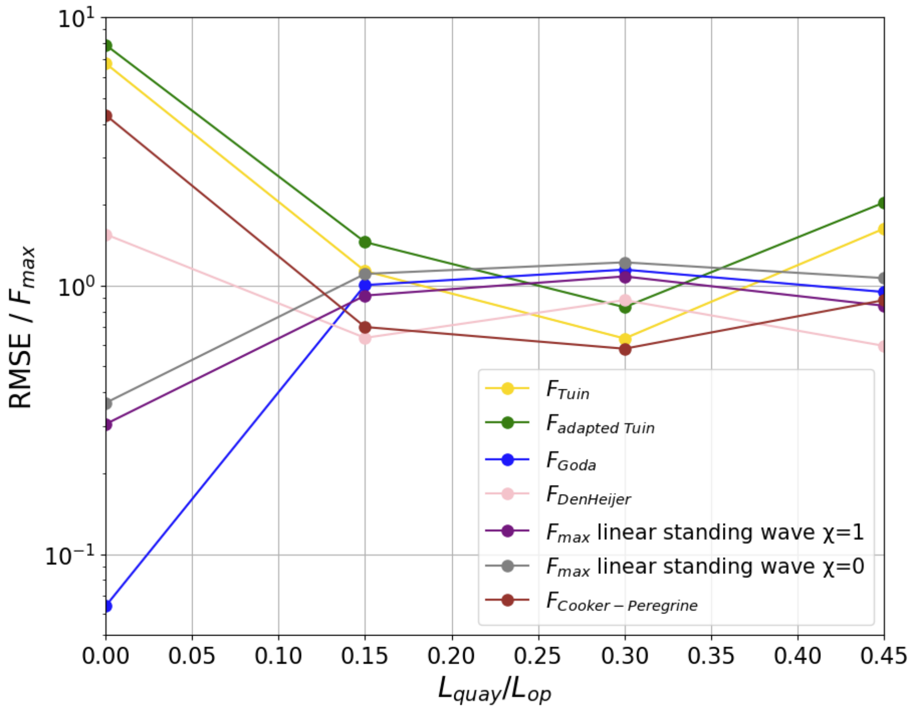

Figure H.5: RMSE theories with respect to maximum irregular wave horizontal force in DualSPHysics per relative quay length

Table H.5: RMSE theories with respect to maximum irregular wave horizontal force in DualSPHysics per relative quay length

L_{quay} / L_{op}	**0.0**	**0.15**	**0.30**	**0.45**
F_{Tuin}	6.73	1.13	0.63	1.63
$F_{adapted\ Tuin}$	7.89	1.45	0.83	2.04
F_{Goda}	0.06	1.00	1.14	0.95
$F_{DenHeijer}$	1.55	0.64	0.88	0.60
F_{max} linear standing wave χ = 1	0.30	0.92	1.08	1.2
F_{max} linear standing wave χ = 0	0.37	1.11	1.22	1.07
$F_{Cooker-Peregrine}$	4.32	0.70	0.58	0.88

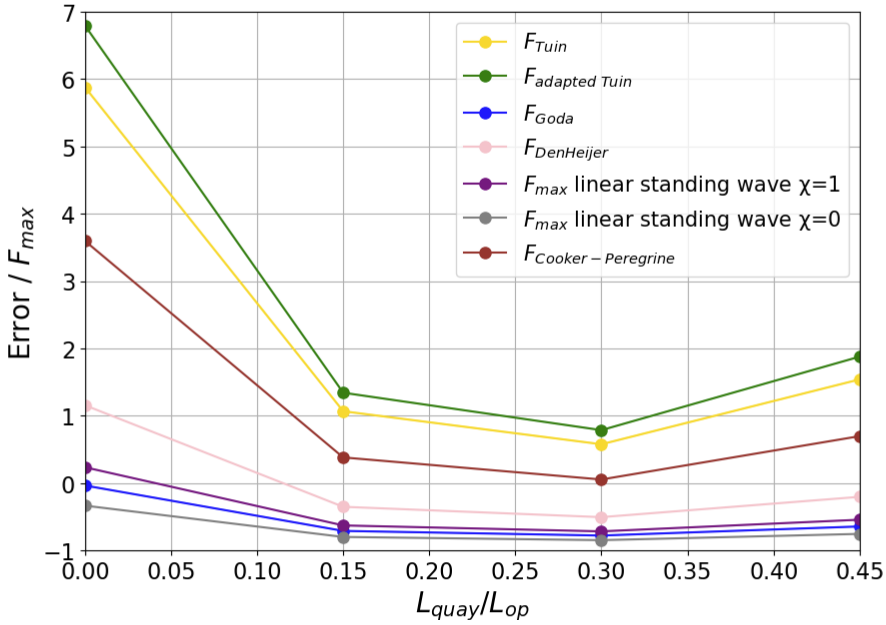

Figure H.6: Error theories (theory - F_{max}) with respect to maximum irregular wave horizontal force in DualSPHysics per relative quay length

Table H.6: Error theories (theory - F_{max}) with respect to maximum irregular wave horizontal force in DualSPHysics per relative quay length

L_{quay} / L_{op}	**0.0**	**0.15**	**0.30**	**0.45**
F_{Tuin}	5.88	1.07	0.58	1.54
$F_{adapted\ Tuin}$	6.80	1.34	0.79	1.88
F_{Goda}	-0.04	-0.71	-0.78	-0.64
$F_{DenHeijer}$	1.16	-0.35	-0.50	-0.20
F_{max} linear standing wave χ = 1	0.23	-0.63	-0.72	-0.54
F_{max} linear standing wave χ = 0	-0.34	-0.80	-0.85	-0.75
$F_{Cooker-Peregrine}$	3.60	0.38	0.05	0.70

When looking at other parameters, similar patterns are visible. Figure H.7 and H.8 show the relative root mean squared error (RSME) and the relative error respectively with the relative depth (d_{wq} / H) on the horizontal axis instead of the relative quay length. The values can be found in Table H.7 and H.8.

Here for lower d_{wq} / H, where broken or breaking waves are expected. The formulas which are based on an impact force on the storm wall again perform the best. With higher values of d_{wq} / H quasi-standing waves occur more often and these formulas perform worse. Again Tuin consequently gives an overestimation.

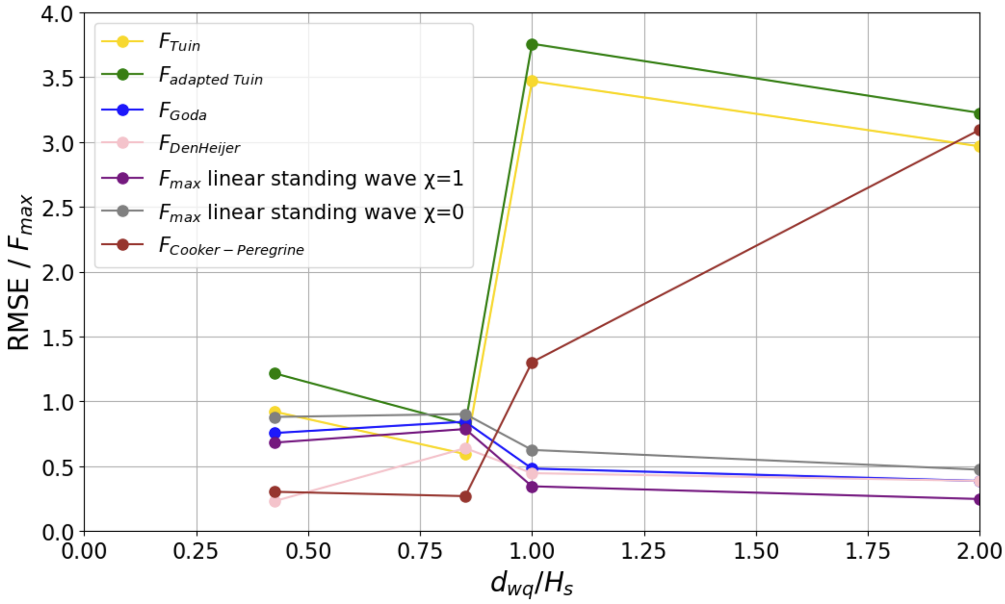

Figure H.7: RMSE theories with respect to maximum irregular wave horizontal force in DualSPHysics per relative quay water depth

Table H.7: RMSE theories with respect to maximum irregular wave horizontal force in DualSPHysics per relative quay water depth

d_{wq} / H_s	**0.43**	**0.85**	**1.0**	**2.0**
F_{Tuin}	0.92	0.59	3.47	2.97
$F_{adapted\ Tuin}$	1.22	0.82	3.76	3.23
F_{Goda}	0.76	0.84	0.48	0.38
$F_{DenHeijer}$	0.23	0.64	0.45	0.39
F_{max} linear standing wave χ = 1	0.68	0.79	0.34	0.24
F_{max} linear standing wave χ = 0	0.88	0.90	0.63	0.47
$F_{Cooker-Peregrine}$	0.30	0.27	1.30	3.10

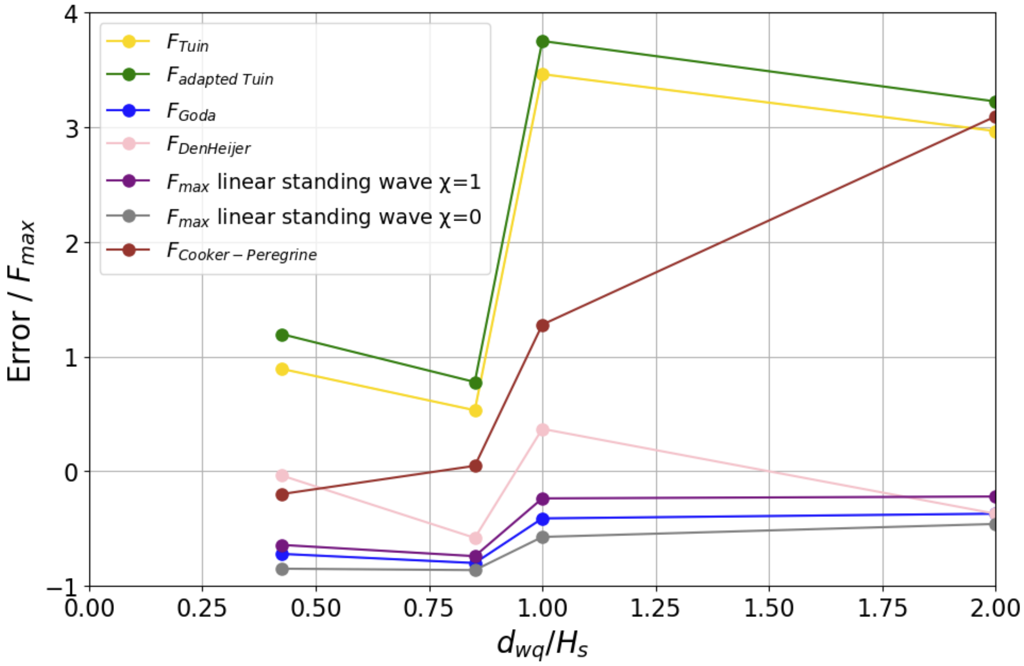

Figure H.8: Error theories (theory - Fmax) with respect to maximum irregular wave horizontal force in DualSPHysics per relative quay water depth

Table H.8: Error theories (theory - Fmax) with respect to maximum irregular wave horizontal force in DualSPHysics per relative quay water depth

d_{wq} / H_s	0.43	0.85	1.0	2.0
F_{Tuin}	0.89	0.53	3.46	2.97
$F_{adapted\ Tuin}$	1.19	0.78	3.75	3.22
F_{Goda}	-0.72	-0.80	-0.41	-0.37
$F_{DenHeijer}$	-0.04	-0.58	0.37	-0.37
F_{max} linear standing wave χ = 1	-0.64	-0.74	-0.24	-0.22
F_{max} linear standing wave χ = 0	-0.85	-0.86	-0.57	-0.46
$F_{Cooker-Peregrine}$	-0.20	0.05	1.28	3.09

Appendix I: Mathematical fits

This chapter contains the results of the different mathematical fits to the DualSPHysics data. Based on the pattern the data shows, five fits are tried. These are a logarithmic, exponential, a parabola, a power, and a fraction fit, shown in Equations I.1 – I.5.

$$a log_b(x) + c \quad \text{Equation I.1}$$

$$ae^{bx} + c \quad \text{Equation I.2}$$

$$ax^2 + bx + c \quad \text{Equation I.3}$$

$$ax^b \quad \text{Equation I.4}$$

$$\frac{a}{x} + b \quad \text{Equation I.5}$$

Where a, b and c are coefficients to be fitted. These are fitted using the curve_fit function from scipy. The best fit is chosen based on the coefficient of determination denoted as R^2, computed with Equation I.6.

$$R^2 = 1 - \frac{sum\ of\ squared\ residuals}{total\ sum\ of\ squares} \quad \text{Equation I.6}$$

The fits, together with the relative residuals, are shown in Figure I.1 - Figure I.5 for regular waves and in Figure I.6 - Figure I.10 for irregular waves. For both wave types the exponential fit scores the best.

Regular waves

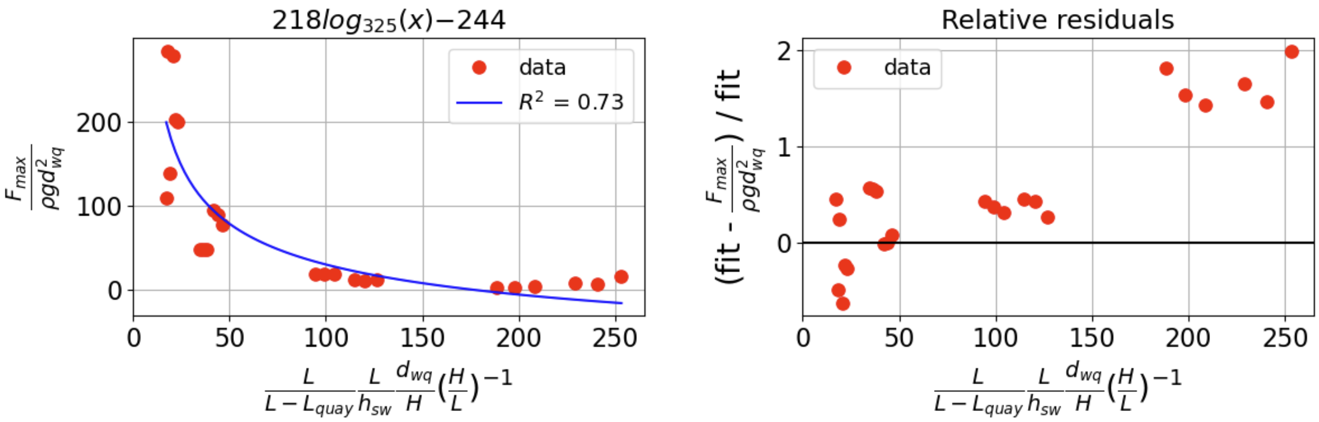

Figure I.1: Logarithmic fit regular waves data

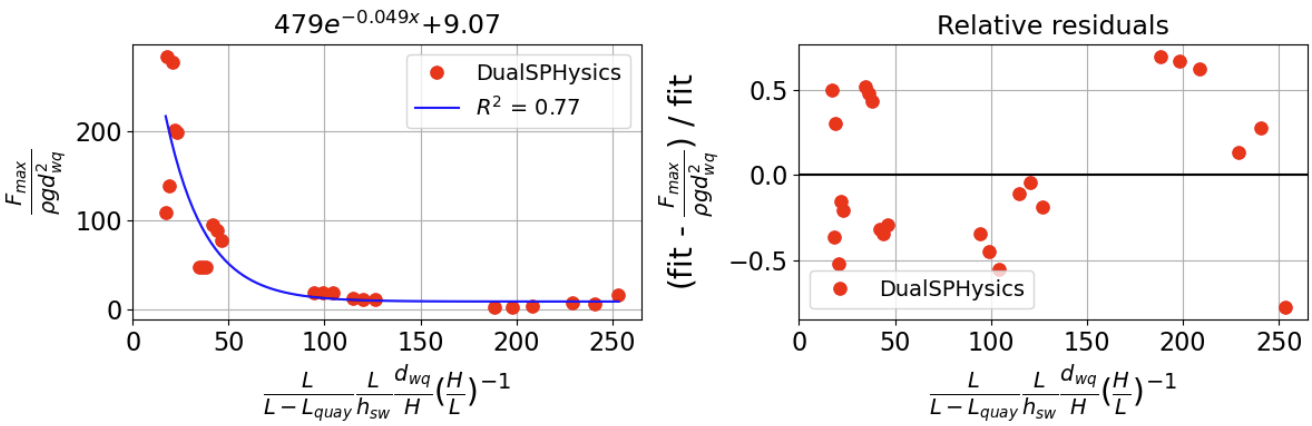

Figure I.2: Exponential fit regular waves data

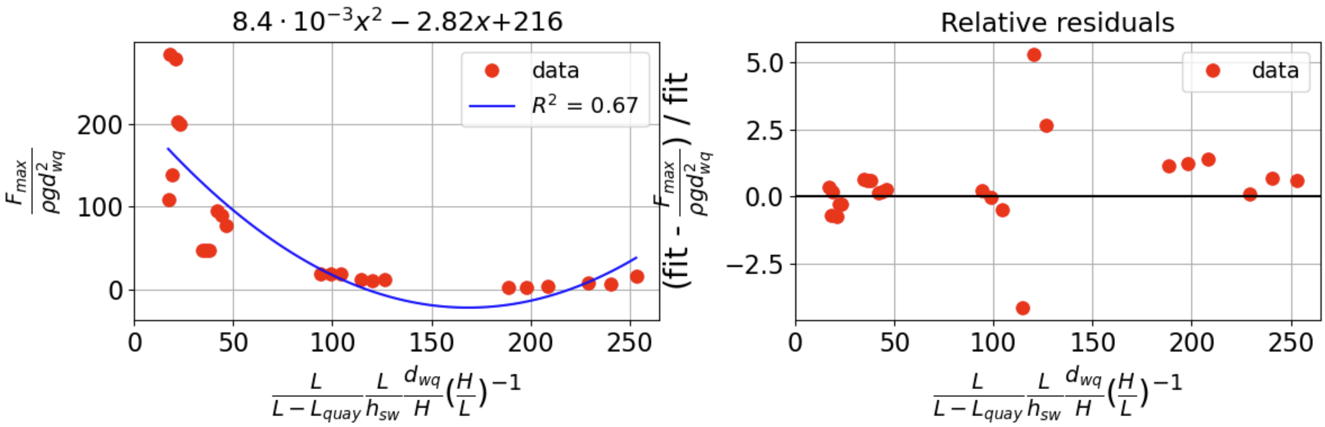

Figure I.3: Parabola fit regular waves data

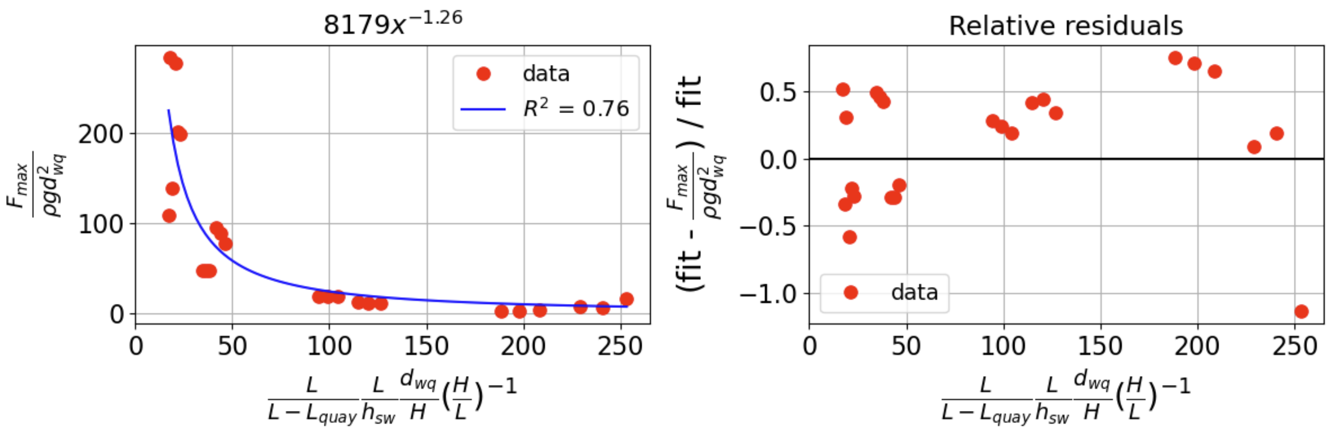

Figure I.4: Power fit regular waves data

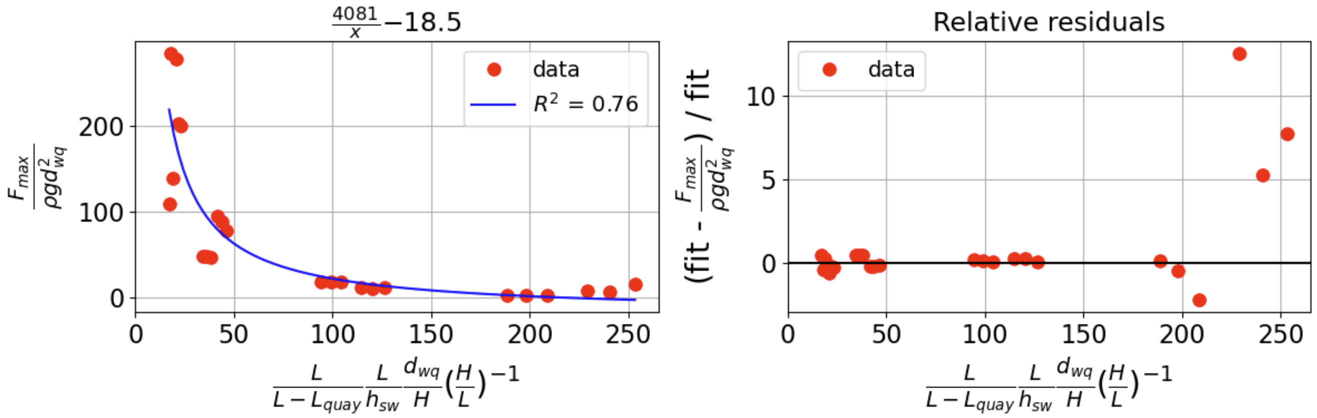

Figure I.5: Fraction fit regular wave data

Irregular waves

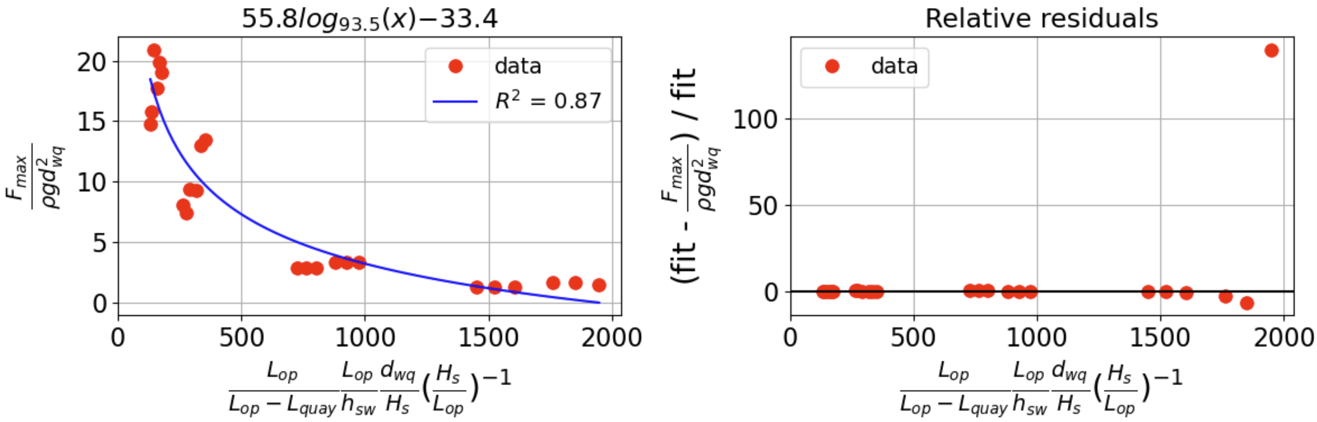

Figure I.6: Logarithmic fit irregular waves data

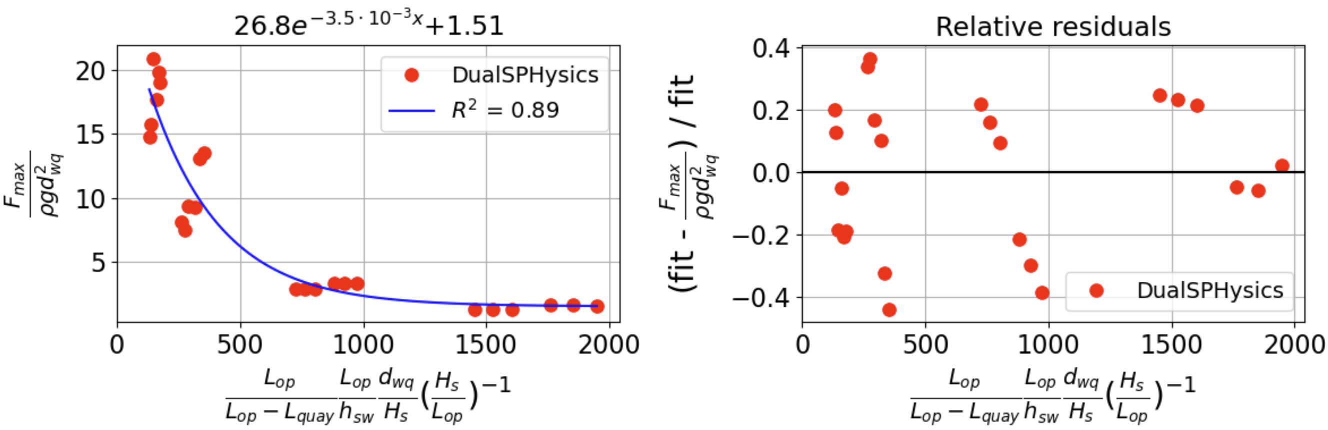

Figure I.7: Exponential fit irregular waves data

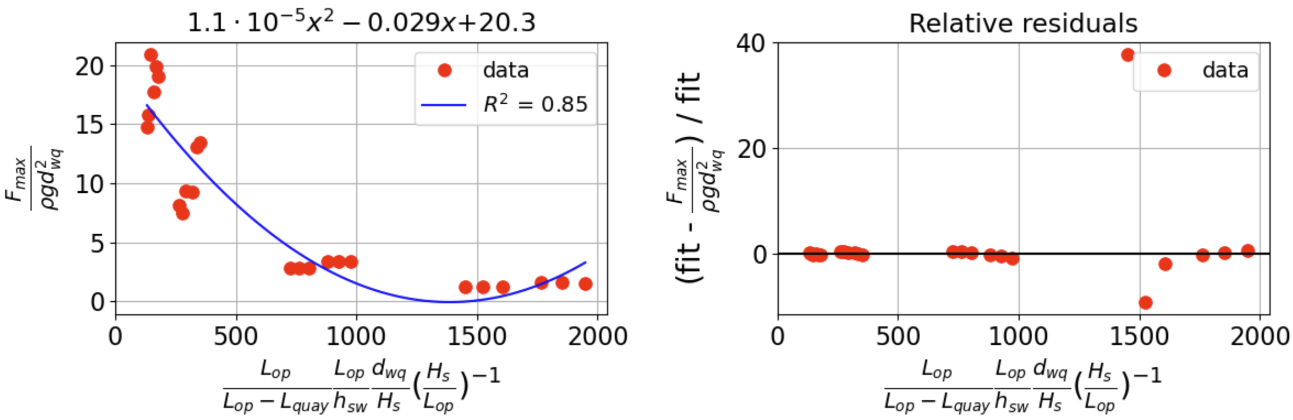

Figure I.8: Parabola fit irregular waves

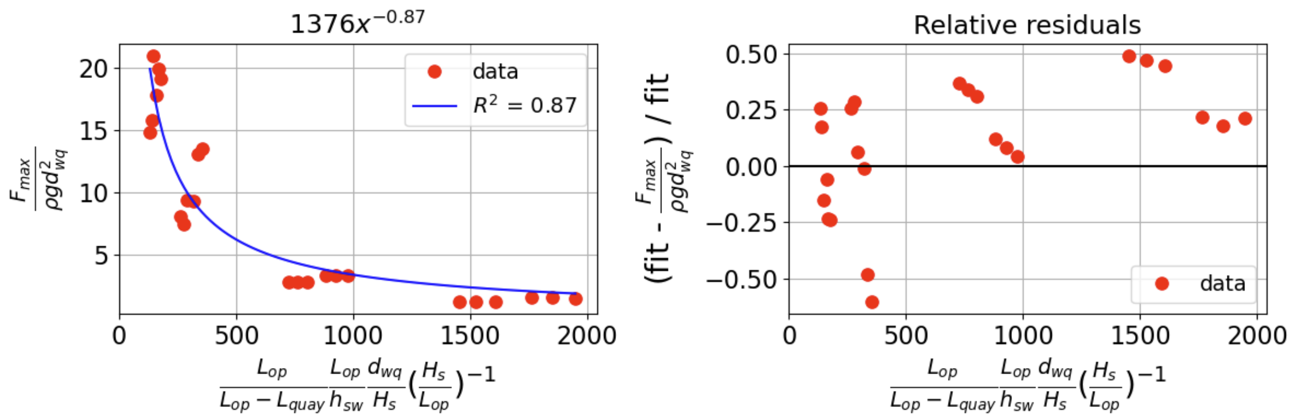

Figure I.9: Power fit irregular waves data

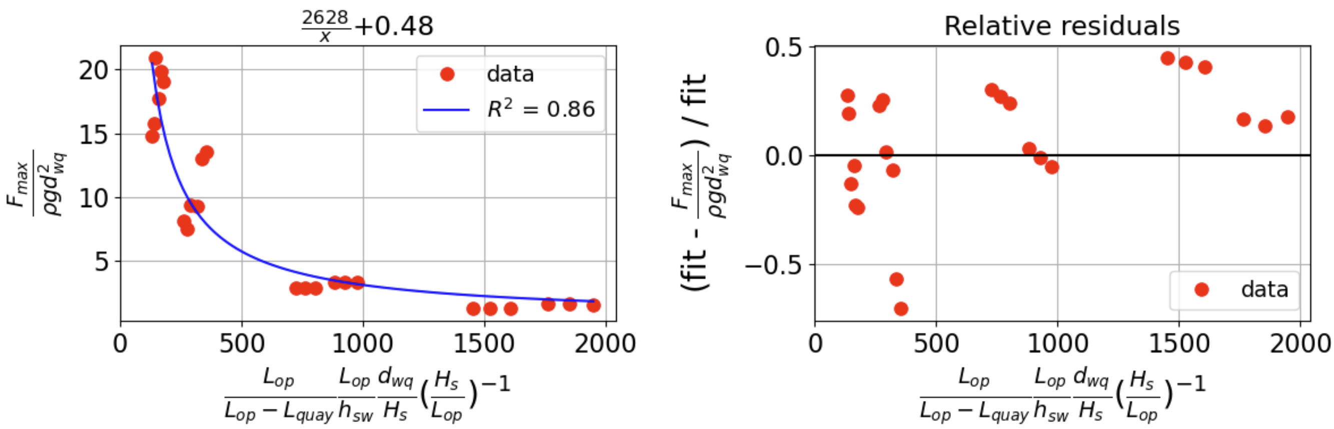

Figure I.10: Fraction fit irregular waves data

Appendix J: Irregular quay surface

This appendix treats a possible solution to the occurrence of numerical instabilities: an irregular quay surface. In the animations of the simulations a build-up of pressure between particles causing them to turn has been observed. Therefore an irregular surface has been used to prevent such a pressure build-up. An example of such a surface is shown in Figure J.1.

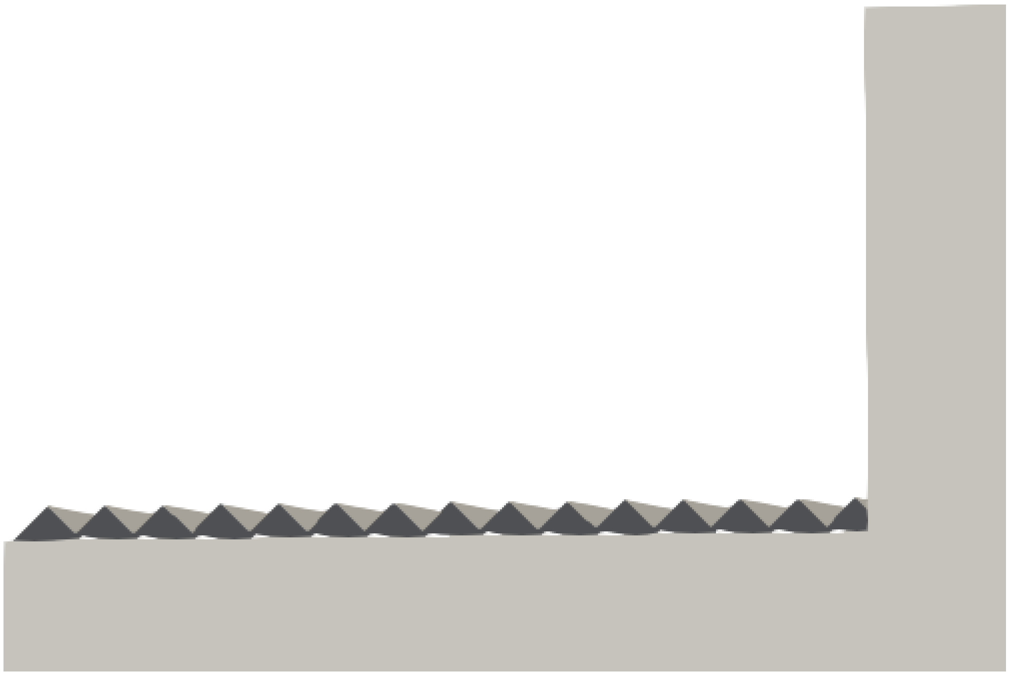

Figure J.1: Irregular quay surface

The irregular surface has been tested for two simulations in which numerical instabilities occurred. One of these simulations has a negative freeboard, while the other has a positive freeboard. Figure J.2 and J.3 show the configuration with the negative freeboard with and without irregular surface respectively. The high numerical instability peak at the end of the simulation has disappeared. The second highest peak around time = 250 s has disappeared as well. Therefore, for a negative freeboard, the irregular quay surface seems to work to prevent numerical instabilities. This is however only tested for one simulation so it might still cause numerical instabilities for different configurations.

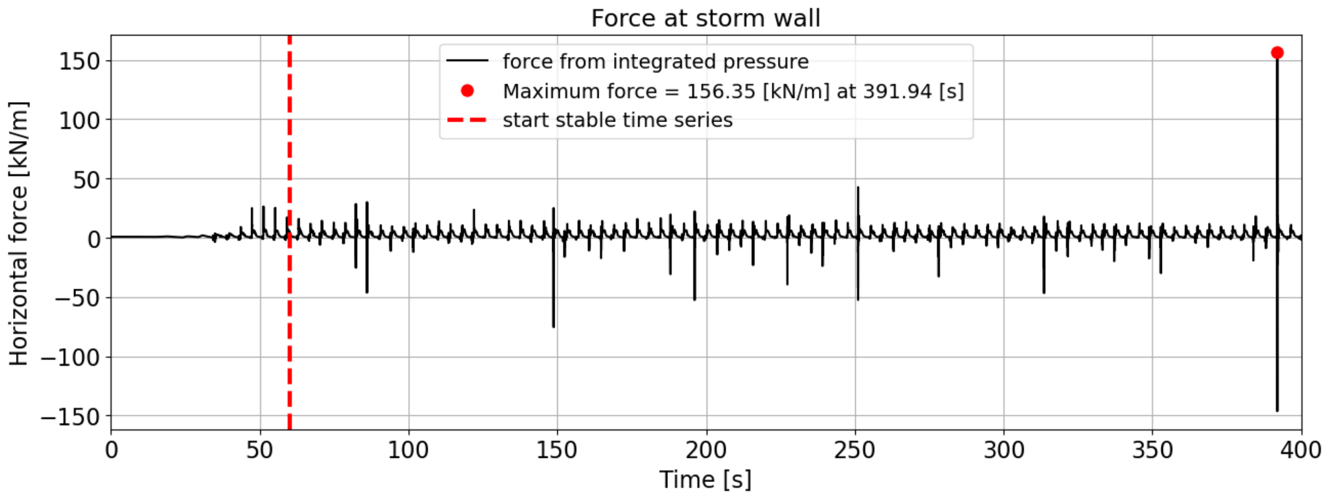

Figure J.2: Force on storm wall over time, negative freeboard (d_{wq}/L = 0.02), smooth quay surface

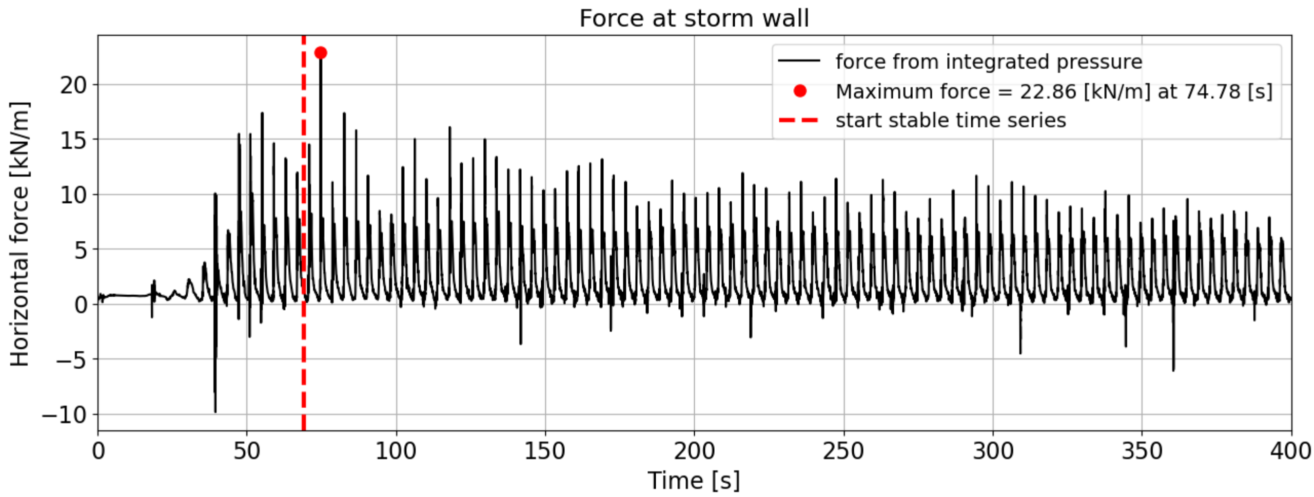

Figure J.3: Force on storm wall over time, negative freeboard (d_{wq}/L = 0.02), irregular quay surface

The method has also been tested for a positive freeboard. Since numerical instabilities occurred here often, only a short simulation has been run. Figure J.4 and J.5 show the configuration with the positive freeboard with and without irregular surface respectively. There is still a high peak with a deep negative valley visible in the stable part of the simulation when using the irregular surface. Generating an animation shows that numerical instabilities still occur in this case. Therefore, for a positive freeboard, the irregular surface is not sufficient to prevent numerical instabilities.

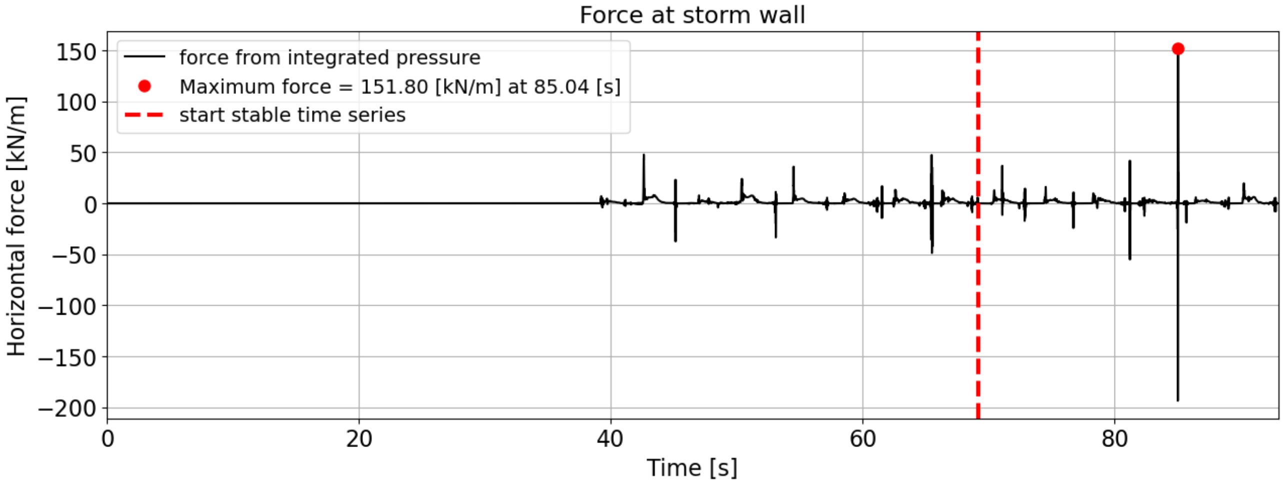

Figure J.4: Force on storm wall over time, positive freeboard (dwq/L = -0.02), smooth quay surface

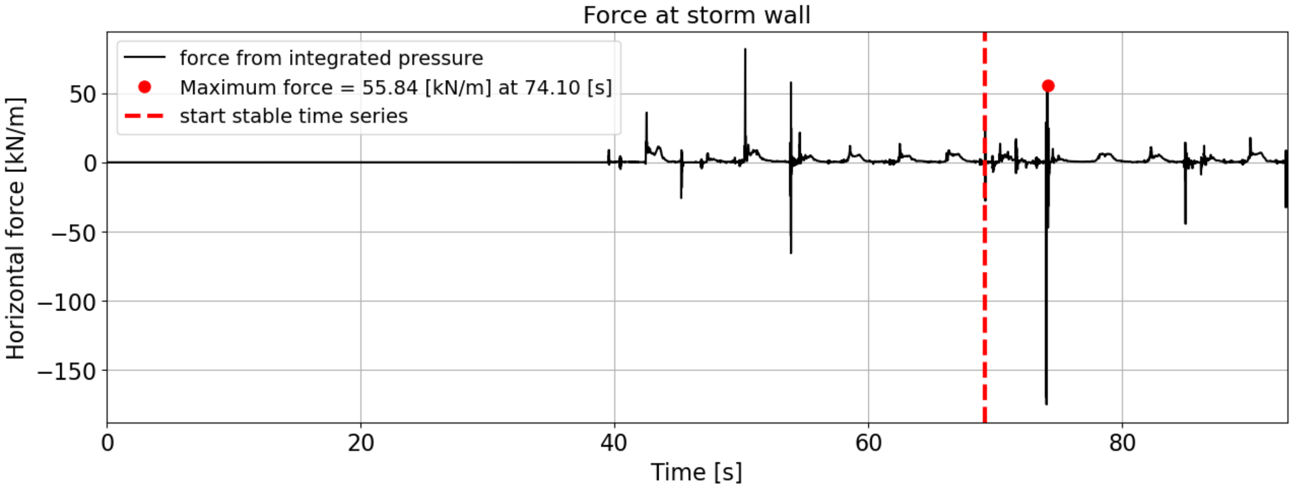

Figure J.5: Force on storm wall over time, positive freeboard (dwq/L = -0.02), irregular quay surface